Systems Biology of HIF Metabolism in Cancer

A thesis submitted to The University of Manchester for the degree of Doctor of Philosophy in the Faculty of Engineering and Physical Sciences

Emily Grace Armitage
2012

The University of Manchester
Faculty of Engineering and Physical Sciences
School of Chemical Engineering and Analytical Science

Contents

Final word count 63,700

List of Figures

List of Tables

List of Equations

Abstract

The University of Manchester
Faculty of Engineering and Physical Sciences

Abstract of thesis entitled 'Systems Biology of HIF Metabolism in Cancer'
Submitted by Emily Grace Armitage for the degree of Doctor of Philosophy, September 2012

Cancer is one of the most devastating human diseases that cause a vast number of mortalities worldwide each year. Cancer research is one of the largest fields in the life sciences and despite many astounding breakthroughs and contributions over the past few decades, there is still a considerable amount to unveil on the function of cancer that would improve diagnostics, prognostics and therapy. Since cancer is known to involve a wide range of processes, applying methods to study it from a systems perspective could reveal new properties of cancer. Systems biology is becoming an increasingly popular tool in the life sciences. The approach has been applied to many biological and biomedical analyses drawing upon recent advancements in technology that make high throughput analyses of samples and computational modelling possible. In this thesis, the effect of hypoxia inducible factor-1 (HIF-1) on cancer metabolism, the entity considered most closely related to phenotype has been investigated. This transcription factor is known to regulate a multitude of genes and proteins to promote survival in a low oxygen environment that is prevalent in solid tumours. However its effect on the metabolome is less well characterised. By revealing the effect of HIF-1 on the metabolome as a system it is hoped that phenotypic signatures, key metabolic pathways indicative of cancer function and potential targets for future cancer therapy, can be revealed.

The system has been studied using two cell models: mouse hepatocellular carcinoma and human colon carcinoma, whereby metabolism has been profiled using a range of analytical platforms. In each model, wild type cells have been compared to cells deficient in HIF-1 to reveal its effect on cellular metabolism. Gas chromatography - mass spectrometry (GC-MS) and ultra high performance liquid chromatography - mass spectrometry (UHPLC-MS) have been employed for metabolic profiling of cells exposed to a range of oxygen conditions. Additionally, time-of-flight secondary ion mass spectrometry (ToF-SIMS) has been employed for imaging mass spectrometric analysis of multicellular tumour spheroids cultured from wild type cells and cells with dysfunctional HIF-1 to represent small initiating tumours. Using these techniques in metabolic profiling it has been possible to reveal metabolites associated with the effect of oxygen and HIF-1 on cancer metabolism along with key pathways and hubs that could be targeted in future therapy. Using imaging mass spectrometry it has been possible to localise metabolites *in situ* revealing how tumour structure relates to function. Finally, a novel approach to consider how metabolites are correlated with one another in the response to oxygen level or presence or absence of functional HIF-1 has been undertaken to better understand the systems properties of cancer metabolism. Metabolites found to be differently correlated with respect to oxygen and/or HIF-1 have been mapped onto a human metabolic network to determine their network-based origins. This allowed the simulation of sub-networks of metabolism most affected by oxygen and HIF-1, highlighting the key mechanisms in HIF-1 mediated cancer cell survival.

Declaration

No portion of the work referred to in the thesis has been submitted in support of an application for another degree or qualification of this or any other university or other institute of learning.

Copyright Statement

i. The author of this thesis (including any appendices and/or schedules to this thesis) owns certain copyright or related rights in it (the "Copyright") and s/he has given The University of Manchester certain rights to use such Copyright, including for administrative purposes.

ii. Copies of this thesis, either in full or in extracts and whether in hard or electronic copy, may be made only in accordance with the Copyright, Designs and Patents Act 1988 (as amended) and regulations issued under it or, where appropriate, in accordance with licensing agreements which the University has from time to time. This page must form part of any such copies made.

iii. The ownership of any patents, designs, trademarks and any and all other intellectual property rights except for the Copyright (the "Intellectual Property Rights") and any reproductions of copyright works, for example graphs and tables ("Reproductions"), which may be described in this thesis, may not be owned by the author and may be owned by third parties. Such Intellectual Property Rights and Reproductions cannot and must not be made available for use without the prior written permission of the owner(s) of the relevant Intellectual Property Rights and/or Reproductions

iv. Further information on the conditions under which disclosure, publication and exploitation of this thesis, the Copyright and any Intellectual Property Rights and/or Reproductions described in it may take place is available from the Head of School of Chemical Engineering and Analytical Science(or the Vice-President) and the Dean of the Faculty of Engineering and Physical Sciences, for Faculty of Engineering and Physical Sciences candidates.

Acknowledgements

I would firstly like to thank my supervisors at The University of Manchester. They include Professor Kaye Williams for supervision on Cancer Biology, Professor Hans Westerhoff for supervision on Systems Biology, Professor Royston Goodacre for supervision on metabolomics and Dr Nicholas Lockyer for supervision on ToF-SIMS.

I would secondly like to thank the members of each of my supervisor's research groups. In particular I would like to acknowledge Professor John Vickerman and Dr John Fletcher for their help and guidance using ToF-SIMS; Dr Warwick Dunn and Dr Graham Mullard for acquisition and preparation of peak output files for UHPLC-MS data; Dr William Allwood for pre-processing of GC-MS data; Dr Alex Henderson for his advice on the use of multivariate analysis methods and Dr McMahon for his contribution to the designing of this PhD project.

Finally I would like to acknowledge Helen Kotze: a fellow Systems Biology Doctoral Training Centre student here at the University of Manchester. Together Helen and I have developed some of the methods that are presented in this thesis. These include the engineering of a chamber for hypoxia exposure in *in vitro* cell experiments as well as the division of methods for culturing multicellular tumour spheroids and for network-based correlation analysis of metabolites detected by GC-MS. Helen Kotze, Dr John Fletcher and I have also worked closely on the generation of a ToF-SIMS standards library of metabolites, my contribution to which is presented in this thesis.

Preface / The Author

I graduated from The University of Sheffield in 2008 with a 2.1 honors BSc in Biology. I began my PhD studies at the Doctoral Training Centre for Integrative Systems Biology in The University of Manchester in the same year. Whilst studying at Manchester I have been a student member of the Biochemical society as well as the British Association for Cancer Research.

Alongside my studies in Manchester I have has the opportunity to present aspects of my research at a range of international conferences. The following list summarises the presentations associated with my PhD research I have given at conferences.

- Poster presentation at the '13th International conference on Systems Biology' Toronto, Canada, August 19th – 23rd 2012
- Oral presentation at the '18th International conference on Secondary Ion Mass Spectrometry' Riva del Garda, Italy, September 18th – 23rd 2011
- Poster presentation at the '12th International conference on Systems Biology' Heidelberg/Mannheim, Germany, August 28th – September 1st 2011
- Poster presentation at the 'Association for Radiation Research/UK Environmental Mutagen Society joint meeting' Nottingham, UK, June 29th –July 1st 2011
- Poster presentation at 'Cancer and Metabolism: Pathways to the Future' Edinburgh, UK, September 19th – 21st 2010
- Poster presentation at 'British Association for Cancer Research 50th anniversary meeting: Hallmarks of cancer- from mechanisms to therapies', Edinburgh, UK, 13th –14th June 2010
- Oral presentation at the 'International Course on Systems Biology of Metabolism' Gothenburg, Sweden, May 24th - June 11th 2010
- Poster presentation at 'Metabolomics and More' Freising-Weihenstephan, Germany, March 10th – 12th 2010

Throughout my time at Manchester University, I have also been granted the following awards following successful application.

- Bursary from the school of Chemical Engineering and Analytical Science at The University of Manchester towards attendance at the '8th annual international meeting of the metabolomics society' Washington DC, USA, June 25th – 28th 2012
- Bursary (excluding travel) from the association of radiation research awarded to attend the 'Association for Radiation Research/UK Environmental Mutagen Society joint meeting' Nottingham, UK, June 29th –July 1st 2011
- Bursary (including travel) from Federation of the Societies of Biochemistry and Molecular Biology applied for as a member of the biochemical society awarded to attend the 'International Course on Systems Biology of Metabolism' Gothenburg, Sweden, May 24th – June 11th 2010

Finally I have had the opportunity to publish some of my work completed as part of my PhD research in academic journals. The following list includes articles already published, articles submitted for publication and articles in preparation for publication.

E.G. Armitage, H.L. Kotze, J.S. Fletcher, A. Henderson, K.J. Williams, N.P. Lockyer, J.C. Vickerman (2012) Time-of-flight SIMS as a novel approach to unlocking the hypoxic properties of cancer. *Surface Interface Analysis* (available online).

H.L. Kotze, **E.G. Armitage**, J.S. Fletcher, A. Henderson, K.J. Williams, NP Lockyer, J.C. Vickerman (2012) ToF-SIMS as a tool for metabolic profiling small biomolecules in cancer systems. *Surface Interface Analysis* (available online).

E.G. Armitage, H.L. Kotze and N.P. Lockyer (2012) Spatiotemporal imaging of metabolites using Secondary Ion Mass Spectrometry. *Metabolomics* (submitted)

J.S. Fletcher, H.L. Kotze, **E.G. Armitage**, N.P. Lockyer and J.C. Vickerman (2012) Time-of-Fight Secondary Ion Mass Spectrometry for Metabolomics – An Assessment of the Challenges for Metabolite Identification and Quantification. *Metabolomics* (submitted).

H.L. Kotze, **E.G. Armitage**, K.J. Sharkey, W.B Dunn, K.J.Williams and R. Goodacre (2012) Network-based correlation analysis: a new systems biology approach to analysing metabolic profiling data (in preparation).

E.G. Armitage, H.L. Kotze, G. Mullard, W.B Dunn, R. Goodacre, and K.J. Williams (2013) Metabolic profiling reveals potential metabolic markers associated with the role of HIF-1 in hypoxic cancer cells (in preparation).

H.L. Kotze, **E.G. Armitage**, W.B Dunn, R. Goodacre, and K.J. Williams (2013) Network-based correlation analysis of metabolic profiling data reveals pathway targets to overcome hypoxia-induced chemoresistance in cancer cells (in preparation).

In addition to publishing in academic journals I have also been approached by Springer (New York, USA) with a proposal to write a book on network-based correlation analysis of metabolic profiling data. The book will form part of a series in Springer briefs on Systems Biology. This is in the early stages of development with an intention of publication in 2013.

Abbreviations

ADP	Adenosine-5'-diphosphate
ANOVA	Analysis of variance
ATP	Adenosine-5'-triphosphate
CVA	Canonical variates analysis
DAG	Diradylglycerol/diacylglycerol
DART	Direct analysis in real time
DESI	Desorption electrospray ionisation
DMSO	Dimethyl sulphoxide
DN	Dominant negative
DNA	Deoxyribonucleic acid
DTGS	Deuterated triglycine sulfate
EDTA	Ethylenediaminetetraacetic acid
EHMN	Edinburgh human metabolic network
EI	Electron ionisation
EMSC	Extended multiplicative scatter correction
ESI	Electrospray ionisation
EV	Empty vector
FA	Fatty acid
FCS	Foetal calf serum
FH	Fumarate hydratase
FIH	Factor inhibiting HIF-1
FT-IR	Fourier transform – infrared
G1	Gap phase 1
G2/M	Gap phase 2/mitotic phase
GC-MS	Gas chromatography mass spectrometry
GLUT	Glucose transporter
HIF	Hypoxia inducible factor
HMDB	Human metabolic database
HRE	Hypoxia response element
IDH	Isocitrate dehydrogenase
IMS	Imaging mass spectrometry
KEGG	Kyoto encyclopedia of genes and genomes
LDH	Lactate dehydrogenase
LIMS	Laboratory information management systems
MAG	Monoradylglycerol/monoacylglycerol
MALDI	Matrix assisted laser desorption ionisation
MCT	Monocarboxylate transporter
MEM	Minimal essential medium
MRI	Magnetic resonance imaging
MS	Mass spectrometry/spectrum
MSI	Metabolomics standard initiative
MSTFA	N-methyl-N-trifluoroacetamide
MTS	Multicellular tumour spheroid
NAD(H)	Nicotinamide adenine dinucleotide (reduced)
NIST	National institute of standards and technology
NMR	Nuclear magnetic resonance
OCT	Optimal cutting temperature
ODC	Ornithine decarboxylase
PBS	Phosphate buffered saline
PCA	Principal components analysis
PDH	Pyruvate dehydrogenase
PDK	Pyruvate dehydrogenase kinase
PET	Positron emission tomography
PHD	Proline hydroxylase
PK	Pyruvate kinase
PLB	Passive lysis buffer
QC	Quality control
RI	Retention index
RNA	Ribonucleic acid
ROS	Reactive oxygen species
SDH	Succinate dehydrogenase
SIMS	Secondary ion mass spectrometry
TCA	Tricarboxylic acid
ToF	Time-of-flight
UHPLC-MS	Ultra high performance liquid chromatography
VHL	von Hippel Lindau
WT	Wild type

Chapter 1. Introduction

1.1. Systems biology and cancer

1.1.1. Systems biology

Systems biology can be considered in terms of the causal theory for explanation. This states that higher entities are caused by occurrences, laws or theories at lower entities[1]. For example the way in which a human functions is caused by how its organs function and how the tissues of the organ function, how the cells of a tissue function, and how the molecules in a cell function.

Reducing a system to its lowest entity and understanding function, structure and behaviour of molecules in isolation can be used to predict how a molecule may interact with other molecules in a micro-system[2]. Further to this, considering many micro-systems and how they can interact and consequently change their function or behaviour can lead to a fuller understanding of a macro-system such as a human organ. It is implied that the structure and function of molecules causes them to interact in a certain way, ultimately contributing to the function of the system. This theory is applicable to cancer research as knowledge of how individual genes, factors and metabolites vary under certain conditions to alter the behaviour at the cellular level (micro-system) can be used to predict how cells may interact within a larger system such as a tumour under similar conditions. This could potentially bridge the gap between *in vitro* and *in vivo* studies.

The field of systems biology is relatively new and has stemmed from the combined successes of molecular biosciences and bioinformatics[3]. This has led to the 'omic' and related data generation technologies that currently dominate systems biology[4,5], and that are used to elucidate information from the genome and transcriptome to the proteome and metabolome. It is becoming increasingly popular in the study of diseases.

Systems biology draws upon knowledge and techniques from various disciplines across the physical, information and life sciences with an aim to fill gaps in biological knowledge. It is an approach commonly used to study the biochemical interactions of genes, proteins and/or metabolites as emergent properties of a biological system, rather

than as isolated biological features. Figure 1 illustrates how different science disciplines can interact in systems biology. Many systems biology experiments are driven by a hypothesis or biological question that has not been resolved using traditional techniques. The experiment is carefully designed and samples collected for analysis using often high-throughput technologies capable of generating reproducible, qualitative or (semi-) quantitative data that can be analysed using intelligent computational methods including multivariate analysis and modelling. Data and data models are usually reported in an accepted systems biology language that if made publically available in databases can be compatible with other data across the world. Subsequently a collection of genomic, transcriptomic, proteomic and metabolomics data is generated for a range of biological systems and used to reveal structural and functional properties that can lead to further hypotheses.

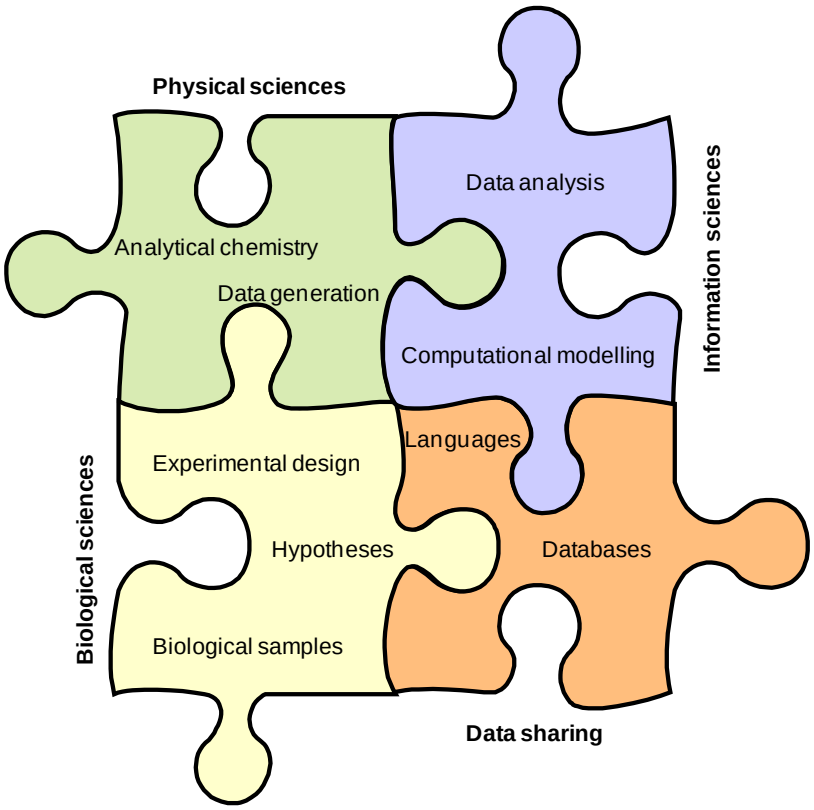

Figure 1: The components that fit together to form systems biology. Examples are given for each of the four major components to show how each scientific aspect contributes to a systems biology study.

Recent advancements in technology especially in the physical and information sciences have enhanced the quality of experimental data and its analysis. For example there are many techniques employed in analytical chemistry for the acquisition of reproducible (semi-) quantitative data and there are many software packages available for complex data analysis of large datasets and modelling of systems biology data. Furthermore, the

increased use of standardised languages and databases for data sharing enables combining of data on one biological system.

1.1.1. Cancer: A systems biology disease

For decades, cancer research has involved studying the molecular features that are different between cancer cells and their healthy counterparts, with the aim of revealing molecular biomarkers representative of the cancer phenotype as well as possible therapeutic targets[6]. This has led to the identification of many molecular features involved in cancer that function in signal transduction[7], cell senescence[8] and other hallmarks of cancer cells[9]. What remains to be done is to reveal more information on the complex connections and interactions between these molecular features beyond the individual pathways in which they function. A systems biology approach that considers how genes, proteins or metabolites interact with each other at each level could start a paradigm shift in cancer research.

The system of cancer is hugely complex and requires to some extent detailed knowledge of its components. Although the biochemistry is by no means fully understood to the detail required to prevent or cure cancer, systems biology can be employed to link components together to reveal their system properties. This could help highlight the most important aspects of the cancer phenotype that should be further investigated, perhaps even using traditional reductionist methods. Considering the system from a top-down perspective could lead to revealing new biomarkers or potential targets for future therapy.

The research presented in this thesis mainly utilises the biological and physical science aspects of systems biology, while specific features of the information sciences are drawn upon. A key component of systems biology involves the information sciences in *in silico* modelling. Numerous computational models have been built for public use (several available at the JWS online model database[10], and the BiGG database[11]) and many systems biologists are building computational models for a variety of biological systems. Computational models range both in terms of size and complexity.

Computational and mathematical analyses and the generation of predictive biochemical models are becoming increasingly popular as a mechanism to predict systems properties quantitatively which could be further tested. In this way the focus of biological research is

moving from the molecular level to the network level. Additionally models with conserved properties to the system under investigation that are already available can be used in the analysis of many 'omics' data. For example there are several publically available human metabolic networks[12, 13] whereby many of the biochemical reactions are relevant to cancer cells. These models can be used to reveal the underlying metabolic effects of a specific cancer phenotype using data generated from profiling the metabolome. Once the systems properties have been revealed, new hypotheses about the pathways and sub-networks that appear to control cancer metabolism could be further investigated in the future. Without using such models, profiling data can only be useful for discovery of individual metabolic features.

By incorporating high-throughput data from genomics, transcriptomics, proteomics and/or metabolomics, it may eventually be possible to build a parameterised computational model of a cancer cell that has the potential to illustrate function. By elucidating a greater understanding of cancer through testable and quantifiable models, it is hoped that new targets for therapy will be revealed. Tumour metabolism is highly sensitive and is controlled by a range of factors. Revealing the influence of some of these hierarchical factors will be essential in modeling tumour metabolism in the future. Building a good model for a tumour cell may be key to recognising dynamic features, which may be useful to identify parts of the system that can be perturbed to disrupt cancer progression, while also moving towards improved diagnostics[4]. The approach to model a silicon cell is a key theme in systems biology research that, 'aims to describe the intracellular network of interest precisely, by numerically integrating the precise rate equations that characterise the ways macromolecules interact with each other'[14]. To model a silicon cancer cell would be a great aim to work towards. This would provide a comprehensive resource for understanding the function of a cancer cell at each level. One of the main considerations for building cancer models are the specificities required that make them relevant to cancer as opposed to a general human model or more specifically make them tissue specific. There are examples of tissue specific models in the literature[15, 16] which highlight the advancements in computational modelling, particularly in the field of metabolism that could contribute to a full-scale cancer cell model. Although the present research does not involve model building *per se*, the tools are in place for models to be used in data analysis. Sub-networks have been identified that could also contribute to a full scale cancer model in future research.

1.2. Cancer cell metabolism

The metabolome is considered the closest entity to the phenotype of a biological system. Revealing the complexity of the metabolome is particularly advantageous to understand the phenotypic function of a cancer cell that is governed by the preceding levels. Central carbon metabolism (Figure 2) is a vital metabolic sub-network in cancer cell metabolism and has been explored extensively over decades of cancer research[17, 18].

The respiratory pathway is considered central carbon metabolism which other pathways either feed in to deliver molecules to be catabolised to produce energy or feed out supplying carbon for biosynthesis[19]. Normal cell respiration in aerobic conditions involves three main processes: glycolysis, the tricarboxylic acid (TCA) cycle and oxidative phosphorylation. The ATP synthesised in aerobic respiration is derived either from metabolising glucose to pyruvate *via* glycolysis or from oxidative phosphorylation[20]. In normal cells under anaerobic conditions, the TCA cycle is aborted and pyruvate synthesised in glycolysis is instead converted by lactate dehydrogenase (LDH) into lactate[20].

One of the main features of central carbon metabolism is glycolysis. Glycolysis is a conserved metabolic pathway that converts glucose to pyruvate *via* a series of reactions that ultimately generate ATP and NADH. Following glycolysis, pyruvate is either converted to lactate, a reaction catalysed by LDH that regenerates NAD from NADH produced in glycolysis, or pyruvate enters the mitochondria through the pyruvate transporter where it is converted to acetyl-coA by pyruvate dehydrogenase (PDH) and further fed into the TCA cycle[21]. Pyruvate dehydrogenase kinase (PDK) can prevent the transport of pyruvate into the mitochondria through phosphorylating and therefore inactivating mitochondrial PDH[22].

It has long been suggested that cancer cells preferentially convert pyruvate to lactate rather than fuelling the TCA cycle even in aerobic conditions[20, 23]. Although more recently it has been shown that this is not the exclusive rule for cancer metabolism, it is a common understanding that tumour cells display enhanced glycolytic activity along with a down regulation of the TCA cycle and electron transport chain[24-26]. This is known as the Warburg effect. Hypothesised by Otto Warburg in 1956, the Warburg effect suggests that tumour cells originate from healthy cells in two phases: an irreversible injuring of

respiration followed by a replacement of the lost respiration energy with fermentation energy[25]. Furthermore, the Warburg effect implies cancer cells show elevated uptake of glucose. This is also the main feature of the highly sensitive and accurate positron emission tomography (PET) used in solid tumour diagnostics[27].

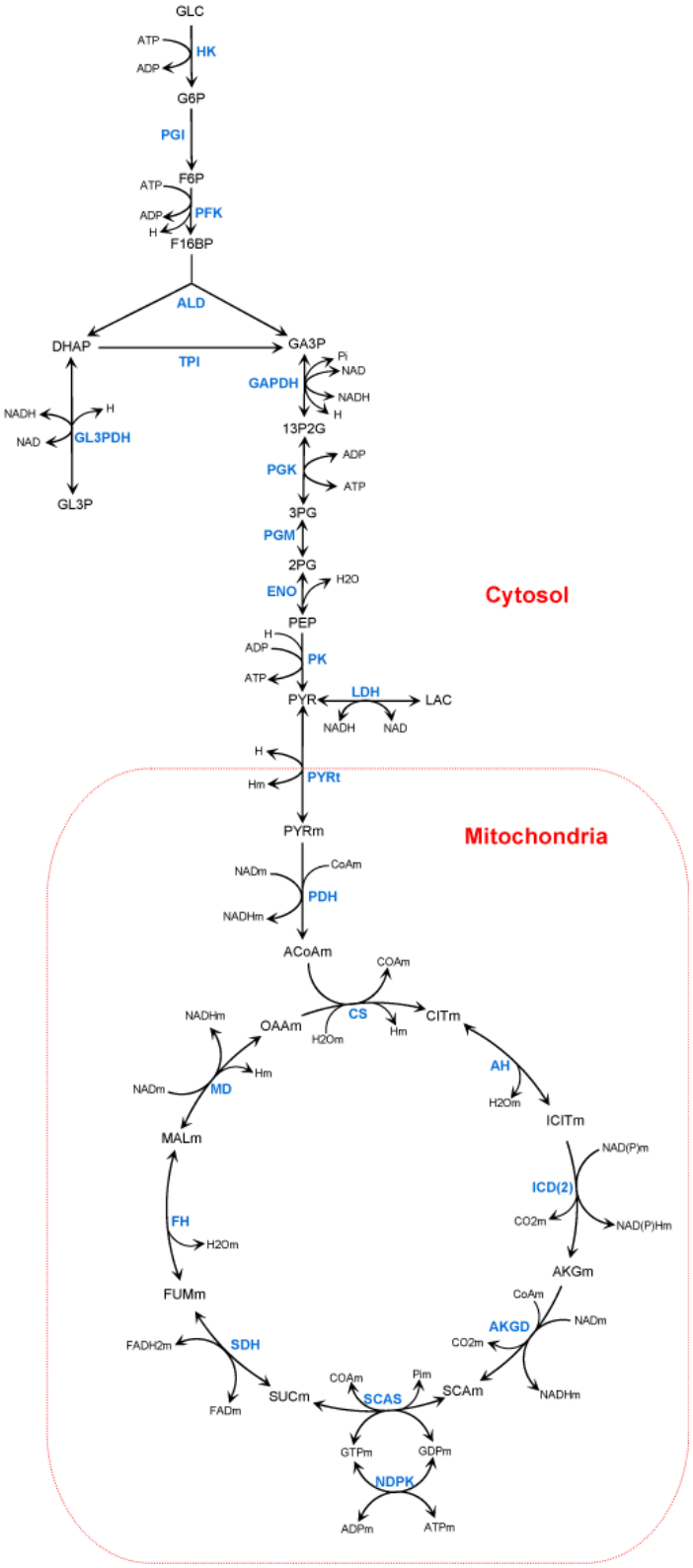

Figure 2: Central carbon metabolism comprised of reactions in glycolysis and the tricarboxylic acid (TCA) cycle.

While the exact mechanism through which the Warburg effect is employed is still undecided[24], the benefits which include enhanced tumour survival and proliferation are clear. Tumour cells display the ability to regulate glycolytic machinery while also down regulating mitochondrial machinery to suit their respiratory system[23], which is almost certainly a result of enhanced expression of glycolytic enzymes[24]. As the glycolytic pathway assists in providing materials for the biosynthesis of molecules such as fatty acids (FAs) and cholesterol, maintaining high glycolytic throughput even in aerobic conditions supports rapid growth and survival of tumours[23]. Further to glycolytic regulation, lactate production which occurs irrespective of oxygen availability is essential to tumour survival. An acidic microenvironment is generated in tissues surrounding the tumour as a result of lactate build up and efflux from the tumour itself. This environment helps prevent attacks from the host's immune system, while also inducing negative effects on surrounding tissues in which the tumour lies[23]. Furthermore, an acidic environment contributes to the success of tumour metastasis[24].

One of the most important regulations in cancer is that of pyruvate kinase (PK). This is an enzyme that catalyses the reaction to yield pyruvate and ATP. The enzyme exists in several isoforms including M1 that is expressed in most adult tissues and M2 that is usually expressed in embryos during development[26]. With reference to cancer metabolism, it has been shown that tumour cells have the ability to switch from an M1 isoform to an M2 isoform of PK and that this switch is observed in conditions that are particularly hypoxic[26]. Additionally, although the M1 isoform is generally the more active isoform of PK, for cell proliferation it is dependent on oxidative phosphorylation[26]. Therefore in the absence of oxygen tumours may be forced to, rather than choose to, express the M2 isoform. Furthermore, cells expressing the M2 isoform were shown to possess an elevated ratio of lactate production to oxygen consumption and it was determined that other glycolytic intermediates are affected by differential expression of these PK isoforms[26]. These data further support the idea of a change in cancer metabolism to elevate lactate production.

Tumour metabolism encompasses processes beyond central carbon metabolism. For example, the pentose phosphate pathway is another key contributor to generate energy in a cancer cell. Here, NADPH is generated that associates with both glycolysis as well as glutaminolysis. Both pathways lead ultimately to the secretion of lactate, from the

oxidation of pyruvate by LDH, that has been identified as a major energy source in tumours, even if they are oxygenated[22].

Additionally, the TCA cycle is extended by cataplerosis (the efflux of biosynthetic intermediates for lipid and amino acid synthesis) and anaplerosis (the influx of biosynthetic intermediates to maintain cycling) involving a vast range of metabolites[28]. Figure 3 shows the interactions of cataplerosis and anaplerosis that maintain the TCA cycle, where citrate and malate are the two most active players in cataplerosis while the main player in anaplerosis is glutamine[22].

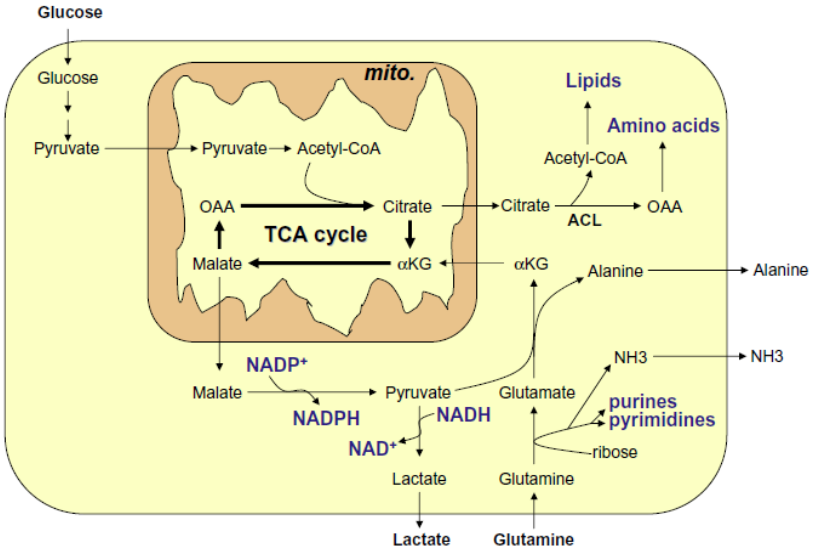

Figure 3: The roles of cataplerosis and anaplerosis in biosynthesis *via* tricarboxylic acid (TCA) cycling. The TCA cycle provides proliferating tumour cells with biosynthetic precursors instead of ATP in cataplerosis and an influx of metabolic intermediates replenish the TCA cycle in anaplerosis. Figure taken from Feron (2009)[22].

The role of glutamine is to feed glutaminolysis, the deamidation of glutamine to glutamate catalysed by glutaminase, generating metabolic intermediates that contribute to and maintain the biosynthetic TCA cycle[22, 29]. Similar to the pentose phosphate pathway, glutaminolysis provides NADPH to the system through metabolising malate from alpha-ketoglutarate which has in turn the potential to be oxidised into pyruvate in the cytosol[22]. Glutamine is therefore considered the other main source of energy to glucose in cells and particularly in tumour cells. In general, tumour cells fuel their metabolism that serves to meet their bio-energetic and bio-synthetic needs essentially from glucose and glutamine[22].

Although numerous aspects of cancer metabolism have been explored previously, few studies have considered less well investigated pathways, or how key pathways interact in

sub-networks of metabolism. Key pathways may be spatially or temporally separated but share the same control in cancer function. Furthermore, the effect of hypoxia on the entire cancer metabolome is not well understood.

1.3. Hypoxia

Mammalian cells have various control mechanisms that regulate homeostasis; the maintenance of a constant cellular environment. This includes regulating oxygen homeostasis, such that the need for oxygen for oxidative phosphorylation and other metabolic reactions is balanced with the risk of oxidative damage within the cell[30]. Hypoxia is the intermediate state between the homeostatic state of normoxia and the complete absence of oxygen in anoxia. Under hypoxia, the survival of a cell, tissue, organ or organism is governed by its ability to detect and respond to oxygen availability before a critical point is reached[31].

Hypoxia is prevalent in solid tumours and is usually associated with oxygen partial pressures below 10 mmHg[32]. It occurs due to the lack of oxygen as a result of poor blood supply[33]. It occurs when cells are located greater than a distance of 100-180μm from the closest capillary through which oxygen is delivered to cells[30]. Figure 4 shows a schematic for this. Rapid cell proliferation and the presence or ongoing production of abnormal blood vessels in tumours contribute to creating distances greater than the threshold, thus causing hypoxia in tumours[30]. The severity of hypoxia is directly proportional to the distance from the oxygen supply and consequently the vast majority of tumours initiate angiogenesis; the recruitment of new capillaries and blood vessels therefore promotes tumour cell survival.

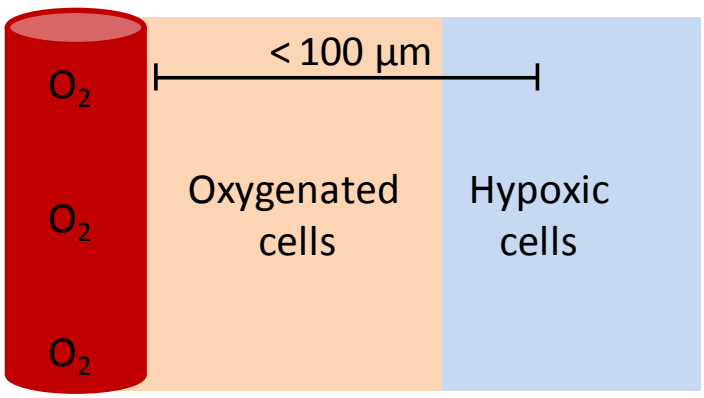

Figure 4: A schematic for hypoxia in a tissue adjacent to a blood supply. Cells situated closest to the blood supply are most oxygenated and a gradient in oxygen availability exists towards cells furthest from the blood supply that are increasingly hypoxic.

Monocarboxylate transporters (MCTs) have received much attention in cancer metabolism research. This is mainly because cancer cells appear to utilise lactate as an alternative to glucose to fuel cellular respiration and MCTs are involved in lactate transport between cells[22, 34]. Another interesting proposal for the effect of hypoxia on cancer cell metabolism with reference to lactate is the model of metabolic symbiosis suggested by Feron (2009)[22]. This explains a possible hypothesis for the relationship between cells in the normoxic region of a tumour and the cells in the more hypoxic regions, further from the blood supply. The model, shown in Figure 5, infers that normoxic tumour cells metabolise lactate over glucose even though their conditions are largely aerobic. Lactate is converted by LDH to pyruvate which is transported into the mitochondria of these cells to continue a normal route for respiration (i.e. through the TCA cycle and oxidative phosphorylation). By not utilising or even taking up glucose, these cells ensure an elevated concentration of glucose in the tumour is available for cells of the hypoxic region to uptake through their glucose transporters. Here glucose is readily converted to pyruvate and transported out of the cell through the hypoxia induced MCT 4 and into the well oxygenated cells through MCT 1. This makes the fluid surrounding the hypoxic cells even more acidic than would be possible if surplus glucose was not left available to these cells.

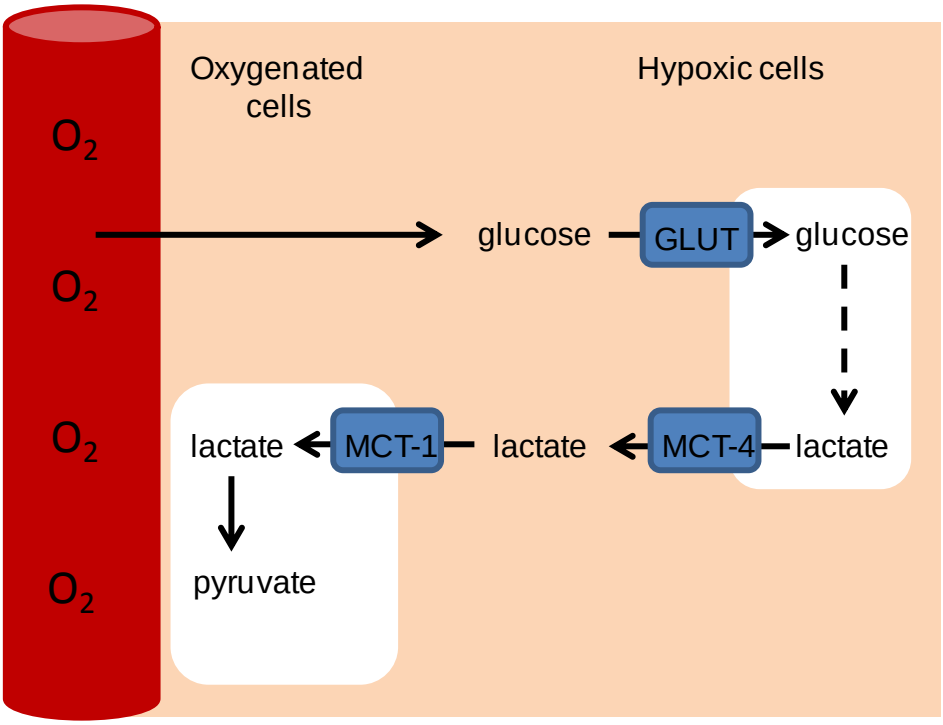

Figure 5: Lactate flux-driven symbiosis in tumours adapted from Feron (2009)[22]. A gradient of oxygen exists with increasing distance away from the blood supply. Glucose is preferentially converted to lactate in the hypoxic cells situated furthest away from the blood supply through increased expression of glucose transporter (GLUT) for glucose influx and monocarboxylate transporter 4 (MCT4) for lactate efflux. Oxygenated cells located close to the blood supply express monocarboxylate transporter 1 (MCT1) to uptake lactate which is then converted to pyruvate, the principal substrate for mitochondrial oxidative

phosphorylation. The preference of aerobic cells to utilise lactate frees excess glucose to be used by hypoxic cells to fuel glycolysis.

1.3.1. Hypoxia inducible factor–1

The responses of cells to hypoxia are orchestrated by the activation of hypoxia inducible factors (HIFs), in particular HIF-1 which was described by Wang and Semenza in 1995[35]. The identification of HIF-1[35], its purification[36] and its molecular characterisation[35] have all been described previously. HIF-1 is responsible for regulating the expression of numerous target genes as summarised in Semenza (2003)[37]. HIF-1 consists of two subunits: HIF-1α and HIF-1β, that can exist independently or as an active complex depending on the state of oxygenation in cells. The HIF-1β subunit is a constitutively expressed nuclear protein and the HIF-1α subunit is stabilised only as a response to low oxygen (oxygen partial pressure <10 mmHg). The mechanisms of this are portrayed in Figure 6.

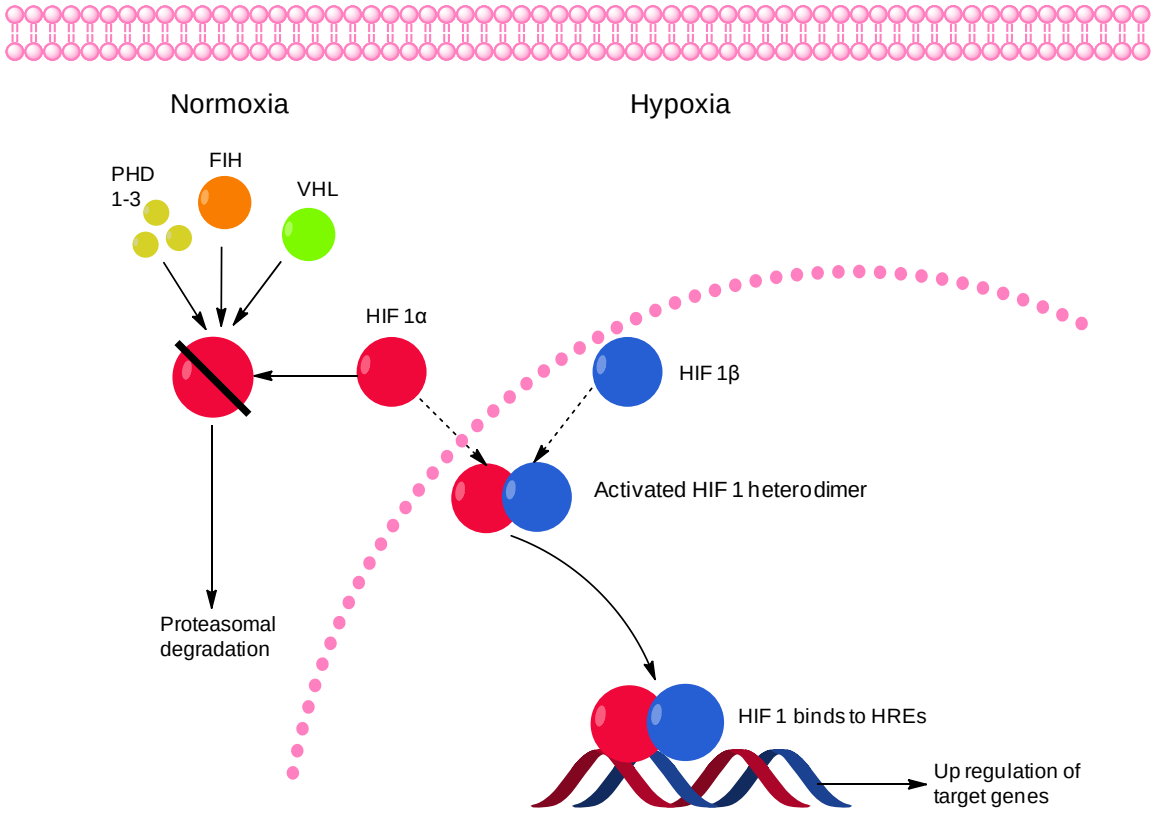

Figure 6: In normoxia, hypoxia inducible factor (HIF)-1α is hydroxylated by proline hydroxylases (PHDs) 1, 2 and 3 after which the von Hippel Lindau protein (product of the von Hippel Lindau tumour suppressor gene) is able to tag HIF-1α to be polyubiquitinated and hence recognisable by the proteasome for degradation. In hypoxia, HIF-1α does not have the binding signature for prolyl hydroxylases (PHDs), von Hippel Lindau (VHL) and factor inhibiting HIF-1 (FIH); therefore HIF-1α is able to form an active heterodimer with the constitutively expressed HIF-1β. The activated heterodimer binds to hypoxia response elements (HREs) in the promoter regions of target genes and recruit transcriptional co-activators to enable transcription.

Deficiencies or blocking of either subunit stops the formation of the active heterodimer and alters the phenotype of the cell in different oxygen potentials, particularly with respect to its metabolic phenotype[38]. For example it has been shown that HIF-1β deficient cells (such as HEPA-1 C4 cells) have an ATP content of up to 80% lower than corresponding wild type cells[33].

HIF-1α is subject to post-translational modification in the presence of oxygen which targets it for degradation[39]. Oxygen sensors such as prolyl hydroxylase (PHD), factor inhibiting HIF-1 (FIH) and von Hippel Lindau (VHL) protein control the repression of HIF in cells exposed to normal oxygen levels (oxygen partial pressure >10 mmHg)[40, 41]. The modification required for targeted degradation is hydroxylation. This occurs on proline residues within the oxygen-dependent degradation domain of HIF-1α [40]. Hydroxylation at these residues allows for the binding of the VHL tumour suppressor protein which targets HIF-1α for degradation *via* the proteasome[40]. In the C-terminal transactivation domain, FIH modifies an asparagine residue, preventing the binding of co-factors necessary for activating the HIF-1 heterodimer[41]. To activate the heterodimer, HIF-1α translocates to the nucleus to complex with HIF-1β. The heterodimer up regulates pathways associated with glucose uptake, glycolytic metabolism and pH regulation as well as other features that contribute to the tumour phenotype such as cellular proliferation and differentiation[38]. The activated HIF-1 complex controls the regulation of genes containing hypoxia response elements (HREs). It does this by interacting with cofactors as well as binding to the promoters of and facilitating the transcription of approximately 100-200 genes[42] that contain HREs[30]. HREs are prevalent in genes which encode stress response enzymes, including glycolytic enzymes[43].

Hypoxia and HIFs (particularly the over expression of HIF-1) are associated with chemotherapy and radiotherapy resistance[30], thus they play a critical role in tumour survival and defence against eradication. Our knowledge and understanding of the mechanisms of HIFs have started to illustrate great scope in the designing and screening of new anticancer therapies[30]. However, simply developing antagonists to the HIF pathway is not enough as it is not yet established that HIF drives the transformation of a normal cell to a cancer cell[44].

One of the main metabolic targets previously investigated with respect to the role of HIF-1 in cancer hypoxia is glycolysis[24, 38]. Targeting the transcription of genes that code for

glucose transporters (such as GLUT 1 and GLUT 3)[33], responsible for eliciting downstream changes in a tumour's metabolic phenotype, are just some of its known activity in regulating glycolysis. It is also thought that HIF-1 mediates an adaptation to hypoxia through down regulating the activity of the TCA cycle as well as mitochondrial oxygen consumption through inhibiting PDK 1[45]. The mechanism for this is thought to be an induced expression of both PDK and LDH-A by a hypoxia driven increase in HIF-1α[45]. In this way, HIF may be directly responsible for controlling the increased conversion of glucose into lactate in low oxygen microenvironments possessed by cancer cells. In another example, it has been shown that inhibiting the HIF pathway significantly reduces glucose uptake and lactate production *in vitro* while also increasing glutamine uptake[46]. This highlights the importance of central carbon metabolism as a target of HIF.

Most research has linked HIF-1 with central carbon metabolism. This potentially plays the most vital role in cancer cell metabolism. However, central carbon metabolism has many associated pathways that supply metabolite precursors or produce precursors necessary for many other metabolic processes. Furthermore, there may be unrelated metabolic features of cancer metabolism that appear to be controlled by HIF-1 that are of equal importance in cancer function. This research has aimed to explore the metabolome to reveal metabolic features and maybe even new targets for cancer therapy, with particular reference to inhibiting HIF-1.

1.4. Metabolomics

Metabolomics is a commonly used tool in systems biology. Since a range of metabolites can be detected in a single assay, metabolomics can be defined as a holistic and data-driven study of the low molecular weight metabolites present in biological systems[47]. The metabolome is made up from endogenous and exogenous components: those catabolised or anabolised by the cell or organism itself, or those that are extra-organism or extracellular respectively. The metabolome includes metabolites present in a cell or organism that participate in metabolic reactions required for growth, maintenance and function, as well as metabolites consumed from the external environment[47]. If considering an organism *in vivo* the external environment could include the metabolomes of interacting organisms, for example from gut microflora in humans[48]. In *in vitro* metabolomics (as presented in this research), the external environment is considered the growth medium.

Although the functional levels of a biological system include the genome, transcriptome, proteome and metabolomes, the latter is considered most representative of the phenotype[47]. Exploring the metabolome following experimental perturbation may be the best way to reveal the phenotypic changes relative to biological function, where subtle changes can be tractable. For these reasons metabolomics is one of the fastest developing disciplines in systems biology and other aspects of modern science.

There are some challenges associated with metabolomics that must be considered prior to undertaking research in this area. For example, the volume of metabolites can be too large to analyse and some metabolites cannot be detected through current experimental methods. Additionally, the fluxes and concentrations of metabolites can originate from more than one hierarchical route, such that changes observed in the metabolic phenotype of a biological system can be ambiguous with respect to their origin. For full elucidation of the biological system, a combination of the 'omics' can be required. Other challenges in the field are owed to metabolomics being less developed than the preceding omic fields. For example there is a lack of a well established, comprehensive and publically available database that would be useful in data interpretation and standardisation. In genomics for example, GenBank provides nucleotide sequences for over 380,000 organisms and involves a daily data exchange from laboratories worldwide to continually enhance it[49]. There have however been advancements towards this for metabolomics, whereby a metabolomics standard initiative (MSI) has been proposed for the identification of metabolites[50] and laboratory information management systems (LIMS)[51] including SetupX[52] have been developed. Additionally metabolite libraries have been compiled, an excellent example of which is the Manchester metabolomics database which includes a range of analysed metabolite standards for both gas chromatography mass spectrometry (GC-MS) and ultra high performance liquid chromatography mass spectrometry (UHPLC-MS)[53]. Libraries are most advanced for GC-MS in metabolomics, a particular breakthrough for which was the Agilent Fiehn metabolomics retention time locked library[54]. Currently the method for identification of features in UPLC-MS data relies upon accurate mass that can be matched to compounds from web-based sources. A recent advancement in this area has been the development of the Taverna work flow for feature identification[55]. For other metabolomics platforms such as nuclear magnetic resonance (NMR) spectroscopy, software such as MetaboHunter are available for feature identification[56]. In the future it is hoped that the number of features it is possible to identify will increase and a combined repository for the whole metabolomics community to use

will be created that contains data from a wider range of analytical platforms. Some aspects have been addressed by the recently introduced metabolights: a database for comparing metabolomics experiments across species and across analytical platforms (http://www.ebi.ac.uk/metabolights/). The advancements in computational metabolomics so far are enough to make biomarker discovery possible and biomarkers are valuable identifications, regardless of their hierarchical origin, for revealing phenotypic properties in a biological system. Furthermore, in the identification of key metabolic pathways it is possible that metabolomics alone can reveal potential targets for cancer therapy. Combining the use of different analytical platforms extends the number of metabolites it is possible to detect in biological samples. For example, the combined use of GC-MS and UHPLC-MS in this research as two of the most developed methods in metabolomics is presented.

1.4.1. Approaches in metabolomics

Metabolomics is an 'umbrella term' for many forms of experiment that can be applied to studying metabolism. It includes, but is not restricted to metabolic profiling which is the branch of metabolomics used to generate data presented in this thesis. Other branches include metabolic target analysis and metabolic flux analysis. Table 1 shows the most commonly used analytical platforms for these three main branches of metabolomics as highlighted by Goodacre (2007)[5]. In each case, metabolism is quenched (typically by adding ice cold methanol to the sample) before analysis to stop any further metabolic changes that may occur.

Metabolic target analysis involves the quantification of particular metabolites of interest. For example in a recent published study, LC-MS was used to quantify glycolytic metabolites to test whether or not an accumulation of glycolytic metabolites and a diversion in glycoytic intermediates to serine metabolism occurs in cells expressing the M2 form of PK. It was revealed that these cells exhibited higher concentrations of phosphoenolpyruvate, 3-phosphoglycerate and serine compared to cells expressing the M1 isoform of PK. Since the former is the substrate of PK and the latter two are involved in serine synthesis, it was concluded that expression of the M2 isoform of PK causes both an accumulation of glycolytic intermediates and diverts them towards serine metabolism[57].

Table 1: Metabolomics approaches and the common analytical platforms used to gain experimental data. Adapted from Goodacre (2007)[5].

Metabolomic approach	Analytical platforms commonly used
Metabolic target analysis	• High performance liquid chromatography - HPLC • Gas chromatography – mass spectrometry - GC-MS • (Ultra (high) performance/pressure) liquid chromatography – mass spectrometry - (U(H)P)LC-MS
Metabolic profiling	• Gas chromatography – mass spectrometry - GC-MS • (Ultra (high) performance/pressure) liquid chromatography – mass spectrometry - (U(H)P)LC-MS • Hydrophobic interaction liquid chromatography (HILIC) • Capillary electrophoresis – mass spectrometry (CE-MS) • (Liquid chromatography–) nuclear magnetic resonance - (LC-)NMR • Direct infusion electrospray ionization – mass spectrometry (DIMS)
Metabolic flux analysis	• Nuclear magnetic resonance (NMR) • Gas chromatography – mass spectrometry (GC-MS) • (Ultra (high) performance/pressure) liquid chromatography – mass spectrometry - (U(H)P)LC-MS

Metabolic profiling is a widely used non-targeted approach in metabolomics. Its application spans from comprehensive studies of all detectable metabolites in biological samples to investigating the fate or effect of an exogenous metabolite on an entire system. Although it is not truly quantitative, it is useful for making relative comparisons between biological systems. The presence, absence or relative difference in concentration of the metabolites detected can be compared between experimental groups. These metabolites can be representative of the entire metabolic network and as such the metabolome-wide effects of an environmental or experimental perturbation can be tested. There are many examples of the analysis of *ex vivo* samples including tissue[58, 59] and biofluids[60-63] in mammalian systems. When considering *in vitro* metabolic profiling of mammalian cells, there are many more examples of intracellular fingerprinting rather than extracellular footprinting. There are advantages of footprinting, mainly with respect to the fact that less sample preparation is required so metabolism can be quenched at a faster rate giving a

more representative analysis or a 'snap shot' of metabolism[64]. However, there is a limit to what metabolites will be present in the footprint. Urine for example is largely composed of waste products that are difficult to connect with biological function. It is clearly advantageous to profile extracellular fluids *ex vivo* since sample retrieval is less invasive and more readily available; however for *in vitro* studies profiling the intracellular fingerprint may be more useful in determining properties of biological function. For this reason the metabolic profiling experiments in this research have been based on *in vitro* intracellular fingerprinting, for which there have been several successful protocols developed[65, 66].

Metabolic flux analysis is the method of recording the rate of movement of atoms usually carbon or nitrogen through metabolism that can highlight biological function in a system. For example, cells can be fed labelled metabolites (e.g. ^{13}C glucose) and the fate of ^{13}C atoms can be traced over time to reveal which metabolic pathways are being employed under the environmental conditions being tested. One of the most recent examples of the use of metabolic flux analysis in cancer research came from the Gottlieb laboratory in the Beatson Institute for Cancer Research, Glasgow. Metabolic flux analysis using ^{13}C glucose and ^{13}C glutamine was employed to determine the effects of a fumarate hydratase (FH) knockout on the carbon supply to the TCA cycle in a modified kidney mouse cell model[67]. FH is an enzyme of the TCA cycle that is mutated in patients with hereditary leiomyomatosis and renal-cell cancer and causes fumarate accumulation that appears to activate HIFs and promote cell survival despite a dysfunctional TCA cycle[68, 69]. Tracing the fate of ^{13}C allowed the identification of a key pathway involved in cells with the FH knockout. It was subsequently shown that targeting this pathway provides a new target for treatment in patients with hereditary leiomyomatosis and renal-cell cancer[67].

1.4.2. Chromatography coupled mass spectrometry in metabolomics

Mass spectrometry (MS) is a widely accepted technique used for the detection and quantification of analytes such as metabolites or proteins. This well developed analytical platform is used across many scientific disciplines to measure the mass-to-charge (*m/z*) ratio of elemental and molecular species[47]. There has been much technological advancement in the field that has allowed rapid progression of mass spectrometry for use in the 'omics'. For example, improvements in sensitivity, mass accuracy and speed make it appropriate for high-throughput analyses of biological samples.

The workflow for MS, involves four main operations[47]amples are first introduced at atmospheric pressure. Mechanical pumps can be employed in conjunction with cryogenic, turbomolecular or diffusion pumps to provide a low pressure high vacuum environment for ionisation of the sample at the source[70]. For other types of ionisation that occurs under atmospheric conditions (*e.g.* electrospray ionisation), these pumping systems are employed during ion focusing. Ions are subsequently separated on a space or time continuum based on their *m/z* ratio by the mass analyser. Ions are finally detected either physically or as orbital frequencies and the signal is transmitted to a computer for processing[47, 70]. A schematic of the mass spectrometry operation is shown in Figure 7.

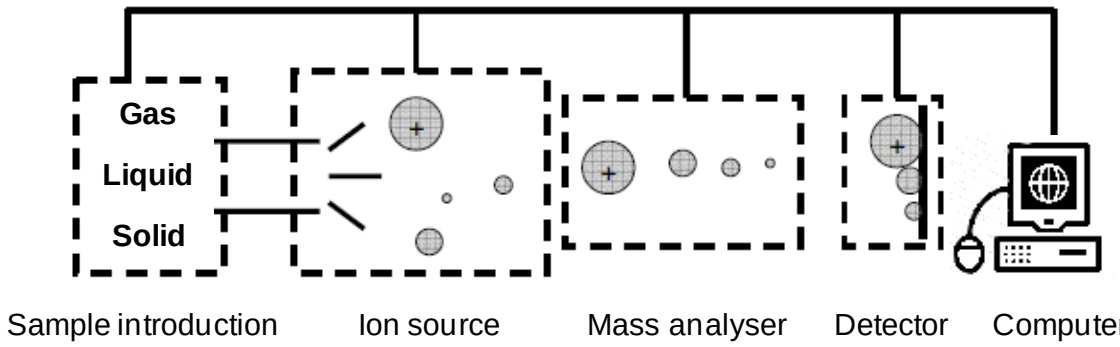

Figure 7: Workflow for mass spectrometry (MS) adapted from Dunn (2008)[47]. The sample is first introduced, then ionised by the source. Ions of positive or negative charge are created and subsequently separated according to their mass-to-charge ratio (*m/z*) in the mass analyser. Finally, ions are detected and the signals are processed using a computer.

Two MS platforms extensively used in metabolomics and chosen here for metabolic profiling of cancer metabolism with respect to HIF-1 are GC-MS and UHPLC-MS. Both are chromatography coupled platforms where metabolites are separated prior to mass spectrometric analysis to aid their detection.

Gas chromatography allows the separation of volatile and thermally stable metabolites[63]. To increase the number of metabolites meeting these requirements, chemical derivatisation can be employed. This involves altering the ionisation characteristics of chemical functional groups and aids in their chromatographic separation on a column of low polarity[71]. In this way it allows the detection of a wider range of chemicals and it is possible to analyse volatile and semi-volatile compounds in a single experiment. The ion source typically employed in GC-MS is electron ionisation (EI). This source is optimal for ionising many gas-phase molecules, causes extensive fragmentation, but is used to provide structural information that enable identification of unknown analytes[70].

Liquid chromatography, and in particular liquid chromatography operated using ultra high performance, is suited to the analysis of chemicals of higher polarity and lower volatility to those analysed by GC-MS[71]. While many metabolic profiling studies involving GC-MS utilise time-of-flight (ToF) mass analysers, metabolic profiling by (U(H)P)LC-MS involves a wider range of mass analysers including ToF[72], QToF[73] and LTQ-Orbitrap[74]. The latter was selected for UHPLC-MS analysis in this research since it is ideally suited to high-throughput analysis (capable of generating 1 spectrum per s), with nominal mass resolving power up to 60 000 and high accuracy mass measurements below 5 ppm[75]. The ion source typically employed in (U(H)P)LC-MS is electrospray ionisation (ESI). This source is sensitive to concentration, but is useful in the high sensitivity identification of a wide range of chemical species from proteins to small polar metabolites[70]. Utilising liquid chromatography in a metabolic profiling analytical platform is highly applicable for the analysis of lipids. There are clinical requirements for the analysis of lipids including cholesterol and triglycerides in blood plasma and it has been shown that LC-MS is ideal for the broad-range profiling of the lipidome in mammals[72].

There are many examples of metabolic profiling using GC-MS and/or (U(H)P)LC-MS in the literature and many are associated with the characterisation of colon cancer[73, 76-78]. Although many of these examples have involved the analysis of *ex vivo* bio-fluids, they have highlighted the effectiveness of studying colon carcinoma by metabolic profiling which supports its application in the present research. The combination of GC-MS and UPLC-MS has been employed previously in metabolic profiling of human colorectal cancer. For example, they were utilised in the metabolic analysis of serum from 64 colorectal cancer patients and 65 control subjects to test the hypothesis that bio-fluids contain relevant biomarkers of tumour malignancy to assess the relevance of metabolic profiling of biofluids[78]. Using both analytical platforms, metabolites were identified to be statistically significantly different between the test and control groups. Of these, pyruvate, lactate, tryptophan, tyrosine and uridine were analysed by both analytical techniques, where pyruvate and lactate were significantly increased while tryptophan, tyrosine and uridine were decreased in the cancer patients[78]. From the study it was concluded that the combination of these analytical platforms was useful in the characterisation of colon cancer metabolism to broaden the range of metabolites that could be detected and to increase the confidence of conclusion determined for metabolites detected using both techniques[78].

1.5. Time-of-flight secondary ion imaging mass spectrometry

Imaging plays a vital role in cancer research and allows improvement of cancer diagnostics and prognostics based on spatially localising molecular features. For example, one of the most successful applications in current cancer diagnostics is PET scanning. Imaging with ^{18}F deoxyglucose allows the detection of metabolic abnormalities common to neoplastic cells in a range of tumorous tissues[27]. This is an advancement in cancer diagnostics offering the capability of distinguishing benign and malignant tumours and pre- or post-therapeutic anatomical alterations[27]. Advancements have also been made in the use of magnetic resonance imaging (MRI). For example, a recent publication has explored the utilisation of susceptibility contrast MRI as a non-invasive technique for quantification of vessel size *in vivo*[79]. This technique highlighted the potential to image changes in vascular morphology following anti-vascular therapies *in situ*.

Imaging mass spectrometry (IMS) is an up and coming field in disease biology that is less well established than methods such as MRI or PET. However, it has been continually developed and extensively applied in other fields for many years. IMS is a label free approach offering the potential to identify biological elements *in situ*. It bridges the gap between the application of non-imaging mass spectrometry (including GC- and LC-MS) and other imaging techniques and therefore is particularly applicable to the present research. Time-of-flight - secondary ion mass spectrometry (ToF-SIMS) is just one method in IMS. Other established techniques include matrix assisted laser desorption ionisation (MALDI)[80], desorption electrospray ionisation (DESI)[81] and direct analysis in real time (DART)[82].

There are many advantages of IMS in biological and biomedical analysis. The main is the use of endogenous biomolecules as labels rather than fluorescent or antibody labels that can interfere with biological functions including post-translational modifications[83]. The localisation and co-localisation of biomolecules in a tissue or cell can be observed as the sample remains undisrupted and resembling biological structure in comparison to traditional mass spectrometric techniques which require the biomolecules of interest to be extracted. Additionally, with some mass spectrometric imagers it is possible to study frozen samples, for example from the addition of a cold stage and freeze fracture facilities in ToF-SIMS[84]. This retains the sample structure further as no fixing or extreme vacuum drying has occurred which may have altered the anatomy of tissue or cell samples.

Information that can be obtained from IMS of a biological surface is complex with respect to other MS as for every pixel imaged a full spectra can be produced. Likewise considering the intensity of peak(s) of interest across an entire image can reveal its localisation that can be related to its structure and even perhaps its function. Although it is relatively pioneering in biological and biomedical analyses, IMS may have future potential in providing the molecular insight necessary to better understand the morphology and molecular pathology of the diseases [83].

ToF-SIMS and MALDI are both great contenders in IMS and in some examples they have been used sequentially to benefit from the advantages of each[85]. Since its introduction in 1988[86], MALDI has been particularly successful in imaging peptides and proteins[80, 87] as well as lipids[88, 89] and drugs[90] in biological samples. The choice of matrix is dependent on the sample and the desired class of compound to be detected[91]. For example sinapinic acid is particularly applicable to the detection of proteins[92], whereas smaller molecules including peptides lipids and drugs are best detected using 2,5-dihydrobenzoic acid or cyano-4-hydroxycinnamic acid[93]. Perhaps the most impressive MALDI MS experiment to date is the protein analysis of a whole rat body[94]. Using a mixed matrix of sinapinic acid and 2,5-dihydrobenzoic acid, it was possible to localise specific proteins in the different tissues within the whole body section including the brain, thymus, liver, kidney cortex and testis. A second related investigation involved dosing the rat with olanzapine and localising the drug and related fragments within the body[94]. Both were highly successful experiments.

ToF-SIMS involves a surface irradiation by primary particles (electrons, ions or neutrals) to emit secondary particles (electrons, neutrals, atomic ions and cluster ions) to be detected by mass spectrometry[70, 95]. A high energy beam of primary particles bombards the sample surface at high energy (10 – 40 keV), transferring energy to the atoms on the surface in a cascade of collisions, some of which are emitted from the surface and ionised[95]. Common primary particles are atomic ions (including Ar^+, Cs^+, Ga^+, In^+) or cluster ions (including Au_n^+, Bi_n^+ SF_5^+ C_{60}^+).

Amongst the earliest examples of ToF-SIMS imaging using liquid metal ion guns was in the analysis of (phospho)lipids to investigate membrane changes associated with mating in *Tetrahymena* using In^+[96]. Despite the early success of ToF-SIMS using atomic primary ion bombardment, the primary particles must be operated below the static limit and hence less

than 1 % of the surface can be analysed non-destructively. Static SIMS, first introduced by Benninghoven in 1967[97] requires a primary ion dose not exceeding 10^{13} ions/cm^2. The advancement of cluster ion beams was undertaken to improve secondary ion yield and take analyses beyond the static limit. For example cluster primary ions such as SF_5^+ allow the detection of higher mass molecules but without causing chemical damage[98]. This was extended to the development of other cluster ions and polyatomics such as Au_3^{+}[99], Bi_3^{+}[100] and C_{60}^{+}[101]. The latter has enabled the development of *3D* ToF-SIMS or depth profiling beyond the surface[102]. Although ToF-SIMS requires no labelling and is not dependent on enhancement by matrices as in MALDI MS, there have been examples of surface modification to extend the mass range ToF-SIMS is able to cover[103].

Conventional ToF-SIMS instruments require short pulses of primary ions (~1 ns) across an aperture to optimise mass resolution and the compression or rapid movement of the primary ion beam to do so make maintaining a small spot size needed for good spatial resolution exceptionally difficult[104]. Additionally, pulsing significantly reduces the time in which a sample is bombarded making imaging a lengthy process, which can only be relieved by separating periods of analysis with periods of sputtering which in itself causes loss or damage to the sample surface[104]. Therefore, new instruments were developed that enable the use of direct current polyatomic ion beams which separate the sputtering process from the mass spectrometry process while enabling sputtered material to be available for analysis. These include the hybrid quadrupole orthogonal ToF mass spectrometer developed in the Winograd laboratory in Penn State, USA[105] and the J105 *3D Chemical Imager* developed in the Vickerman laboratory in Manchester, UK[106]. Both systems decouple the process of secondary ion generation from generating the mass spectrum such that primary ion conditions and topography no longer influence resolution and have each shown successful applications of the use of C_{60}^+ primary ion beams for biological analysis; however ToF-SIMS imaging with the Winograd instrument is limited by the inability for the primary ion beam to be rastered and the secondary ion transit time since the beam can only be moved to the next pixel once all secondary ions from the previous pixel have been detected[104]. The J105 *3D Chemical Imager* overcomes all of these issues in addition to it having the ability to image biological samples in *2D* and *3D* with a mass resolution $m/\Delta m \approx 10\ 000$ at mass 500 and a mass accuracy of 5 ppm[104]. It was therefore considered the optimal instrument to explore the potential of ToF-SIMS in metabolite analysis through utilising its high mass resolution in generating a reproducible

standards library for metabolite entries as well as its excellent spatial resolution for imaging metabolites in biological samples.

There have been many good examples of the application of ToF-SIMS in biological and biomedical research particularly that highlights its potential in metabolite analysis. Numerous studies have been involved in the characterisation of membrane lipids[107-109] which is probably the most popular application of ToF-SIMS in biological analyses. In a human pathology example, the accumulation of vitamin E was shown for the first time in tissue biopsies from Fabry disease patients along with the localisation of cholesterol sulphate; a potential biomarker for the disease[110]. Vitamin E along with other FAs have also been imaged in single cells including *Aplysia californica* neuronal cells[111], rodent leukemia cells[112] and human benign prostatic hyperplasia cells[106] to name a few.

The most recent bio-application of ToF-SIMS utilised the J105 *3D Chemical imager* in depth profiling. For example, the first investigation was of *Xenopus laevis* oocytes[113]. In this experiment a freeze-dried oocyte was analysed and the differential spatial distribution of cholesterol and phosphocholines with FA side chains were highlighted across a *3D* plane. A further example was in the *3D* localisation of lipids in rodent brain representative of grey and white matter regions[114].

The application of ToF-SIMS in biological and biomedical analyses is growing exponentially, particularly in the field of lipid analysis. Its success in disease characterisation has also been highlighted. It is clear that the technique meets the requirements for the analysis of metabolites, an application that will be explored in this thesis.

1.6. Research aims and methodologies employed

It is known that induction of HIF-1 activity results in the coordinated up-regulation of a large number of proteins that facilitate cell survival in an oxygen compromised environment. What is less well known is the effect of HIF-1 on cancer cell metabolism. The aim of this research was to apply a systems biology approach to investigate the effect of HIF-1 on the metabolome of cancer cells in order to elucidate functional information about the system.

The main focus lies in determining the effect hypoxia has on the phenotype of cancer cells, particularly their metabolome, and how HIF-1 behaves in the system to strengthen or counteract the observed effects. Two cell based models were used: a mouse hepatocellular carcinoma cell line including wild type and HIF-1β knockout varieties (Hepa-1 WT and Hepa-1 C4 respectively); and a human colon carcinoma cell line including wild type and a dominant negative HIF-1α - expressing form (HCT-116 WT and HCT-116 DN). The latter is based on insertion of a vector encoding a HIF-1α fragment that acts as a dominant negative inhibitor of HIF-1. The vector also promotes puromycin resistance enabling cells containing the vector to be selected through culture in puromycin-containing medium. An empty vector form containing only the puromycin resistance factor as a control was also used (HCT-116 EV).

Metabolic profiling is the main theme in the research presented. This 'top-down' approach utilises state-of-the-art technologies for high-throughput analyses of biological samples. The analyses have been exploratory with the aim of revealing areas of metabolism not previously linked with hypoxia and HIF-1. Initial experiments were undertaken to characterise both HEPA-1 and HCT 116 cell models and to optimise conditions for metabolic profiling. This also included analysis of glucose, lactate and glutamine fluxes in all cell lines since these features have been linked to HIF-1 and hypoxia in the literature. Both models have been studied *in vitro* through metabolic profiling analysis by GC-MS. The aim of this was to elucidate unknown functions of HIF-1 with respect to the phenotype and function of tumour cells that are known to survive and often thrive in low oxygen environments. Cells were cultured under varying oxygen levels and the effect of hypoxia with and without functional HIF-1 was compared.

For the HCT 116 model, metabolic profiling experiments were extended to utilise UHPLC-MS and ToF-SIMS. UHPLC-MS was selected as a complementary technique to GC-MS for profiling of different metabolites and ToF-SIMS was selected as a method for IMS that is ideally suited to the detection of metabolites *in situ.* Since the study of metabolites in biological samples is pioneering in the field of ToF-SIMS, many experiments have been undertaken to explore the potential for this technique to play a key role in the analysis of metabolites. For example, the limits of detection for metabolites in samples and the ionisation of metabolites have been explored in addition to the contribution to a new ToF-SIMS metabolite standard library. The main biological samples analysed by ToF-SIMS were multicellular tumour spheroids (MTSs) cultured from both

HCT 116 WT and DN cells to compare the metabolic effect of HIF-1 *in situ*. A systems biology approach involves the use of models to study the system of interest. Commonly these are computational simulations of biological processes; however they can be experimental models studied *in vitro*. In this case MTSs were investigated as models of small initiating tumours allowing exploration of the effect of HIF-1 on tumour function as an intermediate step bridging the gap between *in vitro* and *in vivo*.

The final systems biology approach employed to characterise HIF-1 metabolism in cancer was the use of network-based correlation analysis of metabolites detected by GC-MS in the HCT 116 cells. This was done to consider metabolism beyond the first dimension of revealing individual metabolites. Metabolites found to be differently correlated as a result of HIF-1 were mapped onto a human metabolic network to study the systems properties of the correlations. Sub-networks of differently correlated metabolites have been drawn to reveal new pathways and metabolic hubs not previously linked with cancer metabolism, hypoxia and HIF-1.

Chapter 2. Materials and methods

For all experiments, Phosphate Buffered Saline (PBS) was purchased from Oxoid (Hampshire, UK) in tablet form. This was used in making a sterile solution as directed in the manufacturer's guidelines. The medium used in cell culture and associated experiments was RPMI medium1640 (unless otherwise stated in the method of a particular experiment). Medium, L-glutamine used to supplement the medium and 10 × 0.5% (v/v) trypsin-ethylenediaminetetraacetic acid (EDTA) were supplied by Gibco BRL (Paisley, UK). Foetal calf serum (FCS) used to supplement the medium was purchased from Labtech International (East Sussex, UK). Dimethyl sulphoxide (DMSO) was obtained from Fisher (Leicestershire, UK). All other reagents were of analytical grade and were purchased from Sigma-Aldrich (Dorset, UK) unless otherwise stated. All tissue culture flasks and dishes were supplied by Falcon (Runcorn, UK). Cryotubes were supplied by Cellstar, Greiner Bio-one (Gloucestershire, UK) and eppendorf tubes were purchased from Fisher Scientific (Loughborough, UK). All gas was supplied by BOC (Manchester, UK).

2.1. Routine methods

2.1.1. Cell lines and routine cell culture

HEPA-1 WT, HEPA-1 HIF-1β-deficient C4, WT HCT116, HIF-1α-dominant negative expressing HCT116 DN and empty vector (EV) HCT116 EV cells were obtained from in house cell stocks and have been described previously[115, 116]. Cell lines were routinely checked that they were not contaminated with mycoplasma. Both cell lines were cultured in T75 (with an area of 75 cm^2), or T175 (with an area of 175 cm^2) tissue culture flasks containing 12 ml or 20 ml of medium respectively. The medium consisted of 85 % RPM1 1640 medium, 10 % foetal calf serum (FCS) and 5 % (2 mM) glutamine. All media used in cell culture and experiments was pre-warmed before use. Cells were sub-cultivated (passaged) approximately every three days to maintain a confluency of 80 %. This involved washing with sterile PBS followed by inducing detachment by adding 2 ml 1 × trypsin-EDTA (Trypsin and 0.53 mM EDTA in sterile PBS) and incubating until the cells detached. A fresh tissue culture flask containing complete medium as described above was then prepared, into which a portion of detached cells re-suspended in complete

medium was added. Between passages and experiments, cells were incubated in 95 % air and 5 % CO_2 at 37 ºC and 95 % relative humidity.

2.1.2. Freezing cell stocks

Cells cultured to approximately 80 % confluence were washed in sterile PBS and detached using trypsin-EDTA. Detached cells were then re-suspended in 5 ml medium and centrifuged (Centaur-2, SANYO, USA) at 212 × g for 5 min. The supernatant was removed following centrifugation and the remaining pellet was re-suspended in freezing medium consisting of 50 % medium, 40 % FCS and 10 % DMSO. 1 ml aliquots containing approximately 1-5 × 10^6 cells were frozen in cryotubes which were then insulated before being submitted to -80ºC. The purpose of this was to allow cells to freeze slowly such that cell death or damage was minimised. Long term storage of cells involved transfer to liquid nitrogen (-196ºC) following storage at -80ºC for at least 24 h.

2.1.3. Culture from frozen stocks

Cells were removed from liquid nitrogen and defrosted by incubation at 37 ºC. The defrosted cell suspension was then added to 10 ml of medium and centrifuged at 212 × g for 5 min. Following this, the supernatant was aspirated to remove the freezing medium and the pellet was re-suspended in 5 ml growth medium. This was added to a T75 flask containing 12 ml medium and the flask of cells was incubated until conditions for passage were reached. The medium was changed every 48 h until this time. All cells were maintained for several passages before being used in experiments, ensuring full recovery from freezing.

2.1.4. Cell counting

A suspension of cells to be counted was obtained by washing, detaching cells using trypsin-EDTA and re-suspending in fresh medium as described for passaging. From this suspension 13 µl aliquots were taken for counting. A haemocytometer was set up with a coverslip over the central grid, between which the cell suspension was inserted and dispersed over the grid by capillary action. The haemocytometer was then placed under a light microscope and the number of cells in a 5 × 5 square (containing 0.1 mm^3 cell

suspension) were counted. The count was then multiplied by 10,000 to give the total number of cells per ml (1000mm^3). This was repeated three times at two levels: for 5 × 5 squares over which an average was taken and for aliquots of cell suspension over which an average was taken. Remaining cell suspension was either left to re-adhere to the flask or passaged as required.

2.1.5. Culturing of multicellular tumour spheroids

A high throughput method for the culturing of MTSs was designed in house and used to generate MTSs of HCT-116 WT, DN and EV cells. This method involved seeding approximately 30 × 10^5 cells in 30 ml medium in a T75 flask. Flasks were placed culture side up onto a microtiter plate shaker (Bibby Scientific LTD, Staffordshire UK) within an incubator. Flasks were shaken constantly for 3 weeks which was shown to be the optimum time for MTS production in these cells such that MTSs reached a reasonable size for sectioning and contained a necrotic core. After 3 weeks incubation, MTSs were washed in PBS set directly into 1.5 % gelatine heated to 60 °C that were then immediately snap frozen in liquid nitrogen and stored at -80 °C for sectioning. Using MTSs offers an advantage over studying only monolayer *in vitro* systems since they provide more representative models of tumours.

2.1.6. Oxygen conditions

Three experimental oxygen treatments were used and are described as ‘normoxia’, ‘hypoxia’ and ‘anoxia’, defined as 21 %, 1 % and 0 % oxygen pre-mixed with nitrogen in cylinders respectively. An additional oxygen condition containing 5 % oxygen was used in preliminary investigations. All other incubation parameters were the same as for general cell culture described above and unless otherwise stated, exponential phase cells were used in experiments. The hypoxic condition was achieved using continuous gassing over samples in a sealed chamber within an incubator comparable to that described for the normoxic condition. A photograph of the chamber is shown in Figure 8. This chamber was developed in house using a 5 L ADDIS® airtight container into which 6 mm polytube tubing was connected with a male BSPT-female BSPP reducer and a male parallel straight adaptor in two opposite side panels of the box. To ensure unidirectional flow of gas, a 6 mm 2/2 finger valve with grey tap was connected to each end of tubing that allowed

forward flow of gas when open and could be closed off to prevent any gas flow (re-oxygenation) once the desired gas had been disconnected (all components purchased from RS components LTD, Stockport, U.K.). The box was able to be attached to any desired gas cylinder and multiple boxes could be connected with polytube tubing and correct fitting of taps between boxes to ensure unidirectional flow throughout the whole system. The anoxic condition was achieved using a gloved chamber (Bactron anaerobic chamber, Sheldon Manufacturing, Cornelius, Oregon, USA) in which all parameters other than oxygen were comparable to the other two conditions and all necessary sample preparation and incubation was done in this system. Residual oxygen was removed by flowing supply gas over a palladium catalyst. Cell harvesting in each experiment was conducted in normoxia (for normoxic samples) and in anoxia for hypoxic or anoxic samples whereby the gas taps were locked on the hypoxia chamber after the removal of the hypoxic gas inlet to prevent re-oxygenation of hypoxic samples.

Figure 8: Photograph of the hypoxia chamber. Culture dishes are placed inside the sealed chamber through which hypoxic gas is flowed in one direction controlled by the tap valves.

2.2. Growth curves

Cells in exponential phase were plated in 5 cm diameter cell culture dishes each containing a 10 ml suspension of 5×10^4 cells in fresh medium. A total of ten plates for each cell line were set up to include duplicates for cell counts at 24, 48, 72, 96 and 168 h. Cell counts were taken and averaged over the two plates for each cell line at each indicated time. This was repeated for time points of 72, 96, 120, 144, and 168 h so that together lag phase, exponential phase and plateau phase are represented.

From this data the growth rate and doubling time for each cell line were calculated using the following equations:

$$Y = Y_0 \cdot \exp^{KX}$$

Equation 1: Growth rate assuming constant doubling time where Y_0 denotes the growth rate Y at time zero and K denotes the rate constant.

$$T_d = \frac{\ln(2)}{K}$$

Equation 2: Doubling time of cells (T_d) where K denotes the rate constant.

2.3. MTT assay for the analysis of cell proliferation

A 3-(4,5-Dimethylthiazol-2-yl)-2,5-diphenyltetrazolium bromide (MTT) assay was used to assess proliferation of cells after certain treatments. This method described in Mossman (1983)[117] and below involves a tetrazolium salt in a quantitative colorimetric assay that detects living cells where the signal is relative to mitochondrial enzyme function in the cells[117].

Each cell line was prepared to contain a suspension of 25 000 cells per ml medium which was plated into 6 experimental wells of a 96-well plate per cell line (equivalent to 5000 cells per well). All experimental wells were surrounded by wells containing 200 µl of medium to alleviate dehydration of experimental wells in the incubators and to keep the environmental effects constant between wells. All plates of cells were incubated in normoxia for 24 h then subjected to their treatment (oxygen condition) for a further 24 h. After treatment, plates were either analysed immediately or analysed after a 120 h incubation period in the normoxic condition. The analysis consisted of removing the medium from all wells and replenishing experimental wells with a 200 µl solution of MTT (2.5 mg/ml suspended in PBS) and medium in a ratio of 1:10. Plates were then incubated in normoxia for 4 h, after which the MTT medium solution was removed and all experimental wells plus a line of 6 wells parallel to the experimental wells were replenished with 100 µl DMSO. Plates were shaken (Titramax 1000, Heidolph, Germany) for 5 min and analysed using a microtiter plate reader (BioTek, Vermont, USA) reading at 562nm with Gen5 software. The wells containing only DMSO were used to give control values for readings for plastic and DMSO which were then used as a blank to be taken away from experimental values.

2.4. Luciferase assay for analysing expression of HIF-1

An assessment of HIF-1 proficiency was undertaken prior to subsequent experiments as described in Burrows *et al.* (2010)[118] and below. Two 96-well plates were prepared containing 6000 cells per 200 µl for each cell line in triplicate. All experimental wells were surrounded by wells containing 200 µl medium. Both plates were incubated for 24 h under normoxic conditions. After incubation, all experimental medium was removed and replaced with medium containing HRE luciferase adenovirus at a multiplicity of infection equivalent to 20 viral particles per cell. This adenovirus contains a firefly luciferase reporter construct that is linked to the lactate dehydrogenase HRE sequence as described by Cowen *et al.* (2004)[119]. All reagents were supplied by Promega (Promega corp., Madison, USA) and the analysis was performed in accordance with the manufacturer's guidelines. The plates were then incubated under normoxic conditions for a further 5 h with the virus, after which one plate was transferred to the anoxic condition and both plates were incubated in their conditions for 24 h. Following treatment, all medium was removed from plates and cells were washed twice with ice cold PBS and 50 µl of passive lysis buffer (PLB) solution (1 part PLB in 4 parts distilled water) was added to each experimental well before both plates were shaken in the dark for 15 min. A preset protocol for firefly luciferase on Optima software was used with luciferase assay substrate to measure the luminescence of each well using a MicroLumant LB 96 lumiometer (EG & G Berthold Technologies, Harpenden, U.K.). The degree of luminescence in this case is relative to the expression of HIF-1.

2.5. Optimising seeding density for use in all subsequent experiments

An initial experiment was undertaken to determine the optimal seeding density for maximum biomass that does not compromise the condition of the cells. Cells were seeded at 25 000, 50 000, 100 000, 150 000, 200 000 and 400 000 cells per ml. Duplicate samples were plated for both cell lines at each density in a 6-well plate format. The volume of medium was kept constant at 1.5 ml per sample. Once seeded, all samples were incubated under normoxic conditions for 24 h before being transferred to the appropriate oxygen condition for a further 24 h. After this time medium was removed and cells were washed with PBS. The cells from each well were then collected into pre-weighed eppendorf tubes and the contents lyophilised to form the sample into a dry pellet of cells. The dry biomass

was measured by weighing each tube and subtracting the weight of the eppendorf tube from it, and an average was taken across duplicates.

To assess the effect of hypoxia and anoxia on biomass using this seeding density, growth tests were undertaken This involved plating triplicate replicates for each cell line in each of the three oxygen treatments (normoxia: 21 %, hypoxia: 1 % and anoxia 0 %) in a 6-well plate format. Each well consisted of 1.5×10^5 cells suspended in 1.5ml fresh medium. The samples were incubated in normoxia for 24 h then transferred to the oxygen treatment for a further 24 h. After this time, all samples were removed and cell counts were conducted as described in 2.1.4 for each well to provide an average final cell count expressed as cells/ml for each cell line under each treatment.

2.6. Optimising growth medium for use in all subsequent experiments

Various experiments were undertaken to simplify the medium used in metabolic profiling experiments. The first involved removing glutamine while keeping all other medium constituents constant. Growth tests were undertaken using the latter protocol to test the effect of removing glutamine on the final biomass to assess its appropriateness for metabolic profiling experiments. In addition, an MTT assay, as described in section 2.3, was undertaken to assess the effect of removing glutamine from the medium on cell proliferation. All samples were analysed immediately after the assay and after 120 h incubation in normoxia.

With the aim of testing the effect of reducing the medium further on cell growth, growth curves were obtained using the protocol described in 2.2 for both cell lines cultured in various media. The constituents of each medium are shown in Table 2.

Table 2: Constituents and the percent they represent in the total medium used to culture WT and C4 cells for growth curve analysis.

Medium	Constituents	Percent of total medium
1 (Control)	RPMI 1640	89
	FCS	10
	L-glutamine (0.2M)	1
2	MEM (with Earle's salts)	89
	FCS	10
	L-glutamine (0.2M)	1
3	MEM(with Earle's salts)	89
	FCS	10
	Ammonium Sulphate (0.2M)	1
4	PBS	80
	FCS	10
	L-glutamine (0.2M)	6
	Glucose (0.12M)	4
5	PBS	80
	FCS	10
	Ammonium Sulphate (0.2M)	6
	Glucose (0.12M)	4

2.7. Cell cycle analysis using flow cytometry

2.7.7. Propidium iodide staining

Following incubation under normoxia and experimental oxygen condition (normoxia, hypoxia or anoxia) as described for previous experiments, medium was decanted and cells were washed in 3 × 3 ml PBS and fixed in 70 % ethanol in dH_2O for 1 h. Propidium iodide was used to stain the DNA of cells where the quantity of stain taken up is related to the cells stage in the cell cycle. Propidium iodide is excited by blue light and detected at a wavelength of 488 nm. To prepare cells for propidium iodide staining cells were washed in PBS containing 1 % BSA and 5×10^5 cells were re-suspended in staining buffer composed of 0.1 % Triton X 100 in PBS containing 50 µg/ml propidium iodide and 50 µg/ml ribonuclease A. Cells were incubated in 1 ml staining buffer for 20 min in the dark at room temperature and analysed immediately after.

2.7.8. Data acquisition

Each sample was prepared by diluting 2 µl of sample in 1 ml of PBS and each was analysed using a CyFlow® Space flow cytometry system (Partec) coupled to a computer with flow max software version 2.7 (Quantum Analysis). The flow rate was set to 1 µl/s and forward and side scatter were measured using a 488 nm laser. Fluorescence was

measured using the FL6 filter (excitation: 485/20, emission: 610/20). The gain was kept constant throughout at 350 which was optimised so that cells formed a cluster towards the middle of the plot of forward and side scatter at $\log^3$ scale. Data were collected by counting 10 000 events for each sample, after which, a gate was created using forward and side scatter parameters to ensure only events likely corresponding to cells (and not cellular debris) were included in the analysis. A further gate was applied to the data using the FL6 area and width parameters to ensure only events likely corresponding to single cells were included in analysis. These gates were saved and applied to all subsequent samples to ensure consistency in data analysis. Data were then re-run from file to count and collect data for an equal number of events within the two gates so that samples could be directly compared. Figure 9 shows an example of how each gate was applied to the raw data.

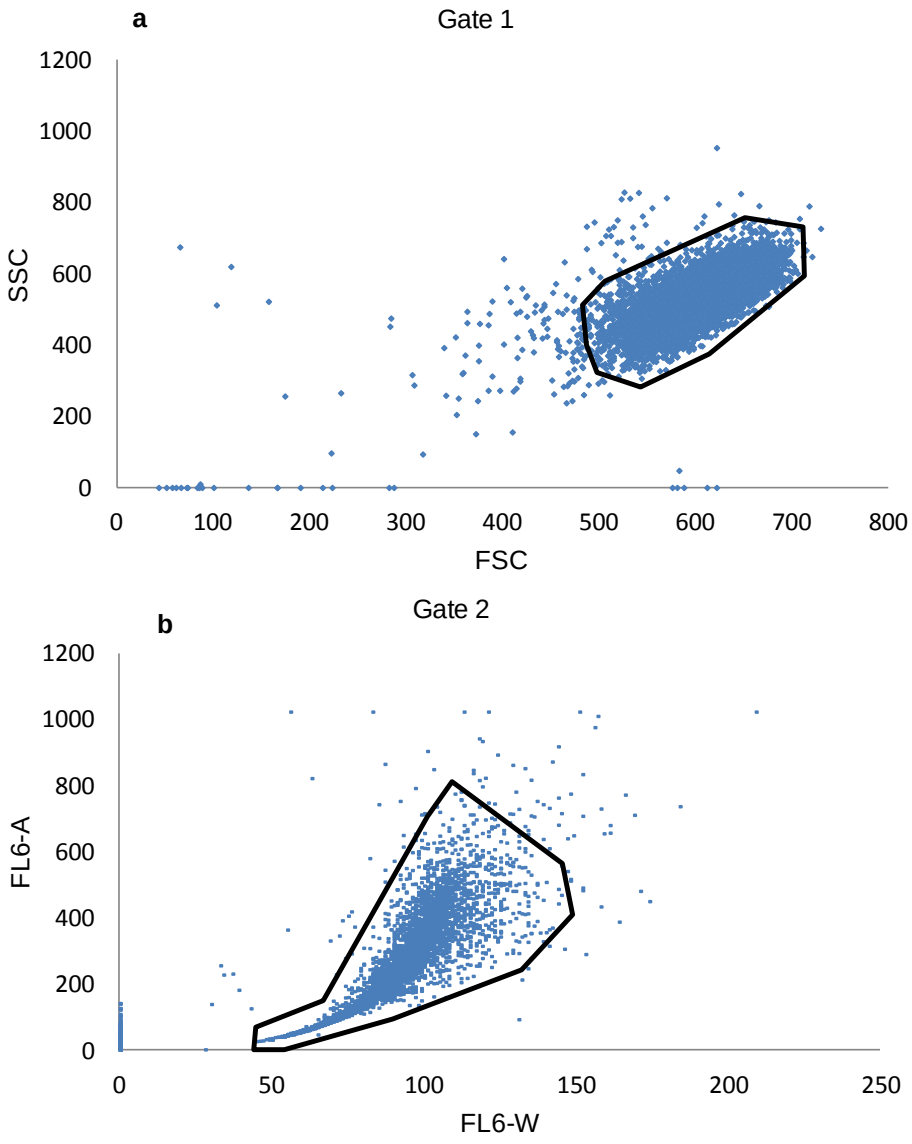

Figure 9: An example of how gate 1 (a) and gate 2 (b) were applied to the total data of 10 000 events detected in FL6. Gate 1 was used to select only events likely corresponding to cells and Gate 2 was used to further gate events in gate 1 that are likely corresponding to single cells.

2.7.9. Data analysis

Gated data were exported to '.txt' files and pasted into Microsoft Excel® (.xls) spreadsheets for analysis. For each sample, a histogram was plotted for counts *vs.* fluorescence, where peaks could be identified at approximately 200 and 400 fluorescence units for cells in gap phase 1 (G1) and gap phase 2/mitotic phase (G2/M) respectively. The percentage of the total number of cells in each phase: G1, G2 and DNA synthesis (S) phase was determined by calculating the number of cells in ½ G1 phase (from the start of the peak to the mean of the peak) and ½ G2 phase (from the mean of the peak to the end of the peak) and the total number of cells counted between the position of the means of these two peaks minus the number of cells calculated in ½ G1 and ½ G2 determined the number of cells in S phase. This is depicted in Figure 10. The percentage of the total number of cells was then calculated from counts for each phase, remembering to double the counts for G1 and G2 to obtain the value for the whole peak of each.

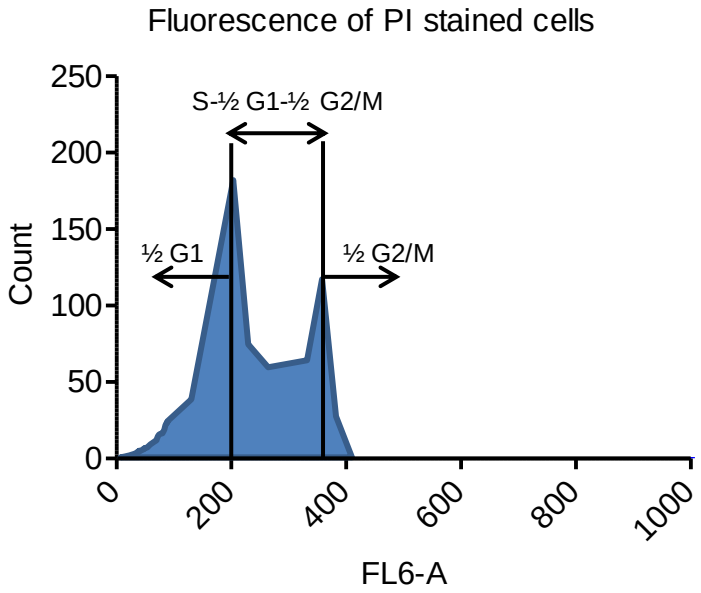

Figure 10: A schematic of how gap 1 (G1), DNA synthesis (S) and gap 2/mitotic (G2/M) phases were defined from the histogram of fluorescence in cells after staining with propidium iodide. ½ G1 and ½ G2/M were calculated from the count of cells from the peak mean to the peak edge and S phase was calculated from the count between the mean peak values minus ½ G1 and ½ G2/M.

2.8. Biochemical assays

All biochemical assays involved the testing of extracellular media. The concentration of glucose, glutamine and lactate was determined from a comparison to fresh medium where the same sample of extracellular medium was used for all 3 tests. 10 cm cell culture dishes were used in which 8×10^5 cells were seeded in 8 ml fresh medium. All samples were reproduced in triplicate. Blank media samples were prepared at the same time as cells were seeded and underwent the exact procedure so that any effect of oxygen on media irrespective of cells could be accounted for. All samples were incubated in normoxia for 24 h then transferred to normoxia or anoxia. An initial aliquot of 100 µl was taken at the start of exposure (0 min) then again at 60, 120, 180, 240, 300 and 360 min of exposure to either normoxia or anoxia. Aliquots were taken from the same vessel for each sample such that less than 10 % of the total volume of medium was removed during the course of the whole experiment. All extracellular extracts were centrifuged at 17000 × g for 10 min and the supernatant was collected for analysis. The cells were then washed in 3 × 1 ml PBS and scraped into eppendorf tubes and the dry mass was recorded for each sample after lyophilisation of the sample pellet (using HETO VR MAXI with RVT 4104 refrigerated vapour trap (Thermo Life Sciences, Basingstoke, UK)).

The uptake or efflux of each metabolite measured was done so by first identifying a period over which cells appeared to be in a steady state and there was a net concentration change of each metabolite (in this case the first 300 min). Then the concentration of the metabolite at 0 min was subtracted from 300 min and the value was converted to mM/gDw/h using the dry weights recorded for each sample.

2.8.1. Determining the concentration of uptake of glucose in cells

The glucose concentration of medium was measured using the glucose (HK) assay kit GAHK-20 (Sigma-Aldrich (Dorset, UK)) following the technical bulletin provided. The kit works by first phosphorylating glucose using ATP in the reaction catalysed by hexokinase then oxidising the product glucose-6-phosphate to 6-phosphogluconate in the presence of NAD catalysed by glucose-6-phosphate dehydrogenase. During this oxidation, NAD is reduced to NADH causing an increase in absorbance at 340 nm that is directionally proportional to glucose concentration[120].

Glucose standards were made from the D-glucose 1 mg/ml in 0.1 % benzoic acid in dH_2O at concentrations of 0, 0.005, 0.0125, 0.025, 0.05, 0.125, 0.25, 0.5 and 1 mg/ml. The hexokinase assay reagent was reconstituted in 20 ml dH_2O and 100 µl was combined with 20 µl of each standard in wells of a 96-well plate. Biological samples were diluted 5 µl in 15 µl dH_2O and 100 µl hexokinase assay reagent was combined with 20 µl of each sample in wells of the same plate. Each standard was plated 3 times and each biological replicate of samples was plated once. The plate was then incubated at 37 °C for 15 min and immediately read at 340 nm using a microtiter plate reader (BioTek, Vermont, USA). A calibration curve for glucose was calculated from the measurements of standards by averaging absorbance across the 3 replicates of standard, minus the 0 mg/ml standard with the hexokinase assay reagent alone. This resulted in a straight line regression that fitted the points closely. The gradient of the line was then used to calculate the concentration of glucose in each sample where the medium and hexokinase assay reagent blank was subtracted from each biological replicate and the concentration was adjusted to the correct value taking into account the dilution factor.

2.8.2. Determining the concentration of uptake of glutamine in cells

The glutamine concentration of medium was measured using the EnzyChrom™ glutamine assay kit EGLN-100 (BioAssay Systems (Hayward, CA USA)) following the technical bulletin provided. The kit works by employing glutaminase to catalyse the reaction from glutamine to glutamate plus ammonia followed by glutamate oxidase to catalyse the reaction from glutamate and O_2 to alpha-ketoglutarate, hydrogen peroxide and ammonia[121]. In the presence of hydrogen peroxide, MTT (also supplied) is reduced to form a purple coloured solution detectable at 565 nm. Since glutamate is also present in the samples, the concentration of glutamine must be calculated accounting for this. Therefore for every biological sample, a working blank is used where the proportion of the colour resulting from naturally occurring glutamate in samples is determined by adding only the glutamate oxidase.

Glutamine standards were made from the 100 mM glutamine standard provided by first diluting 5 µl in 245 µl dH_2O to obtain 2 mM glutamine which was used to make standards in dH_2O at concentrations of 0, 0.0125, 0.025, 0.05, 0.125, 0.25, 0.5, 1 and 2 mM. Sample reagent and working blank reagent were prepared from 65 µl assay buffer, 1 µl enzyme A, 1 µl enzyme B, 2.5 µl NAD and 14 µl MTT per sample for the sample reagent and 65 µl

assay buffer, 1 µl enzyme B, 2.5 µl NAD and 14 µl MTT per blank for the working blank reagent. The working blank reagent was necessary to subtract the concentration of glutamate from the total concentration of glutamine and glutamate for every sample. 20 µl of each standard was plated in triplicate and 20 µl of each sample diluted 5 µl in 15 µl dH_2O was plated in a 96-well plate to which 80 µl sample reagent was added. This was then repeated and 80 µl working blank reagent was added instead. The plate was briefly shaken to mix and incubated at room temperature for 40 min before 100 µl stock reagent was added to each well and the plate was read at 565 nm using a microtiter plate reader (BioTek, Vermont, USA). The absorbance from working blank reagent samples was first subtracted from the corresponding samples to account for glutamate. A calibration curve for glutamine was calculated from the measurements of standards by averaging absorbance across the 3 replicates of standard, minus the 0 mM standard with sample reagent alone. This resulted in a straight line regression that fitted the points closely. The gradient of the line was then used to calculate the concentration of glutamine in each sample where the medium and sample reagent blank was subtracted from each biological replicate and the concentration was adjusted to the correct value taking into account the dilution factor.

2.8.3. Determining the concentration of efflux of lactate in cells

The lactate concentration of medium was measured using the Lactate assay kit 735 (Trinity biotech, Wicklow, Ireland) following the technical bulletin provided. The kit works by converting lactate to pyruvate and hydrogen peroxide catalysed by lactate oxidase. Subsequently peroxidise catalyses the oxidative condensation of chromogen precursors in the presence of hydrogen peroxide to a couloured dye whose absorbance at 540 nm is directionally proportional to lactate concentration[122].

Lactate standards were made at concentrations of 0, 0.0234, 0.0469, 0.0938, 0.1875, 0.375, 0.75, 1.5 and 3 mg/ml. 50 µl lactate reagent was combined with 20 µl of each standard in wells of a 96-well plate. Biological samples were diluted 2 µl in 18 µl dH_2O and 50 µl lactate reagent was combined with 20 µl of each sample in wells of the same plate. Each standard was plated 3 times and each biological replicate of samples was plated once. The plate was shaken for 15 min on a plate shaker (Titramax 1000, Heidolph, Germany) then read at 540 nm using a microtiter plate reader (BioTek, Vermont, USA). A calibration curve for lactate was calculated from the measurements of standards by averaging absorbance across the 3 replicates of standard, minus the 0 mg/ml standard with lactate

reagent alone. This resulted in a straight line regression that fitted the points closely. The gradient of the line was then used to calculate the concentration of lactate in each sample where the medium and lactate reagent blank was subtracted from each biological replicate and the concentration was adjusted to the correct value taking into account the dilution factor.

2.9. Preparation of cell lysates for metabolic analysis

For GC-MS and UHPLC-MS, 10 cm cell culture dishes were used in which 8×10^5 cells were seeded in 8 ml fresh medium. All samples were incubated in normoxia for 24 h then transferred to normoxia, hypoxia or anoxia for a further 24 h. After incubation medium was discarded and cells were washed in 3 × 1 ml PBS. Subsequently 1 ml of ice cold (-40 ºC) methanol was then immediately added to quench the metabolism of cells. Cell scrapers were used to collect samples in eppendorf tubes then exposed to three cycles of snap freezing and thawing using liquid nitrogen (-196 ºC) followed by centrifugation for 15 min at 17000 × g. Finally, the supernatant was collected into fresh eppendorf tubes for analysis and the dry mass obtained after lyophilisation of the intracellular sample pellet (detailed in section 2.8) was used to normalise the samples through determining a final volume of supernatant to be analysed for each sample. Figure 11 shows a schematic of the workflow for collecting cell lysates for MS analyses.

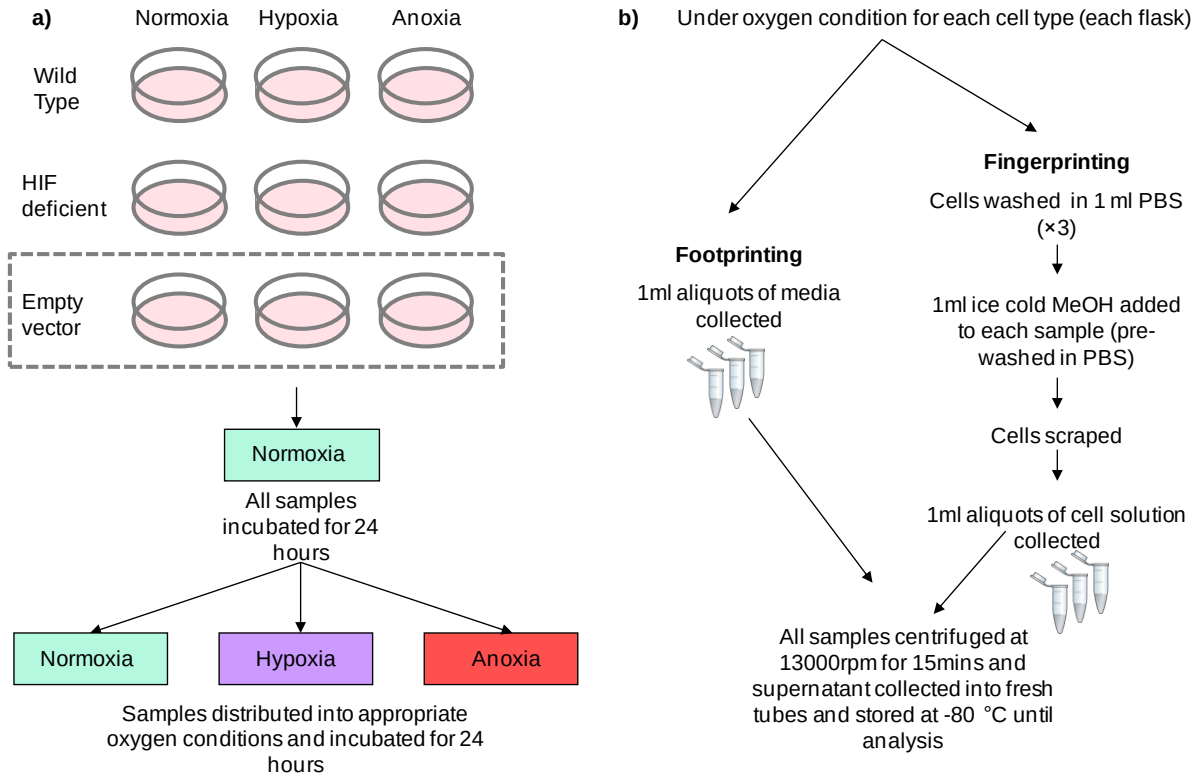

Figure 11: Schematic for the workflow for collecting cell lysates for mass spectrometric analysis. (a) Cells are seeded in replicate culture dishes for each oxygen condition and each cell line. These are incubated in normoxia for 24 h followed by 24 h exposure to experimental oxygen treatment. (b) Fingerprinting (intracellular) and footprinting (extracellular media) samples are prepared for analysis under experimental oxygen condition.

For some analyses quality control samples (QCs) were required. QCs were prepared by pooling small equal volumes (150 µl) of each biological sample into one QC sample from which many 1 ml QC samples were aliquoted. All samples were then prepared and analysed using the protocols for GC-MS, UHPLC-MS or ToF-SIMS. This method was inspired by research from Teng *et al.* (2009)[65], who described this technique as an alternative to using trypsin-EDTA for cell detachment which causes an alteration in metabolic profile since the detachment from extracellular matrix alters cell physiology[65].

To obtain cell lysates for analysis by Fourier transform – infrared (FT-IR) spectroscopy, 3.5 cm cell culture dishes were used in which 1.5×10^5 cells were seeded in 1.5 ml fresh medium. All samples were incubated in normoxia for 24 h then transferred to normoxia or hypoxia for a further 24 h. After incubation 200 µl medium was collected into eppendorfs for analysis and the rest was discarded. Cells were washed in 3 × 500 µl 0.85% saline solution. Subsequently 20 µl distilled H_2O was added and cell lysates were scraped into eppendorf tubes.

2.10. Fourier transform – infrared spectroscopy

FT-IR is a useful tool for the rapid global profiling of biological samples to assess which classes of compounds change or remain constant with respect to the cell line or treatment analysed. Its application is widespread in the biosciences, and with respect to cancer in particular, is thought to be potentially applicable in cancer screening[123]. In general, IR spectroscopy is the method of passing IR radiation through a sample and recording the absorption as a measure of the frequencies and vibrations between chemical bonds that are unique to the chemical material being analysed. Absorption is the $\log_{10}$ reciprocal of transmittance, where transmittance is the ratio between the sample's radiant power and the incident of the radiant power to the sample[124]. Transmittance is measured as a function of absorption. The Fourier transform algorithm is used to express the frequency spectrum by converting time to frequency and a plot of absorbance intensity *vs.* wavenumber (distance of one complete cycle and reciprocal of wavelength)[124] can then be drawn. When a complex mixture is analysed, the spectrum can be compared to absorption frequencies known for particular types of bonds and functional groups in certain chemical classes. Detectable in IR spectra are lipid, carbohydrate and nucleotide and amide peaks due to their shape intensity and position in the spectrum. An example FT-IR spectrum with labelled characteristic peaks is given in Figure 12.

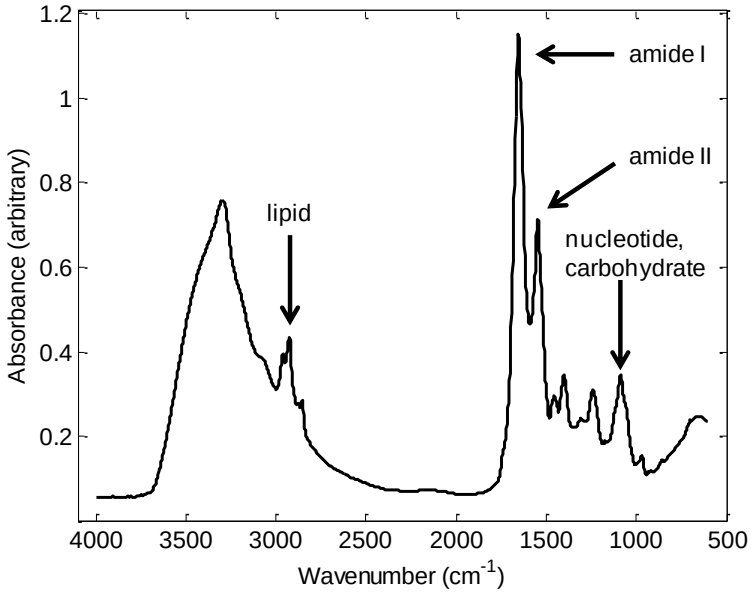

Figure 12: An example Fourier transform-infrared (FT-IR) spectrum showing the approximate wavenumber position of lipid, amide and nucleotide and carbohydrate peaks.

2.10.1. Sample preparation

Prior to use a 96-well silicon plate was rinsed with dH_2O followed by chloroform and ethanol and allowed to dry at room temperature. Leaving the first well blank for acquisition of a reference spectrum, 20 µl aliquots of medium or cell sample were evenly applied to the plate and dried at 50 °C for 30 min.

2.10.2. Fourier transform infrared spectrometer

FT-IR analysis was carried out on a Bruker Equinox 55 infrared spectrometer equipped with a motorised microplate module HTS-XT™ utilising a deuterated triglycine sulfate (DTGS) detector (Bruker Ltd.) described in Winder *et al.* (2006)[125] and below. The plate was loaded onto a motorised microplate module from which the plate is introduced into the airtight optics of the instrument where residual moisture is removed. The DTGS detector was used to measure transmission throughout the samples, collecting spectra which were displayed in terms of absorbance over a 4000 – 600 cm^{-1} wavelength, as controlled by Opus 5.5 FT-IR software. Each spectrum was acquired in approximately 1 min, including the reference spectrum from the blank well in the first position of the plate and all settings were maintained during all measurements. For any one experiment, samples were analysed in a randomised order and multiple plates were used sequentially where the sample number exceeded 95.

2.10.3. Data pre-processing

ASCII data were exported from the OPUS software and imported into Matlab version 9 software (The Mathworks, Inc., Natick, MA, USA). Matlab was programmed to replace CO_2 peaks at approximately 2400-2275 cm^{-1} and 680-660 cm^{-1} with a trend from directly before and after the peak in order to reduce non-biological variation which may affect data processing. Following this, in house routines were programmed to scale the FT-IR spectra using extended multiplicative scatter correction (EMSC)[126].

2.11. Gas chromatography – mass spectrometry

GC-MS was used for metabolic profiling of low molecular weight metabolites (in the approximate range *m/z* 650-1000[71]) and all GC-MS was performed using the following principles. To broaden the range of chemicals detected in the samples, chemical derivatisation was employed prior to analysis. This method facilitates the separation of chemicals, reduces the polarity of the functional groups in chemicals and enhances their volatility and thermal stability prior to GC[71, 127]. Hydroxyl, carboxyl and amino functional groups readily react with the chemical derivatisation agents that are added to convert these polar groups into derivatives with increased volatility[127]. The exact procedure employed for chemical derivatisation in this research is outlined in section 2.11.2. In the process of GC-MS, chemical samples were fractioned in the interaction with the stationary phase (analytical column) and mobile phase (carrier gas). The sample was injected at high temperature and pressure to vaporise the liquid. The carrier gas was then used to deposit the sample onto the analytical column through which the sample migrates and interacts with the stationary phase. This process separates components of the sample mixture that were then eluted and recorded as peaks on the chromatogram[127]. The elutents were ionised by the EI source before entering a ToF mass analyser, whereby an electric field was applied such that ions of the same mass accelerate through the ToF with the same kinetic energy[70]. Fragments were detected based on *m/z* producing a spectrum for every elutent peak of the chromatogram. GC-MS was employed for metabolic profiling of complex samples and many components shared similar or identical EI mass spectra. Therefore the GC retention indices were used to differentiate chemical species[71]. A retention index marker solution containing a range of n-alkanes was mixed with each sample and analysed simultaneously. The purpose of this was to normalise the retention time of each unknown chemical peak to the retention times of adjacently eluting n-alkanes to give a retention index for each peak.

2.11.1. Sample preparation

Solvents were removed by lyophilising all samples (as described in section 2.8). Following this, 100 µl of an internal standard (0.18 mg/ml succinic d_4 acid in water) was added to each sample before samples were re-lyophilised. This resulted in a pellet of metabolites for each sample.

2.11.2. Chemical derivatisation

Prior to injection, all samples were chemically derivatised using a two-stage process of oximation and trimethylsilylation[71]. This was done to increase volatility and thermal stability of the metabolites and ensure their full elution. In the first stage of derivatisation, 50 µl of a 20 mg/ml solution of O-methoxylamine in pyridine was added to each sample, ensuring the pellet of metabolites was fully immersed. Each sample was then vortexed in this solution and heated at 60 ºC for 30 min. The second stage of the process involved adding 50 µl of N-methyl-N-trifluoroacetamide (MSTFA) to each sample which was then vortexed and heated at 60ºC for 30 min. Finally, samples were centrifuged at 17 000 × g for 10 min to pellet the debris and 20 µl of a retention index marker solution containing 0.3 mg/ml n-decane, n-dodecane and n-pentadecane, n-docosane and n-nonadecane in pyridine was added. The resulting supernatant from each sample was collected for analysis.

2.11.3. GC-MS analysis

Where QCs were used, they functioned to condition and equilibrate the analytical platform to provide stability for reproducible data acquisition of biological samples[61] and in data processing described in section 2.13. An acquisition run was formed to start with a derivatisation blank then 5 QC samples followed by 5 samples followed by another QC followed by another 5 samples and so on until the end of one batch (approximately 60 injections). The batch was completed with the analysis of a further 3 QCs and one derivatisation blank. Whether or not QCs were used, all samples were randomised before analysis. All samples were analysed by GC-MS using the optimised method described previously by Begley *et al.* (2009)[128] and as described below. Analyses were carried out using a Leco Pegasus III mass spectrometer (Leco Corp., St. Joseph, MO) coupled with a Gerstel MPS-2 autosampler (Gerstel, Baltimore, MD) and an Agilent 6890N gas chromatograph with a split/splitless injector and Agilent LPD split-mode inlet linear (Agilent Technologies, Stockport, U.K.)[128]. Aliquots of 2 µl sample were injected at a split ratio of 4:1 and at an inlet temperature of 280 °C. The temperature was set to and held at 70°C for 4 min followed by a temperature ramp of 20 °C/min to 300 °C and a subsequent 4 min period at 300 °C. The transfer line between the chromatograph and mass

spectrometer was maintained at 250 °C. The mass spectrometer acquired *m/z* 45-600 at 20 Hz, operating with a source temperature of 220 °C and with ionization energy of 70 eV.

2.11.4. Data pre-processing

All data were pre-processed using the ChromaTOF v3.25 software package. From a set of samples representative of all sample classes, the mass spectrum and retention index of all unique metabolites were exported to a reference table. This reference table was then used to match metabolites in all samples, where it was reported if a mass spectral match between the reference table and the sample peak was greater than 70% and the retention index deviation between them was less than 10. All data were normalised to the peak area of the internal standard (peak area metabolite/peak area internal standard). These data were exported as '.csv' files for subsequent data analysis.

By matching the mass spectrum and retention index to those present in an in-house mass spectral library constructed with data acquired from authentic chemical standards, it was possible to identify a proportion of detected metabolites[129]. A mass spectral match greater than 80 % and a retention index match ± 20 provided a definitive identification. For instances where a definitive identification could not be made, the mass spectrum was searched against other mass spectral libraries. For example, the national institute of standards and technology (NIST) database of retention data for non-polar and polar stationary phases[130] and the publically accessible Golm metabolome database of mass spectral libraries[131] were used to identify metabolites putatively where a match greater than 80 % was observed. The level of identification reported was applied according to reporting guidelines as described by the MSI[50].

2.12. Ultra high performance liquid chromatography – mass spectrometry

UHPLC-MS was used for metabolic profiling as a complementary tool to GC-MS. In general (U(H)P)LC-MS is particularly useful for non-volatile chemicals that are often of high polarity and is therefore able to detect different types of chemical to GC-MS[71]. Combining both techniques provided more diverse profiling of the metabolome. All UHPLC-MS was performed using the following principles. The sample was introduced as a liquid and was combined with the mobile phase for delivery to the column. The sample migrated through the column depending on the physical and chemical interactions with the C18 stationary phase

within the column[127]. The time at which each chemical eluted was recorded as its retention time. The elutents were introduced to the mass spectrometer as a gas by removing the elutent solvent. This was done using ESI which is an application of a strong electric field under atmospheric pressure used to produce highly charged droplets of the elutent from which solvent is evaporated by heat resulting in smaller higher charge droplet formation from each larger droplet[70]. Ions then enter the LTQ Orbitrap mass spectrometer for analysis as described by Makarov (2006)[75] *via* radio frequency-only multipoles into the linear ion trap with two detectors. Ions were then focused and enter the 'C-trap'; a curved structure which enhances ion projection to the Orbitrap. The Orbitrap contains a core electrode and a split barrel shaped electrode surrounds it. Ions enter *via* the break in the outer electrode[75]. The outer electrode remains at ground while the inner electrode applies a voltage (negative for positive ions, positive for negative ions) sufficient to allow oscillation of ions. The current induced by oscillation is converted by Fourier transform to yield the mass spectrum[75]. Figure 13 shows a schematic for the instrument.

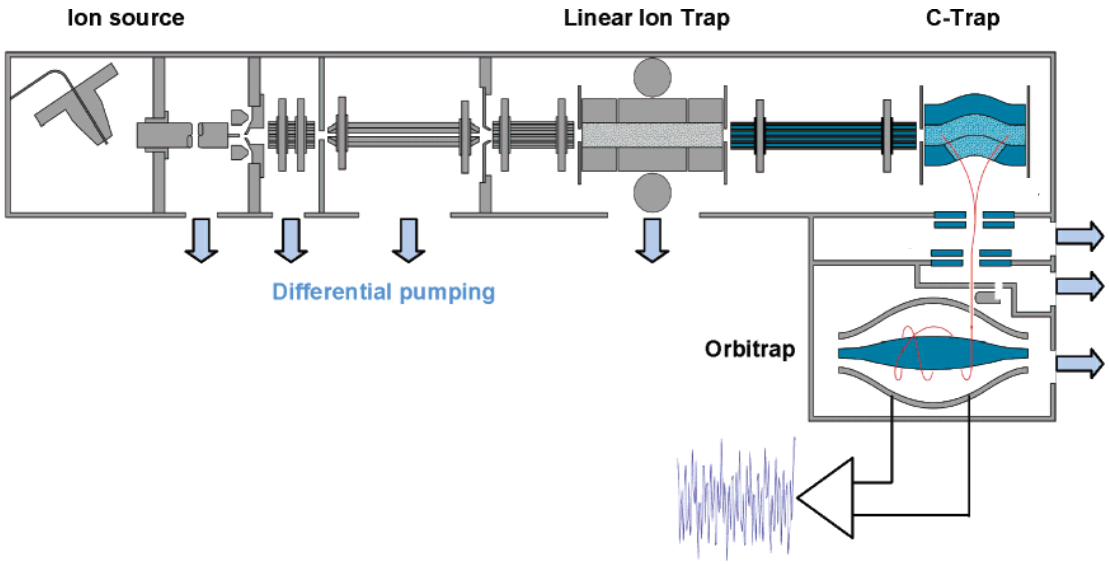

Figure 13: A schematic of the LTQ orbitrap mass spectrometer adapted from Makarov (2006)[75]. The instrument comprises an ion source, linear ion trap, C-trap and orbitrap.

2.12.1. Sample preparation

Solvents were removed by lyophilising all samples (as described in section 2.8). This resulted in a pellet of metabolites for each sample which were reconstituted in 100µl water immediately prior to analysis. QC samples and biological samples were prepared alike.

2.12.2. UHPLC operation

An acquisition run was formed to start with 11 QC samples followed by 5 samples followed by another QC followed by another 5 samples and so on until the end. All samples were randomised before analysis and were analysed separately in positive ion mode and negative ion mode on an Accelaultra high power liquid chromatography (UHPLC) system coupled to an electrospray LTQ-Orbitrap Velos hybrid mass spectrometer (ThermoFisher Scientific, Hemel Hempstead, UK). Chromatographic separations were performed on a Hypersil GOLD column (100 × 2.1 mm, 1.9 μm (ThermoFisher Scientific, Runcorn, UK) which was operated at a temperature of 50 °C.

Two solvents were applied at a flow rate of 400 μL/min. Firstly, solvent A (0.1% formate in water (vol/vol)) was held at 100% for 0.5 min followed by an increase to 100% solvent B (0.1% formate in methanol (vol/vol)) over 4.5 min. Solvent B was then held for a further 5.5 min at 100 % before a step change to 100 % solvent A and holding of solvent A at 100 % to equilibriate for 1.5 min. Subsequently, all column elution was transferred to the mass spectrometer for acquisition of full-scan profiling data. The orbitrap mass analyser was operating with a mass resolution of 30 000 at *m/z* 400.

2.12.3. Data pre-processing

Raw instrument data (in .RAW file format) were converted to netCDF file format with the FileConverter program available in XCalibur (ThermoFisher Scientific, Bremen, Germany). XCMS software, which is freely available[132], was used to deconvolve each 3D data matrix (in the form intensity × *m/z* × time per sample) into a matrix of detected peaks with response (the sum of intensities across a specified mass and time range) *vs.* sample identification. Peak output files were written out to '.csv' files using the built in 'esi' program and pre-processed data were directly exported to Microsoft Excel® (.xls) worksheets for further processing and data analysis.

Metabolites were putatively identified using the method described in Brown *et al.* (2011)[55]. This involved the application of the PUTMEDID-LCMS workflows with a retention time window of 3 s and an *m/z* error of ±5 ppm.

2.13. Time-of-flight - secondary ion mass spectrometry

Prior to analysis, samples were pre-mounted or pre-spotted on silicon wafers (Advent-rm, Oxford, UK) that were pre-washed in dH_2O, then chloroform and finally ethanol to remove any contaminants. All samples were analysed using a J105 *3D chemical imager* ToF-SIMS instrument developed at the University of Manchester (described previously by Fletcher *et al.* (2008)[106] and briefly below). A schematic of the instrument is shown in Figure 14. Currently, ToF-SIMS analysis in negative ion mode is not possible using the J105, therefore all samples were analysed in positive ion mode. All experiments utilised the 40 kV C_{60}^+ ion gun (Ionoptika Ltd., U.K.) mounted at an angle of 45 ° for primary ion bombardment of sample surfaces operated in quasi-dc mode. Using a continuous ion beam greatly enhanced the duty cycle and increased the rate of data acquisition[106]. C_{60}^+ primary ions were chosen as they have been shown to increase secondary ion yield, particularly at higher mass, and because sub-surface damage accumulation is greatly reduced[133]. Therefore the 'static limit'(~ 10^{13} primary impacts/cm^2)[104], the level at which a surface can be bombarded to collect spectral information from one layer without causing damage to the sample surface, can be exceeded. This allowed for some experiments to utilise dynamic ToF-SIMS whereby data is acquired in layers to generate chemical information in *3D* during the process of depth profiling.

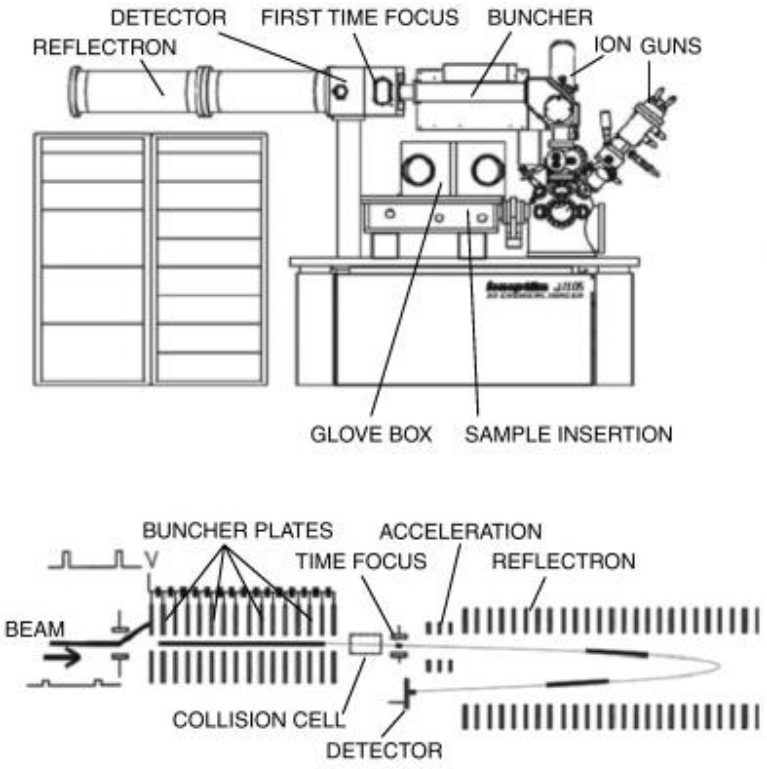

Figure 14: Schematic of the J105 *3D Chemical Imager* taken from Fletcher *et al.* (2008)[106]. Samples are inserted *via* the glove box and transferred to the stage under vacuum using a motorised system. Primary ion bombardment occurs using the ion gun. The buncher creates a temporal focus of ions before acceleration into the harmonic reflectron mass analyser. The collision cell is employed for dissociation in tandem mass spectrometry (MS2) experiments.

The instrument comprises extraction optics with applied voltages that attract secondary ions away from the sample, such that the topography of the sample does not affect the secondary ion yield. A continuous stream of secondary ions are generated from the sample and cooled and focused using a radio frequency-only quadrupole filled with nitrogen gas with a pressure of ~ 3.5 milli-torr. Using the nitrogen gas to cool the ions reduced their translational and vibration energy and prevented further fragmentation. The secondary ions are accelerated to 100 eV as they exit the quadrupole then filtered using an electrostatic analyser to ensure ions have a low energy spread so that they were suitable to fill the buncher. The buncher consists of 30 plates spaced over ~ 30 cm (shown in Figure 14), with a range of 6500 to 500 volts supplied across them. Secondary ions are focussed and fired from the buncher at 10 kHz into a harmonic field ToF reflectron analyser. This process resulted in a 6 keV energy spread across secondary ions and the harmonic field reflectron ToF was used to ensure only the mass and charge of the secondary ions shaped the path of ions (rather than the energy spread). This ensured that ions impacted the detector with the same time spread and focus as they had when entering the reflectron. When ions arrived at the detector the signal was amplified by a collision cascade on the micro channel plate; a plate with a more positive voltage applied at the back, such that

electrons are pulled through the channels placed at angles to induce collisions and creation of further electrons. Subsequently electrons hit the scintilator polymer which yielded photons that then entered a photon multiplier. Finally, photons are converted back to electrons and detected at the analogue-to-digital convertor resulting in a spectrum for one pixel. The primary ion beam was then rastered to the position of a neighbouring pixel and the whole process was repeated to gain a spectrum for that pixel and so on until spectra had been collected for every pixel in a tile (specified area for data acquisition). Where the experiment involved depth profiling, the process was further repeated per analysis area to generate spectra for a sequence of layers that could be summed to give the total ion spectrum for the whole sample analysed or interpreted individually to reveal chemical changes as a function of depth. Due to file size limitations the data were down sampled during acquisition to 0.05 Da bins.

2.13.1. Collection of standards for ToF-SIMS analysis

Standard MS and MS2 spectra were obtained for 20 metabolites and data were combined with a further 20 metabolites that were analysed by another member of the laboratory to provide a repository of 40 standard spectra for use in metabolite identification in the analysis of biological samples by ToF-SIMS[134]. Standards were analysed on the J105 at a primary ion fluence of 1.6×10^{12} ions/cm^2 for MS and 1.6×10^{13} ions/cm^2 for MS2 with a current of 60 pA over a 300 × 300 µm area collecting spectra for each pixel from 200 shots for MS and 2000 shots for MS2 in a 16 × 16 pixel square. Standards were prepared in HPLC grade H_2O to a volume of 1 mM and were spotted at volumes of 2 µl.

In addition to the standard MS spectra, mixtures of two and five standards were also analysed. This was done to observe any influences certain metabolites may have on others with regards to their ionisation efficiencies and detection when combined in a mixture. Since biological samples contain complex mixtures, it was important to consider how metabolites behave in mixtures and how it may change the interpretation of biological data. These mixtures were prepared by combining 1 µl of each desired standard, and spotting 2 µl of solution to be analysed by the J105. These were analysed alongside the standards using the same parameters as described above.

2.13.2. Determining the sensitivity for metabolite detection using the J105

To determine an approximate level of sensitivity for analysis of metabolites known to ionise well using ToF-SIMS, a metabolite was chosen and analysed over a range of quantities. For this 1 µl volumes of guanine were prepared in HPLC grade H_2O to contain 1 nanomole, 1 picomole or 1 femtomole. The whole sample for each was deposited onto clean silicon and analysed using the J105. This was repeated to collect data in layers (dynamic analysis) until the whole sample for picomole and femtomole was consumed. The nanomole sample was not fully consumed as a very good reference spectrum was obtained from a 2 × 2 tiled area over 4 layers where each tile was 800 × 800 µm, included 32 × 32 pixels and was given a current of 80 pA and 200 shots per pixel. The tiles for the picomole sample and the femtomole sample were similar but data were collected from a 4 × 4 tiled area over 7 layers and from a 2 × 2 tiled area over 6 layers respectively, in order to consume the whole sample. Further areas of similar size were analysed on the clean silicon to obtain a background reference spectrum for each experiment: nanomole, picomole and femtomole. The primary ion fluence for all experiments was 1.2×10^{12} ions/cm^2. The total spectral dose (total number of primary ions supplied) for the nanomole sample was 1.2×10^{11} ions, for the picomole sample was 8.6×10^{11} ions and for the femtomole sample was 1.8×10^{11} ions. Within each sample, the spectra from each layer were summed to give a total ion spectrum to be compared to silicon. The molecular ion peak and each of the identified ToF-SIMS fragments for guanine were plotted for each sample and compared to silicon and the sensitivity was determined from the lowest concentration yielding guanine peaks higher than the background signal from the silicon.

2.13.3. Metabolic profiling of whole cells

Suspensions of whole cells were prepared for and analysed by ToF-SIMS using the following method. Culture dishes with a diameter of 6 cm were used in which 3×10^5 cells were seeded in 3 ml fresh medium. All samples were incubated in normoxia for 24 h then retained in normoxia or transferred to hypoxia for a further 24 h as described previously in 2.9. After incubation the medium was discarded and cells were subsequently washed in 3 × 800 µl PBS then 300 µl trypsin-EDTA was added to each sample in which cells were incubated until they detached from the culture surface. Subsequently 1 ml 4% Formaldehyde was added to each sample to fix the cells for 10 min. Samples were

centrifuged at 64 × g for 10 min after which the supernatant was removed and cells were re-suspended in 1 ml 0.15 M ammonium formate solution. This was repeated 6 times with fresh ammonium formate each time to ensure cells were fully washed prior to analysis. After the 6^{th} wash cells were reconstituted in 2 µl ammonium formate solution which was spotted onto silicon wafers. Cells were left to dry before being inserted into the J105 for analysis. Cells were analysed on the J105 at a primary ion fluence of 5.62×10^{14} ions/cm^2 with a current of 20 pA.

2.13.4. Metabolic profiling and imaging of MTSs

MTSs were sectioned at 10 µm using a cryostat-microtome (Bright, Starlet 2212, Instrument Company LTD, UK) operated at approximately -20 °C directly before analysis to minimise degradation from the thawing process. This was achieved by adhering the frozen gelatine block containing the MTSs to a pre cooled disk which was fixed within the cryostat-microtome so that the samples could be accurately cut into sections of 10 µm. The sections were subsequently thaw mounted onto pre cooled silicon substrates prepared as before for ToF-SIMS followed by vacuum desiccation. The embedding medium used to attach the sample to the disk was a polymer for optimal cutting temperature (OCT). This is commonly used in histology to stabilise the tissue and provides a smooth cutting surface. However, it poses problems for samples to be analysed using imaging mass spectrometry as it has been shown to reduce the total ion signal by half[135]. Therefore, for this purpose the amount of OCT used was kept to a minimum to ensure the OCT did not contaminate the cross section to be analysed.

MTS sections were washed three times in 0.15 M ammonium formate each for 1 minand dried on a WS-400-6NPP/LITE spin caster (Laurell technologies, Pennsylvania, USA) operated at 64 × g for 10 min, followed by vacuum desiccation before ToF-SIMS analysis. The C_{60}^+ primary ions were rastered with a current of 20 pA over a 1000 × 1000 µm area collecting spectra for each pixel from 200 shots in a 256 × 256 pixel square. 3 layers were analysed and the total primary ion fluence for this experiment was 3.68×10^{13} ions/cm^2.

2.13.5. Data pre-processing of biological samples

Due to the complexity of the spectra obtained from analysis of MTSs, where stated, peaks of interest were selected using Matlab on which multivariate analysis was performed. This was done to remove non-biological peaks along with unidentified peaks that skew the analysis but that add no value to the data interpretation. Peaks were selected using a list of peaks identified in the analysis of metabolite standards with the addition of sodium and potassium adducts of the molecular ion and known lipid fragments from Passarelli and Winograd (2011)[136]. The intensity for each *m/z* was selected ± a tolerance of 0.05 Da. Where this tolerance resulted in overlap, fragments were averaged and the intensity was selected at this value to encompass all fragment peaks. There were a total of 177 peaks selected from each dataset this was applied to.

2.14. Data analysis

Where QC samples were required to determine the repeatability within analytical batches, data were further processed and to remove metabolic features with excessive drift in signal. The QCs were used to do this by a method of quality assurance as described in Dunn *et al.* (2011)[61]. This process was performed after feature identification and before analysis of GC-MS and UHPLC-MS data. The relative standard deviation of each detected feature was calculated across all QC samples and for features where the coefficient of variance exceeded 20 % for UHPLC-MS data and 30 % for GC-MS data, that feature was removed from the whole data set. The tolerance was greater for GC-MS data as variation due to chemical derivatisation and injection is higher than variation in UHPLC-MS data[61]. QCs were also used in signal correction within, and where necessary between, analytical blocks. For this quality control based robust LOESS (locally estimated scatter-plot smoothing) signal correction (QC-RLSC) was applied. The change in signal between samples for each metabolic feature was corrected by removing the temporal shift in signal observed in QC samples[61], thus reducing instrument drift while retaining biological variation.

For GC-MS, UHPLC-MS, ToF-SIMS and FT-IR spectroscopy analyses, pre-processed data were exported for univariate and multivariate data analysis in Matlab as a data matrix ($m \times n$) where m denoted metabolite features and n denoted sample. Values were

chromatographic peak areas included for each feature detected in each sample. Prior to data analysis, outliers were identified within each experimental group as values greater than 2.5 standard deviations away from the mean for that metabolite in that group and were subsequently replaced by the mean[137].

2.14.1. Univariate analysis

A range of univariate statistical analyses were applied to the data in this research and all were implemented using the Statistics Toolbox in Matlab. For the large scale metabolomics study utilising GC-MS, data were observed to fit an approximately normal distribution after log transformation and therefore parametric tests were applied. A two-way analysis of variance (ANOVA)[138] was employed to identify metabolites that differed significantly due to oxygen level, to HIF-1 presence or absence or due to an interaction between oxygen and HIF-1. Since many metabolites were being tested in parallel and since the sample number was suitable for the application of a false discovery test[139], it was done so using $\alpha = 0.1$ to adjust the critical *p*-value for rejecting the null hypothesis that there was no significant difference between oxygen levels and HIF-1 presence or absence. Box plots were outputted for adjusted significant *p*-values < 0.05. The smaller scale metabolomics study utilising UHPLC-MS yielded data that was non-parametric and therefore non-parametric statistical testing was used to observe differences in experimental groups. A Friedman test[140] was used to observe difference in metabolite concentration between HIF-1 presence and absence after controlling for the effect of oxygen level in each. A Mann-Whitney *U*-test[140] was used to compare WT to HIF-1 deficient samples at normoxia, hypoxia and anoxia and fold changes were calculated for significantly different metabolites.

2.14.2. Multivariate analysis

Multivariate analyses were employed to consider the variance due to experimental condition beyond the first dimension. They are used to assess the variance that may be a combination of many variables such as peak intensities in spectra. Multivariate analyses were performed using programmes developed in-house for Matlab.

The first method for multivariate analysis and the one most commonly used throughout the research was principal components analysis (PCA)[141, 142]. A data matrix of samples *vs.* spectra (where samples represent *x* number of biological replicates from *y* number of experimental conditions) was inputted into Matlab. In many cases the spectra are scaled either by standardisation (autoscaling by dividing by the standard deviation), taking the square root or sum normalising (where the intensity of each peak in a spectrum is expressed as a proportion of total intensity). Scaling accounts for high variance between samples or within spectra which may not be biologically relevant. PCA then works by assessing the variance between each mass in the spectra across all of the samples in a way to fit orthogonal lines of best fit from which the variance is measured[142]. The line of best fit that best describes the data with the highest percentage of variance is termed principal component (PC) 1 and the next PC 2 and so on. Singular value decomposition was the method used to obtain PCs. For each PC the loadings and scores are outputted, where loadings are the cosine angles between the PC and each data point and the scores are the orthogonal projections of the data in the PC space.

For some analyses multivariate analysis was extended to canonical variates analysis (CVA)[143] whereby PCA was performed and a number of PCs were used along with the experimental group structure to build a model for maximising the between-group variance while minimising the within-group variance. This was performed without exceeding the number of PCs that additively describe 95 % of the total variance in the data in order to reduce the likelihood of over fitting which can invalidate the model.

For ToF-SIMS image data of MTS cross sections, image PCA was employed using the image processing toolbox and statistics toolbox in Matlab to assess the variance between spectra from pixels in a single total ion image. For this, the MTS was selected as a region of interest and PCA was performed. Image PCA presents the scores plot is a re-built image of the total ion image with PC loadings displayed as a gradient from green (positive) to red (negative).

2.14.3. Network-based correlation analysis of GC-MS data

Correlation analysis was used as a way to analyse the GC-MS metabolic profiling data in terms of metabolite connections where correlation coefficients were calculated for every pair of metabolites identified. Scripts for this were written and executed in Matlab. The data was transformed by $\log_{10}$ (data+1) to gain an approximately normal distribution necessary for the parametric Pearson's correlation. An $n \times m$ matrix of Pearson's correlation coefficients was calculated for each metabolite by every other metabolite using the statistics toolbox in Matlab. The diagonal of this matrix was then taken and only correlations where there were at least 27 data points for each metabolite were accepted. This value was chosen according to the standard error equation (Equation 3) whereby the weaker the correlation coefficient, the higher the sample number required to the lower the error. This equation was rearranged to reveal the minimum number of samples required to accept a correlation with a standard error less than or equal to 0.1[144]. Correlation coefficients where either metabolite contained less than 27 entries (due to missing values where either the metabolite was not present in the sample or it was present at a concentration not detectable by the GC-MS) were discarded.

$$SE = \frac{(1-\rho^2)}{\sqrt{n-1}}$$

Equation 3: The standard error (*SE*) equation where the required sample size (*n*) is determined for a chosen value for *SE* to accept a chosen correlation with coefficient (ρ).

Correlation coefficient matrices were then compared to observe differences between experimental groups. A difference was reported when the rules that the correlation coefficient of at least one of the two experimental conditions had an absolute value of 0.7 (considered to be the minimum level of a strong correlation) and the difference between the coefficients was at least 0.407 were satisfied. Equation 4a was used to obtain a value Z_i for a chosen correlation coefficient C_i (in this case 0.7) which was then inputted into Equation 4b as Z_1 along with the determined sample size for each experimental group (N_1 and N_2). $\hat{Z}^T$ was selected using Table 3 for a significance level of $\alpha = 0.05$ and rearranged to revel the required threshold value for the compared correlation coefficient and thus the minimum difference in correlations could be calculated.

$$Z_i = \frac{1}{2}\log\frac{1+C_i}{1-C_i} \qquad \hat{Z}^T = \frac{\left|z_1 - z_2\right|}{\sqrt{\frac{1}{N_1 - 3} + \frac{1}{N_2 - 3}}}$$

(a) (b)

Equation 4: Calculations required to assess the difference between correlation coefficients at significance level $\alpha = 0.05$ for a minimum sample size of 27 and a minimum absolute correlation coefficient of ± 0.7 in at least one of the experimental groups compared. (a) is the Fishers z-transformation where C_i is the Pearsons rank correlation coefficient (in this case chosen to be 0.7) and (b) is the permutation test for comparing correlations between metabolites, where $\hat{Z}^T$ is a value that corresponds to the confidence of a correlation, z_1 and z_2 are the values calculated through equation 3a and N_1 and N_2 are the minimum sample sizes for each metabolite. Taken from Steuer (2005)[145]

Table 3: The required value for $\hat{Z}^T$ with a significance of α needed to be inputted into Equation 4b. Taken from Steuer (2005)[145].

α	**10^{-6}**	**10^{-5}**	**10^{-4}**	**10^{-3}**	**0.01**	**0.05**
$\hat{Z}^T$	4.891638	4.4171173	3.890592	3.290527	2.575829	1.959964

Once differently correlated metabolites were identified between experimental groups, pathways between the metabolites were observed on the Edinburgh human metabolic network (EHMN)[12]. To do this, the SBML model was read into Matlab using the SBMLToolbox[146] and the stoichiometric matrix of reactions *vs.* metabolites within the entire network was obtained. From this metabolites produced and consumed were calculated and the transpose of one was multiplied by the other to get a connectivity matrix of metabolites *vs.* metabolites. This matrix was symmetrised to make the reactions reversible and used to calculate the shortest path between a pair of correlations using the Bioinformatics Toolbox (The Mathworks, Inc., Natick, MA, USA).

Chapter 3. Method development, validation and preliminary investigation

3.1. Introduction

The experiments presented in this chapter were aimed at exploring the impact of oxygen level and HIF-1 on cell growth and biomass, cell cycle and cell metabolism. Many of these experiments served to validate the experimental conditions to be used in metabolic profiling in subsequent chapters while others served as initial investigations into the metabolic effects of oxygen and HIF-1 through the analysis of central carbon metabolites known to be targets of both and discussed in sections 1.2 and 1.3.

Prior to the high-throughput analysis of the metabolic profiles of HEPA-1 and or HCT 116 cell models by GC-MS, UHPLC-MS and ToF-SIMS, a range of experiments were undertaken. Experiments mainly using the HEPA-1 model were performed to characterise the growth of cells and to validate experimental conditions such as oxygen treatments, the medium and the seeding density to be used in experiments. Cell cycle analysis was performed using flow cytometry to measure the fluorescence of propidium iodide staining of DNA that is indicative of the stage of the cell cycle cells are in after oxygen treatments. It was considered that differences in cell cycle properties may affect the interpretation of metabolic profiles if certain treatments induce arrest in specific parts of the cell cycle. The effects of oxygen and HIF-1 presence or deficiency on glucose, glutamine and lactate representative of key players in central carbon metabolism were measured and the flux of these metabolites between cell and medium was analysed as a preliminary study of oxygen and HIF-1 related effects on central carbon metabolism. Finally, small scale GC-MS analyses of HEPA-1 WT and C4 and of HCT-116 WT, EV and DN cells were done to develop the method for metabolic profiling of cell lysates by MS and to assess the metabolic phenotype of EV cells compared to WT and DN cells before high throughput analysis of WT and DN cells respectively. Many validation experiments were conducted only on one of the two cell models used and the optimised parameters were applied to the other cell model where necessary since the growth rate of each at each experimental condition was not observed to be significantly different.

HEPA-1 WT, HIF-1β-deficient HEPA-1 C4, HCT 116 WT, HCT 116 DN and HCT 116 EV cells were obtained from in house cell stocks. The development and validation of

HEPA-1 C4 are given in Hoffman *et al.* (1991)[147] and Maxwell *et al.* (1997)[115] and are described also in Troy *et al.* (2005)[38], where HIF-1β was found not to be expressed in these cells. The validation of HEPA-1 C4 cells is illustrated in Figure 15a. From the immunoblot assay of HIF-1β as a response to hypoxia, it was concluded that the activation of the HIF-1 heterodimer was impaired in C4 cells since neither subunit could be detected[38].

The HIF-1α dominant-negative (DN) construct[148] expresses a HIF-1α competitor that binds more readily with HIF-1β and acts as a dominant negative. Thus, unlike the HIF-1β in HEPA-1 C4 cells, HIF-1 activity is inhibited with no effect on HIF-1α stability[116]. The EV construct is used to control for the transfection of the HCT 116 cells. These cells were developed and validated by Dr Rachel Cowen and Professor Kaye Williams. The details of the genetic constructs used in the generation/validation of the cell lines are given in Brown *et al.* (2005)[148] and Roberts *et al.* (2009)[116]. Figure 15b and c show the validation of HCT 116 DN cells. HIF-1α and downstream target glucose transporter-1 (GLUT-1) were compared in HCT 116 DN and EV cells. The expression of HIF-1α was unaffected in DN cells, however hypoxia induced GLUT-1 was absent in both cells and multicellular tumour spheroids (MTSs)[116].

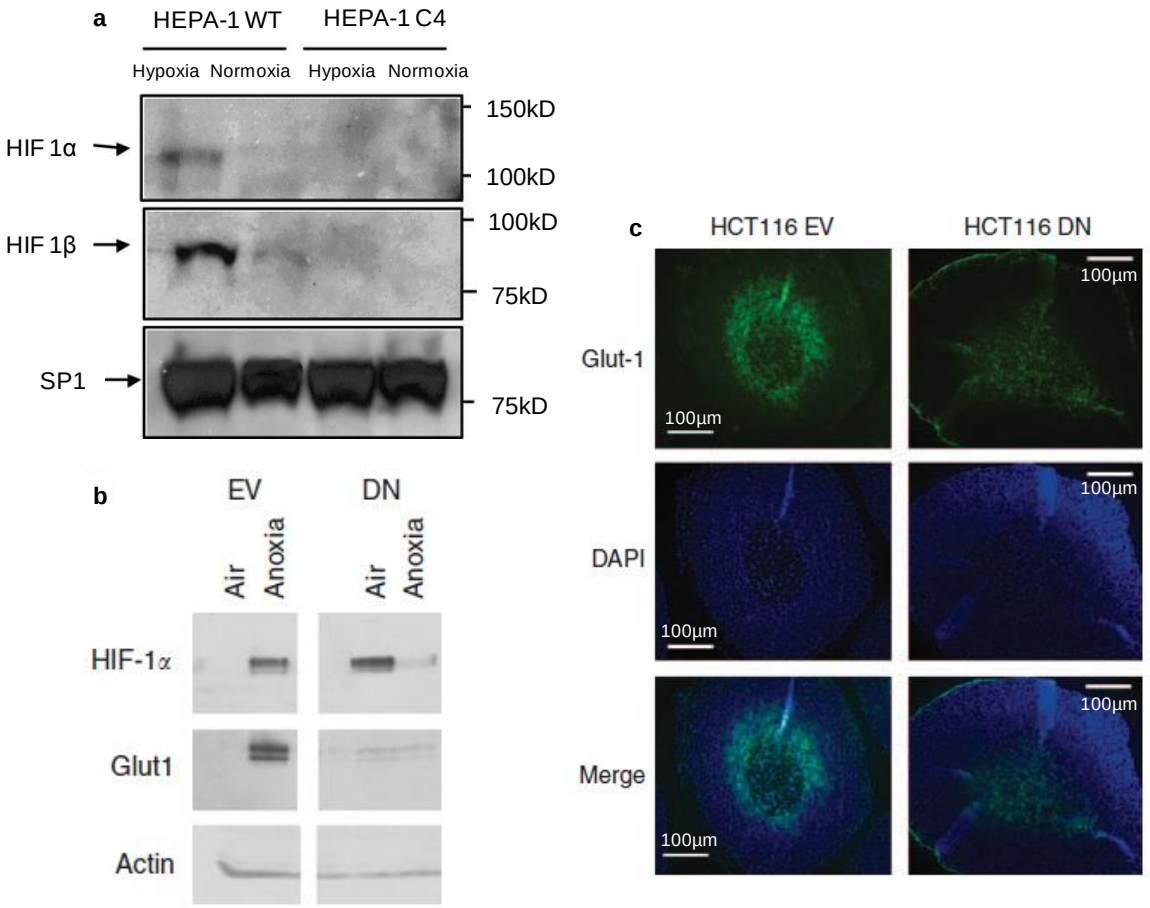

Figure 15: Validation of HEPA-1 C4 cells and HCT 116 dominant negative (DN) cells adapted from (a) Troy *et al.* (2009)[38] and (b-c) Roberts *et al.* (2009)[116]. (a) Immunoblot assay of nuclear extracts from HEPA-1 wild type (WT) and C4 cells for translocation of hypoxia inducible factor (HIF)-1α and HIF-1β as a response to 1 % oxygen exposure (hypoxia) compared to normoxia over an 18 h period. SP1 nuclear transcription factor was loaded as a control. (b) Immunoblot assay of HIF-1α and HIF-1 target glucose transporter-1 (GLUT-1) in HCT 116 empty vector (EV) and DN cells exposed to air or anoxia. Actin was loaded as a control. (c) Multicellular tumour spheroid (MTS) sections immunostained for GLUT-1. HCT 116 EV and DN MTSs were fixed and sectioned when their diameter reached ~ 500. DAPI counterstaining was used to identify cell nuclei.

3.2. Results and discussion

3.2.1. Cell lines

The first cell based investigation was to test for the activity of HIF-1 in each cell line. The analysis was performed using a luciferase reporter-based assay with an adenovirus containing a firefly luciferase reporter construct linked to the LDH HRE sequence. This is an accepted technique for determining HIF-1 deficiency[38] and was therefore used as the method of confirming HIF-1 deficiency in both HEPA-1 and HCT 116 cell models. The assay was first performed to check the proficiency of the cell models by comparing the

transcriptional activity of HIF-1 in WT and HIF-1 deficient cells. The results from this are illustrated in Figure 16 which shows an increase in HIF-1 transcriptional activity in WT cells under anoxia compared to normoxia which is lower in the HIF-deficient cells. This highlighted the deficiency in HIF-1 in the C4 and DN cells, indicating that they were good models to study HIF-1 related effects.

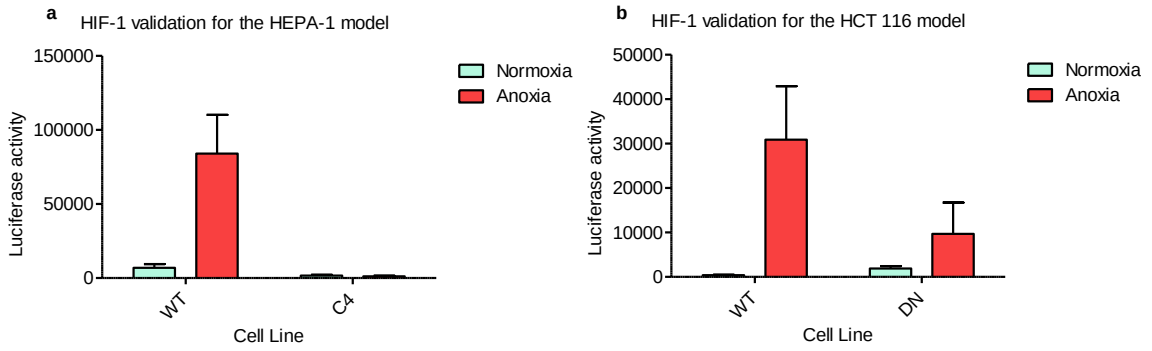

Figure 16: The absolute luciferase activity as a representation of hypoxia inducible factor (HIF)-1 activity. The activity was analysed using a luciferase reporter-based assay with an adenovirus containing a firefly luciferase reporter construct linked to the lactate dehydrogenase HRE sequence. The luminescence was measured for HEPA-1 wild type (WT) and C4 cells (a) and HCT 116 WT and dominant negative (DN) cells (b) exposed to normoxia compared to anoxia, indicating the degree of HIF-1 expression. The mean ± 1 s.e.m from 3 biological replicates is shown for each. The difference between WT cells exposed to normoxia compared to anoxia differed significantly in both cell lines ($p<0.01$) and no significant difference was observed between DN or C4 cells exposed to normoxia compared to anoxia ($p>0.05$).

In another initial experiment, the relative growth rates of HEPA-1 WT and C4 cells were also determined. Cells were seeded at a density of 5×10^4 and measurements were taken at 24, 48, 72, 96 and 168 h. Although the initial growth rate (where Y_0 is the growth rate Y at time zero) of WT and C4 cells was slightly different ($Y_0 = 8705$ and $Y_0 = 7605$ for WT and C4 cells respectively), the doubling time was similar (22.05 h and 21.59 h for WT and C4 cells respectively). It was therefore deemed applicable to use the same experimental design for all subsequent experiments. The observed growth rates and doubling times for WT and C4 cells were similar to that reported in the literature[38].

3.2.2. The effect of seeding density on biomass

An experiment was undertaken to determine the seeding density required for maximum biomass that did not compromise the condition of cells. The aim of this was to establish a suitable seeding density for metabolic profiling experiments. Cells were seeded at 25 000, 50 000, 100 000, 150 000, 200 000 and 400 000 cells/ml. The optimal seeding density,

shown in Figure 17, was 100 000 cells/ml based on having no more than 15 000 cells/cm^2 and no less than 200 µl medium/cm^2 (as recommended by culture vessel manufacturer). The data from this experiment have been used to establish the number of cells and the volume of medium needed for varying culture vessels to be used in all subsequent experiments.

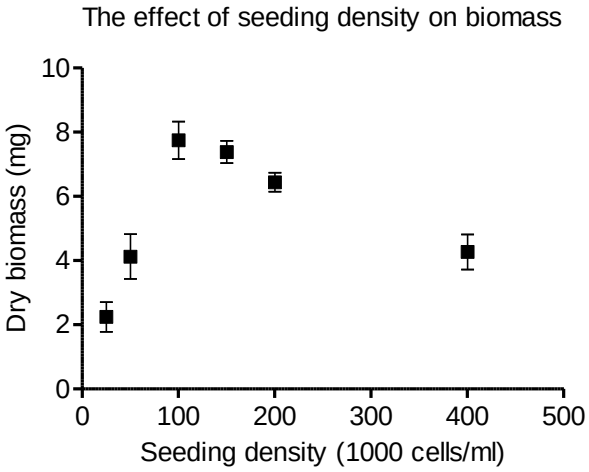

Figure 17: The dry biomass obtained from increasing seeding density expressed as an average for both cell lines under normoxia (21 % oxygen) or anoxia (0 % oxygen). The mean ± 1 s.e.m from 2 biological replicates is shown for each. Cells were seeded at a range of densities and cultured in normoxia for 24 h before being transferred to anoxia or kept in normoxia as appropriate for a further 24 h.

To assess the effect of the hypoxia (1 % oxygen) and anoxia (0 % oxygen) on final biomass, growth tests were undertaken for all 3 oxygen exposure treatments to assess the appropriateness of the seeding number and density for cells. The final cell count for WT and C4 cells after exposure to all three oxygen treatments showed that biomass decreased with oxygen potential. The final biomass for each cell line under each condition is shown in Figure 18. There was a reduction in biomass with a decrease in oxygen however it was decided that this maybe within an acceptable tolerance if enough biomass is yielded for the proposed analyses.

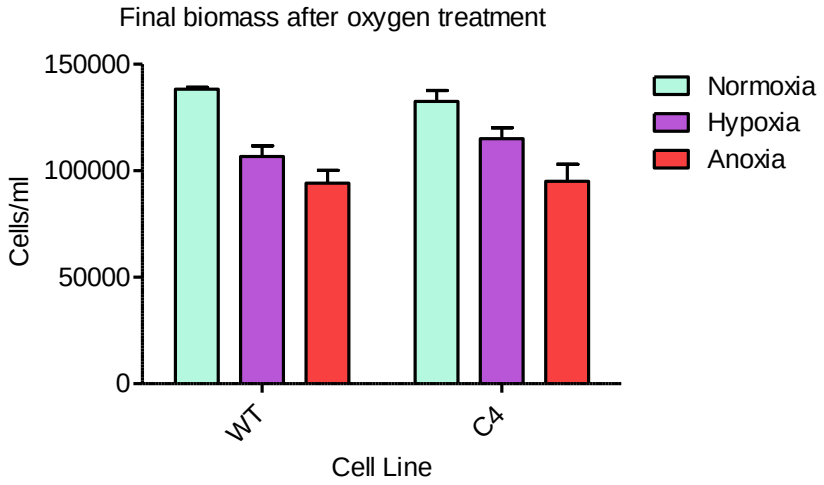

Figure 18: Final cell counts representative of biomass (expressed as cells/ml) after oxygen treatment, where initial seeding was 100 000 cells/ml. The mean ± 1 s.e.m from 3 biological replicates is shown for each cell line in each condition. WT normoxia differed significantly from both hypoxia (p<0.05) and anoxia (p<0.01). C4 normoxia differed significantly from anoxia (p<0.05). All other differences were not statistically significant.

To assess whether or not there was sufficient biomass for GC-MS analysis of anoxia samples, an experiment was undertaken to reveal any effects on signal. The signal was assessed from the analysis of HEPA-1 WT and C4 cell lysates from one 10 cm culture dish and was compared to the analysis of cell lysate from two 10 cm culture dishes combined. Although the biomass of anoxia samples was lower than other samples, the effect on GC signal was minimal. Figure 19 shows the comparison between gas chromatograms for the highest (normoxia sample) and lowest (anoxia sample) biomass samples. There was some reduction in signal intensity for anoxia samples when compared to normoxia, however peak definition was maintained for all chromatograms and the spectral coverage was comparable across all. The quality of the spectrum was not increased from the two dish test and therefore it was decided that one 10 cm dish per sample yields an appropriate amount of biomass and was used in all subsequent metabolic profiling experiments by MS. This validated the seeding density and all other experimental conditions for metabolite extraction and profiling.

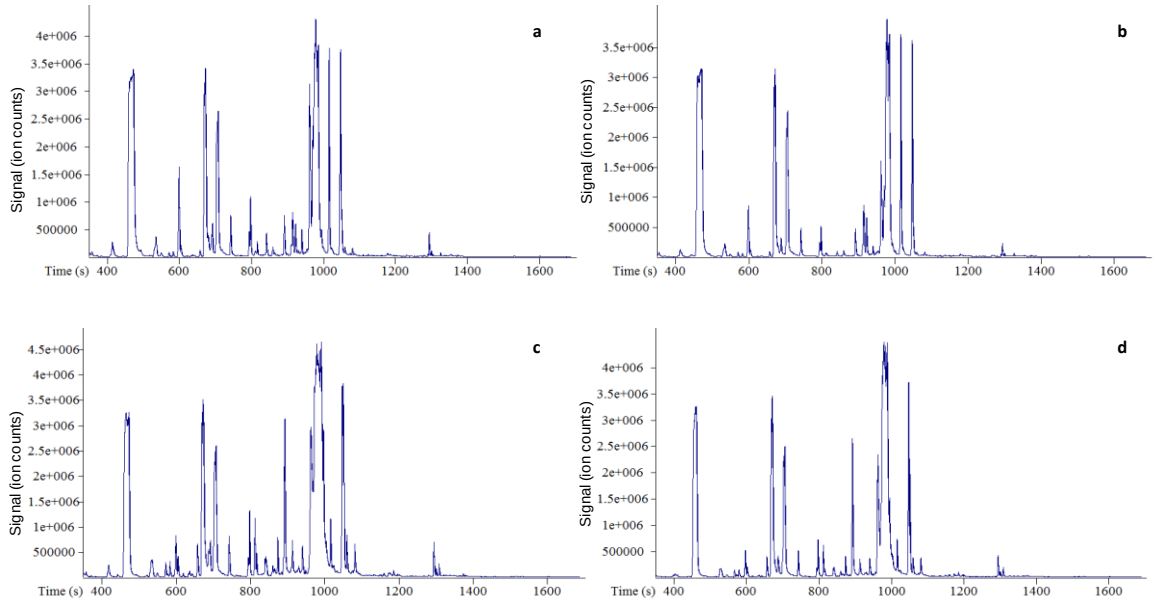

Figure 19: Gas Chromatograms for HEPA-1 (a) wild type (WT) normoxia (21 % oxygen), (b) WT anoxia (0 % oxygen), (c) C4 normoxia and (d) C4 anoxia intracellular fingerprint samples to show the effect of lowered biomass yielded in anoxia samples compared to their normoxia counterparts on signal.

3.2.3. Exploring the effect of using reduced media on cell growth

Experimental data on optimising the medium to be used in cell culture for metabolic profiling was collected with the aim of reducing the complexity of the extracellular footprint. Unlike yeast, mammalian cells require a complex medium to sustain growth and proliferation at steady state. Although metabolic profiling of the extracellular footprint has been successful in other systems such as *Saccharomyces cerevisiae*[64], with the capability for normal function in minimal medium, it is more challenging for mammalian systems that require a complex medium for growth. Complex media often contain many metabolites at higher concentrations than exist in the exometabolome itself. This can result in real biological signals being lost in noise of a mass spectrum relative to the high intensity medium peaks. Also, metabolites that may vary subtly between samples for comparison can be missed, particularly if this metabolite also exists in the medium itself at a high concentration such that differences cannot be observed. A range of experiments were undertaken to investigate whether or not the complexity of the medium could be reduced, starting with the effect of removing glutamine. This was done in an attempt to reduce complexity by removing it as an alternative carbon source to glucose. When glutamine was removed from the growth medium, the biomass was significantly reduced and cells were observed to be undergoing stress as a consequence of nutrient deprivation. Figure 20 shows that after seeding in glutamine free medium, incubating in normoxic

conditions followed by oxygen treatment for a further 24 h, the percent biomass decreased for all oxygen treatments. There was also a reduction in biomass for cells cultured in control medium when exposed to anoxia, however the decrease was much lower and cells did not appear to be stressed under this condition compared to what was observed when glutamine was removed.

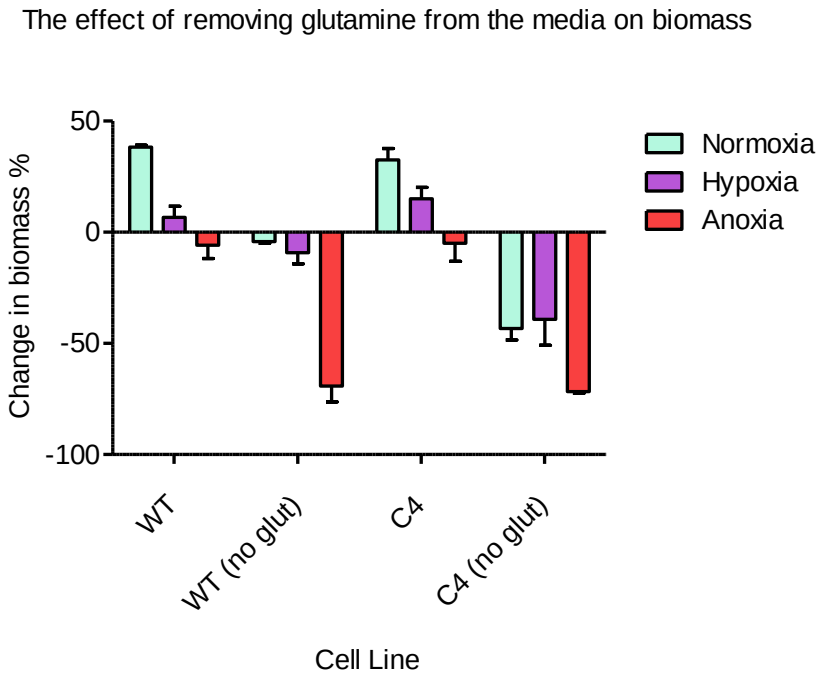

Figure 20: Final cell counts representative of biomass (expressed as percent increase from time of seeding to harvesting) after oxygen treatment, where cells were initial seeding was 100 000 cells/ml. Both HEPA-1 wild type (WT) and C4 cells were cultured in control medium and medium with no glutamine. The mean ± 1 s.e.m from 3 biological replicates is shown for each. For all oxygen conditions and in both cell lines, the biomass was significantly lowered by eliminating glutamine from the media (p<0.001).

MTT assays were undertaken to assess the proliferative ability in cells after exposure to medium containing no glutamine. Neither WT nor C4 cells had the ability to proliferate back to levels observed in the control for each cell line after exposure to glutamine free medium. Assays were taken directly after oxygen treatment and a further three days later following re-oxygenation in normoxia. This was done to observe the immediate and long term effects of culturing cells in glutamine free medium. The results from the MTT assay taken directly after exposure to oxygen treatment and a further three days after oxygen treatment are shown in Figure 21 and Figure 22 respectively.

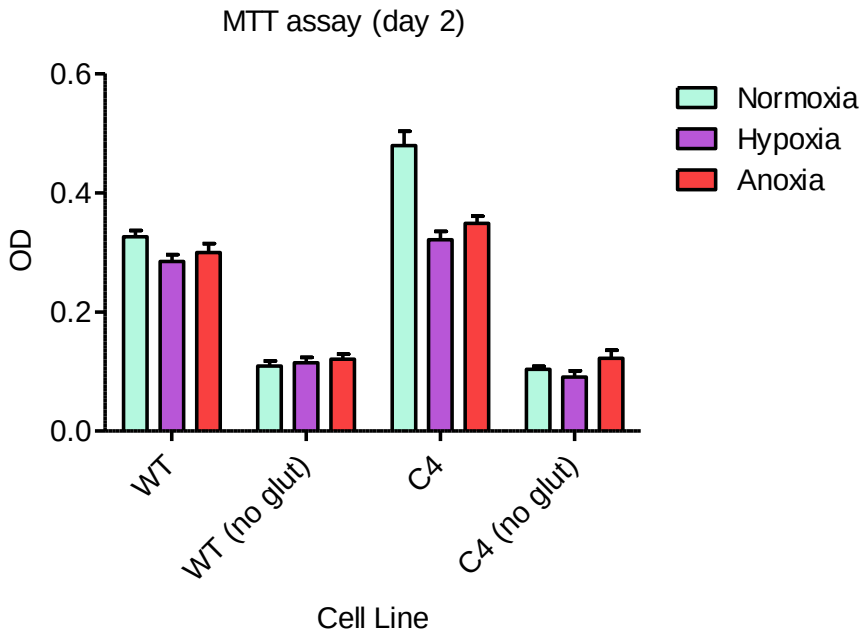

Figure 21: The effect of depriving HEPA-1 cells of glutamine when exposing to normoxia (21 % oxygen), hypoxia (1 % oxygen) and anoxia (0 % oxygen) determined by MTT proliferation assay taken directly after exposure. The mean ± 1 s.e.m from 6 biological replicates is shown for each. For all oxygen conditions and in both cell lines, the biomass was significantly lowered by eliminating glutamine from the media (p<0.001).

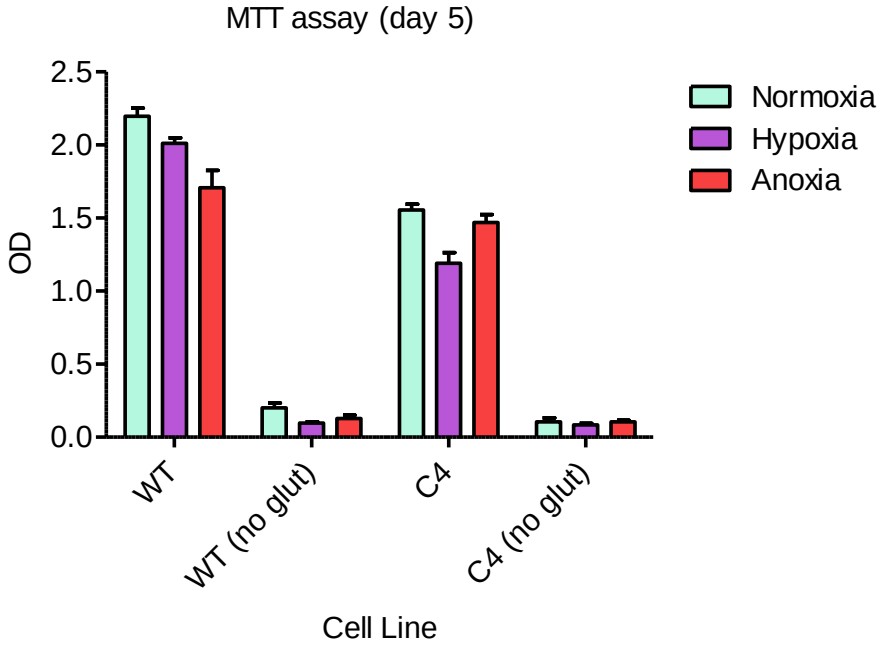

Figure 22: The effect of depriving HEPA-1 cells of glutamine when exposing to normoxia (21 % oxygen), hypoxia (1 % oxygen) and anoxia (0 % oxygen) determined by MTT proliferation assay taken three days after exposure, where cells were restored in control medium after oxygen treatment and incubated in normoxia. The mean ± 1 s.e.m from 6 biological replicates is shown for each. For all oxygen conditions and in both cell lines, the biomass was significantly lowered by eliminating glutamine from the media (p<0.001).

A subsequent set of experiments involved determining the growth of WT and C4 cells in control medium and 4 other reduced media (see Table 2). The curves for each are shown in Figure 23. The curves for both cell lines grown in medium 3: MEM substituted with FCS and ammonium sulphate as the nitrogen source showed no significant growth and very little biomass was yielded. Media 4 and 5 contained a rich supply of FCS, glucose and nitrogen source but no other nutrients, just salts. The curves for both cell lines grown in these media started promising with a peak in growth after the first measurement at 72 h; however the curves indicated cell senescence after this time. It was therefore determined that control medium was the best for representing steady state in growth and for yielding significant biomass for both WT and C4 cells and was therefore the one used in subsequent experiments. The only medium to show a resemblance of a typical sigmoid growth curve and in fact growth in general for either cell line other than the control medium was medium 2: MEM substituted with FCS and glutamine. However, the overall biomass for both WT and particularly C4 cells was reduced when cultured in this medium.

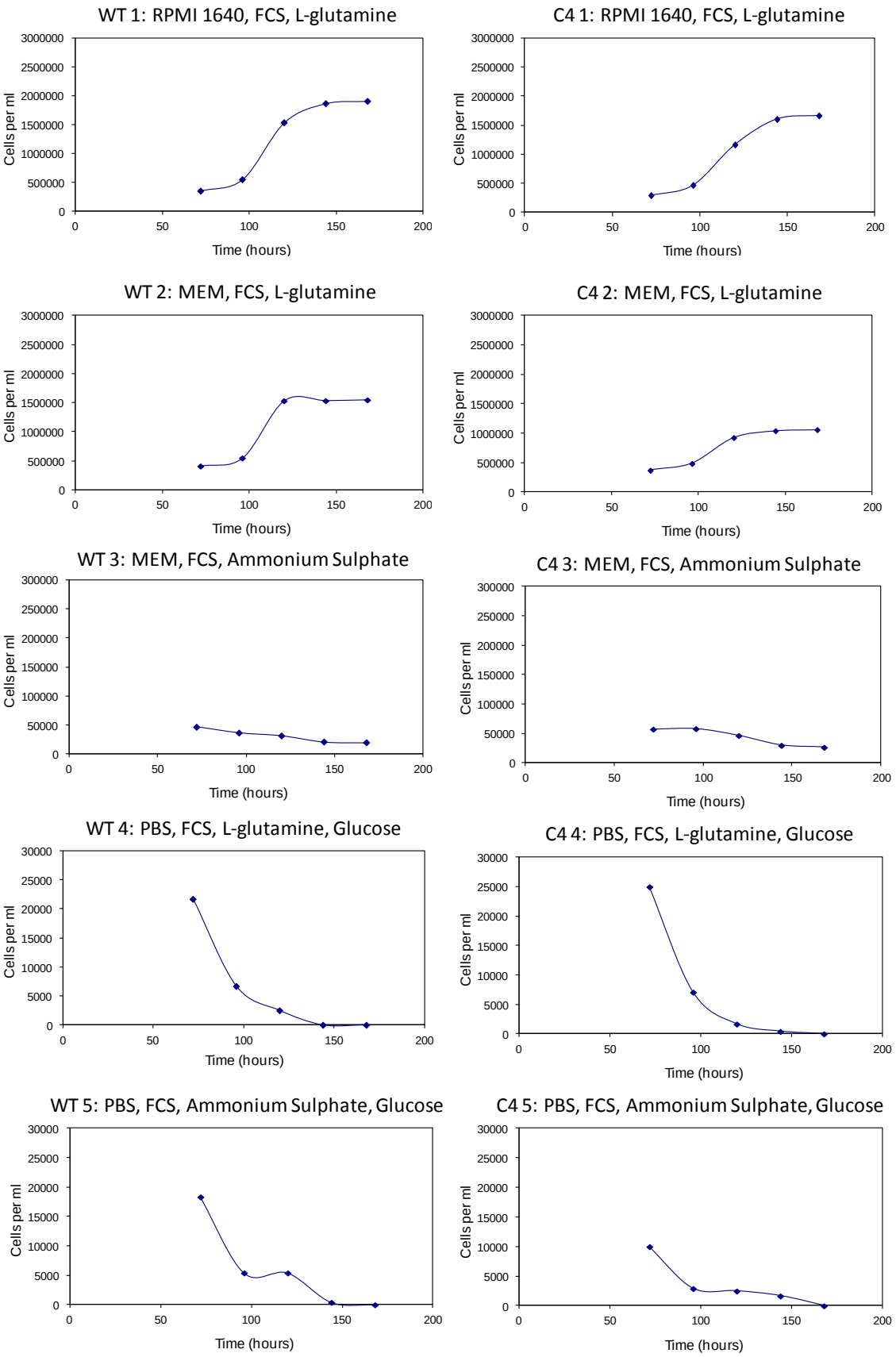

Figure 23: Growth curves for HEPA-1 wild type (WT) and C4 cells grown over 168 h in media described in Table 2. Each graph is scaled according to the number of cells/ml and varies with different media.

Glutamine can be used as an alternative carbon source to glucose through the glutaminolysis pathway[149]. By removing this option, it was hoped that alterations in glycolysis and associated pathways such as the TCA cycle could be inferred directly from the behaviour of cell lines under different oxygen potentials with respect to glucose uptake and utilisation. However, preliminary data suggested that the effect of depriving cells of glutamine was detrimental to cell growth and proliferation. This is consistent with observations in the literature[149, 150]. Furthermore, the effect was amplified after a longer period of time, even when the glutamine was replenished in the medium. Although the length of the experimental procedure is such that the effect was not as bad as it could have been, it is obviously detrimental to remove this metabolite from the growth medium as it allows cells to perturb from steady state, which is not desirable for studying the system's biology. It was hoped that ammonium sulphate could replace glutamine as the nitrogen source in the medium; however this was unsuccessful most likely as glutamine is used as a carbon source as well as nitrogen, particularly in tumours which is a role that cannot be fulfilled by ammonium sulphate.

3.2.4. Investigating which medium constituents are used in cell culture

To assess which metabolites were utilised in the medium, extracellular footprints of HEPA-1 WT and C4 cells exposed to each oxygen treatment were analysed and compared to the constituents of cell free medium. This is shown in Table 4where percent differences between each extracellular footprint and cell free medium from the same batch are expressed. Positive values in the table indicate a net production of a particular metabolite, while negative values indicate a net consumption. All metabolites that are consumed by the cells are utilised by the cells and it is likely that at least some of the metabolites produced by cells are also used by cells to a lesser extent. A smaller volume of 50 µl was used for analysis of each sample to allow observation of cellular differences in the spectra. From this it was observed that a rich proportion of metabolites are consumed by both cell lines exposed to different oxygen potentials, some of which are only available in control medium. This further validates using this medium in experiments. Dialysis of the FCS was considered as a way to reduce the complexity of the control medium. However, this would remove metabolites that are precursors to cellular metabolism. These compounds would be available to a tumour *in situ*, so removing them would cause an alteration in cell behaviour and phenotype which would ultimately lead to a miss-representation of the true metabolic profile. Only metabolites that can be identified are represented in Table 4; however there

were many more metabolites that differed in relative concentration between extracellular footprints and cell free medium. At least some of the consumed metabolites shown in the table only occur in control medium, further indicating the appropriateness of using this medium in profiling experiments as opposed to any other reduced medium.

Table 4: Relative change (%) in metabolic profile of extracellular footprint compared to cell free medium analysed using gas chromatography-mass spectrometry (GC-MS), where positive values indicate net production and negative values indicate net consumption. Values are shown for both HEPA-1 cell lines: wild type (WT) and C4 cells exposed to each oxygen condition: normoxia (21 % oxygen), hypoxia (1 % oxygen) and anoxia (0 % oxygen). The net consumption of metabolites in all conditions is presented in (a), the net production of metabolites in all conditions is presented in (b) and metabolites with condition specific consumption/production are presented in (c).

a) Net consumption in all conditions

WT (21%)	C4 (21%)	WT (1%)	C4 (1%)	WT (0%)	C4 (0%)	Constituent
-100.0	-100.0	-99.3	-99.2	-99.0	-100.0	Nonadecanoic acid
-93.1	-92.1	-88.9	-91.0	-18.0	-89.0	Leucine
-74.1	-72.5	-52.3	-64.3	-35.6	-96.5	Phenylalanine
-73.6	-59.7	-89.0	-84.8	-81.9	-75.3	Sugar alcohol
-68.2	-66.4	-39.1	-54.8	-29.4	-43.3	Tryptophan
-66.5	-69.5	-45.8	-62.4	-24.4	-47.4	Methionine
-66.2	-67.7	-48.5	-65.6	-31.3	-42.3	Lysine
-58.5	-57.6	-31.8	-51.5	-27.6	-37.4	Tyrosine
-56.2	-73.1	-64.9	-68.3	-91.6	-59.6	Aspartate
-52.4	-56.2	-52.5	-100.0	-12.0	-52.2	Malonate
-47.6	-48.9	-25.1	-24.9	-31.7	-35.8	Monosaccharide
-45.6	-62.6	-29.4	-53.9	-4.4	-32.4	Arginine
-33.4	-30.4	-13.0	-19.7	-11.9	-22.5	Hexadecanoic acid
-31.4	-33.2	-12.2	-21.0	-34.6	-10.2	Pyroglutamate
-31.2	-36.4	-30.2	-36.1	-32.5	-30.5	Fructose
-27.3	-29.6	-13.1	-8.0	-12.6	-15.0	Octadecanoic acid
-13.0	-15.5	-2.0	-14.3	-1.3	-11.6	Myo-inositol
-10.6	-8.8	-50.1	-6.3	-48.4	-57.4	Phosphate

b) Net production in all conditions

WT (21%)	C4 (21%)	WT (1%)	C4 (1%)	WT (0%)	C4 (0%)	Constituent
8.8	5.3	65.7	19.4	14.7	43.2	Isoleucine
10.1	5.7	29.4	11.8	25.9	12.3	Urea
15.3	11.1	131.9	89.0	114	114.3	Cysteine
22.4	3.3	39.5	12.3	41.2	7.9	Benzoic acid
27.8	2.4	100.3	13.3	610.6	26.2	Alanine
28.3	18.9	77.8	44.8	64.0	51.5	Glycerol
55.6	19.0	94.8	26.2	5.4	44.8	Creatinine
75.7	62.0	120.3	80.4	47.0	102.6	Glutamine
100.0	100.0	100.0	100.0	100.0	100.0	4-hydroxyproline
100.0	100.0	100.0	100.0	100.0	100.0	Fumarate

114.9	94.7	219.5	178.2	184.0	178.8	Lactate
118.5	93.5	192.4	118.5	46.7	148.0	Sugar alcohol
137.0	-48.8	-33.8	-72.5	-20.2	-44.4	Histidine
151.9	94.2	135.6	64.1	44.1	61.6	Citrate
201.0	204.3	296.9	227.9	338.7	273.3	Succinate
321.9	230.7	177.6	140.0	7.1	98.9	Uracil
327.5	295.0	419.7	308.5	127.8	298.4	Malate
559.7	606.0	628.8	473.2	455.1	333.3	Pyruvate
801.7	1333.2	1076	1167.7	1167	1467.2	Lactose

c) Condition specific consumption/production

WT (21%)	C4 (21%)	WT (1%)	C4 (1%)	WT (0%)	C4 (0%)	Constituent
23.0	38.7	-32.2	-75.3	-74.4	-7.8	Glucose
3.6	-12.0	31.5	-6.0	57.6	21.2	Ornithine
-18.7	-17.2	68.3	34.9	-7.8	54.7	Threonine
-25.5	-34.6	3.3	-30.9	-31.6	-16.6	Asparagine
-26.3	-42.1	-2.2	-43.7	5.9	-14.9	Citrulline
-28.3	-37.9	33.1	-8.5	12.9	11.8	Proline
-29.7	-25.5	22.8	-3.4	-9.8	31.3	Serine
-41.4	-36.5	6.1	-15.7	-16.1	-0.2	Valine
-53.4	-40.2	-24.8	-35.3	7.6	-23.2	Glycine

While some metabolic profiling studies have used MEM[38], it was decided in preliminary experiments for this research that this had too negative an effect on the growth and biomass of cells using the optimised experimental procedure for metabolite extraction and profiling. Furthermore, many constituents of the control medium were shown to be used in cell growth, so removing such metabolites could not be justified when aiming to analyse cells in as steady a state as possible, an essential requirement for modelling in systems biology. A trade off must be done between obtaining some information regarding the extracellular footprint and the validity of data for either extracellular footprint or intracellular fingerprint. Subsequently it has been decided that in order to gain a truer representative of the system, metabolic profiling will only be used to analyse the intracellular fingerprint. Measurements of the movement of cellular metabolites into the medium can be more appropriately obtained using other experimental techniques such as flux analysis[151].

3.2.5. Validation of the normoxic treatment

Although the oxygen conditions selected are acceptable to represent normoxia, hypoxia and anoxia in the literature[116], 21 % oxygen is particularly high and not a physiologically relevant condition. Although the peri-cellular oxygen level would be much lower than the oxygen level in the gas, further investigation was done to confirm 21 % a reasonable oxygen condition to use rather than 5 % which may be considered to be closer to the physiological level. FT-IR spectroscopy was used as a global profiling method to confirm 21 % oxygen as a valid condition to represent normoxia. For this, the intracellular fingerprints of HEPA-1 WT and C4 cells cultured at 21 %, 5 %, 1 % or 0 % were compared. Figure 24 shows the scores plots of PC 1 versus PC 2 for WT and C4 cells; where in both cases there is a grouping of 21 % and 5 % samples that separate from the lower oxygen samples. This indicated that there was no significant difference between the profiles of cells cultured at 21 % compared to 5 % suggesting that the peri-cellular level of oxygen may even be similar between the two conditions. It was therefore decided that either could be used to represent the normoxic condition, thus validating the use of 21 % oxygen in metabolic profiling experiments.

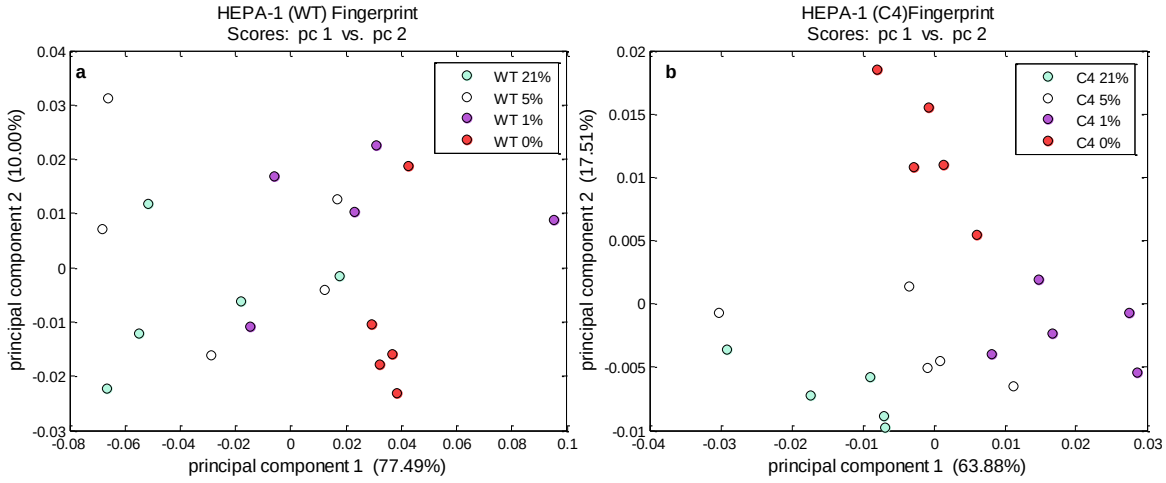

Figure 24: Principal component analysis (PCA) scores plots of principal component (PC) 1 versus PC 2 for intracellular fingerprints of HEPA-1 wild type (WT) (left) and C4 (right) cells exposed to 21 % oxygen, 1 %, 5 % and 0 % oxygen. In both cell lines, intracellular profiles from 21 % and 5 % oxygen group and separate from 1 % and 0 % highlighting the similarity between 21 % and 5 %.

3.2.6. Cell cycle analysis

Flow cell cytometry was used as a method to determine cell cycle characteristics after oxygen treatments and to compare WT and HIF-1 deficient cell models under varying oxygen conditions. In the HCT 116 model, EV cells were also analysed to control for properties of the construct. The analysis was done by exposing all cell lines to experimental oxygen for 24 h following 24 h in normoxic conditions (21 %). Cells were ethanol fixed and treated with propidium iodide to stain the DNA from which the fluorescence was detected as described in section 2.7. This experiment was undertaken to compare the effect of HIF-1 or oxygen exposure on the cell cycle that may affect the interpretation of metabolic profiling results. The percentage of cells in each stage of the cell cycle is shown in Figure 25 and Figure 26 for the HEPA-1 model and the HCT 116 model respectively.

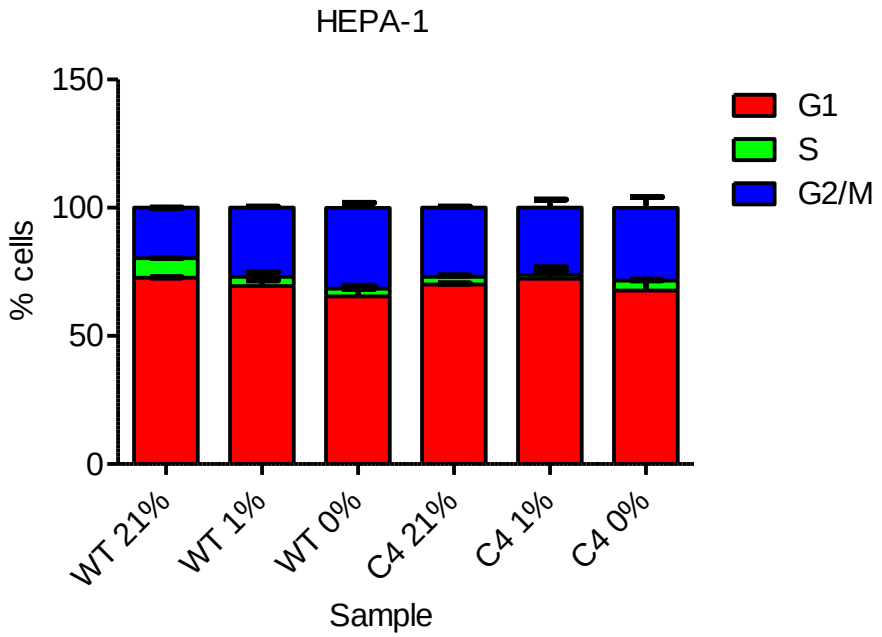

Figure 25: Composite bar chart for the percentage of cells in each phase of the cell cycle for each cell line and experimental oxygen condition in the HEPA-1 model. The mean ± 1 s.e.m from 3 biological replicates is shown for each. There was no obvious difference in the percentage of cells in each stage of the cell cycle caused by cell oxygen or hypoxia inducible factor 1 (HIF-1) (p>0.05).

The percentage of cells in S phase was low for all cell lines exposed to all oxygen treatments. In the HEPA-1 model, there was little observed difference in the distribution of cells in each phase as a result of HIF-1 or oxygen. In the HCT 116 model, there was evidence of a decrease in the number of cells in G1 phase and increase in G2 phase with decreasing oxygen. However, this was consistent between WT, EV and DN cells. It is suggested in the literature that hypoxia can cause G1 arrest[152-154], but since the G1 peak did

not increase with a decrease in oxygen exposure, it was concluded that this was not the case over the exposure time assessed. This provided confidence that the exposure time chosen for oxygen conditions was appropriate for metabolic profiling.

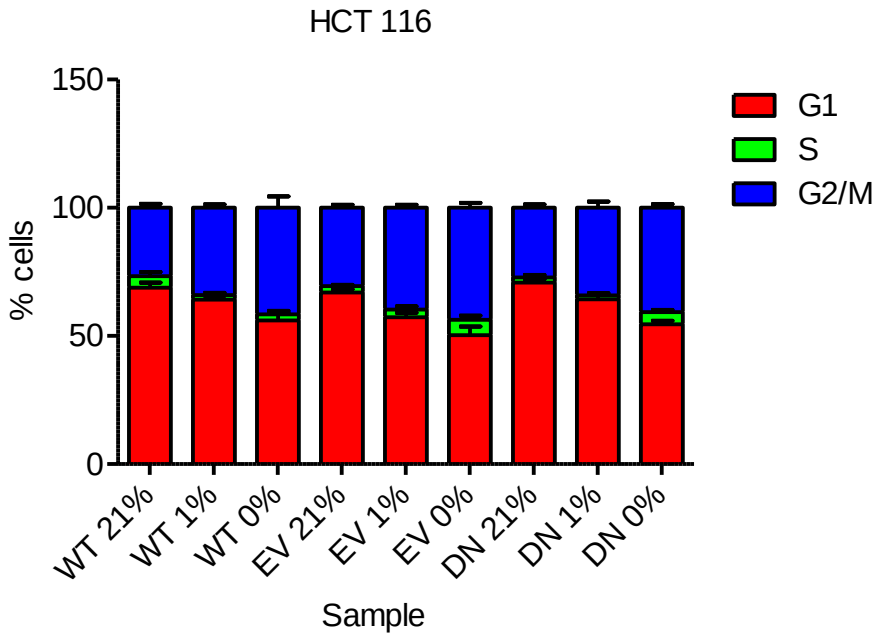

Figure 26: Composite bar chart for the percentage of cells in each phase of the cell cycle (G1, S or G2/M) for each cell line (wild type (WT), empty vector (EV) and dominant negative (DN)) and experimental oxygen condition (normoxia: 21 % oxygen, hypoxia: 1 % oxygen and anoxia: 0 % oxygen) in the HCT 116 model as determined from flow cytometry. The mean ± 1 s.e.m from 3 biological replicates is shown for each. Although there was a slight shift from gap 1 (G1) to gap 2/mitotic (G2/M) phase with decreasing oxygen there was no significant difference resulting from hypoxia inducible factor 1(HIF-1) (p>0.05) and the relative percentage of cells in each phase remains the same with most cells in G1.

3.2.7. Biochemical assays

Central carbon metabolism is a vital metabolic sub-network in cancer cell survival. The sub-network comprises the glycolytic pathway, TCA cycle and other pathways that either feed in to deliver molecules to be catabolised to produce energy or feed out supplying carbon for biosynthesis[19]. Glucose, glutamine and lactate are key metabolites within central carbon metabolism and the flux of these metabolites has been measured to assess how they are changed in the presence or absence of HIF-1 and under high or low oxygen. For this all cell lines were compared having been exposed to anoxia or maintained in normoxia to compare the extreme oxygen conditions. The flux of each metabolite was determined by calculating the difference in metabolite concentration from 0 min to 300 min exposure and expressing it in terms of mM/gDw/h. These experiments were not designed to be compared to metabolic profiling in subsequent chapters since the exposure

time was much shorter. Rather, the aim of these experiments was to unveil the initial effect of oxygen exposure on central carbon metabolite flux while cells were at an approximate steady state.

It is thought that hypoxic cells rely on the glycolytic pathway for energy production and that HIF-1 stimulates extracellular glucose import[155]. Figure 27 shows the net intracellular flux of glucose from the extracellular medium. Although extracellular glucose import is stimulated in WT cells where HIF-1 is active, and is increased in anoxia for the HEPA-1 model, it is decreased in anoxia for the HCT 116 model. The uptake of glucose for EV cells follows the same pattern as WT cells when comparing oxygen levels, suggesting that the construct itself is not affecting the results for DN cells.

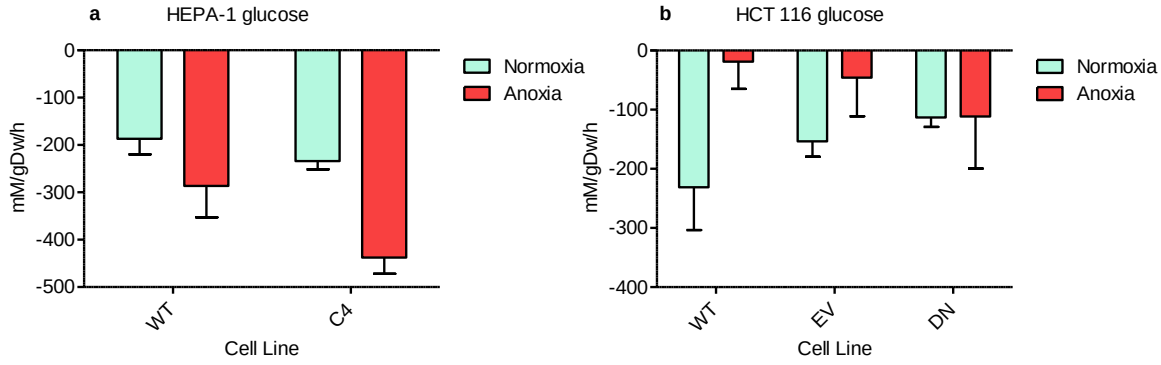

Figure 27: Net flux of glucose from the media over 300 min for (a) cell lines in the HEPA-1 model and (b) cell lines in the HCT 116 model. The negative flux indicates uptake of glucose from the medium into the cells over time. The mean ± 1 s.e.m from 3 biological replicates is shown for each. The difference between normoxia and anoxia was significant in C4 cells (p<0.05), but in all other cases the differences were not significant.

Since the efficiency of mitochondria is thought to be decreased in hypoxic cancer cells, pyruvate is not used by mitochondria in hypoxia and is instead converted to lactate which is subsequently effluxed from the cell[155]. This is consistent with the observed fluxes of lactate in all cell lines measured and shown in Figure 28. In all cases the efflux of lactate was higher in anoxia since when oxygen is limiting, oxidative phosphorylation cannot provide the necessary ATP production and therefore pyruvate is converted to lactate rather than translocating to the mitochondria to supply the TCA cycle and subsequently oxidative phosphorylation. Again, HCT 116 EV cells behave similarly to the WT cells, suggesting the construct itself has no influence on the result for DN cells. It is also suggested in the literature that the accumulation of pyruvate and NADH in the cytoplasm that induces LDH conversion of these products into lactate and NAD is HIF-1 activated[156]. There was not enough evidence from this investigation to reject the null hypothesis that this was not a

HIF-1 mediated process since in both cell lines the standard error is too great to conclude a significant difference between WT and HIF-1 deficient cells in either HEPA-1 or HCT 116 models. Similarly this data alone cannot indicate whether the efflux of lactate through the MCT 4 is HIF-1 mediated as suggested in the literature[157].

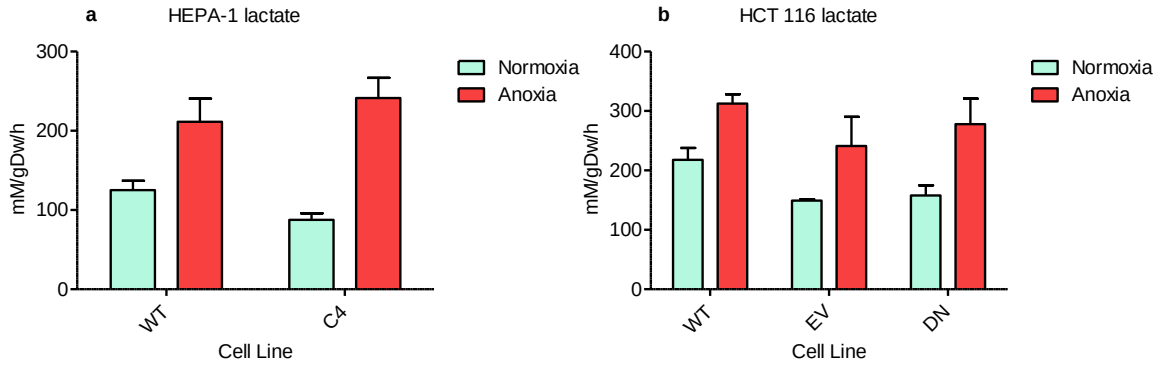

Figure 28: Net flux of lactate to the media over 300 min for (a) cell lines in the HEPA-1 model and (b) cell lines in the HCT 116 model. The positive flux indicates efflux of lactate from the medium into the cells over time. The mean ± 1 s.e.m from 3 biological replicates is shown for each. In the HEPA-1 model there was a significant difference between normoxia and anoxia for WT (p<0.05) and C4 cells (p<0.01). In the HCT 116 model the difference between normoxia and anoxia was significant in DN cells (p<0.05).

The uptake of glutamine was observed to be lower under anoxic conditions for all cell lines and is shown in Figure 29. It is known that glutamine is an important carbon source in cancer cells but that its induction is not likely linked to hypoxia[158]. This is consistent with these data since the uptake of glutamine is higher in normoxic cells than anoxic cells. There was no apparent effect of HIF-1 on glutamine uptake from these data; however the flux of glutamine for all cells was similarly as high as glucose, confirming that glutamine is a vital metabolite for cancer cell survival irrespective of HIF-1.

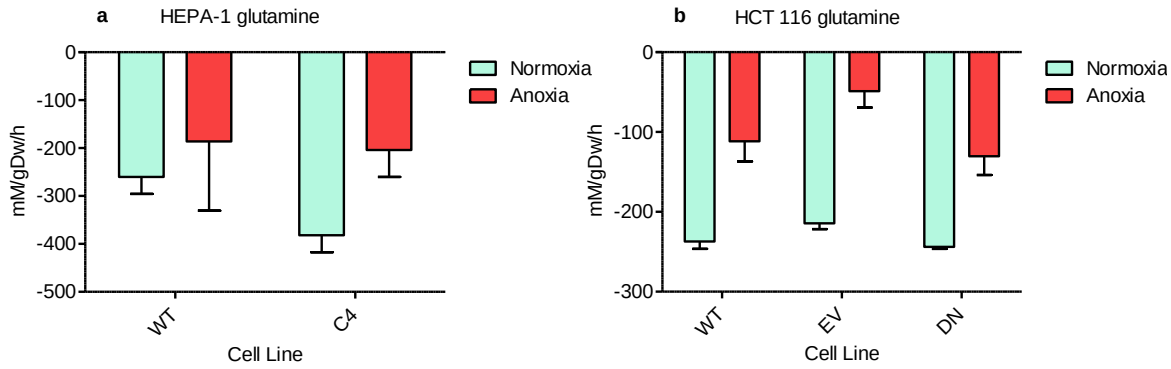

Figure 29: Net flux of glutamine from the media over 300 min for (a) cell lines in the HEPA-1 model and (b) cell lines in the HCT 116 model. The negative flux indicates uptake of glutamine from the medium into the cells over time. The mean ± 1 s.e.m from 3 biological replicates is shown for each. The results were not statistically significant in the HEPA-1 model; however there were significant differences between normoxia and anoxia in WT and EV cells (p<0.01) as well as DN cells (p<0.05).

3.2.8. Developing a method for metabolic profiling

Before high throughput metabolic profiling analysis by GC-MS a robust protocol was needed with the aim of identifying the suitability of the method to test the hypothesis that there are metabolic changes in phenotype with respect to oxygen exposure and HIF-1. Due to laboratory restrictions, the number of conditions to be tested (HEPA-1 WT and C4 cells and HCT 116 WT and DN cells exposed to normoxia, hypoxia and anoxia) and the large scale of the investigation (30 biological replicates) included in the high-throughput analysis meant that samples had to be collected sequentially over a period of 2 weeks per cell model (2 weeks for HEPA-1 and 2 weeks for the HCT 116 model). Preliminary metabolic profiling studies were performed for the HEPA-1 model using GC-MS to test whether or not the oxygen conditions chosen are appropriate to show a metabolic change due to oxygen and to see if HIF-1 has an effect on metabolic phenotype under different oxygen conditions. Samples were collected in 3 batches between which cells were passaged once and all batches were collected over 3 weeks. This was done to ensure the results were not sensitive to which batch in which samples were collected and that the experimental design of collecting samples over a series of batches can be used with confidence in high throughput metabolic profiling. Another experiment was done to compare WT, EV and DN cells in the HCT 116 model. This was done to identify any effects of the construct on metabolic profile such that any similarities between EV and DN cells that are not apparent in WT cells will not be recorded as differences between WT and DN cells attributed to HIF-1 in subsequent metabolic profiling by any method.

For the first investigation to test whether it was viable to collect samples over a number of weeks/passages, cell lysates were prepared for HEPA-1 WT and C4 cells exposed to normoxia, hypoxia or anoxia. This included 5 replicates for each cell line under each condition cultured and harvested over a three week period where the first biological replicate for each condition came from week 1, the second 2 from week 2 and the last 2 from week 3. Each week cells were seeded at one passage higher than the previous but cells were seeded in medium from the same batch. This resulted in 30 samples in total for intracellular fingerprinting which were analysed in a randomised order by GC-MS. The drift of internal standard (succinic d_4 acid in water) with respect to variation in peak area within each sample was calculated and accounted for by normalising all metabolite peaks to this.

After normalisation, PCA was used to show the chemical differences in each cell line exposed to each oxygen condition. The results from this for the intracellular fingerprints are shown in Figure 30. These are scores plots which separate samples as being positive or negative for a particular chemical phenotype described by each PC; those samples that possess a certain phenotype described by PC 1 lie in the positive region of the x-axis while those that don't lie in the negative portion after this separation. Those samples that possess a certain phenotype described by PC 2 lie in the positive region of the y-axis while those that don't lie in the negative portion. The percent of the total variation described by each PC 1 and 2 are shown on the x and y axis respectively. Figure 30 shows the separation in normoxia samples and low oxygen samples (hypoxia and anoxia) for WT cells described in PC 1 representing 50% of the total variance in WT samples. There is no true separation in C4 cells across the first four PCs accounting for over 87 % of the total variance, suggesting that oxygen tension has no clear effect on the metabolome of C4 cells.

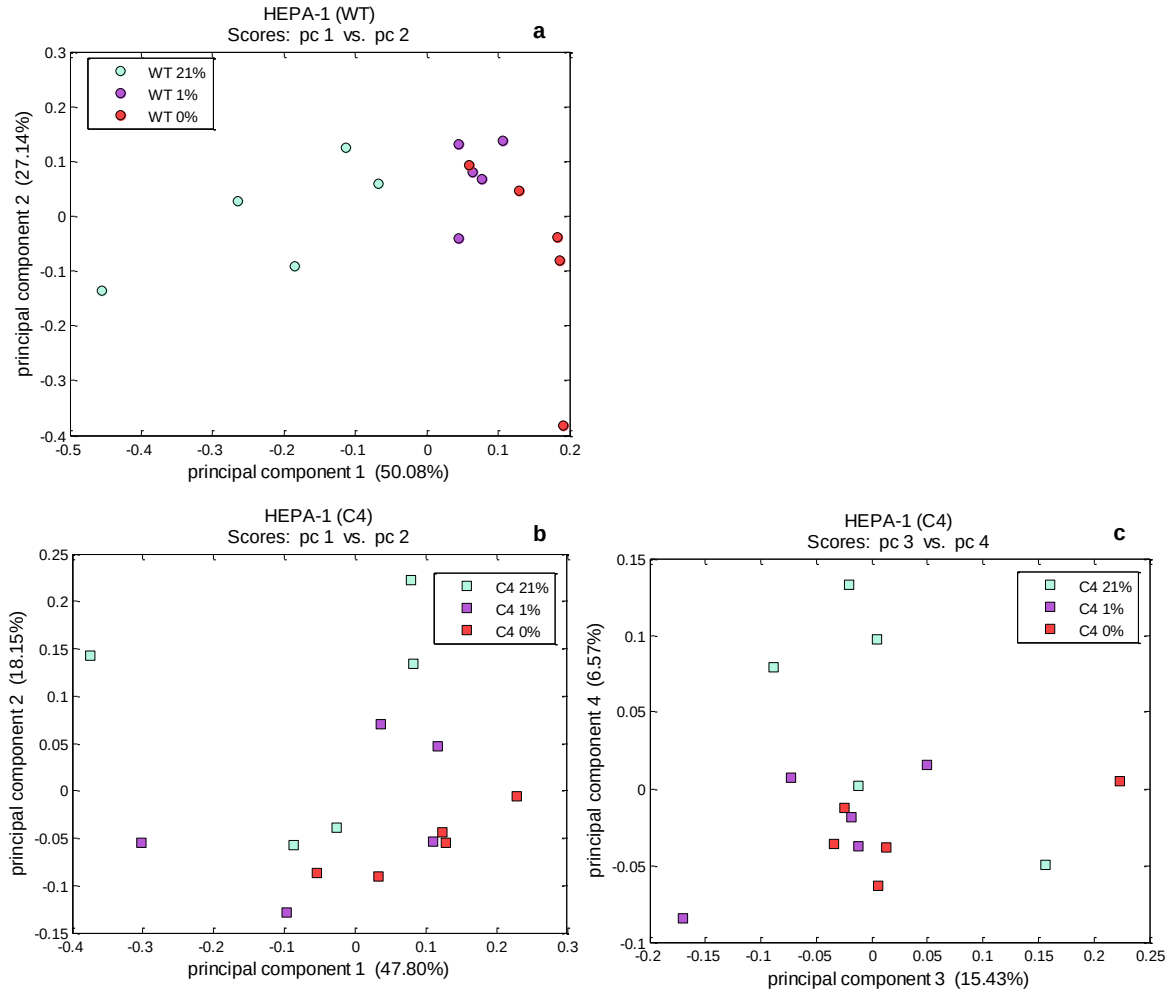

Figure 30: Principal components analysis (PCA) scores plots for intracellular fingerprints of HEPA-1 wild type (WT) and C4 cells exposed to oxygen treatments: normoxia (21 % oxygen), hypoxia (1 % oxygen) and anoxia (0 % oxygen). (a) shows the separation between normoxia and low oxygen in the metabolome of WT cells in principal component (PC) 1 and (b) and (c) show there is no separation in the first four PCs accounting for over 87 % of the total variation in C4 cells, suggesting the separation in WT cells could be due to a hypoxia inducible factor 1 (HIF-1) related metabolic mechanism.

PCA was also applied to the same data labelled by the week in which the biological samples were collected. Although it is possible to analyse a vast quantity of samples sequentially by GC-MS, the acquisition of samples on a much larger scale would not be possible in one session from cells of the same passage. Therefore it was necessary to determine whether or not it is possible to collect samples in batches over a period of up to three weeks where cells are passaged up to six times. Figure 31 shows there is no separation due to weeks and so any variation in either cell line can be confirmed as biological.

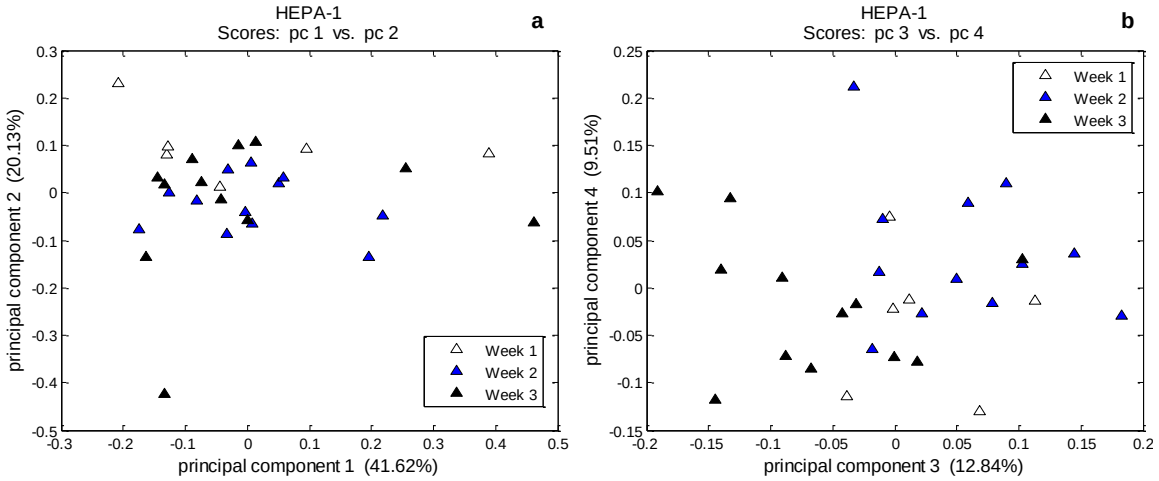

Figure 31: Principal components analysis (PCA) applied to HEPA-1 gas chromatography-mass spectrometry (GC-MS) data labelled by the week in which the biological sample was collected. There was no separation due to the week in which any sample was harvested which gives confidence to the confirmation of biological separation validates harvesting samples over a series of up to three weeks.

For the second investigation to control for differences in HCT 116 WT and DN cells that are due to the construct and not HIF-1 itself, cell lysates were prepared for HCT 116 WT, EV and DN cells exposed to normoxia, hypoxia or anoxia. This included six replicates for each cell line under each condition and a total of 54 samples were analysed in random order by GC-MS.

As before the drift of internal standard (succinic d_4 acid in water) with respect to variation in peak area within each sample was calculated and accounted for by normalising all metabolite peaks to this. After normalisation, PCA analysis was used to show the chemical differences in each cell line exposed to each oxygen condition and is shown in Figure 32. In all 3 cases there is no suggestion of a chemical grouping between EV and DN cells due to the construct. In normoxia and anoxia, WT cells group with EV cells and group away from DN cells suggesting that either can be used as a control to compare DN cells to. In hypoxia there is no clear separation but there is no suggestion of a construct based

separation either so the appropriateness of using only WT cells as a control for metabolic high throughput metabolic profiling of HIF-1 in the HCT 116 model.

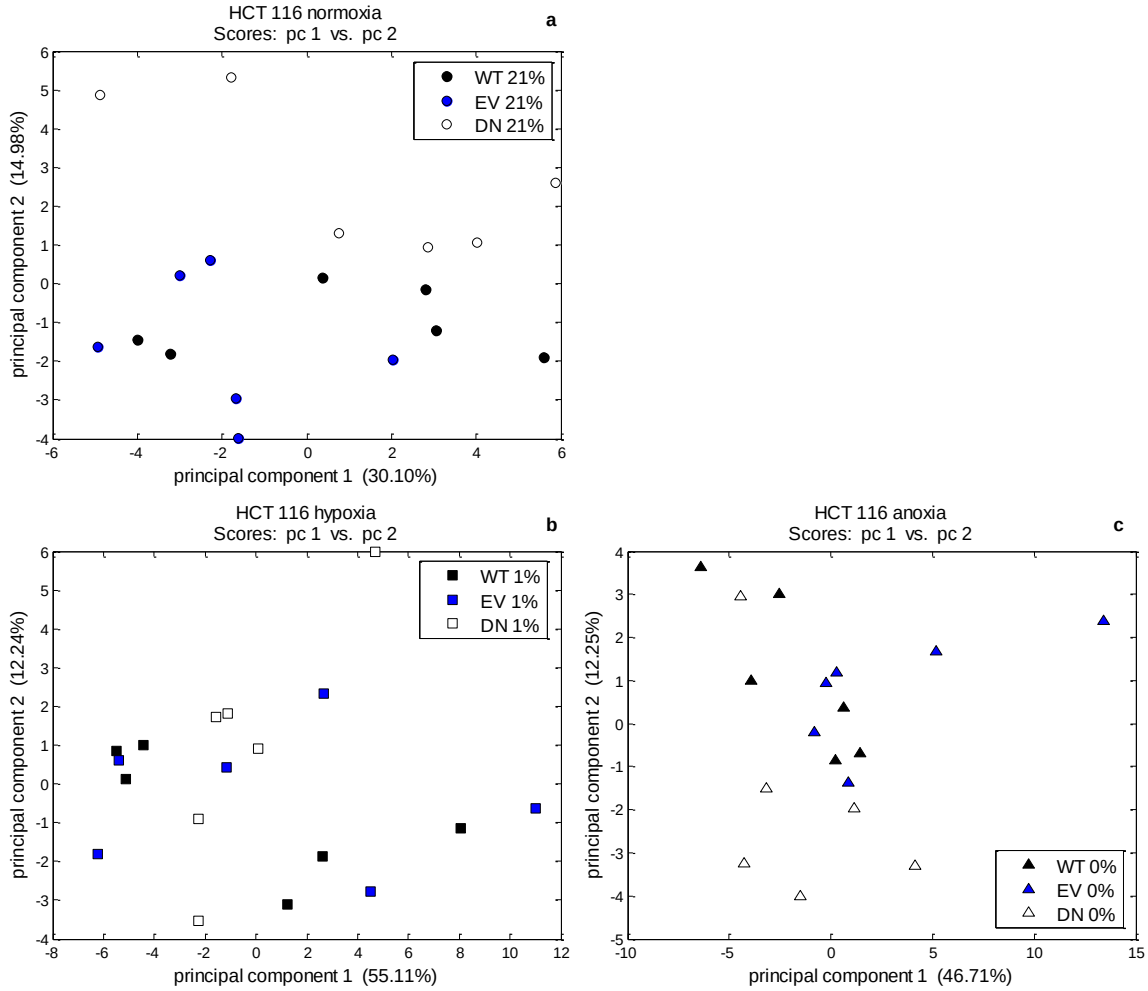

Figure 32: Principal components analysis (PCA) scores plots for intracellular fingerprints of HCT 116 wild type (WT), empty vector (EV) and dominant negative (DN) cells exposed to oxygen treatments: (a) normoxia (21 % oxygen), (b) hypoxia (1 % oxygen) and (c) anoxia (0 % oxygen). In normoxia and anoxia, WT cells group with EV cells and group away from DN cells suggesting that their metabolic phenotype is more similar to each other than with DN cells. In hypoxia there is no clear separation but there is no suggestion of a construct based separation.

3.3. Conclusion

A range of investigations were undertaken to test the characteristics of each cell line that are useful for the interpretation of data in subsequent chapters. The HEPA-1 model was tested to compare its growth rate to the literature, to optimise seeding density and medium to be used in all subsequent experiments and to develop a method for metabolic profiling by GC-MS, many aspects of which will be maintained for metabolic profiling by UHPLC-MS or ToF-SIMS. It was also used to show that 21 % oxygen is a suitable control to represent normoxia. The HCT 116 model was used to assess the effects of the construct

that is used to silence HIF-1α in DN cells by comparing EV cells to WT and DN cells. This seemed to have no effect on the metabolic profile determined by GC-MS and therefore DN cells can be compared only to WT cells in subsequent metabolic profiling. The expression of HIF-1 was tested using the luciferase assay in both cell models and showed HIF-1 deficiency where expected, thus validating the cell models for subsequent experiments. Cell cycle analysis of all cell lines was done to ensure the experimental design with respect to the cell lines and oxygen treatments chosen was appropriate and that differences in the metabolic phenotype between experimental groups will not be due to effects on cell cycle such as apoptosis or cell cycle arrest. Finally, the flux of 3 central carbon metabolites was determined for all cell lines as an initial investigation into whether or not oxygen availability and HIF-1 show to have an effect on central carbon metabolism. From this study alone, it is not clear whether or not HIF-1 mediated responses to oxygen availability affect central carbon metabolism, which leads to the requirement for a more global profile of the metabolism to observe its effects on cellular phenotype.

Chapter 4. Metabolic profiling using GC- and UHPLC-MS

4.1. Introduction

Metabolic profiling is a widely accepted technique in the metabolomics community for the 'top-down' exploration of a biological system. There are many applications of metabolic profiling described in the literature for the study of a diverse range of systems, particularly in plant biology[159-162], microbiology[163-166] and medicine[62, 167-169]. It can be applied to the study of cell or tissue extracts[170, 171], or to extracellular fluids[63, 172], with the aim of better understanding the function of a system through analysing its components and exchange of components between intracellular and extracellular compartments. Furthermore there have been examples of metabolic profiling *in situ*[173-176], an interesting development that enables formation of a link between structure and function with respect to the metabolome. One of the main purposes in metabolic profiling is for biomarker discovery[177, 178]: the identification of metabolic signatures that appear to be representative of a particular system. For example, the identification of biomarkers can be particularly useful in the diagnosis or prognosis of a metabolic disorder or disease, or in identifying features in the metabolic phenotype that could be targeted in disease therapy. In this research metabolic profiling has been employed to discover potential biomarkers for HIF-1 metabolism in cancer through identifying metabolic signatures representative of HIF-1 function in hypoxia. Both human HCT 116 and murine HEPA-1 cell models have been investigated and metabolic profiles of WT and HIF-1 deficient cells have been analysed using GC-MS and in the HCT 116 model UHPLC-MS.

GC-MS is a widely used technique in metabolic profiling[63, 128, 159, 168, 179]. The technique benefits from being highly reproducible at a relatively low cost compared to other metabolomics platforms including UHPLC-MS, but above all capillary GC is excellent for complex metabolic profiling due to its high resolution, separation efficiency and sensitivity[180]. This highlights its appropriateness in the present research which involved the high-throughput GC-MS analysis of hundreds of metabolically complex samples. It is able to detect naturally volatile and thermally stable chemical species inclusive of low molecular weight hydrocarbons and lipids[180], and many other chemical species that meet the requirements for detection following chemical derivatisation[71], including amino acids and sugars. It is therefore highly valuable in profiling metabolites associated with central

carbon metabolism: a key area of the metabolome known to be affected by hypoxia and in particular HIF-1[181]. UHPLC-MS is a much more expensive technique with respect to instrument costs and the method for identifying chemicals is less advanced than GC-MS relying on identification by mass accuracy rather than chemical standards in libraries[180]. That aside, it is capable of analysing heat-liable chemicals and the high pressures and sub 2µm stationary phase particles in the column enhance chromatographic resolution and efficiency such that it is highly appropriate for resolving complex mixtures[180]. UHPLC-MS is complementary to GC-MS for metabolic profiling in terms of the metabolites it can detect, including a broad range of higher molecular weight metabolites and lipids, so for this reason it was decided to perform metabolic profiling with both analytical techniques. A much smaller sample set was analysed using UHPLC-MS compared to GC-MS mainly due to the higher associated cost and it being more challenging to identify metabolites and lipids. Nevertheless it was still valuable in profiling further beyond central carbon metabolism to elucidate the effects of HIF-1 in human HCT 116 cancer cells.

Intracellular extracts were prepared as described in chapter 2.9 and analysed as described in chapters 2.11 and 2.12. Extracts from cells without HIF-1function have been compared to WT cell extracts to observe what features are missing when HIF-1 is not functional but also to discover what features are added to promote cell survival in low oxygen environments despite the lack of HIF-1. The latter would be potentially as important as identifying apparent HIF-1 regulated metabolites as it allows one to pre-empt how cancer cells may respond if metabolic pathways controlled by HIF-1 were perturbed by a way of therapy to attempt to reduce its function in cancer. Cancer therapy based on perturbing pathways associated with identified metabolites will require both the knowledge of how the system functions preferentially (utilising HIF-1) and what back-up functions may be employed in the absence of HIF-1. Aside from revealing potential metabolic targets for future cancer therapy, revealing markers of HIF-1 metabolism could lead to a better understanding of the phenotype and may enable better diagnosis and prognosis of cancer in patients if certain biomarkers are screened for. Screening tumour extracts for relevant biomarkers determined for each oxygen level in these *in vitro* experiments could help identify the level of hypoxia in the tumour and whether or not it is likely that the cells in the tumour are showing signs of survival as opposed to cell death. In the present studies, cells were cultured in conditions with the aim of controlling effects on growth, proliferation and cell cycle as best as possible and the data in the previous chapter

suggested that any metabolites identified in the present chapter should be a function of cancer cell survival and not cell death.

4.2. Results and discussion

Samples for metabolic profiling by GC-MS and UHPLC-MS were collected over 4 batches for HCT 116 cells and 4 batches for HEPA-1 cells, where each batch contained an equal number of WT and HIF-1 deficient cells exposed to normoxia, hypoxia or anoxia. In total there were 6 experimental groups per cell model (WT and HIF-1 deficient forms exposed to normoxia, hypoxia or anoxia). In every batch, the level of HIF-1 transcriptional activity was measured for a sample in each experimental group using a luciferase reporter-based assay described previously (section 2.4). This was performed as a quality check to ensure HIF-1 transcriptional activity consistency between batches of samples collected for GC- and UHPLC-MS analysis. In all cases, HIF-1 was shown to increase in hypoxic and anoxic WT cells compared to normoxic WT cells; a trend that was not observed, or observed to a much lower effect, in HIF-1 deficient cells. The results from this are shown in Figure 33.

For GC-MS profiling of HCT 116 and HEPA-1 samples, 4 analytical batches were formed for each cell model by randomly selecting samples from each experimental group from all 4 sample collection batches. For UHPLC-MS analysis of HCT 116 samples, one analytical batch was formed in the same way. This reduced variability that many have occurred between sample collection batches. The QC samples were used to pre-process the GC-MS data in a way to reduce variability between analytical batches[61].

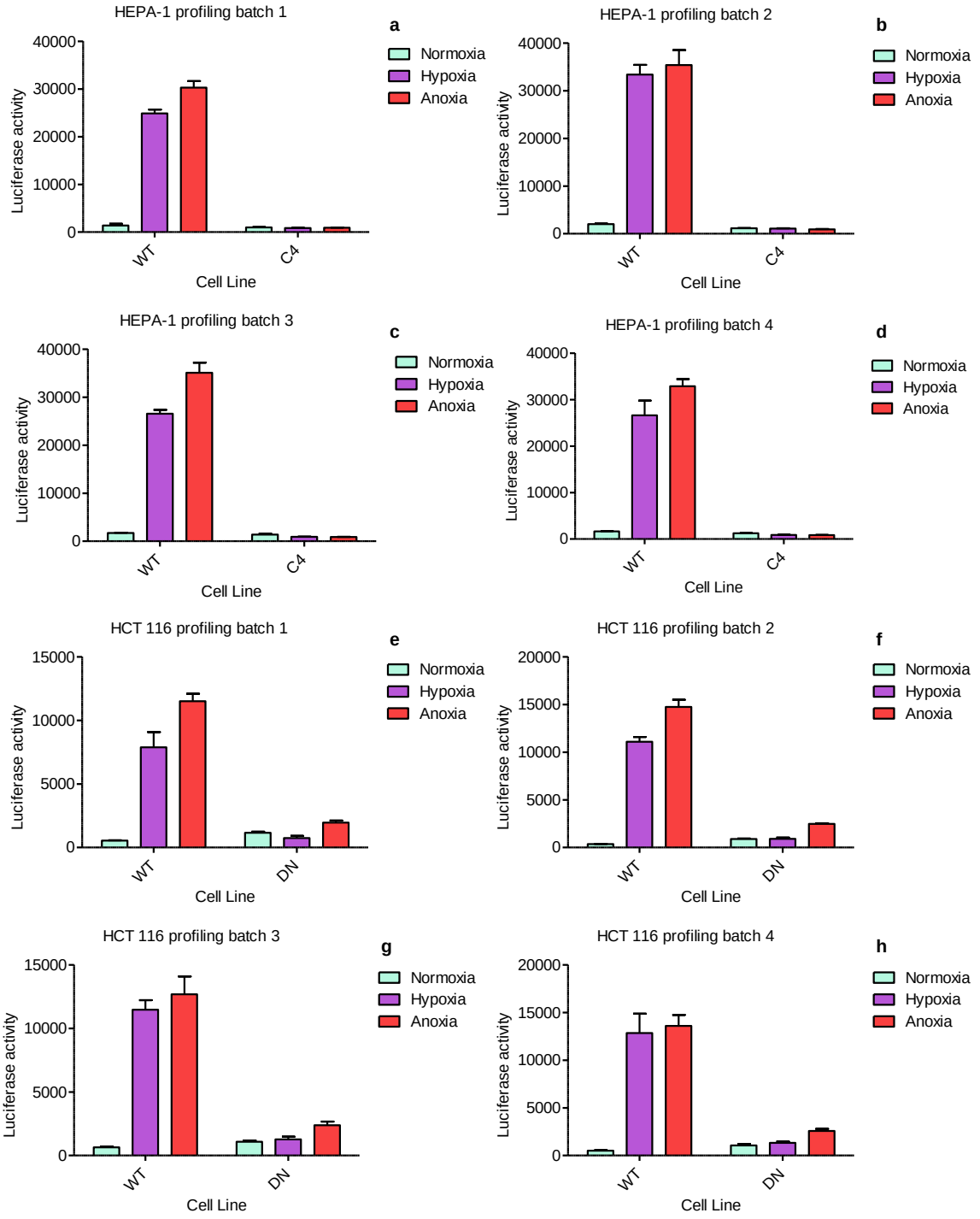

Figure 33: The absolute luciferase activity as a representation of hypoxia inducible factor 1 (HIF-1) activity. The activity was analysed using a luciferase reporter-based assay with an adenovirus containing a firefly luciferase reporter construct linked to the lactate dehydrogenase (LDH) hypoxia response element (HRE) sequence. The luminescence was measured to indicate the degree of HIF-1 expression for HEPA-1 wild type (WT) and C4 cells exposed to normoxia (21 % oxygen), hypoxia (1 % oxygen) and anoxia (0 % oxygen) in each of the four batches of profiling samples (a-d) and for HCT-116 WT and dominant negative (DN) cells exposed to normoxia, hypoxia or anoxia in each of the four batches of profiling samples (e-h). The mean ± 1 s.e.m from 3 biological replicates is shown for each and in all cases there was statistically significant increase in luciferase activity in WT cells exposed to hypoxia or anoxia (p<0.001) but not in C4 or DN cells exposed to hypoxia or anoxia.

A total of 42 and 41 peaks were identified as metabolites that had a relative standard deviation lower than 30 % in the GC-MS profiling of QC samples in the HCT 116 and

HEPA-1 models respectively. The level of identification reported was determined according to reporting guidelines as described by The Metabolomics Standards Initiative (MSI)[50]. In many cases peaks were singly identified with high confidence; however some peaks were putatively identified as multiple metabolites, usually due to several metabolites sharing identical EI mass spectra. Other singly identified metabolites were only identified putatively due to a low mass spectrum (MS) match score (below 80 % match) or due to an error in the observed retention index (RI) (outside the accepted tolerance of ±20 RI units). For some metabolites, for example aspartate, identifications were assigned to multiple peaks due to the presence of different derivatisation products of that metabolite, eluting with different RIs. Table 5 lists the metabolites identified by GC-MS including a unique identifier for each as determined by the Kyoto encyclopedia of genes and genomes (KEGG)[182].

Table 5: Metabolites identified in gas chromatography-mass spectrometry (GC-MS) data, showing only metabolites with a relative standard deviation lower than 30 % in quality control (QC) samples. All metabolites were identified in both HCT 116 and HEPA-1 cells except for leucine and xylitol/ribitol which were only identified in HCT 116 cells and phosphocreatinine which was only observed in HEPA-1 cells. The quality of identification is given for each, where putative identifications are explained. Where there were multiple peaks with a single identification these are numbered. Kyoto encyclopedia of genes and genomes (KEGG) compound identifiers are given where available.

Metabolite peak	Quality of identification	KEGG compound ID
Glycine	High Confidence	C00037
Lactate	High Confidence	C00186
Pyruvate	High Confidence	C00022
Leucine	High Confidence	C00123
Glycerol	High Confidence	C00116
Norleucine	High Confidence	C01933
Malonate	High Confidence	C00383
Phosphate	High Confidence	C00009
Threonine	Putative due to low MS match score	C00188
Phosphocreatinine	High Confidence	N/A
Beta-alanine	High Confidence	C00099
Erythronate/ Threonate	Putative (alternative library match)	C01620
Malate	High Confidence	C00149
4-aminobutyrate	High Confidence	C00334
Aspartate (1)	High Confidence	C00049
Aspartate (2)	High Confidence	C00049
4-hydroxyproline	High Confidence	C01015
Xylitol/ Ribitol	Putative due to RI error	C00379/ C00474
Cysteine	High Confidence	C00097
2-hydroxyglutarate	High Confidence	C02630
Methionine	High Confidence	C00073
Creatinine	Putative due to RI error	C00791
Glutamine	High Confidence	C00064

Putrescine	High Confidence	C00134
Glutamate	Putative due to low MS match score	C00025
Hypotaurine	High Confidence	C00519
Pyroglutamate	High Confidence	C01879
Fructose (1)	Putative due to RI error	C00095
2-oxoglutarate	Putative due to RI error	C00026
Fructose (2)	Putative, due to RI error	C00095
Fructose / Sorbose (1)	Putative due to RI error and identical EI mass spectra	C00095/C00764
Fructose / Sorbose (2)	Putative due to RI error and identical EI mass spectra	C00095/C00764
Glycerol-3-phosphate	Putative,due to RI error	C00093
Allose/Mannose/ Galactose /Glucose (1)	Putative due to RI error and identical EI mass spectra	C01487/C00159/ C00124/C00031
Allose/Mannose/ Galactose /Glucose (2)	Putative due to RI error and identical EI mass spectra	C01487/C00159/ C00124/C00031
Citrate	Putative due to RI error	C00158
Lysine	High Confidence	C00047
Allose/Mannose/ Galactose /Glucose (3)	Putative due to RI error and identical EI mass spectra	C01487/C00159/ C00124/C00031
Scyllo/*Myo*-inositol	Putative due to RI error and identical EI mass spectra	C06153/C00137
Tyrosine	Putative due to RI error	C00082
Tyramine/ Tyrosine	Putative due to RI error and identical EI mass spectra	C00483/ C00082
Hexadecanoic acid	High Confidence	C00249
Octadecenoic acid	High Confidence	C00712

In the UHPLC-MS metabolic profiling of HCT 116 samples, 5244 features were detected in positive ion mode of which over 1340 could be putatively identified as peaks from one or more metabolite or lipid and 1957 features were detected in negative ion mode of which over 920 could be putatively identified as peaks from one or more metabolite or lipid after application of the Taverna workflow for LC-MS metabolite identification[55]. This workflow utilised the HMDB[183], KEGG[182], LIPIDMAPS[184], BioCyc[185], and DrugBank[186] and therefore annotated metabolites from mammalian, plant, microbial or drug origin[55]. For this reason the identifications were manually assessed for their feasibility in mammalian systems and likely non-mammalian identifications were subsequently removed.

4.2.1. Univariate analysis of GC-MS data

Statistical testing in the form of ANOVA was applied to GC-MS data to identify peaks with significantly different mean areas between experimental groups. The data were observed to follow an approximately normal distribution after log transformation which, along with the replacement of statistical outliers with a mean value for the experimental group in which it was identified and along with being a large data set, made parametric testing applicable. The mean GC peak areas between each experimental group: HCT 116

WT and DN samples and HEPA-1 WT and C4 samples exposed to normoxia, hypoxia or anoxia were compared using a two-way ANOVA. Each cell model: HCT 116 or HEPA-1 was considered in turn to assess whether or not there were significant differences in metabolites from GC-MS with respect to oxygen across both WT and HIF-1 deficient samples or with respect to HIF-1 across all 3 oxygen levels. In both HCT 116 and HEPA-1 samples, almost all metabolites were found to differ significantly with respect to oxygen. The 4 most significantly different metabolites with respect to oxygen in the HCT 116 model were lactate, leucine, glycerol and beta-alanine. All 4 metabolites differed significantly with $p < 0.0001$ and box plots of peak areas in each experimental group are shown in Figure 34.

Lactate, leucine and glycerol all increased with a decrease in oxygen. Beta-alanine was higher in normoxic cells irrespective of HIF-1, where DN cells contained most beta-alanine. In WT samples beta-alanine was lowest in hypoxia then increased in anoxia to levels similar to normoxia, however equally low levels of beta-alanine existed in hypoxic and anoxic DN cells. This suggests that a non-HIF-1 mediated response to hypoxia is responsible for lowering the concentration of beta-alanine but in extreme oxygen deprivation HIF-1 instigates processes that raise the level of beta-alanine, or focus is moved from the process that suppresses beta-alanine in hypoxia to other HIF-1 mediated processes such that the concentration naturally rises back to normoxic levels as it is no longer controlled.

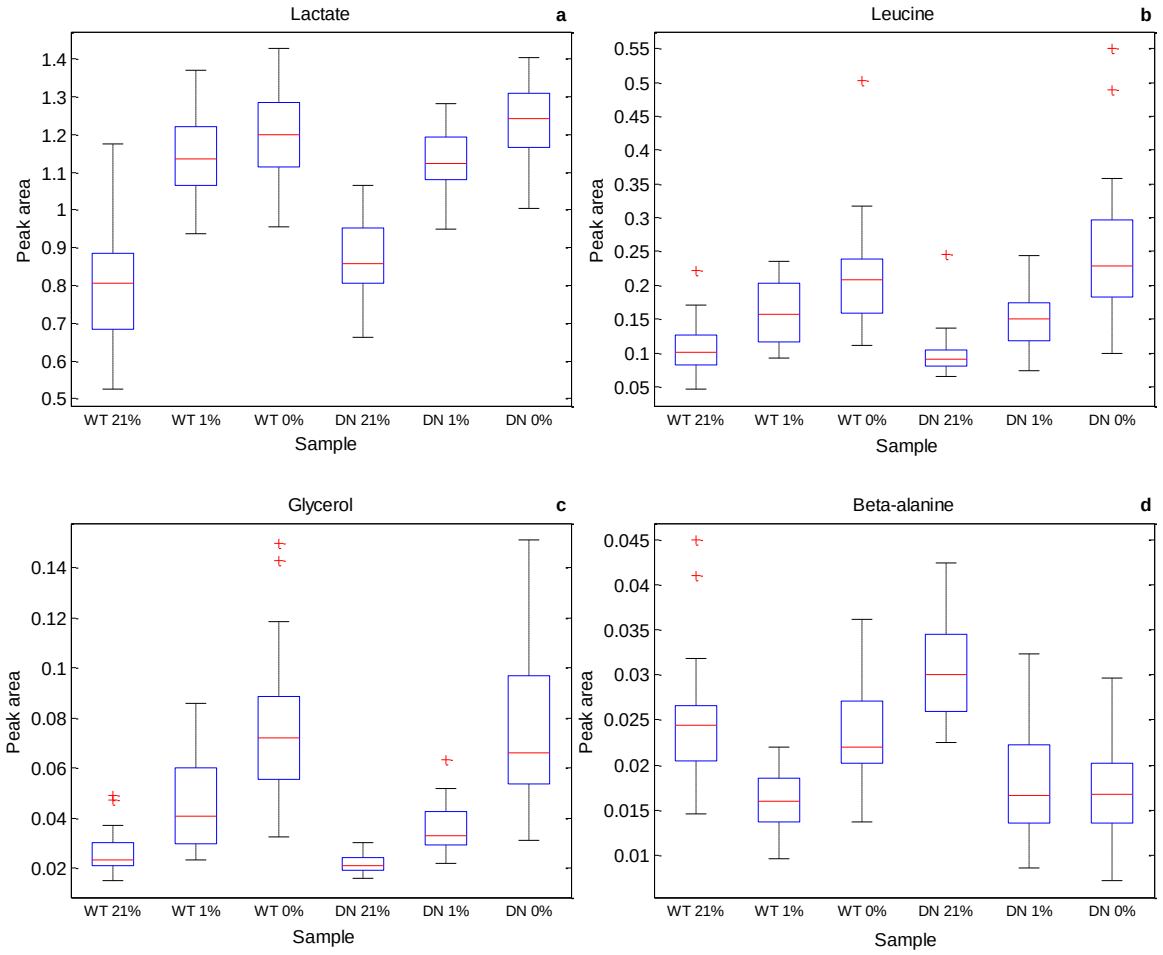

Figure 34: Box plots for the 4 most significant metabolites that differed in gas chromatography-mass spectrometry (GC-MS) data with respect to oxygen in HCT 116 cells.

The 4 most significantly different metabolites with respect to oxygen in the HEPA-1 model were glycine, lactate, norleucine and aspartate (Figure 35). Glycine, lactate and norleucine increased with a decrease in oxygen whereas aspartate decreased. The profiles for aspartate were not dissimilar from beta-alanine in HCT 116 cells suggesting that a similar mechanism relating these metabolites could be a key regulator in response to low oxygen irrespective of HIF-1. For example, both metabolites are involved in beta-alanine metabolism (KEGG pathway ko00410)[182] which could be down-regulated as a non-essential pathway in low oxygen.

The profiles for lactate in both HCT 116 and HEPA-1 models were expected as lactate is a feature of anaerobic respiration in hypoxic and anoxic cells. In accordance with the data presented on the lactate efflux from cells in (section 3.2.7), there was similarly no apparent difference between lactate production or efflux in WT or HIF-1deficient cells. What this data did add however was that elevated levels of intracellular lactate provides an implication that its production is more efficient than its efflux.

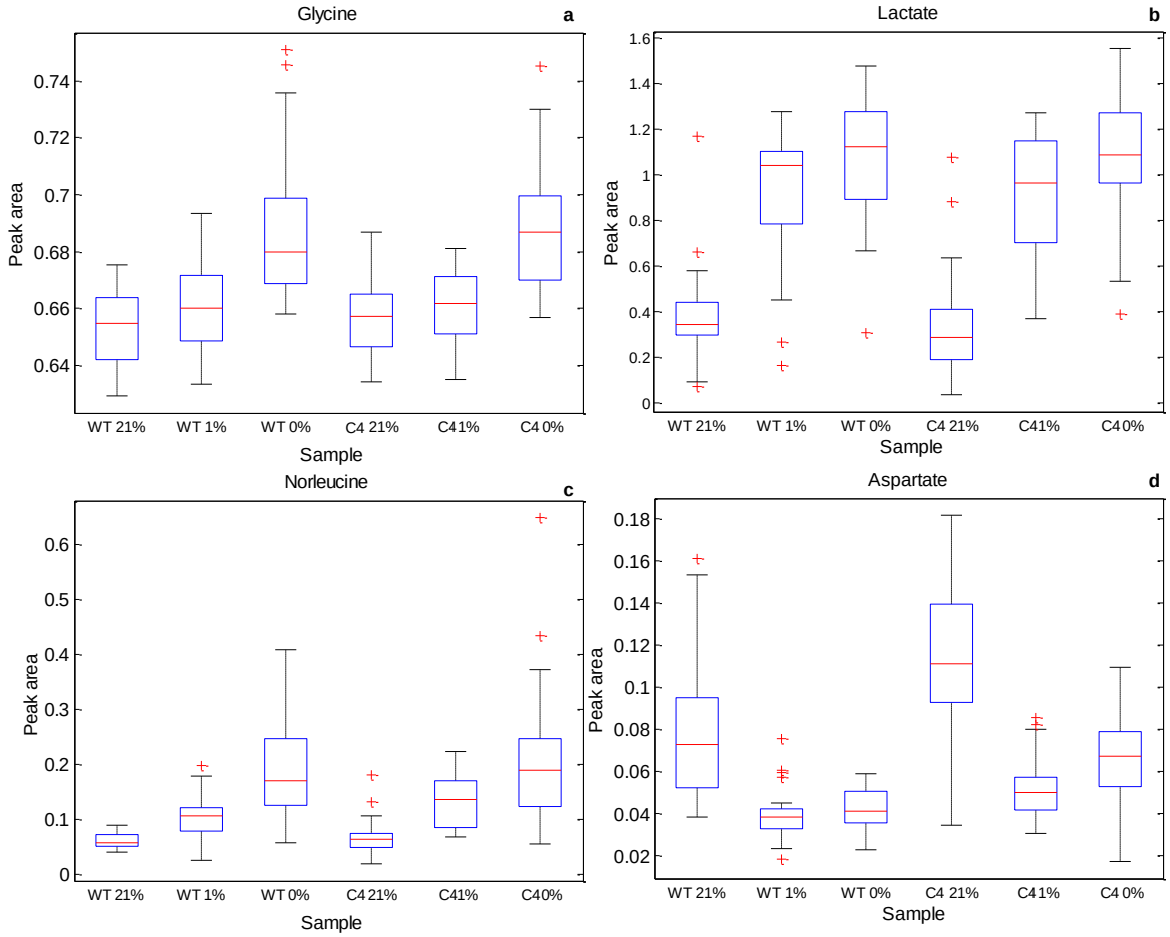

Figure 35: Box plots for the 4 most significant metabolites that differed in gas chromatography-mass spectrometry (GC-MS) data with respect to oxygen in HEPA-1 cells.

Additionally, in both models, leucine isomers were highlighted as metabolic signatures of hypoxia and anoxia. The elevated levels could be due to a down-regulation of the leucine degradation pathway or an increase in its biosynthesis. Both biosynthesis (KEGG pathway ko00290)[182] and degradation (KEGG pathway ko00280)[182] pathways connect leucine to the TCA cycle *via* acetyl-CoA. Norleucine (leucine) aminotransferase (KEGG enzyme 2.6.1.67)[182] catalyses the reversible reaction between Nor(leucine) and glutamate. An increase in leucine under low oxygen could be an indication that acetyl-coA is used in leucine biosynthesis rather than feeding into the TCA cycle, while the conversion of glutamate to leucine and 2-oxoglutarate replenishes the TCA cycle and further elevates the concentration of leucine. Figure 36 shows a schematic for how leucine interacts with the TCA cycle.

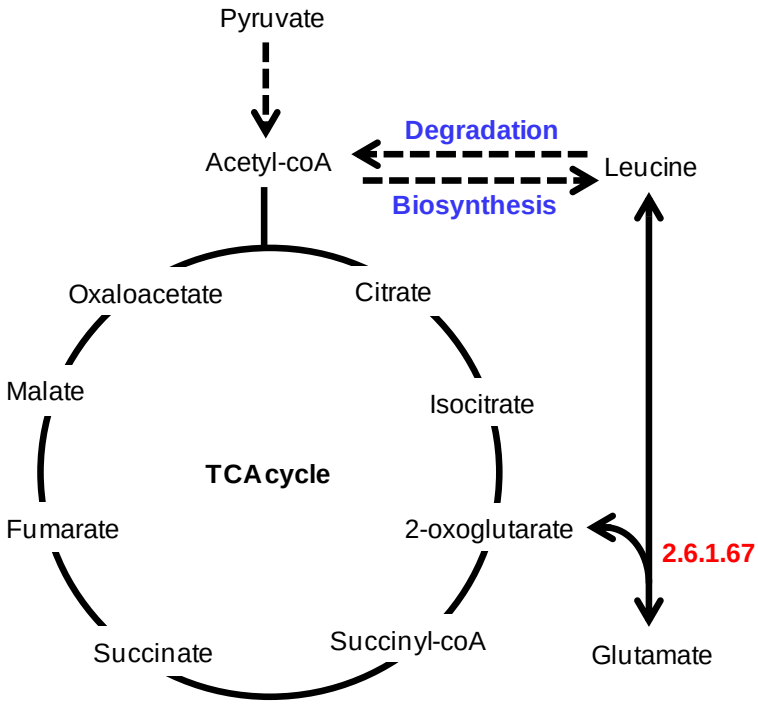

Figure 36: The interaction of leucine (and isomers) with the tricarboxylic acid (TCA) cycle. Norleucine (leucine) aminotransferase (KEGG enzyme 2.6.1.67) catalyses a reversible reaction from glutamate to leucine and 2-oxoglutarate. The leucine biosynthesis and degradation pathways connect leucine to the TCA cycle *via* acetyl-coA.

With respect to HIF-1, 6 features were found to be significantly different between WT and DN cells in the HCT 116 model and 19 were found to be significantly different between WT and C4 cells in the HEPA-1 model. This is summarised in Table 6. All 6 significantly different metabolites in the HCT 116 model were also significantly different in the HEPA-1 model and the remaining 13 metabolites found to be significantly different in the HEPA-1 model were assumed to be either cell line/species specific or HIF-1 subunit specific. One explanation for the extra significant differences between WT and C4 cells in the HEPA-1 model could be due to the absence of HIF-1β which is known to have functions independent of the HIF-1 heterodimer[187]. Since all significant differences in the HCT 116 model were also observed in the HEPA-1 model, it could be more confidently proposed that these differences were due to the lack of functional HIF-1 heterodimer.

Table 6: Significantly different metabolites with respect to hypoxia inducible factor 1 (HIF-1) as determined using a two-way analysis of variance (ANOVA).

Metabolite peak	***p*-value in HEPA-1**	***p*-value in HCT 116**
Aspartate (1)	<0.000001	
Scyllo-/*Myo*-inositol	<0.000001	0.010637
Glycerol-3-phosphate	<0.000001	
Allose/Mannose/Galactose/Glucose (3)	<0.000001	0.000097
Allose/Mannose/Galactose/Glucose (2)	<0.000001	0.000055
Allose/Mannose/Galactose/Glucose (1)	0.000001	0.000080
Glutamate	0.000001	
Malate	0.000004	
Fructose (2)	0.000018	0.013969
Glutamine	0.000050	
Pyroglutamate	0.000214	
Hexadecanoic acid	0.000652	
Citrate	0.000703	
2-hydroxyglutarate	0.003133	0.002245
Putrescine	0.009859	
Tyramine/Tyrosine	0.011640	
4-aminobutyrate	0.017584	
Fructose (1)	0.022678	
4-hydroxyproline	0.026443	

All 3 peaks identified as allose/mannose/galactose/glucose were significantly different between WT and HIF-1 deficient cells in both cell models (and the most significantly different peaks in the HCT 116 model). This is suggestive that all 3 peaks were derived from a single metabolite, which could be glucose since it is known that HIF-1 controls the uptake of glucose through up-regulating the expression of glucose transporters GLUT-1 and 3[155].

4.2.2. Multivariate analysis of GC-MS data

The fact that almost all metabolites were found to be significantly affected by oxygen in univariate analysis highlighted a metabolome-wide effect on cells irrespective of HIF-1 function. Multivariate analysis was therefore performed in an attempt to link metabolites together with the aim of revealing specific regions of metabolism that were directly affected by oxygen availability. Further analyses were applied to consider the metabolic profile of each sample type as a system, rather than its individual metabolites in isolation. Prior to any multivariate analyses an initial PCA was performed on all samples from each cell line including QC samples to confirm the batch matching process was successful. The

plot generated from this analysis of the HCT 116 cell line is shown in Figure 37, where QC samples were observed to fall amongst other data points suggesting the data were correctly pre-processed.

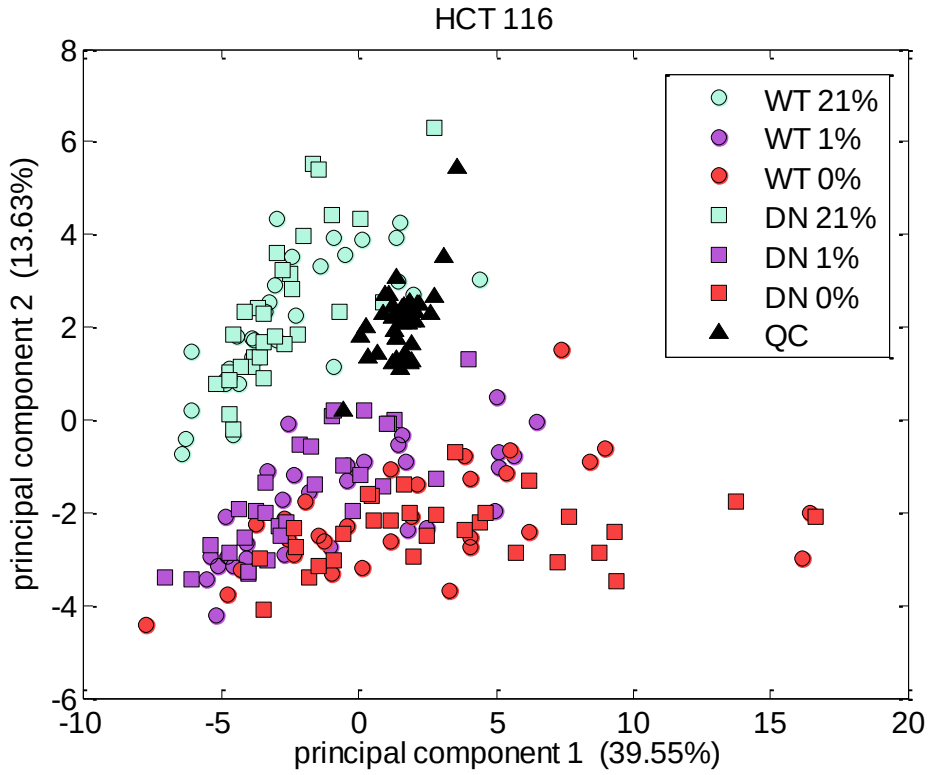

Figure 37: Principal components analysis (PCA) on all HCT 116 metabolic fingerprints analysed using gas chromatography-mass spectrometry (GC-MS). The quality control (QC) samples formed from pooling small quantities from each sample displayed on the plot fall approximately in the middle.

CVA was applied to the PCs in each cell model and the results for the HCT 116 cell model are shown in Figure 38. This was performed without exceeding the number of PCs that additively describe 95 % of the total variance in the data in order to reduce the likelihood of over fitting which can invalidate the model. From the analysis of the scores plot it can be seen that the greatest multi-variance in the data was due to oxygen and that by assessing all samples together it was not possible to tease out the subtle metabolic difference between WT and HIF-1 deficient samples.

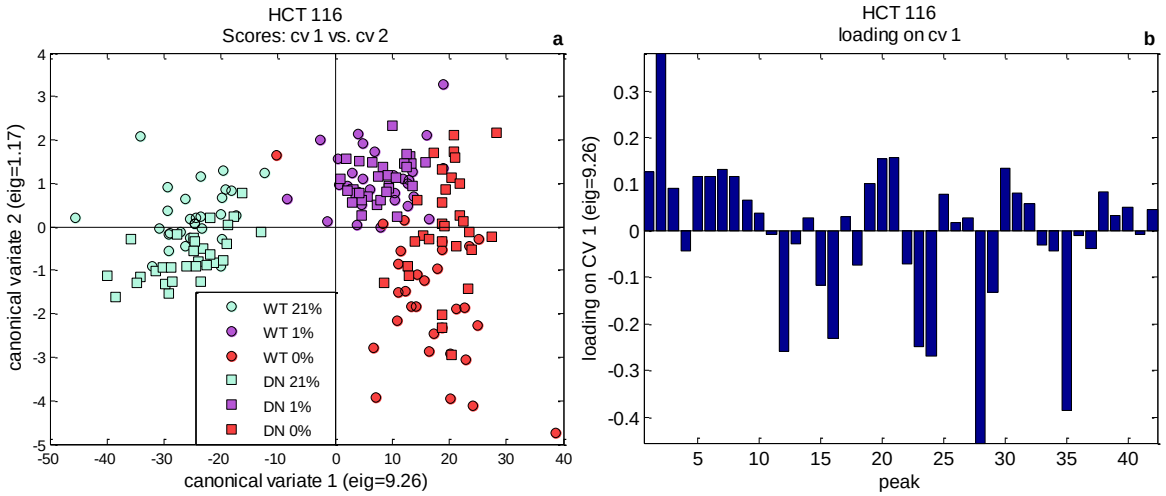

Figure 38: Canonical variates analysis (CVA) on all HCT 116 samples. The model was built using 8 principal components (PCs) collectively accounting for approximately 77 % of the total explained variance in the data. The largest separation in the data is seen on the scores plot (a) between normoxic samples and low oxygen samples in canonical variate (CV) 1. The loading on this CV is shown in (b), where the negative loadings correspond to negative scores (normoxic samples) and the positive loadings correspond to metabolites corresponding to low oxygen samples.

In order to identify individually how WT and HIF-1 deficient cells respond to the range of oxygen treatments, CVA was performed separately on HCT 116 WT samples, HCT 116 DN samples, HEPA-1 WT samples and HEPA-1 C4 samples. In all cases a gradient between oxygen tensions could be identified with a clear separation in CV 1 between normoxic samples and low oxygen samples (Figure 39). These separations were caused by different anti-correlations between metabolite features that appeared to be controlled by HIF-1. The loadings from these analyses were assessed in turn to identify features of normoxia and low oxygen samples in each plot which were then compared to each other to find similarities as a function of oxygen exposure and as a function of HIF-1 presence or absence in each cell model. The results from this are summarised in Table 7.

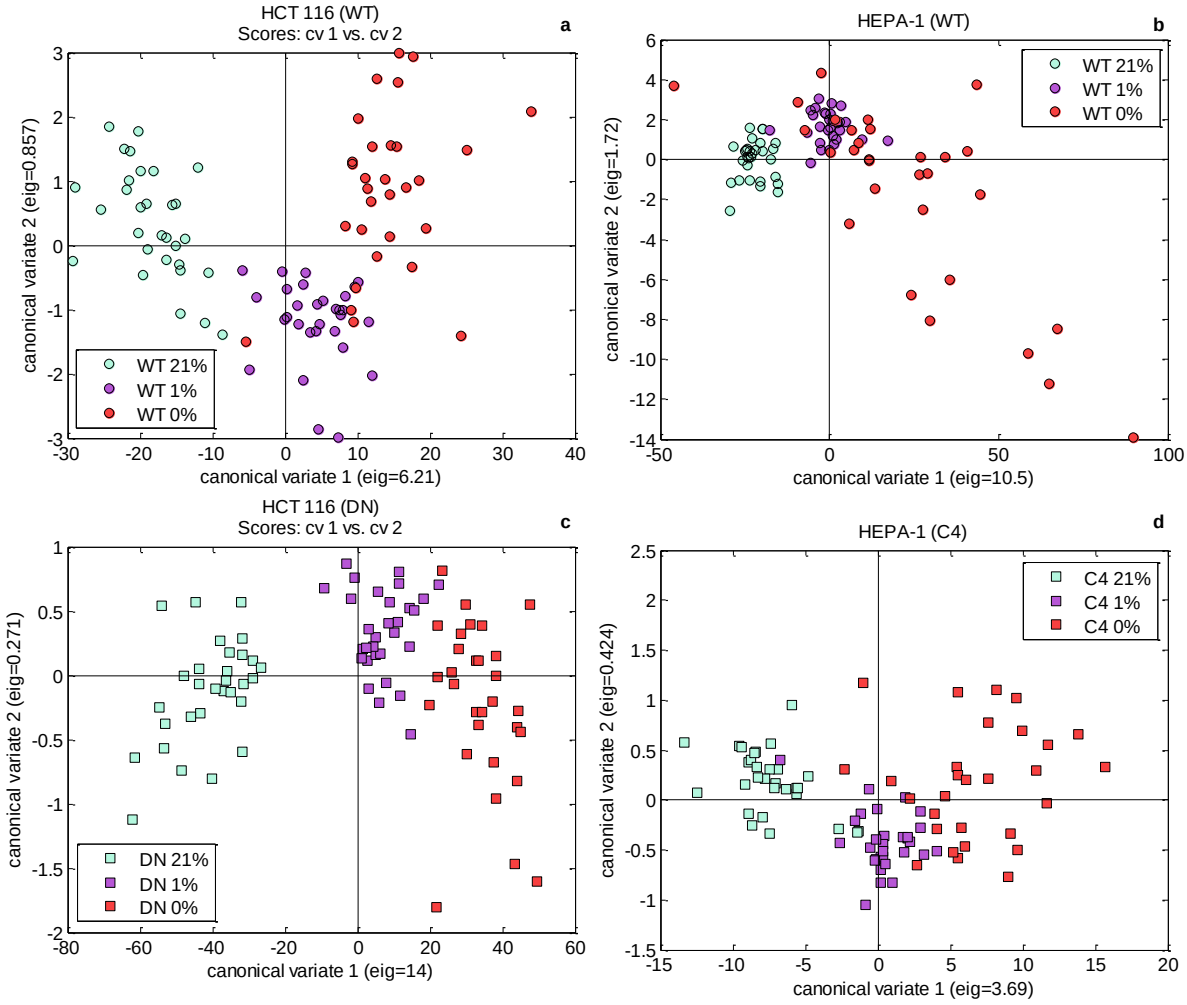

Figure 39: Canonical variates analysis (CVA) scores plots for (a) HCT 116 wild type (WT), (b) HEPA-1 WT, (c) HCT 116 dominant negative (DN) and (d) HEPA-1 C4 samples comparing all 3 oxygen conditions. Each CVA model was built using 8 principal components (PCs) collectively accounting for between 80 % and 90 % of the total explained variance from each analysis. In all cases the greatest separation in the data was between normoxic samples and low oxygen samples in canonical variate (CV) 1.

From Table 7, it is possible to subdivide metabolites into 4 types of metabolic signatures. First are metabolites in normoxia or low oxygen for all 4 cell lines (i.e. irrespective of cell line or HIF-1), where metabolites are labelled normoxia or low oxygen and marked with asterisks. Second are metabolites in normoxia or low oxygen that are cell line specific but not HIF-1 specific, where metabolites are labelled in the appropriate column. Third are metabolites that were similar between WT and HIF-1 deficient cells and labelled in one cell line but different in the other and finally fourth are metabolites that were HIF-1 specific in both cell models marked only with asterisks. All subdivisions of metabolites are useful to consider since it is interesting to assess whether a response to low oxygen is HIF-1 specific, and whether or not the response is conserved between species. Many responses were conserved between HCT 116 and HEPA-1 cells which provided confidence in recognising the results as HIF-1 related metabolites.

Table 7: Comparison of the loadings from canonical variate analysis (CVA) of all 3 oxygen conditions that was performed for HCT 116 wild type (WT) samples, HCT 116 dominant negative (DN) samples HEPA-1 WT samples and HEPA-1 C4 samples (Figure 39 a-d). Metabolites labelled 'normoxia' were identified in the loadings as being features of normoxia that were common between WT and HIF-1 deficient cells, while metabolites labelled 'low oxygen' were identified in the loadings as being features of low oxygen that were common between WT and hypoxia inducible factor 1 (HIF-1) deficient cells. Un-labelled metabolites represent HIF-1 mediated responses to oxygen since the loadings were not common between WT and HIF-1 deficient cells. Metabolites marked with an asterisk (*) indicate cell line similarities such that the same behaviour was observed in both HCT 116 and HEPA-1cell lines.

Metabolite peak	**HCT 116: loading common between WT and DN**	**HEPA-1: loading common between WT and C4**
4-aminobutyrate	normoxia	
4-hydroxyproline	normoxia	
Allose/Mannose/Galactose /Glucose (1)	*	*
Allose/Mannose/Galactose /Glucose (2)	*	*
Allose/Mannose/Galactose /Glucose (3)		normoxia
2-hydroxyglutarate	low oxygen	
2-oxoglutarate	normoxia *	normoxia *
Aspartate (1)		normoxia
Aspartate (2)	normoxia *	normoxia *
Beta-alanine		normoxia
Citrate	normoxia *	normoxia *
Creatinine		low oxygen
Cysteine	normoxia	
Erythronate /Threonate	low oxygen *	low oxygen *
Fructose (1)	*	*
Fructose (2)	normoxia	
Fructose / Sorbose (1)	low oxygen	
Fructose / Sorbose (2)	low oxygen *	low oxygen *
Glutamate	normoxia	low oxygen
Glutamine	normoxia *	normoxia *
Glycerol	low oxygen *	low oxygen *
Glycerol-3-phosphate		low oxygen
Glycine		low oxygen
Hexadecanoic acid	*	*
Hypotaurine	low oxygen *	low oxygen *
Lactate	low oxygen *	low oxygen *
Leucine		N/A
Lysine	low oxygen	
Malate	normoxia	
Malonate	low oxygen *	low oxygen *
Methionine	low oxygen *	low oxygen *
Norleucine	low oxygen *	low oxygen *
Phosphate	low oxygen *	low oxygen *
Phosphocreatinine	N/A	
Putrescine	normoxia *	normoxia *
Pyroglutamate	normoxia	
Pyruvate		normoxia
Scyllo-/*Myo*-inositol	*	*

Octadecenoic acid	*	*
Threonine	low oxygen *	low oxygen *
Tyramine/Tyrosine	low oxygen	
Tyrosine	normoxia *	normoxia *
xylitol/Ribitol	low oxygen	N/A

A direct comparison between cells with and without functional HIF-1 could be made by performing CVA on hypoxic WT and DN cells or WT and C4 cells for HCT 116 and HEPA-1 cell models respectively. It was hoped that understanding the multi-component variation in the metabolome as a response to hypoxia with respect to HIF-1 activity would lead to elucidating the role of HIF-1 in cancer cell metabolism. Furthermore, comparing HCT 116 and HEPA-1 analyses identified the conserved responses of WT and HIF-1 deficiency. The results from this CVA are shown in Figure 40.

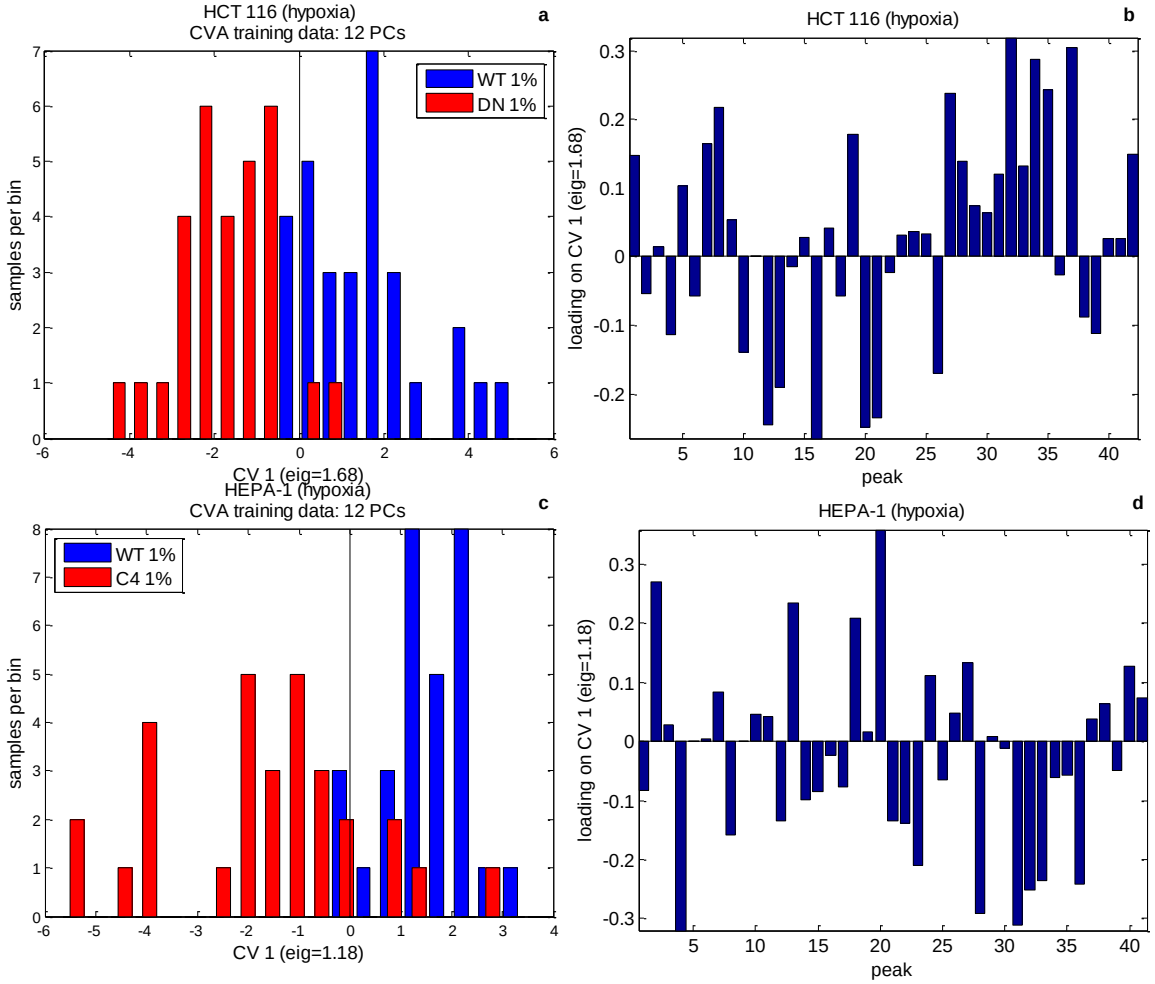

Figure 40: Canonical variates analysis (CVA) of hypoxic (1 % oxygen) samples in the HCT 116 (a and b) and HEPA-1 (c and d) cell models. In each case the CVA models were built using 12 principal components (PCs) accounting for approximately 90 % or the total explained variance. The distributions of samples in canonical variate (CV) 1 for each cell model are represented as bar charts (a and c) where the number of samples per bin is shown. The loadings for CV 1 for each cell model are shown (b and d).

Although the loadings showed a considerable amount of variance between the two cell lines there were some similarities in the anti-correlation between metabolites causing the separation between WT and HIF-1 deficient cells in each. The positive loadings and features of WT cells for each cell line consisted of 2-hydroxyglutarate, 2-oxoglutarate, fructose, hexadecanoic acid, hypotaurine, phosphate, pyruvate and octadecenoic acid which were anti-correlated with 4-hydroxyproline, aspartate, cysteine, glutamine, lysine, malate and pyroglutamate in the negative loadings. It is likely that 2-hydroxyglutarate, 2-oxoglutarate, fructose, hexadecanoic acid, hypotaurine, phosphate, pyruvate and octadecenoic acid are targets of HIF-1 and that targets are conserved across species.

Pyruvate, 2-oxoglutarate and 2-hydroxyglutarate are all connected to central carbon metabolism *via* the TCA cycle. Figure 41 shows a schematic for how these 3 metabolites interact. Since they are affected by the presence of absence of HIF-1, this provides some evidence that HIF-1 targets central carbon metabolism.

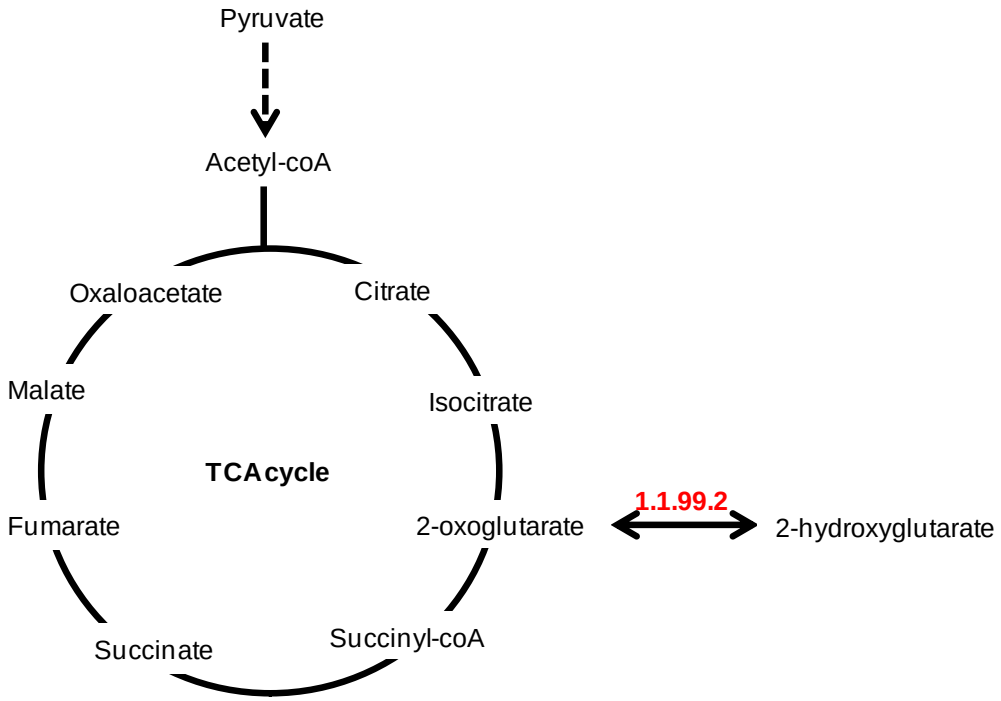

Figure 41: The interaction between pyruvate, 2-oxoglutarate and 2-hydroxyglutarate and central carbon metabolism. 2-hydroxyglutarate dehydrogenase (KEGG enzyme 1.1.99.2) catalyses a reversible reaction between 2-oxoglutarate and 2-hydroxyglutarate. All 3 metabolites feed into the tricarboxylic acid (TCA) cycle.

Hexadecanoic acid and octadecenoic acid are both features of FA biosynthesis (KEGG pathway ko00061)[182]. Figure 42 shows a schematic for FA biosynthesis of which hexadecanoic acid and octadecenoic acid are endpoints. This was the other main pathway highlighted by comparing WT and HIF-1 deficient cells to elucidate the role of HIF-1 on metabolism.

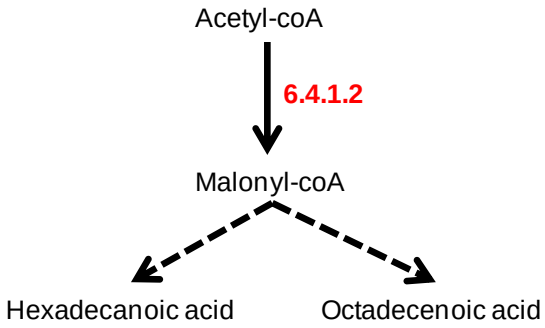

Figure 42: Fatty acid (FA) biosynthesis. Hexadecanoic acid and octadecenoic acid are two of the end points of FA biosynthesis that metabolises acetyl-coA *via* malonyl-coA. Acetyl-CoA carboxylase alpha (KEGG enzyme 6.4.1.2).

Although entire pathways cannot be targeted in cancer therapy, it is useful to identify pathways that link correlated metabolites to determine the enzymes that are responsible for their production and consumption. HIF-1 cannot target metabolites directly, it must target the enzymes that produce or consume the metabolite either directly or *via* a particular signalling cascade. Identifying metabolites in isolation is useful in revealing metabolic signatures but not in hypothesising potential targets for therapy. For example, in excess of 25 enzymes are described in KEGG[182] for their associations with fructose. Without linking fructose to another metabolite of HIF-1 metabolism it is not possible to identify pathways to narrow down which enzymes HIF-1 could be using to control the level of fructose. Identifying specific pathways offers a way to consider certain enzymes over others in their likelihood as HIF-1 targets and inhibiting these enzymes could be the way to inhibit HIF-1 metabolism.

4.2.3. Univariate analysis of UHPLC-MS data

Although statistical outliers were treated in the same way in the data analysed by UHPLC-MS as GC-MS, the dataset was still relatively small and did not follow a normal distribution. For that reason non-parametric statistical testing was applied. The median UHPLC peak areas between each experimental group: HCT 116 WT and DN samples exposed to normoxia, hypoxia or anoxia were compared using a Friedman statistical test[140]. This was performed to assess the effect of HIF-1 from all samples, after correcting for the effect of oxygen. The most significantly different metabolites identified in positive ion mode are shown in Figure 43. In each case the difference was highly significant with $p < 0.0001$. Hexanoylcarnitine was the most significantly different metabolite between WT and DN samples. The median peak area increased in both cell lines with a decrease in oxygen but the range of concentration inferred from peak area was much greater in DN samples than WT samples. Another significant peak was identified as either tetradecanoylcarnitine or a monoradylglycerol/monoacylglycerol (MAG). In both cell lines its presence was found to be highest in anoxia and the concentration was elevated in both hypoxia and anoxia in DN samples relative to WT. Tetradecanoylcarnitine and hexanoylcarnitine are both examples of acylcarnitines that form long-chain esters that function in transporting FAs into the mitochondria[188]. FA metabolism was also exposed in the GC-MS data analysis (Figure 42). Together the data suggest FA metabolism could be as important as central carbon metabolism in HIF-1 control of metabolism in low oxygen environments.

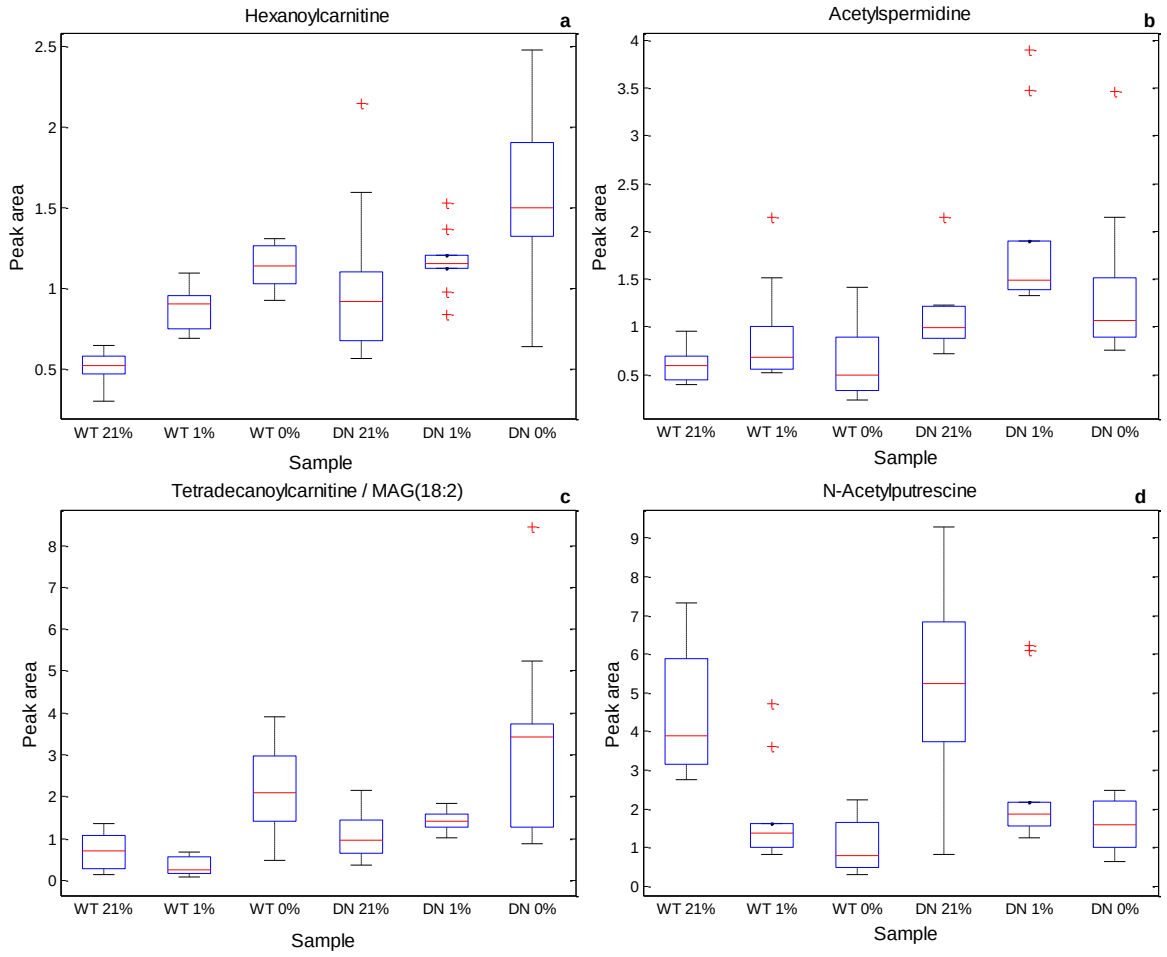

Figure 43: Box plots for the most significant metabolites that could be identified between HCT 116 wild type (WT) and dominant negative (DN) samples from Friedman analysis of ultra high performance liquid chromatography (UHPLC) peak areas (positive ion mode).

Acetylspermidine and N-acetylputrescine are features of polyamine metabolism that along with putrescine, spermidine, spermine and related chemicals have described associations with cancer cell growth and proliferation[189]. The concentration of acetylspermidine was relatively higher in DN cells compared to WT cells, but in both cases was highest in hypoxic conditions. This suggests that acetylspermidine may be a feature of non-HIF-1 mediated responses to low oxygen that occur in both WT and DN cells but that are greater relied upon in the absence of HIF-1. The concentration of N-Acetylputrescine was higher in DN samples at each oxygen level. It was on average more abundant in normoxic DN samples but the range was much greater than in WT samples where the concentration was always higher in normoxia. The concentration was decreased with oxygen irrespective of HIF-1, suggesting another non-HIF-1 mediated response to low oxygen exposure. However, in this case the reduction in N-acetylputrescine was representative of hypoxia.

It has long been thought that polyamine metabolism could be a target for cancer therapy and chemotherapy agents have been explored in the past[190], however it has been difficult

to strike the balance between successfully inducing cytotoxicity in cancer cells without inducing toxic effects on non-cancerous cells[189]. Also, drugs have been developed that target specific enzymes in polyamine metabolism[189, 190]. These data may suggest that a successful therapy may need to target more enzymes of the pathway, blocking several sites for polyamine synthesis. Similarly, since the profiles of different metabolites in this pathway are differentially regulated under different oxygen levels, the severity of hypoxia should be determined to decide which enzymes of the pathway should be targeted to enhance its potential success.

The most significantly different metabolites identified in negative ion mode are shown in Figure 44. In WT samples, the median peak area for the feature identified as lysophosphatidylserine (16:0) increased in hypoxia and decreased in anoxia, although the range in anoxia was much greater than in the other conditions. In DN samples, the median peak areas at each oxygen level were similar to normoxic WT cells suggesting lysophosphatidylserine may be a downstream target of HIF-1 in low oxygen. A previous study has shown that lysophosphatidylserine can increase the concentration of intracellular calcium in HCT 116[191]. In general, the role of calcium in cancer cells is largely for the allosteric regulation of a range of enzymes involved in cell proliferation and the activation of nuclear transcription factors and factors involved in DNA replication[192]. Furthermore, it has been proposed that blocking calcium channels in cell and organelle membranes can suppress growth in human cancer cells[192]. The data could suggest that in hypoxia, HIF-1 may be up-regulating calcium induced proliferation and DNA replication *via* lysophosphatidylserine, which is maintained in anoxia to a certain extent. The range in concentration of many metabolites and lipids was greater in anoxia than in other oxygen conditions most likely due to a difference between samples containing more or less cells continuing hypoxia-based cancer cell survival or cells starting the early stages of apoptosis. Although the experimental design aimed to reduce the latter, in the extreme cellular stress induced by anoxia was correlated with some cell death as seen in (Figure 18).

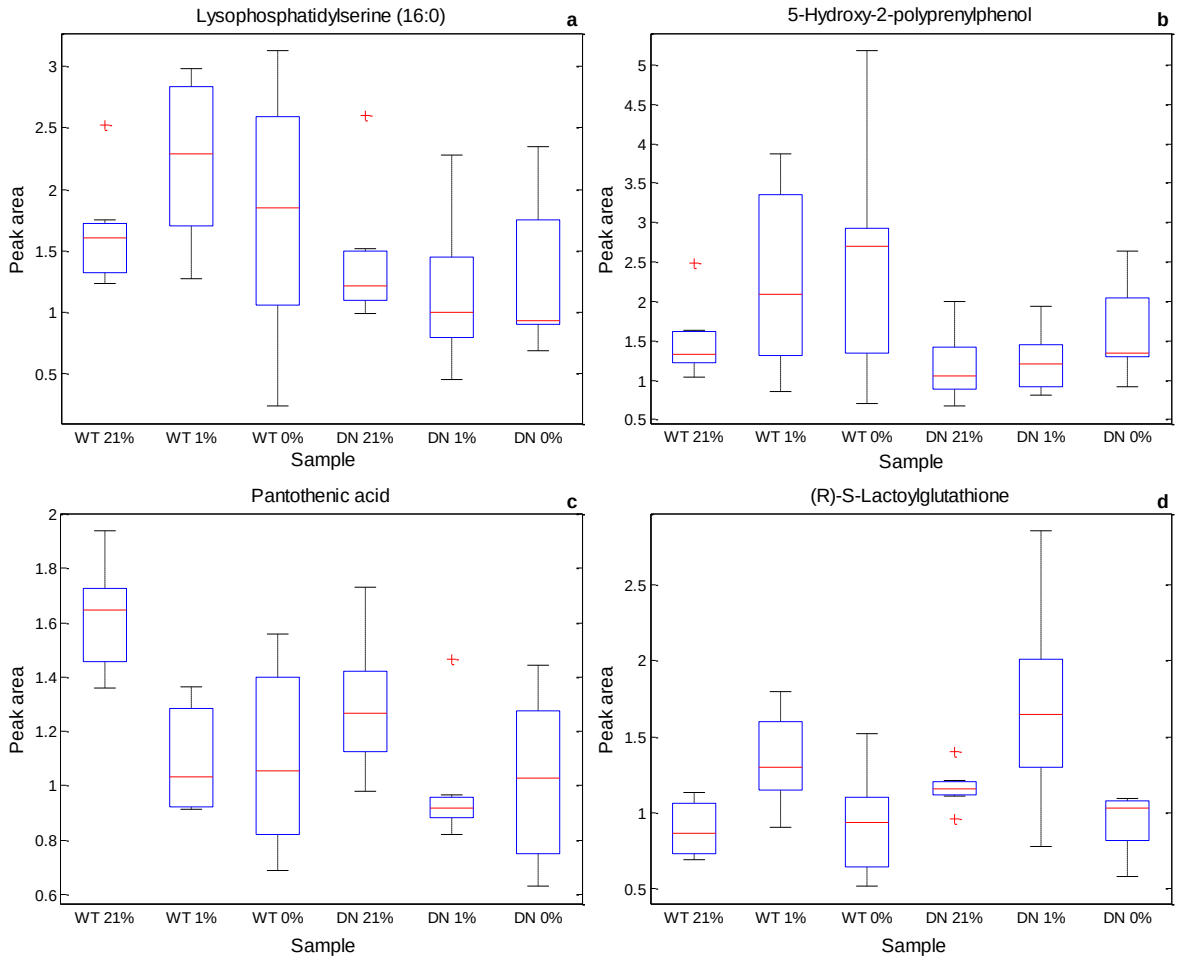

Figure 44: Box plots for the most significant metabolites that could be identified between HCT 116 wild type (WT) and dominant negative (DN) samples from Friedman analysis of ultra high performance liquid chromatography (UHPLC) peak areas (negative ion mode).

Pantothenic acid appeared to be suppressed in hypoxia, seemingly irrespective of HIF-1, although its concentration was marginally lower in hypoxic DN cells. Therefore it could be involved in a non-essential pathway in cellular response to hypoxia. (R)-S-Lactoylglutathione, involved in pyruvate metabolism (KEGG pathway ko00620)[182], exhibited the same pattern with respect to oxygen in both WT and DN samples where the concentration was increased by hypoxia relative to normoxia but in anoxia it was maintained to be similar to normoxia. This suggests a non-HIF-1 response to hypoxia but that may not be useful in the absence of oxygen.

Fold changes were calculated for significantly different features identified between mean WT and DN sample UHPLC peak areas at each oxygen level separately using Mann-Whitney *U*-statistical testing[140]. The most significant results from this are summarised in Table 8, where for each feature identified, the level of significance, the fold change in DN samples relative to WT samples and the ion mode in which the feature was detected are

given. In all cases, the fold change was calculated to be ±1.5, where positive fold changes were indicative of an increase in DN samples and negative fold changes indicated a decrease relative to WT. Many of the significant features were identified as a range of phospholipids or lysophospholipids. Since each peak was putatively identified as many different phospholipids, and a range of peaks were identified as being one or more of the same, a fold change and *p*-value was collected representative of an average. Positive and negative fold changes were averaged separately and a net difference between them was calculated for each oxygen level. The (lyso)phospholipids identified included different (lyso)phosphatidylcholines, (lyso)phosphatidylserines and (lyso)phosphatidylethanolamines and significant differences were observed between WT and DN profiles in both Friedman and Mann-Whitney *U*-analyses. This could suggest that HIF-1 has a distinct effect on the lipid profile of HCT 116 cells. Furthermore, since different phosphatidylcholine, phosphatidylserine and phosphatidylethanolamine peaks were increased and decreased with a loss of functional HIF-1 in DN samples, it is possible that other transcriptional factors control lipid metabolism downstream and that different regulators can cause different effects on the lipidome with respect to the oxygen environment they are exposed to.

Table 8: Summary of the metabolites and lipids found to be significantly different between HCT 116 wild type (WT) and dominant negative (DN) cells at each oxygen level, where peak fold changes exceeded ±1.5. The *p*-value associated with each fold change is given as well as the ion mode in which the peak was detected. For (lyso)phospholipids where each peak fold change exceeded ± 1.5, a net fold change has been calculated and an average *p*-value is quoted.

Oxygen level	ID	*p*-value	Fold change	Ion mode
Normoxia	Choline phosphate/ Indole-3-ethanol/ Methylleucine/ Dehydroxycarnitine	0.0257	3.83	positive
	N-Acetylputrescine	0.0002	2.20	positive
	DAG(34:2)	0.0452	1.91	positive
	ADP / dGDP	0.0073	1.54	positive
	Phospholipids	0.0062	-0.25	positive/ negative
Hypoxia	Acetylspermidine	0.0073	2.08	positive
	Lysophosphatidylserine (16:0)	0.0113	1.84	negative
	N-Acetylputrescine	0.0376	-1.76	positive
	Tetradecanoylcarnitine/ MAG(18:2)	0.0002	-2.12	positive
	2-Oxoarginine/ 5-Guanidino-2-oxopentanoate	0.0257	-2.13	negative
	Phospholipids	0.0142	-3.91	positive/ negative
	GDP-monosaccharide	0.0113	-3.39	negative
Anoxia	N-Acetyl-D-galactosaminyl-(N-acetylneuraminyl)-D-galactosyl-D-/ Neuraminic acid	0.0257	5.59	positive
	5-isobutylthioribose	0.0376	2.63	negative
	Galactosylceramide (d18:1/18:1)/ Glucosylceramide (d18:1/18:1)	0.0113	2.61	negative
	11-hydroxyprogesterone 11-glucuronide/ PC(P-15:0/0:0)/ PE(P-18:0/0:0)	0.0312	1.86	positive
	1-(O-alpha-D-glucopyranosyl)-29-keto-(1,3R,31R)-dotriacontanetriol/ 1-(O-alpha-D-mannopyranosyl)-29-keto-(1,3R,31R)-dotriacontanetriol	0.0376	1.77	positive
	8-Hydroxyguanosine	0.0452	1.71	positive
	Acetylspermidine	0.0173	1.69	positive
	Phospholipids	0.0334	0.08	positive/ negative
	Lysophospholipids	0.0380	-2.07	negative

It was expected that the behaviour or WT and DN cells would be similar in normoxia, however a few significant differences were highlighted between them from the metabolic profiling of each using UHPLC-MS. Figure 33 showed that a basal expression of HIF-1 was present in normoxia and it is possible that its effect on the metabolome, although minimal, may have been significantly different between WT and DN cells. These differences are likely to be the first responses of HIF-1 transcriptional activity and the most sensitive to small fluctuations in oxygen availability. The first feature that was shown to be significantly different was putatively identified as choline phosphate, indole-3-ethanol, methylleucine or dehydroxycarnitine. Although there are clearly similarities in the

structure of these metabolites which has led them to be possible identifiers for the same peak, their biological function is diverse. For this reason, using these data alone it was not possible to derive biological meaning from this significant difference in concentration. Furthermore, there were no other peaks with similar identifications found to be significantly different between normoxic WT and DN samples that could increase the possibility for this feature being one metabolite over the others. The features identified as N-acetylputrescine and diradylglycerol/diacylglycerol (DAG) (34:2) were singly identified and therefore their biological function in normoxic WT and DN samples could be assumed with more confidence. N-acetylputrescine was found to be significantly affected by HIF-1 in normoxia and hypoxia, however in normoxia, the fold change was positive indicating an up-regulation of the metabolite in DN cells relative to WT and in hypoxia the converse was true. Since the peak was more significantly different between WT and DN samples in normoxia and the magnitude of the fold change was higher it is likely that N-acetylputrescine is a metabolite characteristic of DN cell metabolism in normoxia that is present in cells lacking functional HIF-1 but that is not used in the survival mechanism of these cells in lower oxygen.

When comparing WT and DN cells, as oxygen was decreased, the effect on lipid metabolism increased, further enhancing the differential responses to oxygen deprivation dependent on the presence or absence of HIF-1. In normoxia, one DAG and some phospholipid features differed compared to a Lysophosphatidylserine, possibly a MAG and more phospholipids in hypoxia and many (lyso)phospholipids in addition to the the 1-(O-alpha-D-glucopyranosyl)-29-keto-(1,3R,31R)-dotriacontanetriol/1-(O-alpha-D-mannopyranosyl)-29-keto-(1,3R,31R)-dotriacontanetriol peak and the galactosylceramide (d18:1/18:1)/glucosylceramide (d18:1/18:1) peak in anoxia. Lipid metabolism has long been described as a feature of severe oxygen stress especially in cancer. In particular it is known that cellular stress can increase ceramide levels[193] and that chronic hypoxia can affect ceramide moieties of many gangliosides and sphingolipids[194]. The peak identified as galactosylceramide (d18:1/18:1)/glucosylceramide (d18:1/18:1) could be a marker of changes in regulation of the ceramide pathway. Ceramide can be incorporated into less toxic galactosylceramides or glucosylceramides by glycosylation and further modified into complex glycosphingolipids[193]. DN cells are likely to exhibit more cellular stress as an onset of anoxia due to the lack of HIF-1 and it is therefore possible that ceramide levels could be elevated and that the greater than 2.6 fold increase in galactosylceramides and/or

glucosylceramides in DN cells relative to WT cells occurs from a shunting of ceramide into these less cytotoxic forms.

The peak putatively identified as neuraminic acid was also an interesting finding. Neuraminic acid is a generic name for a family of sialic acids that occur in the structures of N-glycans, O-glycans and glycosphingolipids[195]. Previously, glycophospholipids containing sialic acid have been associated with tumour growth and metastasis through overenhancing their role in promoting phosphorylation of membrane receptor tyrosine kinases that promote growth signalling[196]. Furtherrmore, tumour hypoxia has been shown to enhance the expression of sialic acid containing gangliosides *via* the up-regulation of sialic acid transporters[197]. The areas for this peak in the spectra were over 5 times higher in DN cells relative to WT which may suggest a greater reliance on promoting these glycophospholipid species in DN cells when specific HIF-1 mediated processes are not employed. HIF-1 promotes tumour survival in a multitude of ways including increasing the transcriptional activity of the genes encoding vascular endothelial growth factor (VEGF) and insulin-like growth factor 2[198]. Although it was not possible to determine which receptor tyrosine kinases were involved in promoting cancer cell survival in DN cells from these data, it could be interesting to identify which are involved in pathways that are not enhanced by HIF-1 or that are overexpressed to compensate for a lack in HIF-1.

Most fold changes in hypoxia occurred due to an apparent loss of function in DN cells relative to WT cells. In addition to N-acetylputrescine, peaks identified as tetradecanoylcarnitine/MAG (18:2), 2-oxoarginine/5-guanidino-2-oxopentanoate and a GDP-monosaccharide were more than 1.5 times lower with a lack of functional HIF-1. These metabolites are therefore highlighted as being potentially connected to a HIF-1 mediated response to hypoxia. 2-oxoarginine and 5-guanidino-2-oxopentanoate are alternate names for the same compound and are involved with N-acetylputrescine in arginine and proline metabolism (KEGG pathway ko00330)[182] or polyamine metabolism[189]. Further to the Friedman analysis, the data could suggest that this pathway may be one of the key metabolic targets for preventing the action of HIF-1 in hypoxia and could be important for future cancer therapies. The net change in phospholipids were also negative suggesting that while some lipids are up-regulated to a certain degree to compensate for a lack of HIF-1 in cell survival in hypoxia, most phospholipids appear to be specific targets of HIF-1.

Although it is interesting to consider the direct effects of HIF-1 metabolism in cancer, it is also vital to assess how DN cells overcome the lack of HIF-1 and maintain survival in low oxygen environments or what cell death processes are employed with the absence of HIF-1 function. This can be particularly seen from the 8 features found to be significantly more abundant in DN cells relative to WT cells. Amongst those already mentioned are, 11-hydroxyprogesterone 11-glucuronide (although this peak could be a phospholipid derivative) and 8-Hydroxyguanosine. 8-Hydroxyguanosine has been described previously as a product of oxidative DNA damage[199] and its increase in DN samples is suggestive of an increase in oxidative DNA damage in these cells. Oxidative DNA damage caused by low oxygen environments was a controversial topic for many years since it was thought to be only a feature of hyperoxia (highly oxygenated environment), however it has been described since as a possible feature of hypoxia, particularly in mitochondrial DNA[200]. Reactive oxygen species (ROS) produced in the mitochondria are thought to play key roles in both hypoxic and non-hypoxic conditions, are associated with oxidative DNA damage and are involved in regulating HIF activity[201] such that HIF-1 can reverse the effects of DNA damage by ROS. A hypoxia induced accumulation of ROS in DN cells in the low oxygen environment may not be controlled in the absence of HIF-1 and subsequently 8-Hydroxyguanosine could increase as a result of elevated DNA damage caused by ROS.

4.2.4. Conclusion

A range of metabolites have been discovered from the GC-MS and UHPLC-MS analysis of HCT 116 and HEPA-1 cells comparing WT cells to HIF-1 deficient cells exposed to normoxia (21 % oxygen) hypoxia (1 % oxygen) or anoxia (0 % oxygen). Amongst these were metabolites representative of HIF-1 metabolism in cancer, metabolites representative of cancer cell survival or cell death in the absence of HIF-1 and metabolites that are either cell line specific or more interestingly conserved between species. This has enabled an enhanced understanding of the systems biology of HIF-1 metabolism, particularly where metabolites could be linked to possible pathways. The discovered metabolites could be considered in devising cancer therapy to inhibit HIF-1 *via* the metabolome or used in diagnosis or prognosis of cancer in the future. The latter would involve screening suspected tumours for the metabolites and associating the concentrations to the likely level of hypoxia in the tumour. Furthermore, it could be possible to assess whether or not tumour cells appear to be surviving through HIF-1 dependent or independent mechanisms.

Many of the metabolites were related to central carbon metabolism, confirming its role in cancer metabolism. Some of the other most interesting metabolites discovered were 2-hydroxyglutarate, 2-oxoglutarate, hexadecanoic acid, hypotaurine, pyruvate and octadecenoic acid since they appear to be conserved metabolic targets of HIF-1 across species. From the discovery of these particular metabolites it would be interesting to investigate the role of HIF-1 in hypotaurine metabolism, butanoate metabolism, FA biosynthesis and biosynthesis of unsaturated FAs since a few of these metabolites are involved in each suggesting they are likely pathways involved in HIF-1 response to low oxygen. From the UHPLC-MS analysis of HCT 116, it was revealed that targets of HIF-1 requiring investigation are polyamine metabolism, arginine and proline metabolism and the ceramide pathway.

Chapter 5. Network-based correlation analysis of metabolites detected by GC-MS

5.1. Introduction

Cellular phenotype is largely governed by metabolism. There are approximately 2900 endogenous metabolites that are currently detectable in the human body using analytical techniques such as GC-MS, LC-MS or NMR[183]. The human metabolic network involves connections between metabolites through biochemical reactions and links many metabolic pathways together into one representation of metabolic function. The structure of this network gives rise to the relative concentrations of metabolites that are present in cells and naturally, the concentrations of certain metabolites tend to be correlated with others in the network due to their position and influence on other metabolites *via* key enzymatic reactions. The influence of one metabolite on another can be due to a neighbouring interaction; however in reality correlated metabolites tend to be spatially or temporally separated in the network. A correlation can exist between two metabolites that could be due to any number of factors. Many of these are discussed in Camacho *et al.* (2005)[202]. Figure 45 shows schematics for some of these factors. Two metabolites can be highly correlated due to the domination of a single parameter whose variability has more control over the correlation than any other parameter (asymmetric control). In such a case, groups of highly correlated metabolites can form if one metabolite is highly correlated to two others due to a single parameter, then the two others by necessity must also be highly correlated and so on. For example, HIF-1 could control the correlation between metabolites A and B as well as A and C. By asymmetric control, HIF-1 is likely therefore to be accountable for a correlation between B and C as well. Other factors that can cause metabolites to be highly correlated include cases where metabolites are highly positively correlated when they are close to chemical equilibrium or highly negatively correlated when they share a conserved moiety. An example of the latter would be the anti-correlation between ATP and ADP such that the concentration of one is higher while the other is lower because phosphate is a conserved moiety transferred cyclically between them. Finally, correlations can be due to high variability in one parameter. For example high variability in a certain enzyme will pose a negative correlation on its substrates and products.

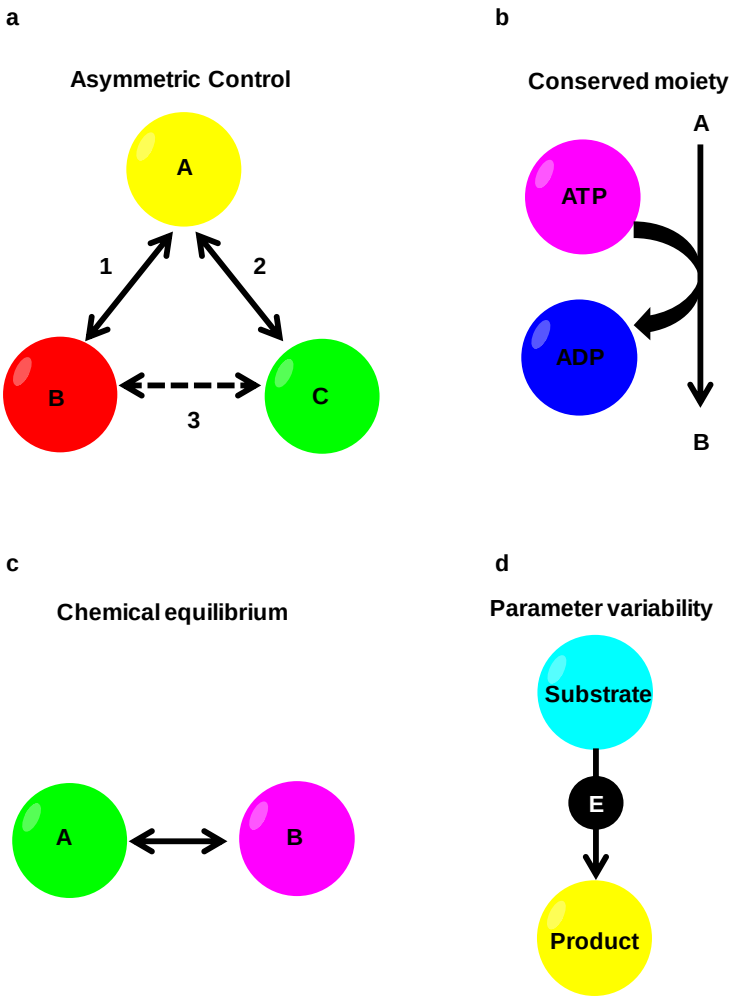

Figure 45: Examples of factors contributing to the correlation between metabolites. (a) an external factor controls correlation 1 between metabolites A and B as well as correlation 2 between A and C. By asymmetric control, this factor also controls a correlation 3 between B and C. (b) In the energy consuming metabolic reaction between A and B, ADP and ATP are negatively correlated. (c) A correlation between A and B can occur when both are close to chemical equilibrium. (d) High variability of enzyme E controls the negative correlation between its substrate and product.

Different metabolites have different levels of connectivity both in reality and in representations of human metabolic networks. Highly connected metabolites feature in many reactions and can be considered ‘hubs’ in the network. These hubs may change when cells are exposed to different environments as alternative metabolic pathways are up- and down-regulated to promote survival in that particular environment. Determining hubs and key pathways that change in response to HIF-1 function or oxygen treatment could give an insight into how cells use metabolism to respond to these stresses and potentially reveal regions of the network that could be targeted in cancer therapy. This was performed by identifying strongly correlated metabolites in cells from each experimental group (WT or DN exposed to normoxia, hypoxia or anoxia) and identifying differences between correlation coefficients due to HIF-1 or oxygen. Once identified, differently correlated metabolites were mapped onto a computational human metabolic network to reveal their

network based origins and the connections between them. This offers a systems biology-based approach to study the metabolic effects of hypoxia in cancer as a system rather than by single entities. After all cancer is a multi-factorial disease and should be studied from a system perspective. Just as cancer is not controlled by a single gene, protein or metabolic pathway, it was expected that there are many correlated metabolites and that a combination of these are responsible for the cancer phenotype.

5.1.1. Correlation analysis

There are many different methods for performing correlation analysis. The type and quality of the data to which correlation analysis will be applied along with the level of robustness required usually provide the basis for choosing certain methods over others. The most commonly used are the Pearson's product correlation and the Spearman's rank correlation methods. In both, a correlation coefficient (*r*) representative of the connectivity between two independent variables (metabolites) is calculated, ranging from -1 to 1; where a coefficient of 0 implies no correlation between variables, coefficients in the range ± 0.7 to 1 usually imply strong correlation between variables and coefficients in the range ± 0 to 0.7 usually imply weak correlation between variables. The Pearson's product-moment correlation method computes a coefficient that is invariant to linear transformation in variables[203] and this type of correlation analysis is only valid when variables are linearly related[202]. Further requirements include data that are approximately normally distributed and do not contain outliers. Although the Spearman's rank correlation can be used to analyse non-parametric data and is less sensitive to outliers[202], the Pearson's product-moment correlation method is statistically more powerful.

The quality and validity of a result from correlation analysis is highly influenced by the sample size. Although the Pearson's product-moment correlation method is less sensitive to sample size than the Spearman's rank correlation method; in general, correlation analysis should be avoided for experiments with fewer than 10 biological replicates[202]. The metabolic profiling data obtained from analysing HCT 116 WT and DN cell lysates described in chapter 4.2 was shown to have an approximately normal distribution after log transformation and any observed metabolite outliers were replaced by a mean peak area from the respective experimental group. The relationships between metabolites were linear in nature and the biological replicate size of $n = 30$ for each experimental group was moderate. The data were therefore deemed suitable for Pearson's product-moment

correlation analysis. Equation 5 shows the calculation used to obtain coefficients for the pair-wise correlation analyses between identified metabolites.

$$r = \frac{\sum_{i=1}^{n}(x_i - \bar{x})(y_i - \bar{y})}{[\sum(x_i - \bar{x})^2 \sum y_i - \bar{y}^2]^{1/2}}$$

Equation 5: The Pearson's product-moment correlation equation (as shown in Rodgers and Nicewander (1988)[203]) where r is the correlation coefficient calculated for the pair-wise correlation of variables x and y.

5.1.2. The network

In order to discover their network based origin, correlations were mapped onto a human metabolic network. There are several genome-scale human metabolic networks freely available for use. The two most popular genome-scale human metabolic models are the global reconstruction of the human metabolic network based on genomic and bibliomic data developed by the Palsson group (HMN-P)[13] and the Edinburgh human metabolic network (EHMN) reconstruction[12]. Both metabolic networks have distinctive features making them more or less valuable for use depending on the investigation. For example, both the EHMN and HMN-P contain a similar number of compounds (approximately 2700) of which more than half have KEGG references in the EHMN[12]. The HMN-P has more reactions (approximately 3800) compared to the EHMN (approximately 2800), however the HMN-P contains compartmentalisation such that some reactions are the same as others occurring in different subdivisions of the cell/network and many reactions involve transport of metabolites between compartments. Therefore the number of different biochemical reactions contained does not differ hugely from the EHMN. Although compartmentalisation provides a more realistic model of metabolism, for this research the EHMN was more suitable since it is not compartmentalised. The analysis of cell lysates means that metabolites are no longer localised to compartments of the cell, rather metabolites are analysed as collective pools from all compartments. Therefore correlations between metabolites are not compartment specific such that it was not clear which compartments metabolites originated. Consequently, using the EHMN allowed a simpler yet more valid network analysis of the correlations observed.

Correlated metabolites were identified within the EHMN and the shortest path between these was computed from the reactions available in the network. This allowed the connection between correlated metabolites to be observed. From a list of differently

correlated metabolites between two experimental groups at a time it was possible to collect pathways between them and together create new sub-networks to describe the network based origin of the differences. For example, the differences between correlations for normoxia and hypoxia show the changes in pathway regulation in response to hypoxia.

5.2. Results and discussion

From the GC-MS analysis of HCT 116 WT and DN cells exposed to normoxia, hypoxia or anoxia, a total of 45 metabolite peaks were identified according to reporting guidelines as described by the MSI[50]. Of these, 3 were removed from the data due to the relative standard deviation of each exceeding 30 % in the QC samples. In some cases peaks were identified as a single metabolite whereas in others peaks could not be definitively identified as a single metabolite. Additionally some identifications were assigned to multiple peaks. This was either due to different derivatisation products of a single metabolite that elute with different retention indices or where metabolites could not be definitively identified due to several metabolites having identical EI mass spectra such as peaks assigned allose/mannose/galactose/glucose.

5.2.3. Correlation analysis

For a direct comparison between cells with and without HIF-1 function, correlation analysis was applied to compare WT and DN cells at each oxygen level. This yielded 16, 42 and 24 pairs of differently correlated metabolites in normoxia, hypoxia and anoxia respectively. The greatest correlation differences between WT and DN cells are summarised in Table 9. They are listed according to the oxygen condition they refer to in descending order of correlation difference. The Pearson's product-moment correlation coefficient observed for each correlation in each cell line (WT or DN) is given.

Table 9: Pair-wise correlations with a difference greater than 0.5. For each pair of metabolites, the Pearson's product-moment correlation coefficients in HCT 116 wild type (WT) and dominant negative (DN) cells are given along with the difference in correlation between them. The table is split into correlation differences observed at each oxygen level: (a) normoxia (21 % oxygen), (b) hypoxia (1 % oxygen) and (c) anoxia (0 % oxygen).

a) Normoxia (21 % oxygen)

Metabolite A	Metabolite B	Difference	Correlation (WT)	Correlation (DN)
Allose/Mannose/ Galactose/Glucose	2-oxoglutarate	0.708	0.792	0.084
Allose/Mannose/ Galactose/Glucose	Threonine	0.679	0.767	0.088
Fructose/Sorbose	2-oxoglutarate	0.638	0.779	0.142
Malate	Threonine	0.595	0.718	0.122
Glutamate	Malate	0.536	0.785	0.249
2-oxoglutarate	5-oxoproline	0.526	0.836	0.309

b) Hypoxia (1 % oxygen)

Metabolite A	Metabolite B	Difference	Correlation (WT)	Correlation (DN)
Tyramine/Tyrosine	Xylitol/Ribitol	0.845	0.918	0.073
Xylitol/Ribitol	Erythronate/threonate	0.811	0.875	0.064
Xylitol/Ribitol	Pyruvate	0.719	0.837	0.118
Xylitol/Ribitol	4-hydroxyproline	0.693	0.834	0.141
Fructose	Xylitol/Ribitol	0.687	0.78	0.093
Allose/Mannose/ Galactose/Glucose	Xylitol/Ribitol	0.656	0.845	0.189
Scyllo/Myo-inositol	Xylitol/Ribitol	0.641	0.966	0.325
Allose/Mannose/ Galactose/Glucose	Glutamine	0.636	0.866	0.23
Xylitol/Ribitol	Malate	0.635	0.704	0.069
Methionine	Xylitol/Ribitol	0.614	0.973	0.359
Xylitol/Ribitol	Aspartate	0.601	0.929	0.329
Allose/Mannose/ Galactose/Glucose	Erythronate/Threonate	0.594	0.924	0.329
Tyramine/Tyrosine	Fructose/Sorbose	0.594	0.905	0.312
Xylitol/Ribitol	Norleucine	0.584	0.934	0.35
Fructose/Sorbose	Glutamine	0.578	0.866	0.288
Creatinine	Xylitol/Ribitol	0.575	0.749	0.174
Glutamate	Xylitol/Ribitol	0.562	0.741	0.179
Allose/Mannose/ Galactose/Glucose	Glycerol	0.534	0.800	0.266

c) Anoxia (0 % oxygen)

Metabolite A	Metabolite B	Difference	Correlation (WT)	Correlation (DN)
Glutamate	Beta-alanine	0.867	0.858	-0.008
Scyllo/Myo-inositol	Malate	0.769	0.805	0.036
Hypotaurine	Putrescine	0.721	0.752	0.030
Hypotaurine	Glutamate	0.698	0.822	0.124
Methionine	Lactate	0.682	0.773	0.091
5-oxoproline	Malate	0.681	0.833	0.152
Tyramine/Tyrosine	Malate	0.657	0.911	0.254
Scyllo/Myo-inositol	Beta-alanine	0.653	0.707	0.054
Malate	Norleucine	0.65	0.870	0.219
Xylitol/Ribitol	Malate	0.613	0.856	0.244
Methionine	Malate	0.607	0.853	0.247
Malate	Glycerol	0.591	0.902	0.311
Xylitol/Ribitol	Lactate	0.587	0.789	0.202
Allose/Mannose/ Galactose/Glucose	4-hydroxyproline	0.552	0.832	0.281
Allose/Mannose/ Galactose/Glucose	Lactate	0.541	0.758	0.217

Significant differences between WT and DN cells occurred between many different metabolites and from this it cannot be concluded that HIF-1 affects any one specific region of metabolism; rather its affect on cells exposed to different oxygen could be metabolome-wide. This potentially makes targeting HIF-1 in a hope to reduce cancer cell survival difficult if specific regions of metabolism are not identified. The best way to target metabolism would be to consider the metabolites that were most correlated in WT samples, irrespective of the difference in correlation between WT and DN. These include xylitol/ribitol strongly correlated to aspartate, methionine, norleucine *scyllo*/*myo*-inositol and tyramine/tyrosine as well as malate correlated to glycerol and tyramine/tyrosine. There are no reported chemical reactions involving ribitol in humans and therefore the peak likely derived from xylitol. Xylitol lies in the pentose and glucuronate interconversions pathway in KEGG (ko00040)[182] and can be converted in humans to D-xylose which is used in starch and sucrose metabolism and can be converted to and from many other sugars including glucose and fructose. Sugar metabolism is known to control many processes in cancer and especially in low oxygen[204] and therefore it is no surprise that these metabolites are highly correlated. More commonly used sugars in human metabolism may be stored in cancer cells as xylitol to be inaccessible by other biochemical reactions until needed. The correlation between xylitol and many other metabolites could be indicative of it being used as a carbon source to fuel many processes under oxidative stress. Malate is a key player in central carbon metabolism that is inter-converted to fumarate which feeds into tyrosine metabolism (involving tyrosine and tyramine). This is

likely the structure behind the correlation between malate and tyrosine/tyramine with HIF-1 regulating both the TCA cycle and tyrosine metabolism together. Succinate can also feed into tyrosine metabolism and could also be involved in this mechanism. Figure 46 shows a schematic for the TCA cycle where fumarate (directly adjacent to malate) and succinate feed into tyrosine metabolism.

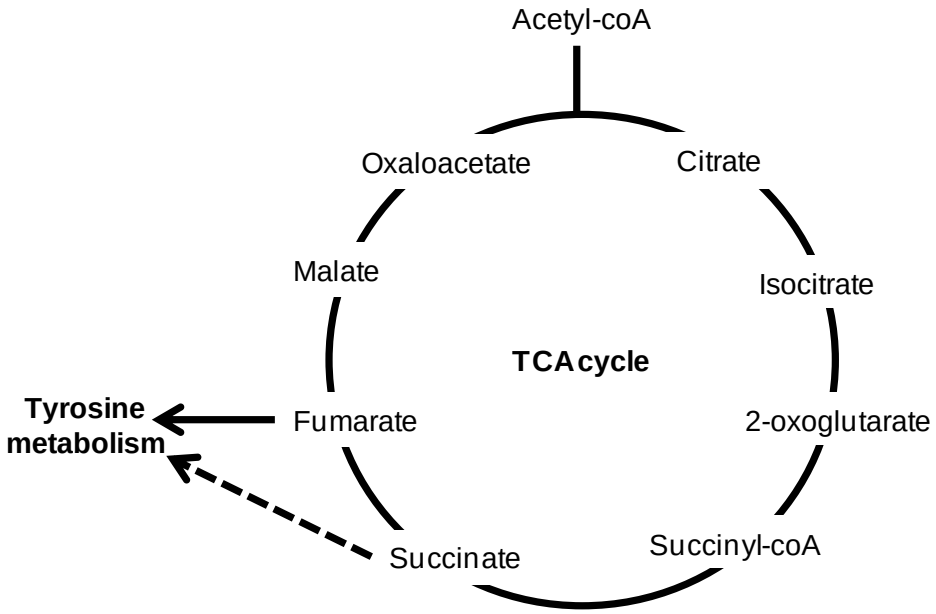

Figure 46: The interaction between the tricarboxylic acid (TCA) cycle and tyrosine metabolism that connects malate to tyrosine. Malate is inter-converted to fumarate that enters tyrosine metabolism along with succinate, another metabolite of the TCA cycle that feeds into tyrosine metabolism.

From the table it can be seen that correlation differences were due to metabolites being correlated in WT cells and the correlation being lost in HIF-1 deficient DN cells. These connections between metabolites potentially provide the structure behind cancer cell survival through HIF-1 mediated processes. There were some significant differences in correlations where metabolites were correlated in DN cells that were not correlated in WT cells but none exceeding a difference of 0.5. Network analysis was applied to these to investigate HIF-1 independent pathways.

Although there were fewer differences in normoxia than in the lower oxygen conditions, it was expected that WT and DN cells should have behaved the same under normoxic conditions and that there should be no significantly differently correlated metabolites. Additionally, these differences were not consistent between oxygen conditions so they could not be considered as artefacts of the cell lines. Rather, correlation analysis may be sensitive to very subtle differences caused by HIF-1 in each oxygen condition including normoxia that are not observed in other data analyses. A low level of HIF-1 expression

was observed in normoxic cells (Figure 33) suggesting that it could be regulating metabolic function in normoxic cells to a certain degree that is minimal and not highlighted in other analyses but that is revealed in correlation analysis.

Whilst direct differences between WT and DN cells at each oxygen level have shown the most important connections between metabolites promoted by HIF-1, a better way to consider the response of cells with and without HIF-1 is to determine differently correlated metabolites as a response to oxygen level change. This would help to elucidate how HIF-1 promotes metabolic changes in response to low oxygen or what mechanisms DN cells use in the absence of HIF-1 to promote survival in low oxygen. Correlation analysis was therefore also performed to compare normoxic WT cells with hypoxic WT cells and normoxic WT cells with anoxic WT cells to elucidate the greatest differences caused by decreasing oxygen availability to the cells. A difference in correlation was significant greater than 0.407 (as determined in chapter 2.14.3). There were 22 correlations exhibiting a difference greater than 0.407 for WT normoxia *vs.* hypoxia and 12 correlations exhibiting a difference greater than 0.407 for WT normoxia *vs.* anoxia. The same correlation analysis was applied to DN cells to elucidate the greatest differences caused by decreasing oxygen availability to the cells, but that could not be due to HIF-1. In this case there were 22 and 20 correlations meeting the requirements for WT normoxia *vs.* hypoxia and normoxia *vs.* anoxia respectively. Although there were 22 differences in pair-wise correlations between normoxia and hypoxia in both WT and DN cells, these pairs were not common, mainly due to the difference in metabolic profiles observed in hypoxia.

The greatest difference in correlation between WT cells exposed to normoxia and WT cells exposed to hypoxia occurred in the correlation between log transformed GC peaks identified as 4-hydroxyproline and allose/mannose/galactose/glucose. The difference was calculated to be 0.804 and was also observed to be the largest difference in correlation between WT cells exposed to normoxia and WT cells exposed to anoxia where the difference was 0.805. The GC peak areas observed for each metabolite in each normoxia and anoxia sample are plotted in Figure 47. These metabolites are correlated in hypoxia and anoxia but are not correlated in normoxia and must therefore be a response to low oxygen. This correlation was not observed when comparing DN cells exposed to normoxia and hypoxia or anoxia which suggests this correlation could be HIF-1 mediated.

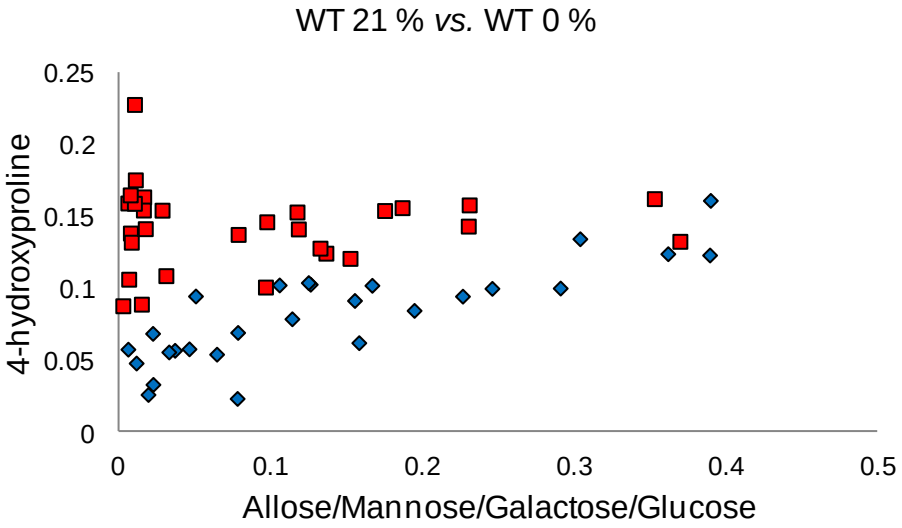

Figure 47: Pearson's product-moment correlation between 4-hydroxyproline and allose/mannose/galactose/glucose in HCT 116 wild type (WT) cells exposed to normoxia (21 %) represented in red squares or anoxia (0 %) represented in blue diamonds. The difference in correlation was calculated to be 0.805, where the correlation coefficients were 0.027 and 0.832 for WT normoxia and WT anoxia samples respectively.

The 4-hydroxyproline peak was correlated with many metabolites in hypoxia and anoxia and could therefore be considered a potential 'hub' in cellular response to low oxygen such that pathways involving this metabolite are changed in regulation. 4-hydroxyproline was correlated with 9 metabolites in addition to allose/mannose/galactose/glucose in hypoxic cells including asparate (r = 0.951), malate (r = 0.902), glutamine (r = 0.862), inositol (r = 0.89), methionine (r = 0.841), fructose (r = 0.815) and 2-hydroxyglutarate (r = 0.809). In anoxic cells 4-hydroxyproline was correlated with 3 metabolites in addition to allose/mannose/galactose/glucose including *scyllo/myo* inositol (r = 0.869), methionine (r = 0.813) and asparate (r = 0.796). None of these metabolites were correlated in normoxic cells suggesting that they were features of cell survival in low oxygen. There were more metabolites correlated with 4-hydroxyproline in hypoxia than anoxia. This was likely due to certain pathways being down regulated in the more stressful environment as cells utilise key pathways for survival which could be between 4-hydroxyproline and *scyllo/myo* inositol, methionine or aspartate; metabolites correlated with 4-hydroxyproline in both hypoxic and anoxic cells. 4-hydroxyproline was correlated with malate in hypoxic DN cells (r = 0.743) and fructose in anoxic DN cells (r = 0.717) which suggests that HIF-1 was not responsible for the correlation between 4-hydroxyproline and these two metabolites. All other metabolites correlated with 4-hydroxyproline were not correlated in DN hypoxic or anoxic cells suggesting they could be HIF-1 regulated. The 4-hydroxyproline metabolite could be related to the proline residues of HIF-1α that are

hydroxylated in normoxic cells and targeted for degradation by the ubiquitin ligase complex[205].

While 4-hydroxyproline seemed to be a controlling 'hub' metabolite in WT cells exposed to low oxygen, threonine appeared to be a 'hub' for normoxic WT cells. It was correlated with pyroglutamate (r = 0.895), aspartate (r = 0.892), erythronate (r = 0.852), lactate (r = 0.764) and malate (r = 0.718). These correlations were lost in low oxygen likely because the pathways between these metabolites are down regulated as they are not required to promote cell survival under low oxygen. These correlations were not flagged up as being different between DN cells exposed to normoxia or low oxygen which indicates that the loss of these correlations may be HIF-1 specific.

When comparing DN cells exposed to normoxia to cells exposed to hypoxia, the greatest difference in correlation was between citrate and malate which were positively correlated in hypoxia (r = 0.708) but weakly negatively correlated in normoxia (r = -0.224). In anoxic conditions the greatest difference in correlation was between citrate and aspartate which were correlated in anoxia (r = 0.9) but not in normoxia (r = 0.137). The log transformed GC peak areas observed for citrate *vs.* malate in normoxia and hypoxia samples are plotted in Figure 48. From this it can be clearly seen that the two metabolites were strongly correlated in hypoxic cells (blue) but a very weak negative correlation occurred between the metabolites in normoxic cells. Similar to 4-hydroxyproline in WT cells, many differences in correlations between normoxic and hypoxic cells involved citrate as a 'hub'. In the absence of HIF-1 citrate could be the control metabolite to promote cell survival in hypoxia. Citrate also appeared to act as a hub correlated with many other metabolites in anoxia. In addition citrate was shown to be differently correlated with a few metabolites in anoxic WT cells compared to normoxic cells. This suggests citrate and its associated pathways play a role in cell survival under extreme oxygen stress (such as anoxia) or in hypoxia as well when additional stress is added by the absence of HIF-1.

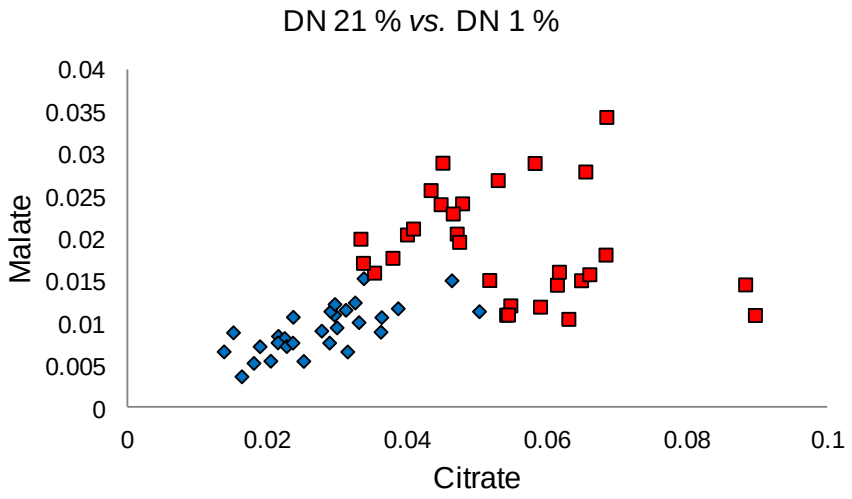

Figure 48: Pearson's product-moment correlation between citrate and malate in HCT 116 dominant negative (DN) cells exposed to normoxia (21 %) represented by red squares or hypoxia (1 %) represented by blue diamonds. The difference in correlation was calculated to be 0.931, where the correlation coefficients were 0.224 and 0.708 for DN normoxia and DN hypoxia samples respectively.

The strongest correlation between any two metabolites in hypoxic DN cells occurred between citrate and glutamine. The log transformed GC peak areas observed for citrate *vs.* malate in normoxia and hypoxia samples are plotted in Figure 49. This could be suggestive of the use of glutamine to fuel the TCA cycle[150].

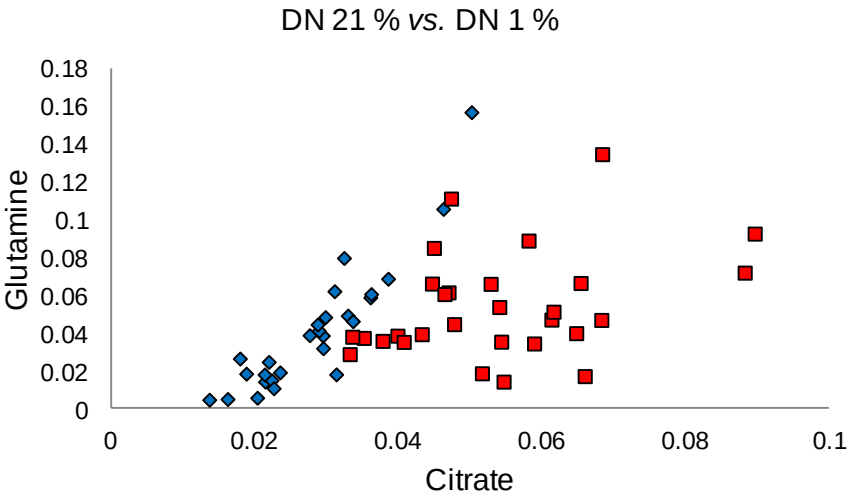

Figure 49: Pearson's product-moment correlation between citrate and glutamine in HCT 116 dominant negative (DN) cells exposed to normoxia (21 %) represented in red squares or hypoxia (1 %) represented in blue diamonds. The difference in correlation was calculated to be 0.563, where the correlation coefficients were 0.346 and 0.909 for DN normoxia and DN hypoxia samples respectively.

5.2.4. Network-based correlation analysis

Cancer is a highly complex disease utilising the differential regulation of many genes, transcription factors, proteins and metabolites. It is therefore no surprise that many different metabolites were correlated and that the environment cancer cells are exposed to changed correlations between metabolites. While correlation analysis was useful to identify key metabolites or phenotypic 'hubs' such as 4-hydroxyproline, threonine and citrate discussed; the information gained from correlation analysis is vast and to some extent ambiguous. Further analysis was required to analyse the data in terms of systems properties. To address this, correlated metabolites were mapped onto the EHMN to reveal the shortest pathway between them which could be vital in promoting cancer cell survival under certain environmental conditions such as hypoxia. Subsequently new sub-networks of these pathways were constructed to distinguish cross over in metabolic pathways and potentially reveal metabolic hubs that are not directly correlated but exist in many pathways connecting correlated metabolites.

Where possible correlations were mapped onto the EHMN and the shortest path between each pair of metabolites in the model was calculated. In some cases singly identified metabolites from the GC-MS data correspond to multiple EHMN metabolites. For example, aspartate corresponded to either L-aspartate or D-aspartate. Since there was no way of identifying which form of this metabolite was detected in the cells, correlations were mapped using both options. It was decided not to map correlations involving the GC peak identified allose/mannose/galactose/glucose as there were too many options and therefore such an exercise would not have enabled further understanding of the system. In some cases where GC peaks were identified to two metabolites, only one existed in the EHMN. In these cases the metabolite present in the EHMN was used. For example *scyllo*-inositol was not in the EHMN but *myo*-inositol was. Mapping correlations involving xylitol/ribitol was not successful since ribitol was not in the EHMN and xylitol was not highly connected in the network and therefore these correlations were not represented in sub-network reconstructions. Similarly, fructose/sorbose was mapped as fructose since sorbose was connected only with one other metabolite in the network and did not link up to any of its correlation paired metabolites.

Not mapping correlations due to metabolites not being present in the model, or there being too many options in the model to sensibly assign pathways, did limit the study to a certain

extent. For example the xylitol/ribitol peak was highly correlated in hypoxic WT cells and these correlations were lost with the absence of HIF-1 in DN cells. More than half of the differences in correlations between WT and DN cells in hypoxia involved this peak. Figure 50 shows the greatest difference between hypoxic WT and DN cells that involved the correlation between tyramine/tyrosine and xylitol/ribitol which were correlated in WT cells (r = 0.918) represented in red but not in DN cells (r = 0.073) represented in blue.

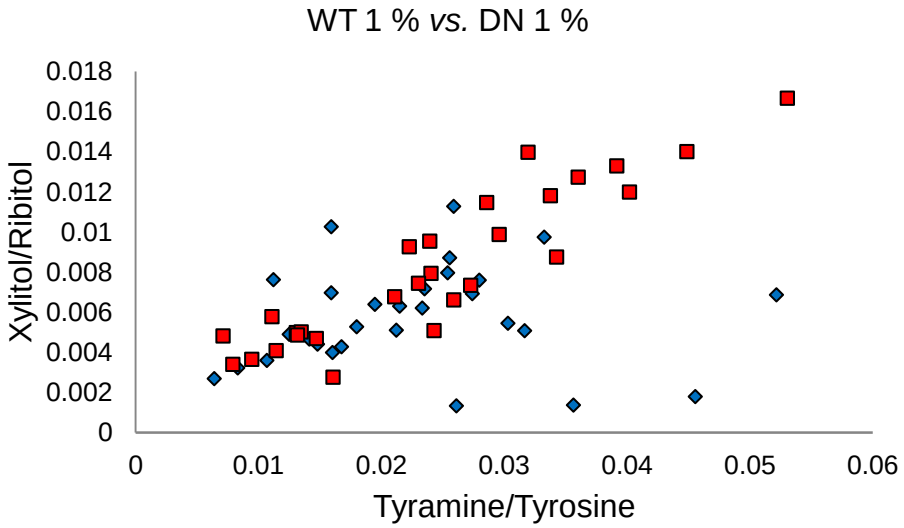

Figure 50: Pearson's product-moment correlation between tyramine/tyrosine and xylitol/ribitol in HCT 116 cells exposed to hypoxia (1 %). The log transformed gas chromatography (GC) peak areas are plotted for these two metabolites where wild type (WT) samples are shown in red squares and dominant negative (DN) samples in blue diamonds. The difference in correlation was calculated to be 0.845, where the correlation coefficients were 0.918 and 0.073 for WT and DN samples respectively.

Additionally some assumptions were made that may or may not be correct, for example when mapping correlations concerning the *scyllo*/*myo*-inositol peak as just *myo*-inositol. Nevertheless many correlations could be mapped onto the network and pathways visualised for different sub-networks as discussed below. Using this technique it was possible to visualise inter-connecting pathways regulated by each cell type under each oxygen tension and identify similarities and differences between sub-networks with respect to the pathways involved and the metabolites that appear to be 'hubs'.

Network analysis was first applied to correlations gained in DN cells that were identified during the comparison between WT and DN samples at each oxygen level. This was done to assess how cells coped with a deficiency in HIF-1 at each oxygen level in isolation. Pathways were identified that could be involved in cancer cell survival over the range of oxygen potentials in the absence of HIF-1 and are shown in Figure 51.

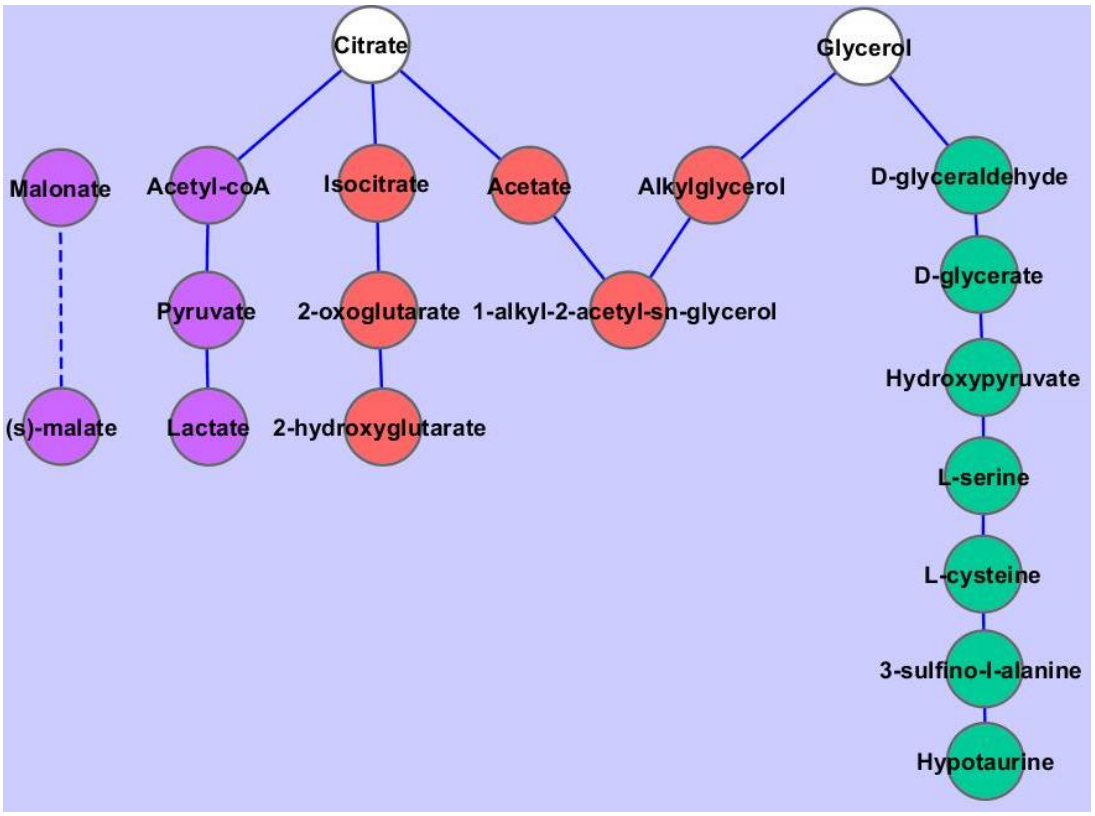

Figure 51: A schematic of all correlations that were identified in HCT 116 dominant negative (DN) samples that were significantly different to wild type (WT) samples. Metabolite nodes coloured in turquoise were normoxic, lilac were hypoxic, red were anoxic and white were shared between oxygen levels. The dotted line connecting malonate to (s)-malate is the only correlation that could not be mapped onto the EHMN due to malonate not being in the model.

The pathway connecting hypotaurine to glycerol in normoxic DN cells involved 3 main pathways as described in KEGG[182]: taurine and hypotaurine metabolism (ko00430) for hypotaurine through to L-cysteine, connected to D-glycerate *via* glycine, serine and threonine metabolism (ko00260) and glycerolipid metabolism (ko00561) to connect D-glycerate through to glycerol. Figure 52 shows how the identified pathway between hypotaurine and glycerol crosses over 3 'traditional' metabolic pathways represented by KEGG. Although it would be expected that hypotaurine metabolism would be a regulatory feature of oxidative stress due to its antioxidant properties[206] irrespective of HIF-1 function, it could be the first response for cells deficient in HIF-1 to either the exceptionally low (background) level of hypoxia (that could be occurring in the normoxic condition over time) or, more likely, as a preventative mechanism in these cells lacking HIF-1 to scavenge free radicals before the effect of hypoxia exceeds a response that this pathway can function (hence why it is not observed as a key feature in hypoxic and anoxic DN cells). L-cysteine and L-serine have been linked previously with colorectal carcinoma metastatic invasion[207], but not with specific roles in hypoxia. It would not be expected that these metabolites be key in DN cellular function in normoxia and not in WT, however the method of generating a shortest path between the two differently correlated metabolites, in

this case hypotaurine and glycerol, may use metabolites whose concentration was not directly affected by a lack of HIF-1.

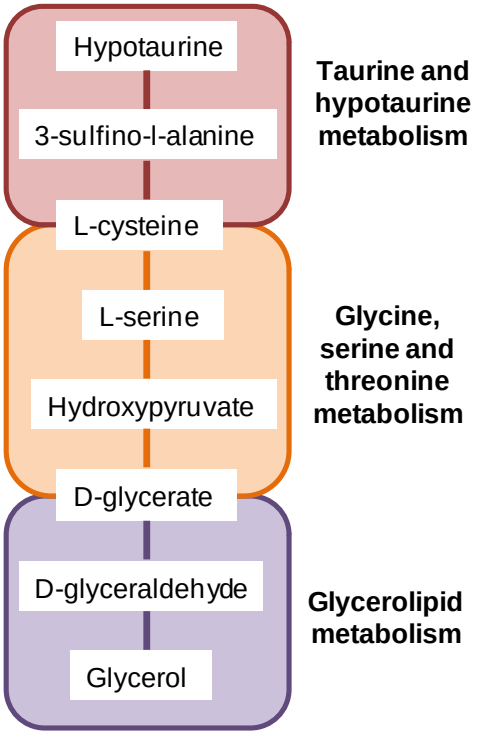

Figure 52: Hypotaurine and glycerol are connected *via* 3 main Kyoto encyclopedia of genes and genomes (KEGG) pathways: taurine and hypotaurine metabolism, glycine serine and threonine metabolism and glycerolipid metabolism.

There were two main responses identified as hypoxic features of DN cells including the pathway connecting citrate and lactate and the correlation between malonate and malate. The connection between citrate and lactate was likely a direct central carbon metabolism response connecting anaerobic metabolism of glucose to lactate and aerobic metabolism of glucose through the TCA cycle. The pathway formed between the two metabolites connects these two mechanisms and suggests a shift between aerobic and anaerobic metabolism as a response to hypoxia. Figure 53 shows a schematic for how citrate and lactate are connected around the TCA cycle. This correlation was also positive in WT cells, but was significantly higher in DN cells suggesting their greater dependence on this mechanism for survival in hypoxia. Malonate is known to be an inhibitor of succinate dehydrogenase (SDH), an enzyme that catalyses reactions in the TCA cycle and in oxidative phosphorylation[208]. SDH catalyses the reaction between succinate and fumarate, the latter of which is subsequently converted to malate in the TCA cycle. The positive correlation between malate and malonate suggests while the concentration of malate is increased through its synthesis in the TCA cycle, the concentration of malonate is increased in a negative feedback response to control the concentration of malate. Similar to

the citrate-lactate response, malate and malonate were also positively correlated in WT cells but were correlated significantly higher in DN cells.

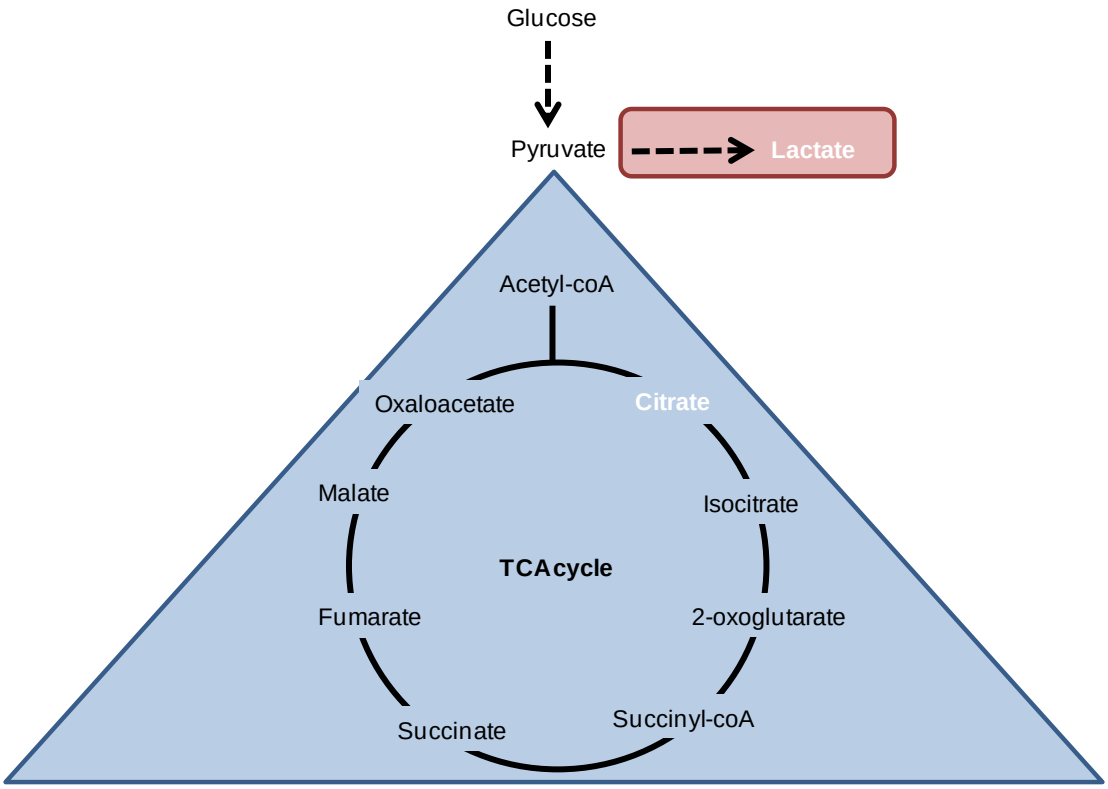

Figure 53: Schematic for the aerobic and anaerobic metabolism of glucose. Glucose is metabolised *via* intermediates to pyruvate which can then be metabolised to lactate (traditionally anaerobic) or enter the tricarboxylic acid (TCA) cycle *via* acetyl-coA (traditionally aerobic as an intermediate between glycolysis and oxidative phosphorylation).

Citrate was correlated to 2-hydroxyglutarate and glycerol, creating two interlinking pathways associated with the DN cellular response to anoxia. The pathway connecting citrate to 2-hydroxyglutarate is likely to be indicative of the effect of 2-hydroxyglutarate on the part of the TCA cycle that connects citrate *via* isocitrate to 2-oxoglutarate. Although it has not been shown in colorectal cancer, it is known that mutations in isocitrate dehydrogenase 1 (IDH1), the enzyme that catalyses the reaction between isocitrate and 2-oxoglutarate, can induce an ability to catalyse a reaction between 2-oxoglutarate and 2-hydroxyglutarate rather than its usual function of oxidative decarboxylation of isocitrate[209]. Thus, 2-hydroxyglutarate has been described as an 'onco-metabolite' in cancer, enabling progression in malignancy and arising from mutations in isocitrate dehydrogenase 1[209]. This pathway has arisen from a strong positive correlation between citrate and 2-hydroxyglutarate. If this was due to a loss of 2-hydroxyglutarate accumulation in DN cells for example, citrate would also be lower since isocitrate is needed for its conversion to 2-oxyglutarate by IDH1 functioning normally. Conversely

these two metabolites could equally be maintained to high concentrations if the function of IDH1 is reduced in DN cells as a result of anoxia, ensuing accumulation of 2-hydroxyglutarate *via* the new induced reaction between 2-oxoglutarate and 2-hydroxyglutarate and an accumulation of citrate since the demand for its conversion into isocitrate is reduced. To estimate which scenario was more likely the mean peak area of 2-oxoglutarate and 2-hydroxyglutarate have been compared in anoxic DN cells and the concentration of the latter was found to be higher, suggesting that citrate and 2-hydroxyglutarate are maintained high by reduced function of IDH1 while the intermediate isocitrate and 2-oxoglutarate are maintained lower. Although the data give reasonable evidence for this, it cannot be definitively confirmed from these data as no comparison can be made between the concentrations of citrate and iscocitrate since the peak area is inclusive of both metabolites. This is because a distinction cannot be made between these isoforms using GC-MS and the identifications of citrate and 2-oxoglutarate were only putative due to a retention index error. The correlation between citrate and glycerol and the pathway connecting them in anoxic DN cells could be indicative of a shift between central carbon metabolism and lipid metabolism using citrate as a substrate for either. Figure 54 shows the relationship between citrate correlations to glycerol and 2-hydroxyglutarate in anoxic DN cells.

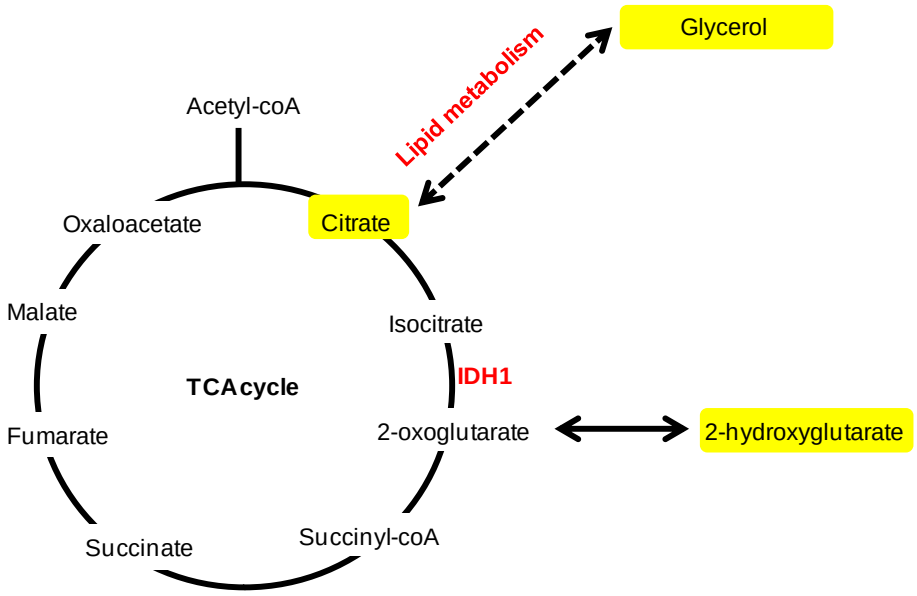

Figure 54: Citrate is a metabolite of the tricarboxylic acid (TCA) cycle and also a precursor for lipid metabolism. It was correlated to glycerol and 2-hydroxyglutarate in anoxic DN cells. The schematic shows how citrate connects to both glycerol and 2-hydroxyglutarate.

Metabolism is usually considered in terms of pathways in the way they are traditionally represented in KEGG etc. However, many of these pathways inter-connect and it is possible to consider new pathways that cross over several 'traditional' pathways that may potentially be more biochemically relevant than each of the traditional pathways. This is depicted in Figure 55. The method used to build sub-networks of differently correlated metabolites in this research has found pathways that connect correlated metabolites *via* the shortest route. This means many pathways form from interactions between traditional pathways and thus cross over them. Sub-networks have been built considering metabolic pathways in this different way and although this is less conventional, it has made it possible to reveal potentially more relevant pathways than if only 'traditional' pathways were considered. An example of this was shown in Figure 52 where the connection between hypotaurine and glycerol crossed 3 traditional pathways.

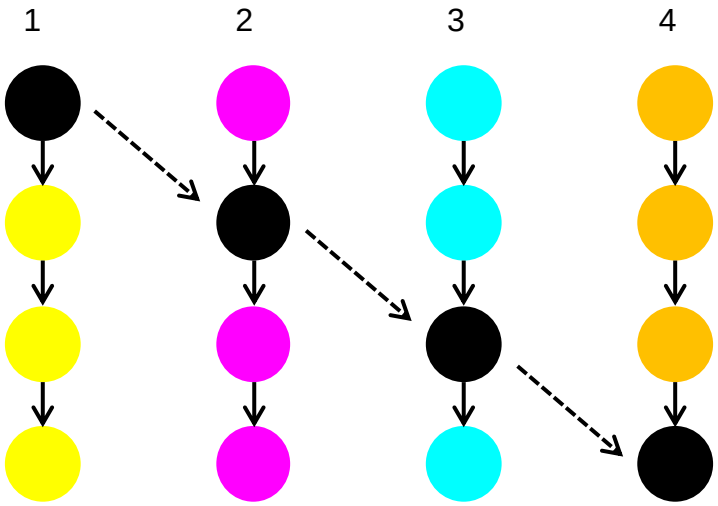

Figure 55: A different way to view metabolic pathways. Metabolism involves many inter-connections between metabolites; however there are traditional ways to represent pathways. In this schematic1, 2, 3 and 4 represent 4 individual pathways as they are traditionally considered, however a pathway exists in metabolism that can connect these 4 pathways *via* the intermediates of each. This pathway (highlighted in black) could be biochemically more important than 1, 2, 3 or 4.

Rather than just considering differences between WT and DN cells at each oxygen tension in isolation, the way in which each cell line responded to low oxygen environments were compared. For this sub-networks of differently correlated pathways were made for WT cells exposed to normoxia compared to hypoxia (Figure 56), for DN cells exposed to normoxia compared to hypoxia (Figure 57), for WT cells exposed to normoxia compared anoxia (Figure 58) and for DN cells exposed to normoxia compared to anoxia (Figure 59). Cross comparisons between WT and DN networks were then made and represented by colouring metabolite nodes on each sub-network in blue where the same pathway was

regulated or yellow where the same metabolite was involved but not in the same pathway(s) irrespective of cell line. Such metabolites are likely to be regulated by non-HIF-1 mediated responses to hypoxia or anoxia. Pathways unique to WT cells were assumed to be regulated by HIF-1 and pathways unique to DN cells were assumed to be regulated as alternative coping mechanisms in the absence of HIF-1. The advantages of assessing these sub-networks are to reveal the HIF-1 specific mechanisms that could be targeted to reduce HIF-1 mediated survival in cancer cells (pink nodes), to identify the alternative metabolic routes HIF-1 deficient cells use that could be employed by WT cells if HIF-1 pathways are truncated in therapy (white nodes) and the pathways that are common (HIF-1 independent) and appear to be central in cancer cell metabolism and perhaps the best target in cancer therapy.

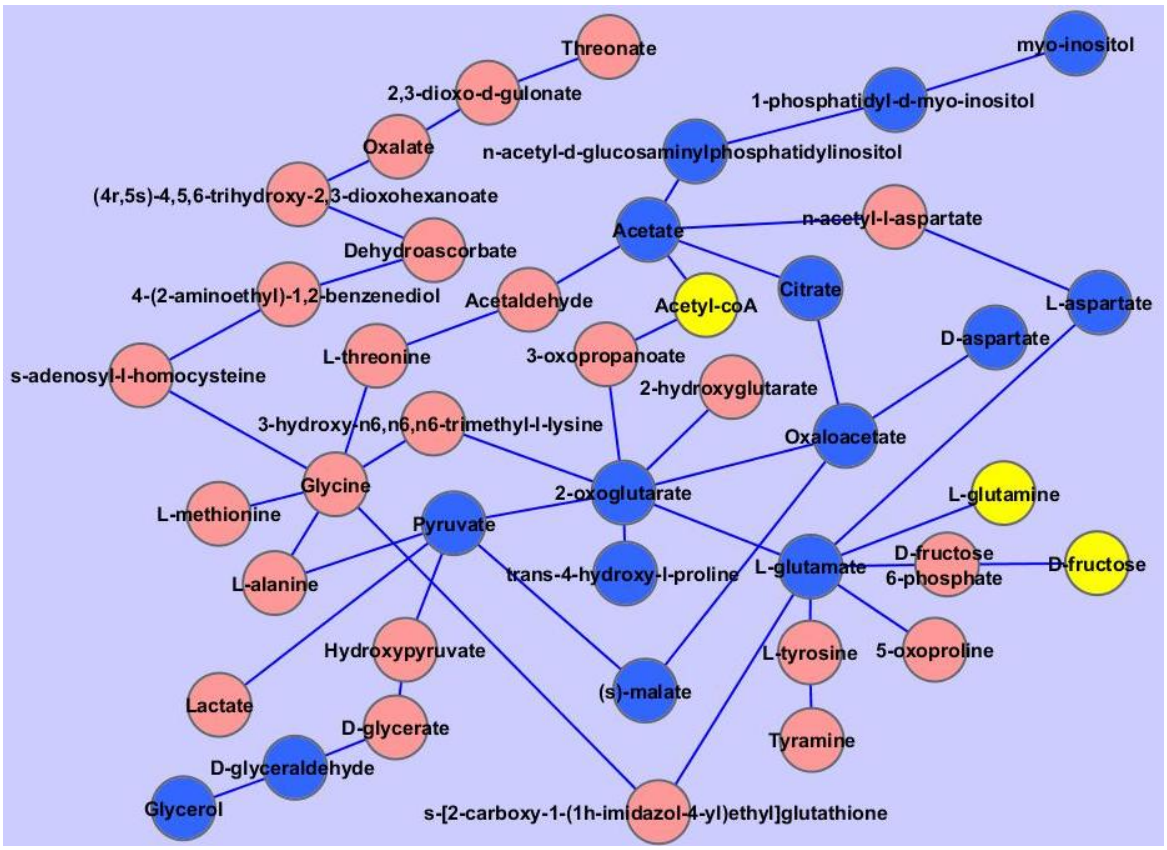

Figure 56: Sub-network representation of pathways between metabolites that were shown to be differently correlated between normoxic and hypoxic HCT 116 wild type (WT) samples. Metabolite nodes coloured pink were unique to WT cells, those coloured in blue were also observed in the comparison between normoxic and hypoxic DN samples and yellow nodes are metabolites that were also observed in the dominant negative (DN) comparison but that were not connected to the same neighbours as they were in WT samples.

One central hub observed in the WT network that does not exist in the DN network for differential correlations between normoxia and hypoxia is glycine. It has been previously shown that glycine is reduced in cells deficient in HIF-1[33, 210], which would explain the

loss of this hub as a regulator of hypoxia in the DN cells. Connected to glycine and the major route for non-HIF-1 dependent regulation of hypoxia (indicated by the blue nodes) is alanine. Previously, alanine has been shown to increase in hypoxic tumours in conjunction with lactate, where the conversion of pyruvate to alanine alleviates a single build up of lactate[211]. Furthermore, lactate may be more indicative of mild hypoxia than severe hypoxia[211], which could explain why lactate is more highly connected in the sub-network for hypoxia compared to anoxia. In DN cells this pathway seemed to be regulated by hypotaurine metabolism which functions biochemically as an antioxidant pathway that protects cells under environmental stress[206]. This may suggest that in the absence of HIF-1 there was a higher demand for protection against reactive oxygen species and free radicals in hypoxic cells.

Myo-inositol is a common node irrespective of HIF-1 function and is known to be involved in volume and osmo-regulation that is particularly important in colon carcinomas[206]. Glutamine, fructose and acetyl-coA are nodes common between WT and DN cells differentially correlated in normoxia and hypoxia but do not connect to the same pathways. Acetyl-coA was connected to acetate in WT cells and citrate in DN cells. This difference may not be biologically relevant, it may be that connecting to one rather than the other offers a shorter route to the metabolite of interest. Therefore this could be an artefact arising from the method rather than a biochemical marker of HIF-1 response. Glutamine however was involved in two very different correlations in WT and DN cells. In WT cells it was strongly correlated with 4-hydroxyproline in hypoxia (r = 0.862) and in DN cells it was strongly correlated with citrate in hypoxia (r = 0.909). In WT cells 4-hydroxyproline could possibly arise from the prolyl-4-hydroxylases that modify HIF-1 such that the α subunit can be marked for degradation in normoxia[205] that may accumulate in hypoxia due to lack of this function and instead be involved in glutamine metabolism. In DN cells, glutamine was correlated with citrate which is a potential marker of glutamine metabolism and the use of glutamine as an alternative carbon source to fuel the TCA cycle[150].

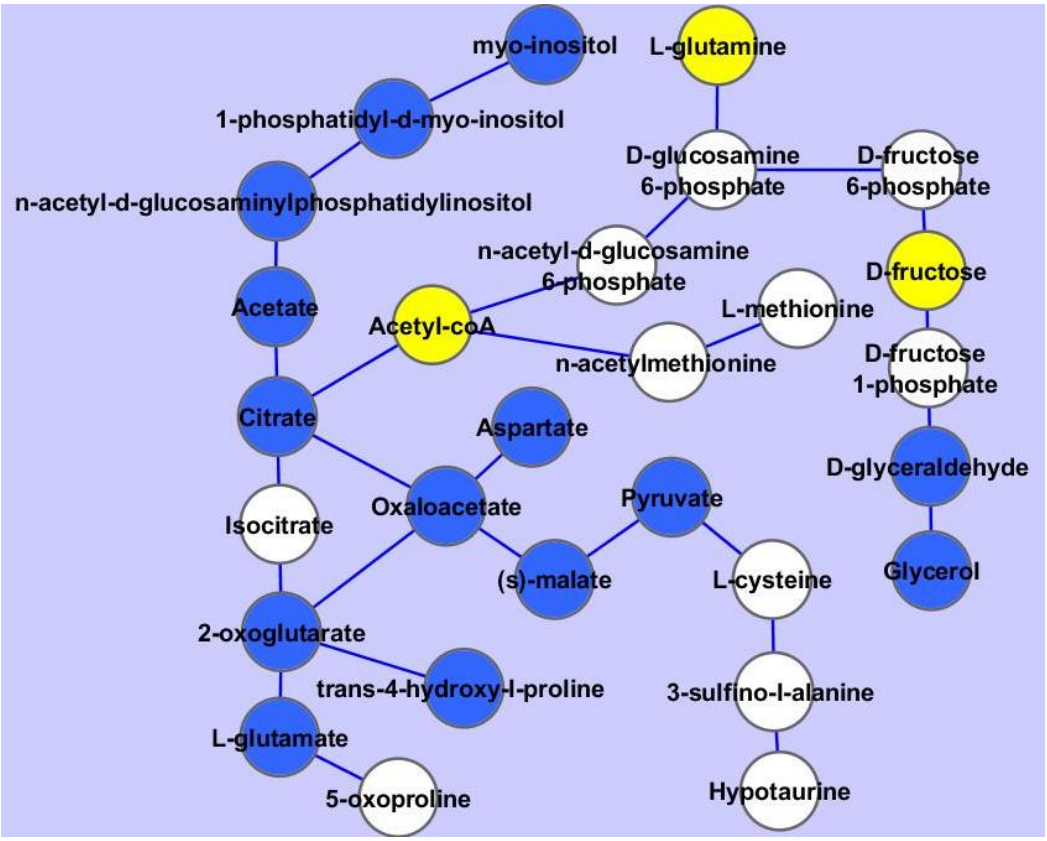

Figure 57: Sub-network representation of pathways between metabolites that were shown to be differently correlated between normoxic and hypoxic HCT 116 dominant negative (DN) samples. Metabolite nodes coloured white were unique to DN cells, those coloured in blue were also observed in the comparison between normoxic and hypoxic wild type (WT) samples and yellow nodes are metabolites that are also observed in the WT comparison but that were not connected to the same neighbours as they were in DN samples.

When considering the common pathways between WT and DN cells in normoxia compared to hypoxia, it appeared that the response was largely centred on citrate with its involvement in the TCA cycle and its connection to *myo*-inositol. Some of these connections were observed to be more significant in DN cells when directly comparing hypoxic and anoxic WT and DN cells (Figure 51), but they were also relevant features of WT metabolism when assessing the metabolic changes associated from the shift from a normoxic to hypoxic environment. Furthermore, this network included more connections that were missed by simply comparing WT and DN cells at each oxygen environment in isolation. Central carbon metabolism controls to some extent most other regions of metabolism through the energy and bio-precursors generated. Carbon utilisation in nucleic acid, polyamine and amino acid metabolism that all sprout from central carbon metabolism are known targets of the proto-oncogene c-Myc as a response to hypoxia[212].

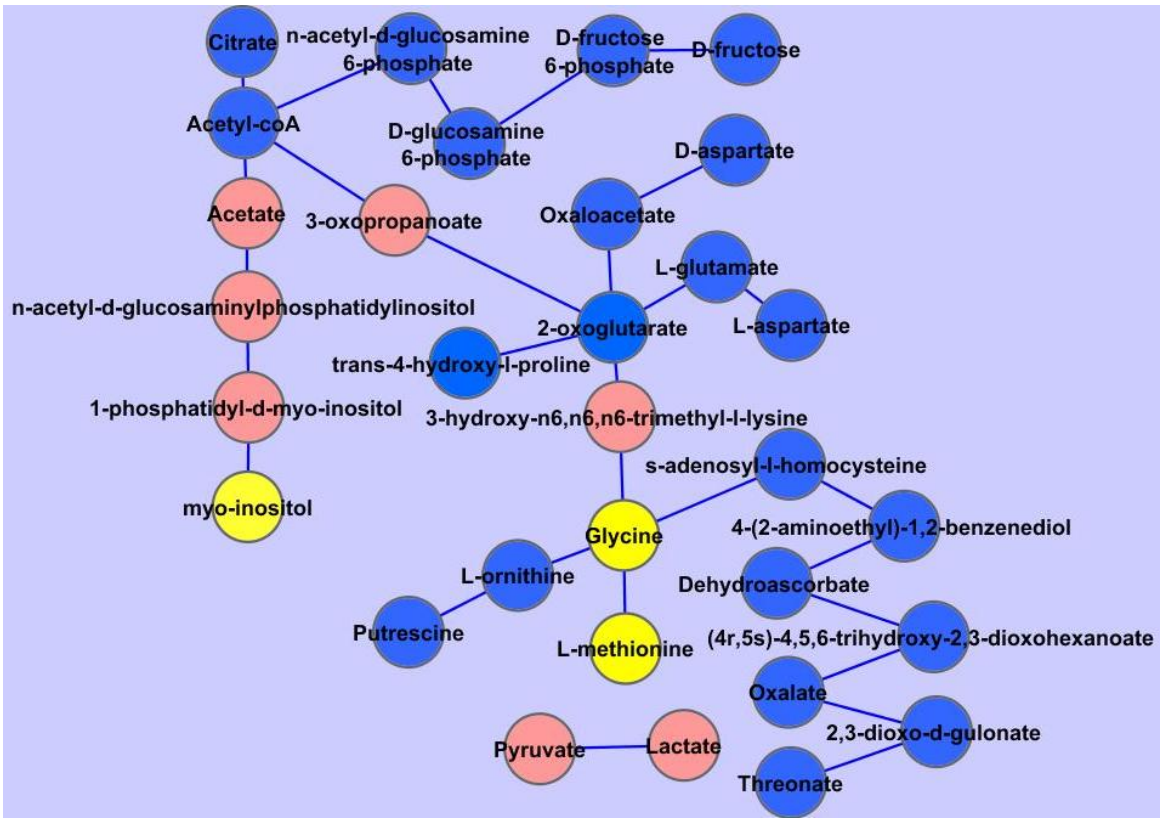

Figure 58: Sub-network representation of pathways between metabolites that were shown to be differently correlated between normoxic and anoxic HCT 116 wild type (WT) samples. Metabolite nodes coloured pink were unique to WT cells, those coloured in blue were also observed in the comparison between normoxic and anoxic dominant negative (DN) samples and yellow nodes are metabolites that were also observed in the DN comparison but that were not connected to the same neighbours as they were in WT samples.

In contrast, when considering the conserved pathways between WT and DN cells in the sub-networks showing the differential correlation network for normoxia compared to anoxia, central carbon metabolism no longer features. Instead vitamin C, tyrosine and amino and nucleotide sugar metabolism are the conserved mechanisms irrespective of HIF-1. DN cells further rely upon amino and nucleotide sugar metabolism by connecting additional sugars into the network. Nucleotide sugars were used metabolically in protein glycosylation to maintain protein stability and aid in protein trafficking within cells[204]. Disturbances in glycosylation patterns expressed in proteins lead to cellular abnormalities and are often associated with cancer phenotype. It is still unknown how hypoxia affects nucleotide sugars[204], however the data could suggest that without HIF-1 it may not be possible to keep glycosylation patterns in check under extremely low oxygen environments and this could be why DN cells indicate a disturbance in the glycosylation processes needed for cells to function normally through nucleotide sugars.

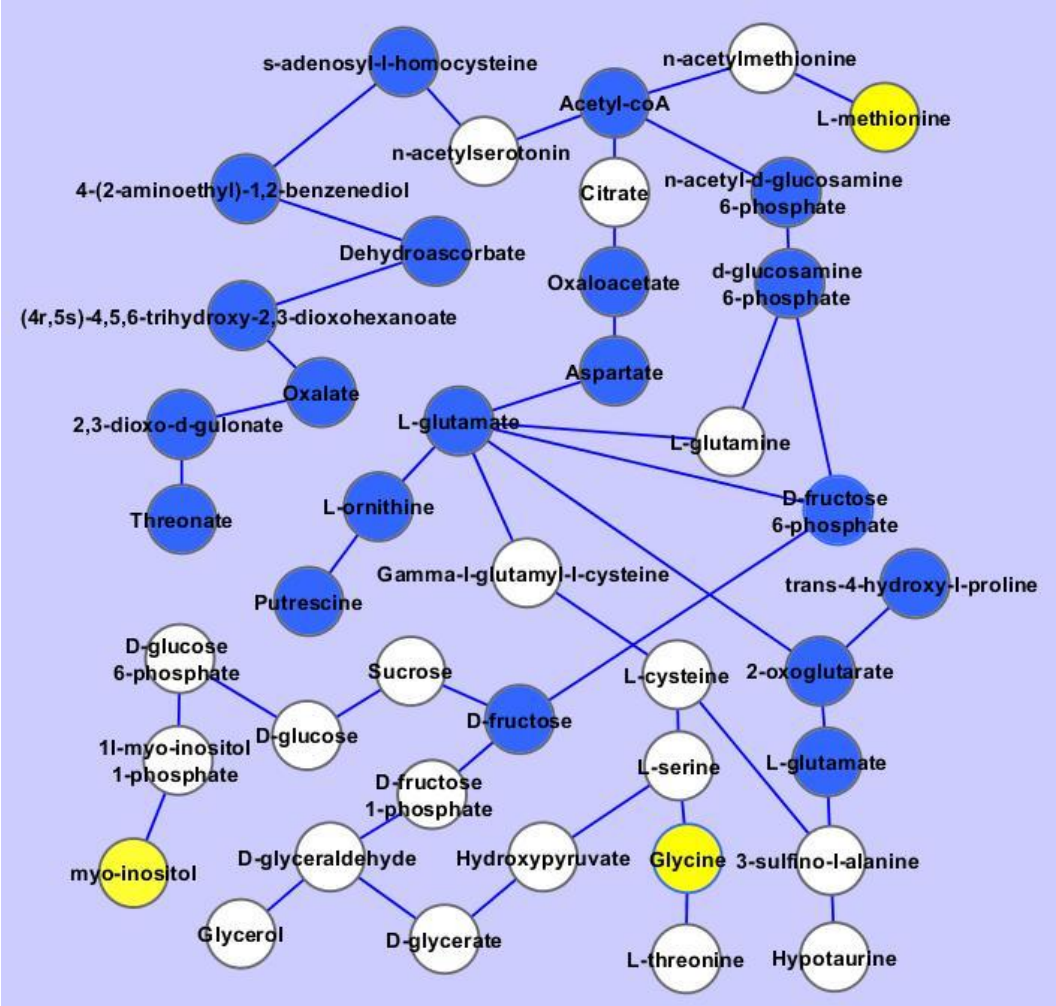

Figure 59: Sub-network representation of pathways between metabolites that were shown to be differently correlated between normoxic and anoxic HCT 116 dominant negative (DN) samples. Metabolite nodes coloured white were unique to DN cells, those coloured in blue were also observed in the comparison between normoxic and anoxic wild type (WT) samples and yellow nodes are metabolites that are also observed in the WT comparison but that were not connected to the same neighbours as they were in DN samples.

5.3. Conclusion

Network-based correlation analysis of metabolites measured using GC-MS has proved a novel and highly useful tool to visualise the responses of HCT 116 cells to hypoxia or anoxia when compared to normoxia. Using this method many correlations were identified including those known to be associated with colon carcinomas, those associated with low oxygen irrespective of HIF-1 function and those that are specifically HIF-1 mediated. Pathways have been identified in each scenario, highlighting regions of the metabolome that could be targeted in cancer therapy, in particular colon carcinoma therapy.

There were interesting findings from both correlation analysis and network-based correlation analysis. Findings from correlation analysis included the revelation of

4-hydroxyproline as an apparent ‘hub’ in WT cells exposed to low oxygen and citrate as an apparent ‘hub’ in DN cells exposed to low oxygen. Sugar metabolism along with the connection between the TCA cycle and tyrosine metabolism were highlighted as some of the main differences between WT and DN cells in the way they respond to low oxygen. The correlations between citrate and glycerol potentially *via* lipid metabolism and between citrate and 2-hydroxyglutarate potentially involving IDH1 with reduced function in anoxic DN cells were also particularly interesting. From network-based correlation analysis, elements of central carbon metabolism including pyruvate, malate, oxoalacetate and citrate appeared to be conserved irrespective of HIF-1. HIF-1 specific pathways that were not observed in DN pathways centred on glyine in hypoxia. In anoxia, a HIF-1 specific ‘hub’ metabolite was not revealed. Rather, the connections appeared to be more linear, for example the pathway between *myo*-inositol and citrate.

Pathways are often compounded of different features within ‘traditional’ pathways but have provided an alternative way of viewing cancer metabolism. Analysing sub-networks showing the change in pathway regulation caused by lowering the oxygen microenvironment cells were exposed to have enabled a clearer understanding of the metabolic effects of HIF-1 and hypoxia in general. Additionally, it has revealed alternative pathways that can mediate cancer cell survival in low oxygen environments if HIF-1 pathways were to be targeted. Truncating HIF-1 metabolic pathways will likely induce an up-regulation of the responses observed in DN cell metabolic profiles. This could be vital when considering new cancer therapies, and would not have been considered using other methods of analysing metabolic profiles. Alternatively, the conserved pathways observed irrespective of HIF-1 function seem to be central in each scenario and therefore targeting these pathways could be potentially the best targets to damage cancer cell metabolism in hypoxia beyond its repair, thus offering sustainable targets for the future.

Chapter 6. Metabolic profiling and imaging using ToF-SIMS

6.1. Introduction

IMS is a novel method for the analysis of biological samples *in situ* combining mass spectrometry and microscopic imaging. The chemical organisation of a sample is likely to be correlated with its physical features and therefore spatially localising and co-localising groups of chemicals elucidates properties of structure and potentially reveals information about their function in a biological system. IMS is currently of paramount importance and receiving significant attention in the mass spectrometric community[83]. While there are a variety of mass spectrometric instruments capable of imaging[80, 96, 213], due to its recent successes in bio-imaging of samples from cells[214] to tissues[215], ToF-SIMS is a popular choice. The information gained from analysing biological samples using IMS depend on numerous parameters including amongst others the sensitivity of ionisation, sample preparation and the spatial and mass resolution offered by the instrument used[216]. Current ToF-SIMS instruments available for IMS benefit from remarkable spatial resolution with reasonable mass resolution[106, 217, 218]. The way in which samples should be prepared to optimise results has been explored[219, 220]. As a technique, it is ideal for analysing at low mass, often but not restricted to masses <1000 Da, making it an ideal choice for the application of IMS in metabolic studies.

In this research, the potential for ToF-SIMS as a key contributor in IMS based identification of metabolites has been explored. Reference data was first collected as evidence for the possibility for metabolite analysis using ToF-SIMS. This included the analyses of a collection of metabolite standards, assessing how the detection of metabolites is influenced by the chemistry of mixtures that are relevant to the analysis of complex biological samples. Additionally, an example limit of detection was obtained using one standard and the level of biomass required to identify metabolites in biological samples using ToF-SIMS was explored.

Subsequently it was determined that ToF-SIMS is capable of metabolic profiling in biological samples highlighting its ability to identify metabolites relevant to biological systems. For this, its value in elucidating spatial biochemical information about the structure and function of MTSs was explored. MTSs are structures formed from cancerous cells to represent initiating tumours that exhibit decreasing gradients of oxygen from the periphery to the core. MTSs and in particular those formed from HCT 116 cells are

regarded as a respectable model for tumour initiation and have been used in a wide variety of experiments to study tumour properties[116, 221, 222]. Success in ToF-SIMS analysis in imaging MTSs would provide an extension to the results revealed from the previous chapters regarding metabolites highlighted for their potential involvement in cancer cell survival in low oxygen environments with and without the expression of HIF-1. This would allow an assessment of how the interaction of cells in such structures changes the metabolic phenotype under a more natural gradient of oxygen availability. Therefore it could be possible to reveal metabolic profiles specific to particular regions of tumours that are indicative of its function. The J105 *3D Chemical Imager* using polyatomic primary ion bombardment benefits from having the ability to image samples in *2D* and *3D* with a mass resolution $m/\Delta m \approx 10\ 000$ at mass 500 and a mass accuracy of 5 ppm[104]. It was therefore considered the optimal instrument to explore the potential of ToF-SIMS in metabolic profiling. Its high mass resolution was utilised in generating a standards library for metabolites that could be identified in high spatial resolution images of MTSs.

6.2. Results and discussion

A range of experiments were performed using ToF-SIMS with C_{60}^+ primary ion bombardment to collect mass spectra and images from metabolite standards to biological samples. Preliminary experiments were done to assess the potential for ToF-SIMS in metabolite analysis, a field in which the technique is ideally suited due to its target mass range (inclusive of metabolites), its potential to profile biological samples *in situ* and its potential to analyse biological samples intact since it requires no prior separation of compounds or injection into disruptive environments such as high temperature (other than vacuum) before mass spectrometric analysis.

6.2.1. Collection of metabolite standards for ToF-SIMS

Since ToF-SIMS is a pioneering technique for metabolic analysis of biological samples, there are very few standard spectra available for metabolites. Therefore 20 metabolite standards were analysed at 1 mM concentrations and standard spectra were obtained in positive ion mode for each. A summary of observed $[M+H]^+$ ions and fragments from the MS and MS2 spectra are given in Table 10 for the 16 metabolites that ionised well. With the exception of glycine, all 16 metabolites had intense fragments in addition to the

$[M+H]^+$ ion that could be used as characteristic ions for defining each metabolite. Arginosuccinate, ATP, cysteine and glutamate did not ionise well in positive ion mode and therefore standard spectra for these metabolites were not obtained.

The standard ToF-SIMS spectra were compared to freely available databases such as MassBank[223] and most standards were found to be highly comparable to standard spectra in the database obtained using LC-ESI-QTOF (highlighted in Table 10). This presents the possibility for using this database and in particular entries from this analytical technique to characterise ToF-SIMS spectra to identify intense fragments in ToF-SIMS profiling spectra[134]. However, since many fragments common between ToF-SIMS and LC-ESI-QTOF spectra are also common between more than one metabolite, it would be advisable to use additional ToF-SIMS fragments for more accurate metabolite identification.

Table 10: Metabolite standards analysed on the J105 and their comparison to standards from other techniques in the literature adapted from Fletcher *et al.* (2012)[134] A summary of the peaks identified in the standard spectra is given for the 16 metabolites of the 20 analysed that yielded spectra characteristic of each metabolite. The observed molecular $[M+H]^+$ ion *m/z* is given for each metabolite along with the most intense fragments observed in the mass spectrometry (MS) spectra (quoted to closest 0.05 Da) and the fragments yielded from tandem mass spectrometry (MS2) (quoted to closest 0.1 Da) of the $[M+H]^+$ ion. Time-of-flight-secondary ion mass spectrometry (ToF-SIMS) spectra were compared to standards in MassBank (unless otherwise stated) and the common fragments between them are given. The *m/z* 265.10 peak identified in the thiamine spectrum is marked with an asterisk due to it being a radical molecular ion that was observed and not the $[M+H]^+$.

Compound	**Molecular ion $[M+H]^+$**	**ToF-SIMS Fragments**	**MS2 fragments from CID of $[M+H]^+$ ion in ToF-SIMS**	**Of which common with MassBank from MS2 of $[M+H]^+$ ion**	**Database spectrum used (from MassBank unless stated otherwise)**
Arginine	175.10	158.10, 130.10, 116.05, 112.10, 70.10, 60.05	-	158.1, 130.1, 116.1, 112.1, 70.2, 60.2	Arginine; ESI-IT-MS/MS; *m/z*: 175.2; $[M+H]^+$
Carbamoyl aspartate	177.05	159.05, 134.05, 116.05, 88.05, 74.05, 70.05	134.1, 88.1	-	Data not currently available in Massbank or Metlin
Fumarate	117.00	99.00,	71.0		Positive ion data not currently in Massbank or Metlin
Glucose	181.1	163.05, 145.05, 127.05, 109.10, 97.10, 95.10, 85.05, 81.1, 71.10, 69.05	-	-	$[M+H]^+$ ion data not currently in Massbank or Metlin.
Glycine	76.00	-	-	76.04	Glycine; LC-ESI-QTOF; MS2; MERGED; $[M+H]^+$

Guanine	152.05	135.05, 110.05	135.1, 110.1,43.0	135.06, 110.06	Guanine; LC-ESI-ITFT; MS2; *m/z*:152.06; POS
Guanosine	284.10	152.05, 135.05, 110.05	152.2	152.06, 135.03, 110.04	Guanosine; LC-ESI-QTOF; MS2; MERGED; $[M+H]^+$
Malate	135.05	117.00, 99.00, 89.00, 71.00	117.0, 89.1, 71.0	-	Data not currently available in Massbank or Metlin
Ornithine	133.10	116.10, 115.10, 70.10	116.1, 70.1, 58.1, 43.1	133.08, 116.07, 115.09, 70.07	L-Ornithine; LC-ESI-QTOF; MS2; MERGED; $[M+H]^+$
Phenylalanine	166.10	120.10, 103.058, 91.05, 77.05	120.1, 91.1, 77.1	120.08, 103.05, 91.05, 77.04	L-(-)-Phenylalanine; LC-ESI-QTOF; MS2; MERGED; $[M+H]^+$
Proline	116.10	70.05, 68.05	70.1	70.07, 68.05	L-(-)-Proline; LC-ESI-QTOF; MS2; MERGED; $[M+H]^+$
Thiamine	265.10	144.05, 122.05, 81.05	122.10	144.05, 122.07, 81.05	Thiamine; LC-ESI-QTOF; MS2; MERGED; $[M+H]^+$
Tryptophan	205.10	188.05, 170.05, 159.10, 146.05, 144.10, 143.05, 132.10, 130.05, 117.05, 115.05	188.10, 130.10	188.07, 170.06, 159.09, 146.06, 144.08, 143.07, 132.08, 130.07, 117.06, 115.05	L-Tryptophan; LC-ESI-QTOF; MS2; MERGED; $[M+H]^+$
Tyrosine	182.10	165.05, 147.05, 136.10, 123.05, 119.05, 107.05, 91.05, 77.05	165.1, 136.1, 123.1, 119.1, 107.1, 91.1, 77.1	165.06, 136.08, 123.04, 119.05, 107.05, 91.05, 77.04	L-Tyrosine; LC-ESI-QTOF; MS2; MERGED; $[M+H]^+$
Urea	61.05	55.05	-	61.0402	Urea; LC-ESI-QTOF; MS2; MERGED; $[M+H]^+$
Valine	118.10	72.10, 55.05	72.1, 57.1, 55.1	72.08, 55.05	L-Valine; LC-ESI-QTOF; MS2; MERGED; $[M+H]^+$

MS2 was performed on the $[M+H]^+$ ion (or $[M]^+$ ion for thiamine) of all 16 metabolites and 12 of these $[M+H]^+$ ions were fragmented by MS2. In most cases the MS2 spectra yielded less fragmentation from the molecular ion than was observed in the MS spectra and in all cases the intensity of fragments was much lower in the MS2 spectra than the MS spectra. This can be observed in Figure 60 where the ToF-SIMS MS and MS2 spectra for thiamine are shown.

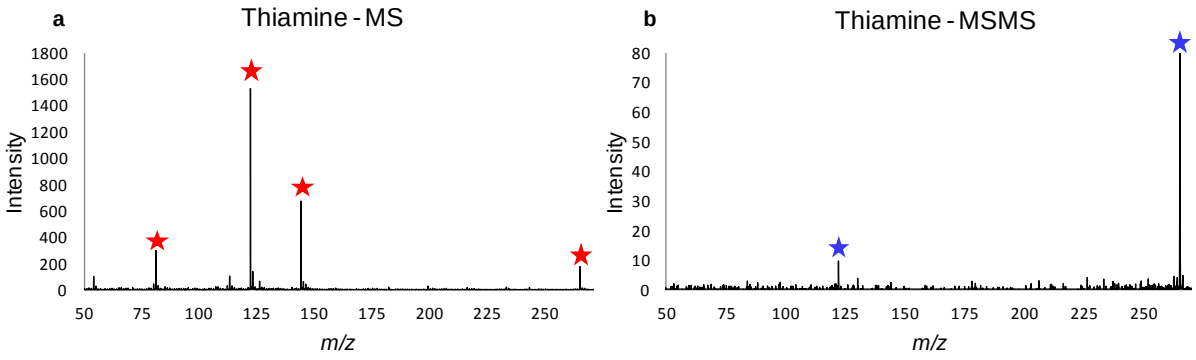

Figure 60: Time-of-flight-secondary ion mass spectrometry (ToF-SIMS) analysis of thiamine in positive ion mode. (a) The mass spectrum (MS) and (b) the tandem (MS2) mass spectrum from the mean intensity per pixel analysed. The $[M]^+$ observed at *m/z* 265.10 along with 3 observed intense fragments are marked with red stars on the MS spectrum. After MS2 on the molecular ion, only one intense fragment was observed. This is marked along with the $[M]^+$ by a blue star.

The standard spectra were combined with other standard spectra acquired in the laboratory to provide a repository of over 30 metabolite standards that can be found in Fletcher *et al.* (2012)[134]. The full repository was used in subsequent experiments for metabolite identification in the analysis of biological samples by ToF-SIMS.

In addition to the standard MS spectra, mixtures of two and five standards were also analysed to observe whether or not the intensity of metabolites detected was dependent on the number and nature of other metabolites present. These mixtures were prepared as described in 2.13.1. This was useful to predict how metabolites would ionise in complex mixtures that exist in real biological samples. First a mixture of valine and tyrosine was analysed. The standard spectra observed for each are shown in Figure 61 along with a predicted spectrum for the mixture of valine and tyrosine generated by summing together the standard spectra from each and the observed spectrum from the ToF-SIMS analysis of the mixture. The intensity of tyrosine fragments from its analysis as a standard exceeded those of valine by approximately two-fold and so it was predicted that tyrosine would ionise more readily in the mixture also. However, in the actual analysis of the mixture, the converse was seen where valine appeared to suppress the ionisation of tyrosine. Secondly a mixture of metabolites was analysed containing valine, tyrosine, thiamine, phenylalanine and guanosine. In this case all metabolites were identifiable in the complex spectrum but guanosine, and in particular it's $[M+H]^+$ ion, appeared to suppress the other 5 metabolites.

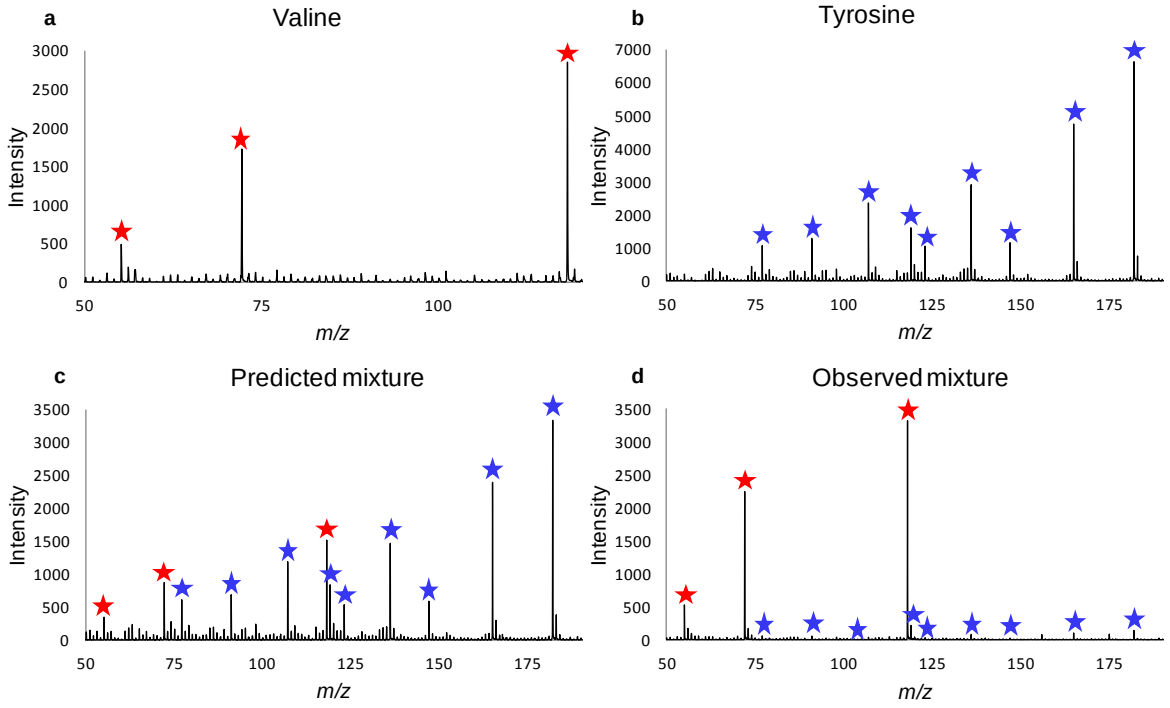

Figure 61: Time-of-flight-secondary ion mass spectrometry (ToF-SIMS) analysis of metabolite mixtures in positive ion mode. The standard spectra observed for (a) valine and (b) tyrosine where the most intense fragments are labelled with red and blue stars respectively. The predicted spectrum calculated from adding 50 % of each standard spectrum together is shown in (c) and the observed spectrum from the analysis of the valine and tyrosine mixture is given in (d) where valine and tyrosine peaks are marked with red and blue stars respectively. All spectra represent an average per pixel analysed.

The ability for certain compounds to influence the detection of another in a mixture is a well known feature of ToF-SIMS analyses and is termed the matrix effect[104]. The secondary ion yield from chemicals in a mixture can vary by a factor of 10-10^7 across a matrix of chemicals such that measured intensities can be dependent on the chemical environment more than actual concentrations[95]. This must be taken into careful consideration, especially when imaging since it can lead to the mis-interpretation of data. For example, it was previously shown problematic in a study where the distribution of the drug raclopride in rat brain was assessed using C_{60}^+ ToF-SIMS imaging. The signal from the drug was enhanced in cholesterol rich regions of the brain leading to the interpretation that its abundance was higher in the white matter of the brain, even though the distribution of the dopamine receptors the drug is known to bind to meant this could not be the case[224].

A particularly notable observation was that the suppression or enhancement of fragments was not equal for any one metabolite. Using the mixture of valine and tyrosine in Figure 61 as an example, more intense fragments of tyrosine from the standard spectrum were suppressed further than less intense fragments such that in the mixture the relative intensities of all tyrosine fragments were approximately equal. Additionally, some

metabolites, for example thiamine, were neither enhanced nor suppressed by the presence of other metabolites. This was probably due to it being directly fragmented from primary ion impact involving no process of proton transfer from other molecules in the sample such that it is not susceptible to the matrix effect in the same way $[M+H]^+$ ions and their fragments are. Similarly, the $[M+H]^+$ ion of valine was suppressed but there was no apparent suppression of its immonium ion at *m/z* 72.1[134].

Knowing which metabolites enhance or suppress the detection of others was useful for the interpretation of ToF-SIMS images in the present research. It was decided that although all fragments could still be used in the identification of any one metabolite since they remain present in mixtures, the relative intensity of fragments from standard spectra should not be used in any interpretation of biological data.

6.2.2. Determining the sensitivity for metabolite detection using the J105

To determine an approximate level of sensitivity for analysis of metabolites known to ionise well using ToF-SIMS, samples containing 1 nanomole, 1 picomole and 1 femtomole guanine were analysed. The standard ToF-SIMS MS spectrum obtained from the analysis of guanine (from section 6.2.1) is shown in Figure 62. The most intense peaks were *m/z* 152.05, 135.05 and 110.05.

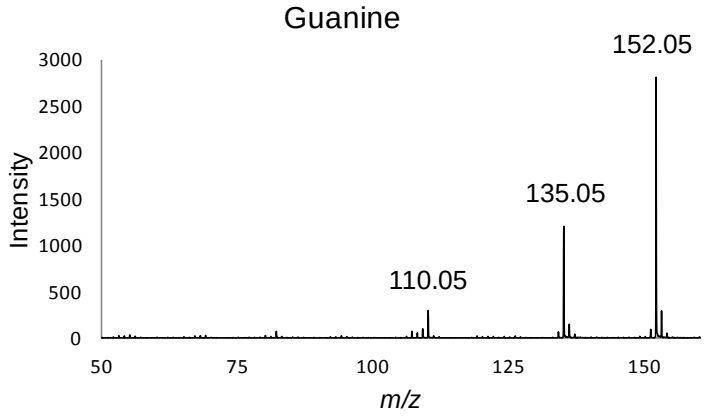

Figure 62: Standard time-of-flight-secondary ion mass spectrometry (ToF-SIMS) spectrum obtained for guanine in positive ion mode. The characteristic peaks for guanine have been labelled including the $[M+H]^+$ at *m/z* 152.05 and fragments at 135.05 and 110.05.

A very good reference spectrum was obtained after the analysis of 4 layers (total spectral dose 1.2×10^{11} ions) of the sample containing 1 nanomole guanine and so the whole sample was not consumed. For the other two samples, the whole sample was consumed in order to obtain total ion spectra for 1 picomole and 1 femtomole guanine respectively. This was compared to a total ion spectrum from the analysis of clean silicon in order to determine the concentration of guanine detectable above the silicon background spectrum.

From the analysis of 1 nanomole guanine, the intensity of the $[M+H]^+$ ion was almost 5×10^6 counts compared to a background intensity of approximately 0.5×10^6 counts from the analysis of silicon. When comparing the total ion spectrum for 1 picomole guanine to a total ion spectrum of silicon from the same sized area the intensity of the $[M+H]^+$ ion for guanine was still slightly higher than the background exhibiting an intensity over 3×10^6 counts. From the comparison of the total ion spectrum for 1 femtomole guanine to a total ion spectrum of silicon from the same sized area the intensity of the $[M+H]^+$ ion for guanine was lower than the background intensity from silicon (just under 4×10^5 and 7×10^5 for 1 femtomole guanine and silicon respectively). In addition to analysing the intensity of the $[M+H]^+$ ion, the intensity of the other two MS fragments from guanine as determined in 6.2.1 were analysed. Figure 63 shows the intensity of each guanine fragment in each sample analysed. This highlights that the limits of detection for metabolites on the J105 fall between the picomole and nanomole range such that 1 picomole can be detected by the J105 but 1 femtomole cannot.

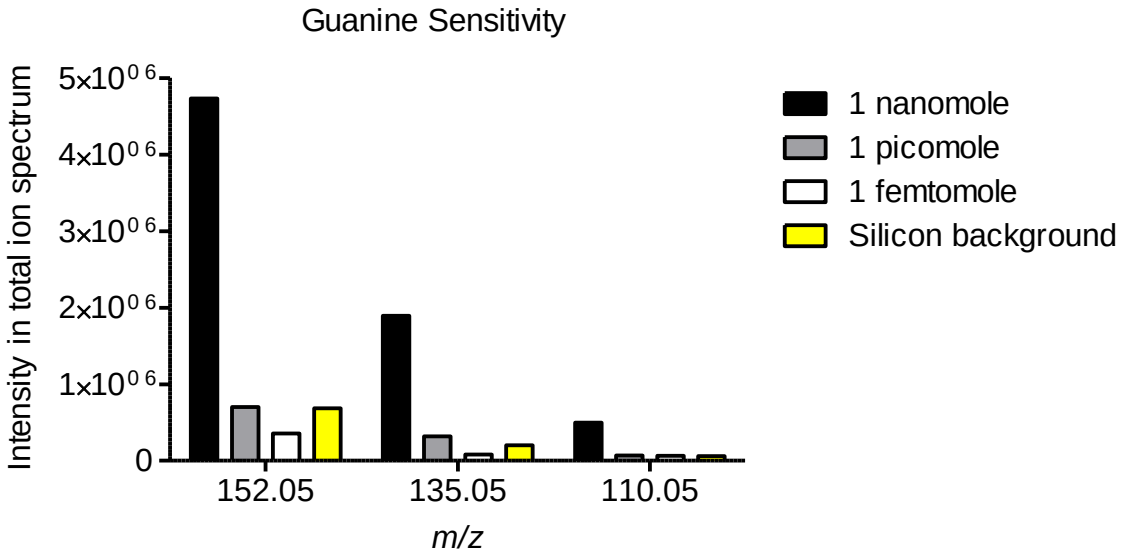

Figure 63: The intensity of the 3 characteristic peaks of guanine as determined from the analysis of the metabolite described in 6.2.1. Guanine was analysed at 1 nanomole, 1 picomole and 1 femtomole concentrations and each was compared to silicon for background signal at each peak.

There is very little information in the literature regarding the per-cell concentration of metabolites. Additionally, the range in concentration of metabolites can be cell specific and naturally, it would be expected that the range would be further influenced by experimental condition and only by measuring the specific concentrations of metabolites in the cell of interest under the condition of interest would one be able to determine such parameters. Lactate has been measured in leukaemia cell lines and found to be present in the picomole range per cell[225]. Since this concentration may not be indicative of a general concentration for all metabolites in single cells and may not be close to the concentrations present in HCT 116 cells it was not possible to confirm whether or not metabolites could be reliably detected at the level of the single cell in this research. Additionally, the level of detection of other metabolites may not be the same as that measured for guanine. Therefore, only samples of relatively high biomass were analysed to ensure reliable identification of metabolites. Despite this, the sensitivity result did highlight the possibility for the future application of ToF-SIMS in single cell analysis if the concentrations of all metabolites of interest are measured in the cell line and under experimental conditions of interest (which in itself is a demanding task[226]) and if the present method for assessing the limits of detection is applied to each metabolite. An additional point that must be considered however, is that the limit of detection for any given metabolite is likely to be affected by the matrix in which it exists in a biological sample such that if it is suppressed (as discussed in 6.2.1), it would need to be abundant in concentrations of a certain magnitude higher than that calculated from the analysis of the metabolite standard to be detectable in the sample. It is therefore more appropriate to compare metabolite levels between related samples rather than to attempt to extract absolute concentrations of metabolites from cells based on reference data.

6.2.3. Metabolic profiling of whole cells to identify metabolites

ToF-SIMS spectra were collected from the analysis of 3 biological replicates of WT and DN cells exposed to normoxia (21 % oxygen) or hypoxia (1 % oxygen). This was required to see if metabolite fragments could be identified in biological samples analysed by ToF-SIMS irrespective of cell line, oxygen treatment or presence or absence of HIF-1. Figure 64 shows average total ion spectra for both WT and DN cells after exposure to normoxia or hypoxia.

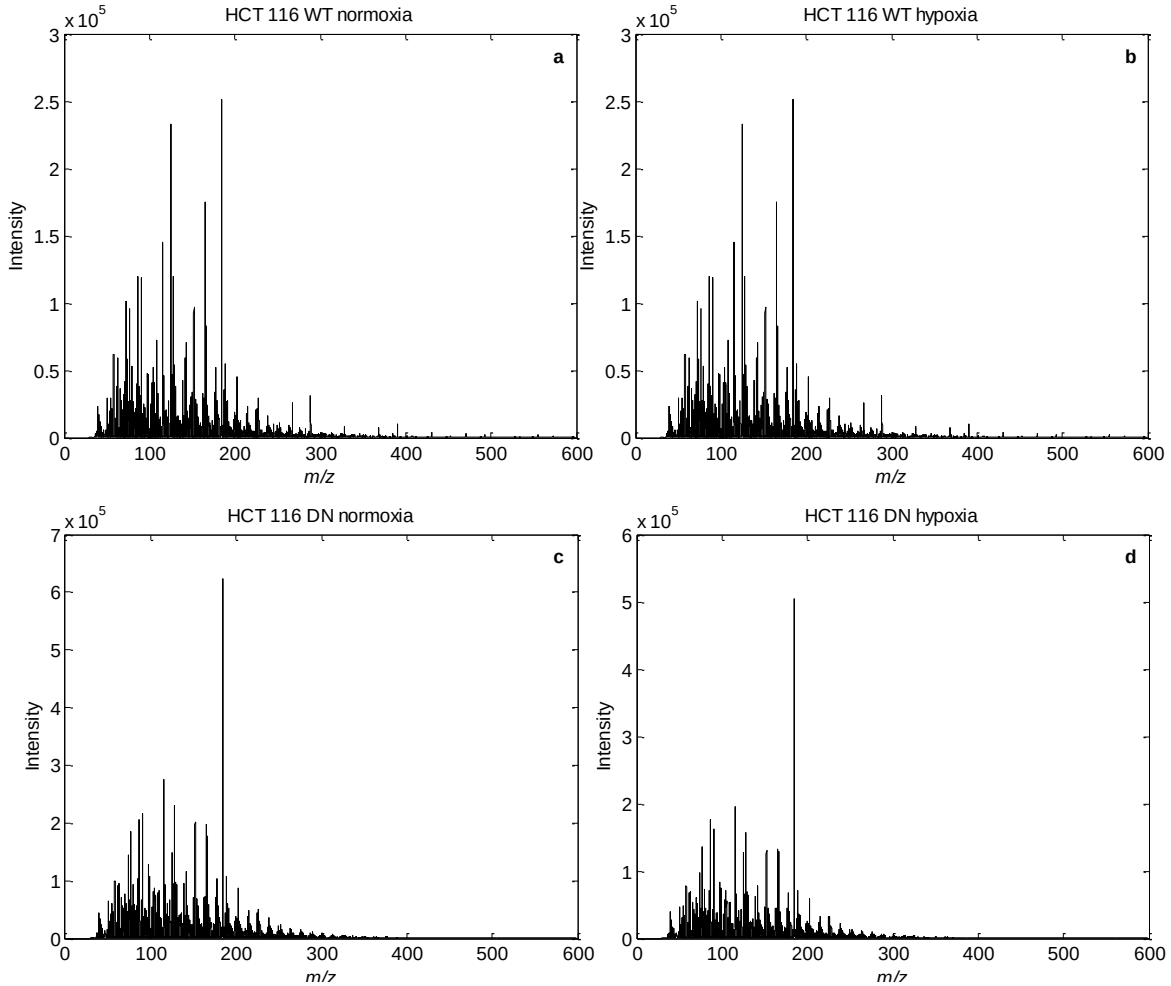

Figure 64: Average total ion spectra from the time-of-flight-secondary ion mass spectrometry (ToF-SIMS) analysis of HCT 116 (a) wild type (WT) cells exposed to normoxia (21 % oxygen), (b) WT cells exposed to hypoxia (1 % oxygen), (c) dominant negative (DN) cells exposed to normoxia and (d) DN cells exposed to hypoxia. All spectra were acquired in positive ion mode.

Using the standard spectra for metabolites, $[M+H]^+$ ion peaks and related fragments could be identified in all 4 spectra and oxygen levels or the presence or absence of HIF-1 had little effect on the number or intensity of species identified in each spectrum. The peak at *m/z* 184 was identified as a phosphocholine head group and is readily detectable in biological ToF-SIMS spectra[136]. This was found to be more intense in DN samples. Choline metabolism has been previously reported as a hallmark of cancer[227] and its particular role in hypoxic tumours has been reported where an increased acidity appears to have distinct effects on different cholines[228, 229]. Phosphocholine metabolism is thought to be activated in hypoxic conditions leading to an increase in total phosphocholine concentration as a direct response of choline kinase, targeted by HIF-1[229]. In the present data, the intensity of phosphocholine peak was higher in DN cells than WT cells and was higher in normoxic DN cells than hypoxic DN cells. These data therefore do not support the idea that HIF-1 is required for an increase in phosphocholine as an effect of hypoxia.

Since there were no observed differences in the metabolic profiles of cells in each experimental group, it was decided not to use cells as a model for studying the effect of HIF-1 and hypoxia on cancer metabolism. The data were however useful in highlighting the potential for metabolic analysis with ToF-SIMS. Therefore, ToF-SIMS was applied to the metabolic profiling of MTS cross sections. In an MTS system there is naturally a greater range of oxygen exposure within one model, giving a chance to observe more oxygen effects that may or may not be HIF-1 specific and to utilise the imaging capability of ToF-SIMS to spatially localise oxygen related metabolic features.

6.2.4. Metabolic profiling of MTS cross sections

Initial experiments were undertaken to decide whether or not MTS sections should be washed in ammonium formate prior to analysis. MTSs were washed three times in 0.15 M ammonium formate each for 1 min. Figure 65 shows the total ion images and spectra of HCT 116 WT MTS cross sections comparing an unwashed MTS (a and b) to an ammonium formate washed MTS (c and d). Due to the higher abundance of salts in the unwashed MTS, some charging occurred that was less significant in the washed MTS. Over-charging resulted in a loss of biochemical information from the unwashed sample due to suppression by salts whereas washing removed some salt, revealing a richer spectrum.

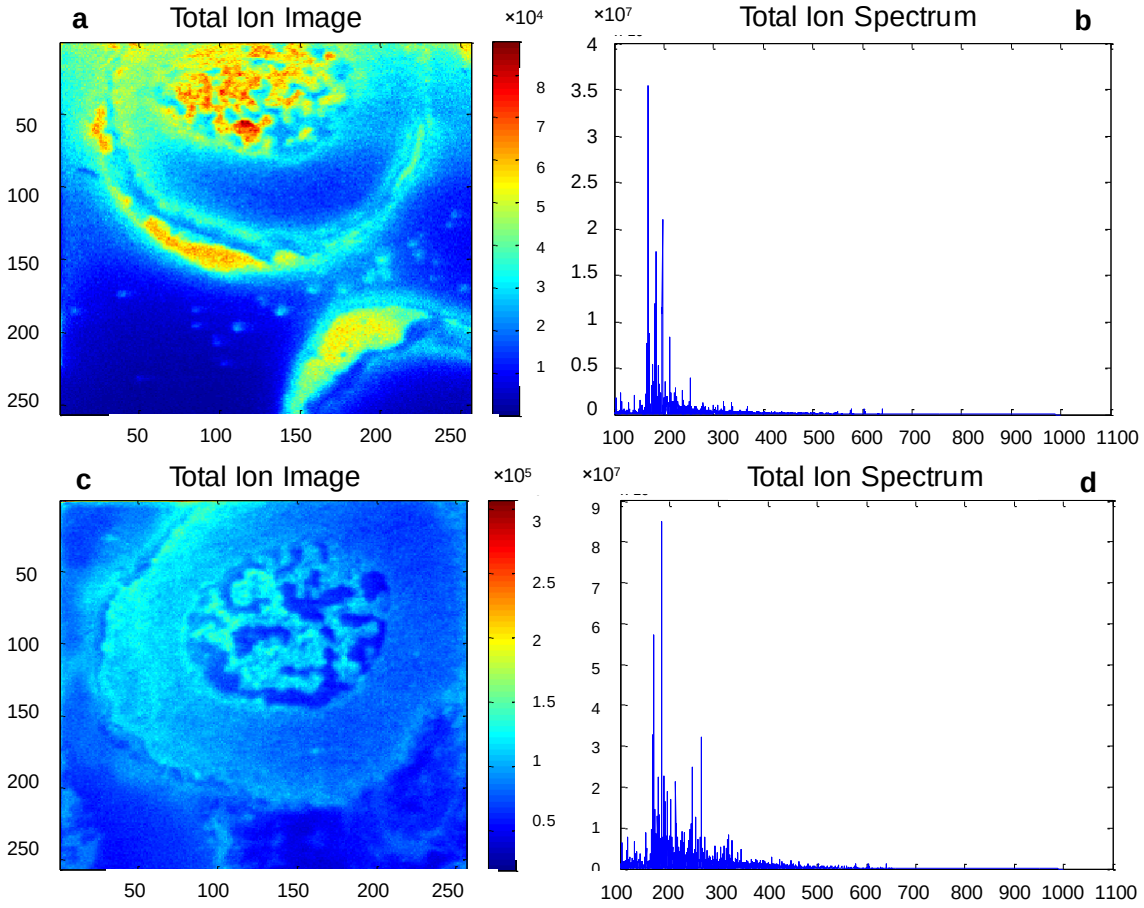

Figure 65: Total ion images and spectra from the time-of-flight-secondary ion mass spectrometry (ToF-SIMS) analysis of an unwashed HCT 116 wild type (WT) multicellular tumour spheroid (MTS) cross section (a and b) and a washed HCT 116 WT MTS cross section (c and d). The images were collected from a 256 × 256 pixel area of 1000 × 1000 µm.

To further investigate the effect of washing on the identification of metabolites in MTSs, the localisation of metabolite quasi-molecular ions were determined for both the unwashed and washed MTSs. This was done to compare the signal from each with respect to sample preparation and using proline as an example it is shown in Figure 66. In Figure 66(a) the localisation of proline is shown in the unwashed MTS compared to the washed MTS in (b). Comparing the scale bars representative of signal intensity on each image, it is clear that the signal from proline is increased with ammonium formate washing. Using the information from both Figure 65 and Figure 66 it was decided to analyse all subsequent MTS cross sections after washing with ammonium formate.

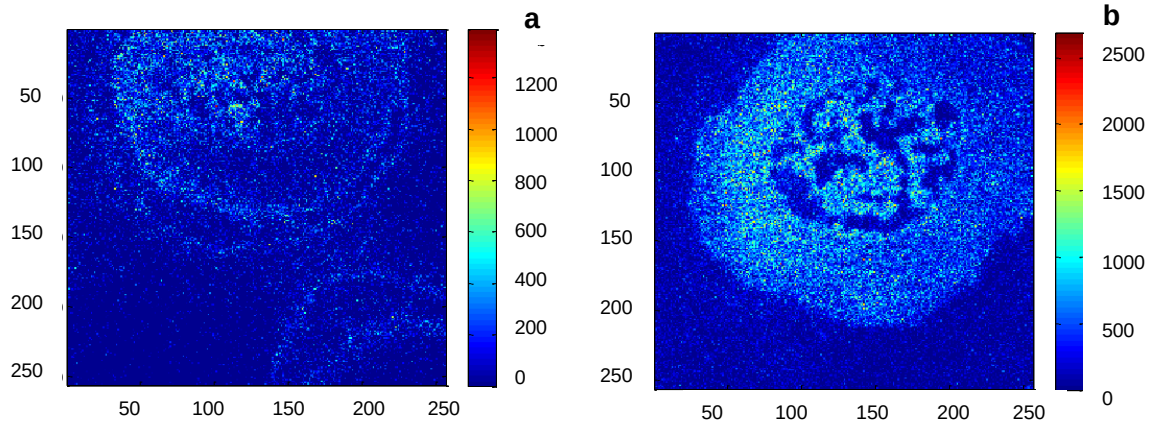

Figure 66: Localisation of the $[M+H]^+$ proline ion in (a) unwashed and (b) ammonium formate washed HCT 116 wild type (WT) multicellular tumour spheroid (MTS) cross section images. The signal from proline is much higher in the image obtained from SIMS analysis of the ammonium formate washed HCT 116 WT MTS.

An initial experiment for the metabolic profiling of HCT 116 MTS cross sections was performed to determine whether or not metabolites could be identified in the total ion spectra, whether or not there was evidence of a change in metabolic profile across the section that was indicative of oxygen level and whether or not the profiles of WT and DN MTSs differ, attributed to effects of HIF-1. For this a HCT 116 WT MTS section was analysed by ToF-SIMS and compared to a HCT 116 DN section using the method described in 2.13.4. This work was published as a novel use of ToF-SIMS imaging in the identification of metabolites in biological samples to spatially explore the metabolic effect of the natural oxygen gradient that exists in small tumours and how HIF-1 is employed to change the metabolic phenotype of tumours[174]. The total ion images from each analysis are shown in Figure 67.

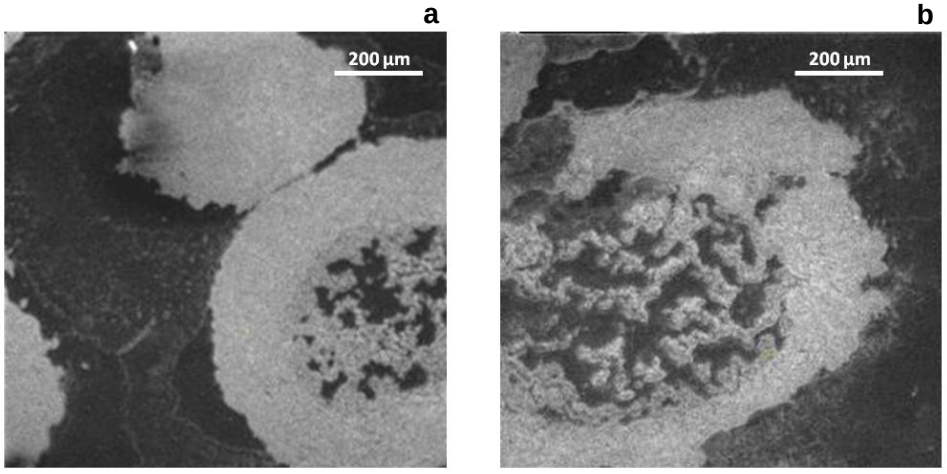

Figure 67**:** Total ion images from the time-of-flight-secondary ion mass spectrometry (ToF-SIMS) analysis of (a) HCT116 wild type (WT) and (b) dominant negative (DN) MTS sections. In the centre of each, regions of necrosis can be identified from the disruption in cellular structure caused by the hypoxic environment generated during growth.

As with any mass spectrometry used to study biological systems, the complexity and quantity of spectra produced in an experiment with a reasonable number of experimental conditions and biological replicates, make it exceptionally difficult to interpret the data without multivariate analysis. The complexity is further enhanced in IMS since every pixel in an image is representative of a spectrum generated from that position in the sample. Therefore, there are often thousands of spectra produced in a single image and multiple images are often collected for a number of biological replicates from a range of experimental conditions. Applying multivariate analysis to the total ion image to determine variation within pixels with the aim of defining regions of differing chemical properties frequently enables the essential spectral features that distinguish one region from the other to be identified[84].

Image PCA was applied to each total ion image and the PC that was observed to represent oxygen variation was selected for each. The loadings were analysed to identify metabolites using the peaks from Table 10, in addition to the other metabolite standards in Fletcher *et al.* (2012)[134], which were anti-correlated in each image as a result of oxygen. Figure 68 shows the results from image PCA of HCT 116 WT and DN MTS cross sections where the positive loadings in PC 3 are represented in green and the negative in red on the scores plot. In both MTSs all peaks determined from the analysis of the metabolite standard for valine were found to be correlated with tyrosine peaks in the higher oxygen region of the MTSs[174]. Likewise, glutamine was shown to be a feature of the low oxygen region of both MTSs. In the WT MTS, thiamine was found to anti-correlate with guanosine and/or guanine, features that were not conserved in the DN MTS suggesting a HIF-1 related effect[174]. This may suggest that HIF-1 may function at the level of RNA or DNA since guanine is a nucleobase and guanosine is a ribonucleoside.

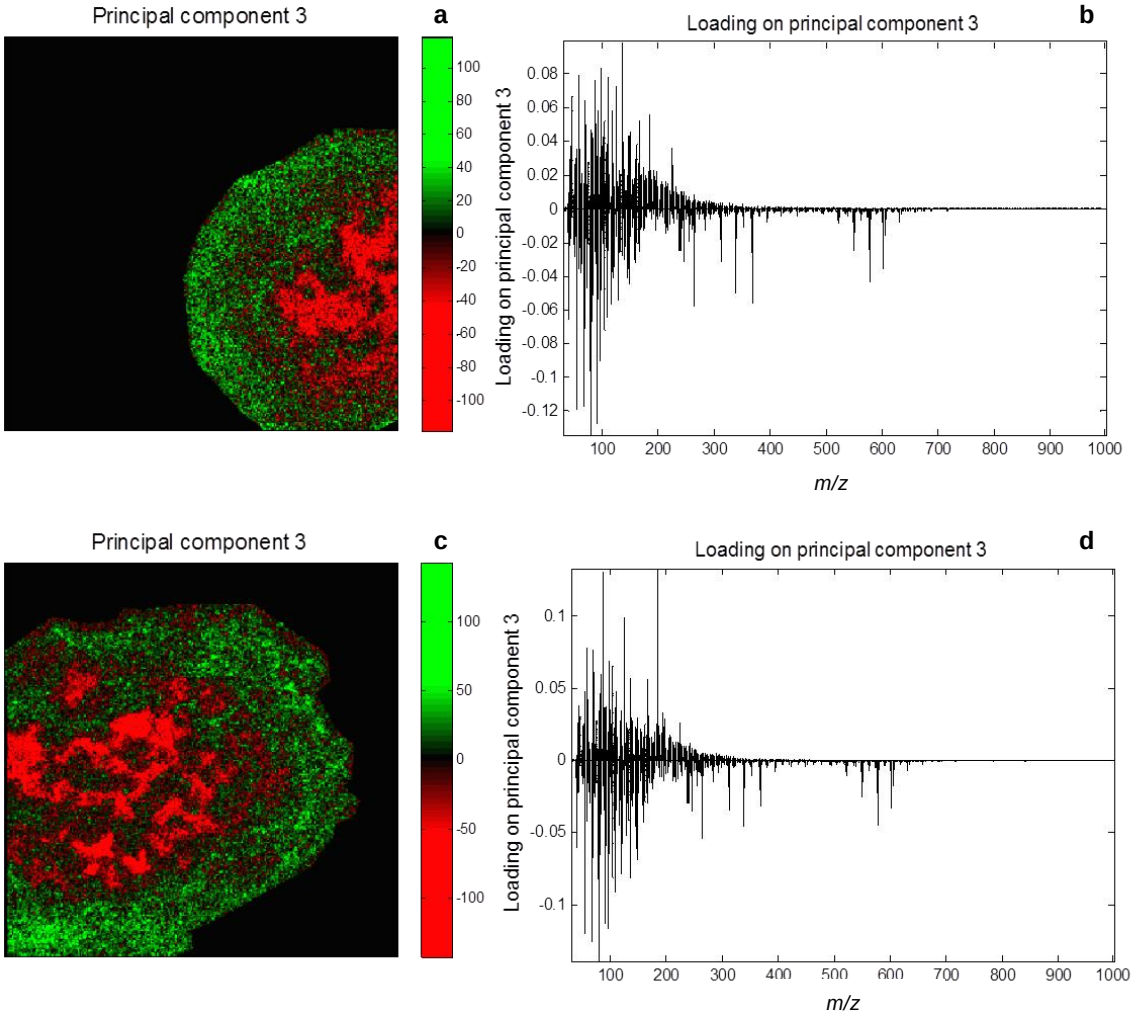

Figure 68: Image principal components analysis (PCA) of HCT 116 multicellular tumour spheroid (MTS) cross sections analysed using time-of-flight-secondary ion mass spectrometry (ToF-SIMS) adapted from Armitage *et al.* (2012)[174]. Scores and loadings for wild type (WT) (a and b) and dominant negative (DN) (c and d) MTSs are shown where anti-correlations in the loadings are shown in the scores images where peaks in the positive region are highlighted green and peaks in the negative region red.

This initial experiment was successful in highlighting the potential for ToF-SIMS imaging of MTS cross sections in metabolic profiling of biological samples and that image PCA was a valuable tool in the analysis of this type of data. There is another example of this in the literature whereby a similar method was employed in the investigation of chemotherapy resistance to hypoxia[175]. In this example, MTSs cultured from MDA-MB-231 breast cancer cells were treated with different concentrations of doxorubicin to highlight the metabolites that appeared to promote or were a consequence of chemo-resistance in the hypoxic cores of the MTSs.

Regardless of its success, it was decided that this method of data analysis could be improved upon by including a series of biological replicates, analysing HCT 116 EV MTS cross sections in addition to WT and DN and performing image PCA on only identified metabolite peaks from the metabolite standards in Table 10 and Fletcher *et al.* (2012)[134] in

addition to some common ToF-SIMS lipid peaks summarised in Passarelli *et al.* (2011)[136]. Predicted fragments for sodium and potassium adducts of each metabolite's molecular ion were also considered since they are known to be prevalent in biological samples[53]. Including 3 biological replicates per cell line allowed more confidence in the biological interpretation of data. Analysing EV MTSs controlled for differences in DN MTSs being due to HIF-1 silencing, rather than transfection in general. Finally, selecting peaks for PCA allowed the removal of non-biological peaks along with peaks that could not be identified that skew the PCA but that added no value to the data interpretation.

It has been shown previously that the inner region of an MTS is hypoxic with respect to the outer cell layers[116]. From the new analyses, the PC that appeared to account for variation in oxygen in each MTS was analysed and for each sample, the region of MTS each metabolite or lipid appeared to be associated with was recorded. Figure 69 shows a loadings plot for the PC that appeared to account for oxygen variation in each cell line. The similarity between WT and EV observed here was used to confirm that the process of cell transfection added no artefacts to the DN results. From the loadings plots for WT and DN MTSs, the main peak differences are labelled in both positive (higher oxygen region) and negative (lower oxygen region) loadings. Peaks were selected for PCA with a tolerance of 0.05 Da, and as such, many peaks were inclusive of fragments from more than one metabolite. In the WT MTSs the two most prominent peaks in the positive loadings that were lost in the DN MTSs were at *m/z* 130.05 (fragment from glutamine, glutathione and tryptophan) and *m/z* 136.10 (fragment from adenosine and tryptophan). Although the weighting on the loadings varied, most of the intense positive loadings in the WT MTSs were also positive in DN MTSs. This was expected since the effect of HIF-1 in the outer more oxygenated region should be minimal between WT and DN MTSs compared to the less oxygenated core. There were a few differences in the negative loadings observed from an initial comparison of WT and DN PC loadings. For example, the peak at *m/z* 178.10 (fragment from adenosine), *m/z* 165.05 (fragment from cholesterol and tyrosine) and *m/z* 152.05 (fragment from guanine, guanosine and cholesterol) were distinct features of the hypoxic region in WT MTSs. In the DN MTSs, the negative loadings were heavily weighted by peaks at *m/z* 519.44-579.54 (diradylglycerols/diacylglycerols (DAGs)), *m/z* 311.26, 313.27, 339.29 and 341.31 (monoradylglycerols/monoacylglycerols (MAGs)), *m/z* 255.23 (FA fragment (16:0)), *m/z* 109.10 (fragment from glucose), *m/z* 67.05 (fragment from cysteine) and *m/z* 55.05 (fragment from lactate, succinate, urea and valine).

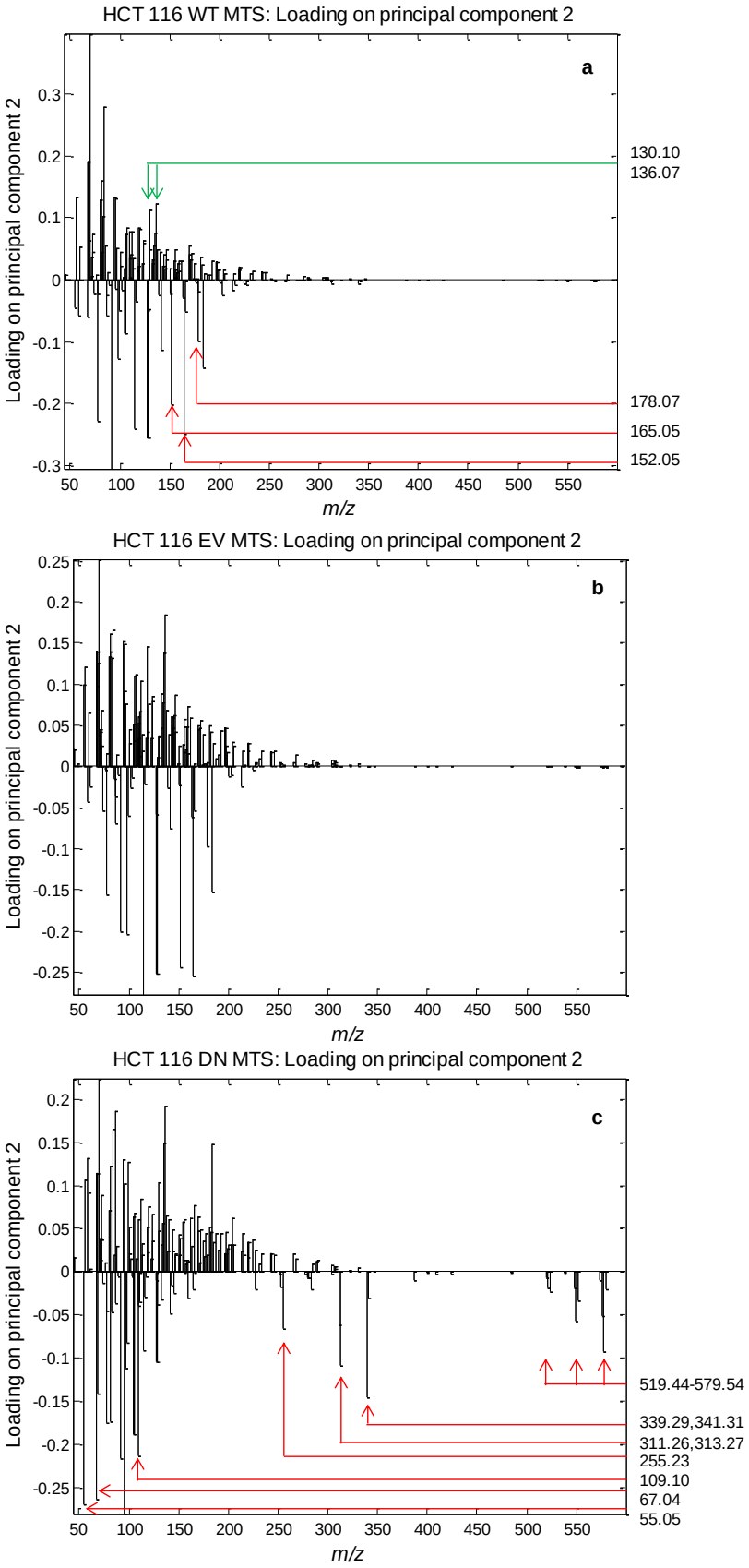

Figure 69: Principal component (PC) loading plots from image principal components analysis (PCA) of HCT 116 (a) wild type (WT), (b) empty vector (EV) and (c) dominant negative (DN) multicellular tumour spheroids (MTSs). The main peak differences due to hypoxia inducible factor 1 (HIF-1) are labelled using green and red arrows for positive (higher oxygen region) and negative (lower oxygen region) loadings respectively.

Although it is interesting to assess which individual peaks were most responsible for the separation between higher and lower oxygen regions of MTSs, considering all characteristic peaks from each metabolite and assessing whether or not these peaks are correlated to one region of an MTS provides more confidence in assigning metabolites that are oxygen specific and that may differ with the presence or absence of HIF-1. Additionally, the weighting of peaks in the PCA loadings could be due to matrix effects of metabolite peaks. For example, the most dominant peaks may have arisen from metabolites that ionise more readily than others in a biological matrix (as discussed in section 6.2.1). The loadings were therefore further analysed to classify metabolites to be associated more closely to either the inner or outer regions. A summary of metabolite identifications are given in Table 11. Many metabolites and lipids were observed to be features of the same region independent of HIF-1. The effect of oxygen level was greater than the specific effect of HIF-1. There were 4 lipid features and 3 metabolite features whose spatial localisation appeared to be dependent on HIF-1. FA(16:2), FA(18:3) and FA(20:4) were all correlated in the higher oxygen region of WT MTSs but correlated in the lower oxygen region of DN MTSs. Conversely, DAG (36:4) was correlated in the lower oxygen region of WT MTSs but correlated in the higher oxygen region of DN MTSs. Malate, ornithine and putrescine were observed to be localised in the higher oxygen region of WT MTSs but could not be spatially localised to a specific region in DN MTSs.

Table 11: Comparison of average metabolic profiles observed for HCT 116 wild type (WT) and dominant negative (DN) multicellular tumour spheroids (MTSs) using image principal component analysis (PCA). Metabolites and lipids found to be spatially localised to the outer more oxygenated region of MTSs are given in the first column. Metabolites and lipids found to be spatially localised to the inner less oxygenated region of MTSs are given in the second column. Metabolites and lipids found to be spatially localised to different regions as an apparent effect of hypoxia inducible factor 1 (HIF-1) are given in the third column.

Metabolites in higher oxygen region of both WT and DN MTSs	**Metabolites in lower oxygen region of both WT and DN MTSs**	**Metabolites in different oxygen regions as a consequence of HIF-1**
Adenosine	7-ketocholesterol	DAG(36:4)
Alanine	Cholesterol	FA(16:2)
Arginine	DAG(30:0)	FA(18:3)
Alpha-ketoglutarate	DAG(30:1)	FA(20:4)
Carbamoyl aspartate	DAG(30:2)	Malate
Carnitine	DAG(32:0)	Ornithine
Citrate	DAG(32:1)	Putrescine
Citrulline	DAG(32:2)	
Cysteine	DAG(34:0)	
Glutamine	DAG(34:1)	
Glutathione	DAG(34:2)	
glycerophosphocholine	DAG(34:3)	
Glycine	FA(14:0)	
Glutathione disulphide	FA(16:0)	
Guanine	FA(16:1)	
Guanosine	FA(16:2)	
Methionine	FA(18:0)	
Nicotinic acid	FA(18:0) /MAG(16:0)	
Phosphocholine	FA(18:1) (oleic acid) FA(18:2)	
Phosphocholine head group	FA(18:2)	
Phenylalanine	MAG(16:1)	
Proline	MAG(18:0)	
Thiamine	MAG(18:1)	
Tryptophan		
Tyrosine		
Uracil		
Urea		
Valine		

Similar to the preliminary investigation where image PCA was performed on the total ion images of WT and DN MTSs, valine was still correlated with tyrosine in the higher oxygen region of each. However, guanosine and thiamine were also correlated in both WT and DN MTSs from this investigation but were found to be anti-correlated previously. In DN MTSs, all guanosine peaks were found to exhibit positive loadings indicating their abundance in the more oxygenated regions, whereas in all WT MTSs the quasi molecular ion for guanosine was found in the negative loadings representative of the low oxygen core but the other 6 peaks were found to be positive leading to the classification of guanosine as a marker of the higher oxygen region in these MTSs as well. One drawback with metabolic analysis using mass spectrometry is that although a more definitive identification of metabolites can be made in biological samples by using the full range of characteristic peaks from the standard spectra, many peaks from many metabolites are similar in *m/z*.

This can be due to metabolites sharing identical fragments such that there is no way to correlate them to the correct parent ion or it can be due to similar mass despite different chemistry. The latter currently cannot be distinguished using ToF-SIMS when a complex mixture of compounds exists in biological samples. Thus, it could be possible that either the quasi-molecular ion was skewed by other metabolites that share the same peak or the other peaks from guanosine were skewed by metabolites sharing similar fragments. Therefore, only putative classifications could be made using this type of analysis. This was not a problem with GC-MS or UHPLC-MS since the PCA was performed on chromatograph peak areas for metabolites, irrespective of mass spectra which will have also contained peaks similar between metabolites.

Most of the peaks in the negative PC loadings representative of the low oxygen cores of each MTS were lipids. Cholesterol and all MAGs were found to be markers of this region in both WT and DN MTSs. Most DAGs were observed to be markers of the low oxygen region in both WT and DN MTSs. Similarly most FA peaks were markers of low oxygen, although some were observed to be in different regions of WT and DN MTSs. This suggests that although lipid species are generally features of tumour hypoxia, HIF-1 can act on the lipid profile to some extent to change the expression of lipids as a response to oxygen. It is known that tumour hypoxia instigates an accumulation of DAGS and it has been investigated whether or not the expressions of DAGs influence or are influenced by HIF-1[230]. From this cited research it was concluded that there was no apparent link between HIF-1 and DAGs which suggests why there are no significant difference observed in their profiles in WT and DN MTSs in the present research. Fatty acid synthase (FAS), the gene that encodes for the synthesis of many FAs has been found previously to be up-regulated by hypoxia in cancer[231]. Therefore the concentration of most FAs was expected to be in the more hypoxic regions of MTSs. The up-regulation of FAs is further increased by HIF-1 in hypoxia[231]. Although the outer region is described as the more oxygenated region of the MTS it is not likely to be normoxic since it is comprised of several layers of cells and some level of hypoxia is bound to be formed in this area, just that it is expected to be much less hypoxic than the inner core. Therefore, some FA synthesis is expected in the outer region of the MTSs and the fact that this is more prevalent in WT MTSs suggests that HIF-1 is required to instigate these processes under mild hypoxia.

Ornithine and putrescine were the main features identified to be different between WT and DN MTSs. Both were localised to the more oxygenated outer regions of WT MTSs but not

in DN MTSs. The profiles of ornithine and putrescine are likely to be controlled by the enzyme ornithine decarboxylase (ODC) that converts ornithine to putrescine and is a metabolic feature of cancer due to its over expression[232]. The induction of ODC is thought to be HIF-1 regulated and it has been shown that in cells lacking HIF-1, activation of ODC is reduced[233]. Putrescine plays an important role in tumour cell proliferation that occurs when ODC is overexpressed[232]. This explains why these metabolites would be more abundant in the proliferative cells at the periphery of the WT MTS.

6.3. Conclusion

The data presented demonstrate the potential of ToF-SIMS as a useful platform in metabolite analysis. It has been shown that many metabolites ionise well using ToF-SIMS in positive ion mode, they can be detected in quantities relevant to biological samples and can be identified in complex spectra. ToF-SIMS and image PCA have been useful in identifying metabolites in MTSs representative of small non-vascularised initiating tumours. Limitations of ToF-SIMS imaging for metabolic profiling of MTSs include the inability to make definitive identifications due to many metabolites sharing similar peaks in addition to multivariate analysis separating individual peaks that are additive of many metabolites. Nevertheless, it has a useful technique for the spatial localisation of metabolites within MTSs. Metabolites were highlighted that appeared to promote the proliferation of tumours in the more oxygenated outer region of MTSs that were both HIF-1 and non-HIF-1 specific. Similarly, metabolic signatures were also identified in the hypoxic core that could promote tumour survival in low oxygen. Both should be considered in future cancer therapy since combating the ability for tumours to proliferate at such a rapid rate and targeting their capability to survive in such oxygen compromised conditions may prevent, slow or stop tumour progression in patients. This type of analysis shows the successful application of ToF-SIMS imaging which could be applied in similar studies of tumour xenografts.

Chapter 7. Summary

The metabolome can be considered as the most relevant entity to study biological phenotype. Metabolism plays a vital role in many diseases and cancer metabolism has been studied for many decades, particularly with respect to central carbon metabolism[17, 18]. In 1956, Warburg suggested that tumour cells are associated with an irreversible injuring of respiration followed by a replacement of the lost respiration energy with fermentation energy[25]. Since then it has been accepted that central carbon metabolism plays a vital role in cancer survival, provides possible targets for therapy and is useful in prognosis and diagnosis. Furthermore, it has been revealed that cell survival in hypoxia, the low oxygen state that exists in solid tumours, is also to an extent dependable on central carbon metabolism[22]. HIF-1 is an important factor in cancer cell survival in hypoxic environments. Its metabolic targets that have previously been investigated have also featured central carbon metabolism. For example, a known target of HIF-1 in cancer hypoxia is glycolysis[24, 38]. This has been explored revealing its function in targeting the transcription of genes that code for glucose transporters (such as GLUT 1 and GLUT 3)[33]. Additionally, HIF-1 mediates other processes in central carbon metabolism such as cellular adaptation to hypoxia through down regulating the activity of the TCA cycle as well as mitochondrial oxygen consumption through inhibiting PDK 1[45].

The aim of this research was to further explore the effect of hypoxia, and more specifically HIF-1, in cancer metabolism. Although investigations were not limited to metabolic profiling, it has formed a major component in revealing the effect of HIF-1 on cancer metabolism. Through applying a systems biology approach whereby the metabolomes of WT and HIF-1 deficient cells and MTSs have been profiled, effects of hypoxia and HIF-1 have been revealed. Metabolic profiling is a ‘top-down’ method for exploring the relative changes in detectable metabolites caused by experimental perturbation. Although it is only semi-quantitative, it offers a distinct advantage over targeted approaches in metabolomics since its exploratory properties mean it is useful to reveal metabolites not previously linked with the system. Using a range of analytical and computational methods, both metabolites and pathways that have not previously been connected with each other or with cancer function in hypoxia have been identified.

A successful method for metabolic profiling of HEPA-1 and HCT 116 cells was devised for GC-MS and used to study cells with and without functional HIF-1 that had been exposed to a range of oxygen conditions. This proved to be an excellent approach to

revealing statistically significant changes in metabolite concentrations as a result of experimental condition and allowed the cross comparison of the effect of low oxygen and HIF-1 on cancer cell metabolism in different cell lines. Metabolites found to be significantly different in HCT 116 cells were also significantly different in HEPA-1 cells with respect to HIF-1. This included 3 peaks putatively identified as allose/mannose/galactose/glucose. With the prior knowledge that HIF-1 controls the uptake of glucose through up-regulating the expression of glucose transporters GLUT-1 and 3[155], it was suggested that this peak was derived from glucose.

In both cell models lactate increased with a decrease in oxygen, a result that was expected since lactate is a feature of anaerobic respiration in hypoxic and anoxic cells. Together with the data from the analysis of lactate efflux in both cell models, it was shown that there was no apparent difference between lactate production or efflux in WT or HIF-1deficient cells. The data from GC-MS analysis of intracellular extracts provided an implication that its production is more efficient than its efflux. From this research central carbon metabolism was considered still to be of pinnacle importance since many metabolites identified as being HIF-1 targets in both cell models were either features of or closely related to central carbon metabolism. These included, 2-hydroxyglutarate, 2-oxoglutarate, hexadecanoic acid, hypotaurine, pyruvate and octadecenoic acid.

Network-based correlation analysis of metabolites detected by GC-MS was performed for the HCT 116 model. This involved identifying differently correlated metabolites as a result of oxygen level or HIF-1. Some of the most notable correlation differences were strongly correlated metabolites in WT samples that were lost in DN cells. These included xylitol/ribitol strongly correlated to aspartate, methionine, norleucine *scyllo*/*myo*-inositol and tyramine/tyrosine as well as malate correlated to glycerol and tyramine/tyrosine. Comparing correlations for WT and DN cells at each oxygen level revealed important connections between metabolites promoted by HIF-1. In another way to consider the response of cells to low oxygen with and without HIF-1, differently correlated metabolites were determined as a response to oxygen level change. This suggested how HIF-1 promotes metabolic changes in response to low oxygen as well as considering the mechanisms DN cells use in the absence of HIF-1 to promote survival in low oxygen. Metabolites found to be differently correlated were subsequently mapped onto the EHMN, (a human metabolic network) in order to study the systems properties of the correlations. Although numerous aspects of cancer metabolism have been explored previously, few

studies have considered less well investigated pathways or how key pathways interact in sub-networks of metabolism. Key pathways may be spatially or temporally separated but share the same control in the cancer function. Therefore, sub-networks of differently correlated metabolites were drawn to reveal new pathways and metabolic hubs not previously linked with cancer metabolism, hypoxia and HIF-1. Pathways were revealed to compare differently correlated metabolites in hypoxia or anoxia compared to normoxia as a control for WT and DN correlations separately. Some pathways were conserved irrespective of HIF-1 indicating non-HIF-1 mediated responses to low oxygen. For example key elements of central carbon metabolism were connected including pyruvate, malate, oxoalacetate and citrate. Other pathways associated with HIF-1 function that were not observed in modelling of DN pathways were centred on glyine in hypoxia. In anoxia, a HIF-1 specific 'hub' metabolite (one that is highly connected within the network) was not revealed. The connections were more linear, for example the pathway between *myo*-inositol and citrate. Network-based correlation analysis has offered a novel approach to studying the systems properties of HIF-1 metabolism. Although it considers metabolic pathways in a less conventional manner, it has allowed the revelation of pathways associated with low oxygen and HIF-1 response that appear to stem from central carbon metabolism but that encompass metabolic processes beyond glycolysis and the TCA cycle. It has been useful to identify which elements of the TCA cycle appear to change in their interactions with different metabolites.

For the HCT 116 model, metabolic profiling experiments were extended to utilise UHPLC-MS and ToF-SIMS. UHPLC-MS was selected as a complementary technique to GC-MS for profiling of metabolites with different chemical properties. It was useful in identifying additional metabolites separate from central carbon metabolism that appear to be targets of HIF-1 or whose concentrations are affected by low oxygen. These were interpreted with respect to linking identified metabolites into biochemical pathways and revealed that targets of HIF-1 that could be investigated in future research are polyamine metabolism, arginine and proline metabolism and the ceramide pathway.

ToF-SIMS was selected as a method for IMS that is ideally suited to the detection of metabolites *in situ*. The J105 *3D chemical imager* was advantageous for such experiments due to its high specifications with respect to mass resolution $m/\Delta m \approx 10\,000$ at mass 500, a mass accuracy of 5 ppm[104] and a capable spatial resolution as low as 1 µm. HCT 116 WT and DN MTSs were compared and metabolites spatially localised to the outer cell layers

assumed to be more oxygenated compared to the inner core. The effect of hypoxia was greater than the specific effect of HIF-1 and many metabolites were spatially localised to the same region of MTS in both WT and DN MTSs. For example, the inner core was lipid rich and mainly comprised DAGs, MAGs, and FAs. The outer cell layers were metabolite rich and 25 metabolites in addition to choline species could be correlated in this region. Metabolites that were highlighted as differently located based on the functionality of HIF-1 were malate ornithine and putrescine.

The study of metabolites in biological samples is pioneering in the field of ToF-SIMS. Therefore certain experiments were undertaken to explore the potential for this technique in metabolite analysis. The limit of detection for metabolites in samples was determined using guanine as an example. This revealed that for this particular metabolite, quantities as low as 1 picomole can be detected using the J105 *3D chemical imager*. Additionally, the ionisation efficiencies of metabolites were explored, highlighting a limitation of ToF-SIMS for metabolite analysis whereby the presence of certain metabolites can enhance or suppress the ionisation of other. To this end, the technique was only capable of analysing comparable biological samples with respect to relative changes in metabolic profile. Finally, 20 metabolites were analysed and contributed to a new ToF-SIMS metabolite standard library.

Together the data presented in this thesis have highlighted the effects of HIF-1 on cancer cell metabolism. Many metabolites apparently involved in cellular response to low oxygen and HIF-1 are features of, or are closely connected to, central carbon metabolism. However, other important regions of the metabolome that should be considered in relation to understanding the function of HIF-1 in metabolism include polyamine metabolism, arginine and proline metabolism and the ceramide pathway in addition to FA biosynthesis and beta-alanine metabolism. Using a range of complementary profiling mass spectrometry tools, it has been possible to analyse a wider range of metabolites offering a fuller view of the metabolic effects of low oxygen and HIF-1. It has also been possible to analyse the temporal and spatial variation of particular metabolites. For example, the flux of 3 key metabolites known to be associated with cancer hypoxia metabolism have been analysed temporally and metabolites detectable using ToF-SIMS have been analysed spatially. Ultimately this research has involved innovative methods has revealed novel findings and has formed a potentially valuable contribution to both cancer research and metabolomics.

The data presented in this thesis provides scope for future research that could be undertaken to extend on the knowledge of systems biology of HIF metabolism in cancer. For example, by analysing a larger dataset using UHPLC-MS it would be possible to perform correlation analysis. Furthermore, it may be possible to devise a method that would allow alignment of GC-MS data with UHPLC-MS data such that a larger-scale correlation analysis of all detected metabolites could be performed. This would enable pathway analysis between all metabolites and would be particularly useful to highlight some of the possible routes connecting primary metabolites, including central carbon metabolites detected using GC-MS and secondary metabolites including lipids detected using UHPLC-MS.

It may also be useful to develop a method for profiling lysates from different cellular compartments individually. Since many computational models consider compartmentalisation, particularly distinguishing cytosolic metabolic reactions from mitochondrial metabolic reactions, it would be useful to have data that would be compatible with these models. Many tissue specific models include compartmentalisation and without separating cellular components for metabolic profiling, it is not possible to use these models which may provide a better representation of the system.

A selection of flux based metabolomics experiments tracing key components of central carbon metabolism could allow elucidation of the pathways that are relied upon in both WT and HIF-1 deficient cells and how they change in response to hypoxia. This would involve using labelled substrates such as ^{13}C glucose and tracing the fate of this carbon through the system. Such studies would confirm whether or not the pathways highlighted in network-based correlation analysis were truly representative of cellular metabolism *in vitro*.

Finally, with regards to extending the work presented for ToF-SIMS, it would be interesting to analyse cross sections of tumours grown *in vivo* and to include an analysis of tissue surrounding the tumour. This would be useful to determine how comparable MTSs are to tumours grown *in vivo*. Profiling the tissue surrounding the tumour may provide information on the possible metabolic interactions between tumerous and non-tumerous cells that may be representative of mechanisms for symbiosis or tumour metastasis.

Bibliography

1. Kim, J. Making sense of emergence. *Philosophical Studies* **95**, 3-36 (1999).
2. Ahn, A.C., Tewari, M., Poon, C.-S. & Phillips, R.S. The Clinical Applications of a Systems Approach. *PLoS Med* **3**, e209 (2006).
3. Bruggeman, F.J. & Westerhoff, H.V. The nature of systems biology. *Trends Microbiol.* **15**, 45-50 (2007).
4. Laubenbacher, R. *et al.* A systems biology view of cancer. *Biochim. Biophys. Acta* **1796**, 129-139 (2009).
5. Goodacre, R. Metabolomics of a superorganism. *J. Nutr.* **137**, 259S-266S (2007).
6. Hornberg, J.J., Bruggeman, F.J., Westerhoff, H.V. & Lankelma, J. in 5th International Conference on Systems Biology (ICSB 2004) 81-90 (Elsevier Sci Ltd, Heidelberg, Germany; 2004).
7. Bianco, R.B., Melisi, D., Ciardiello, F. & Tortora, G. Key cancer cell signal transduction pathways as therapeutic targets. *Eur. J. Cancer* **42**, 290-294 (2006).
8. Mathon, N.E. & Lloyd, A.C. Cell senescence and cancer. *Nature Reviews Cancer* **1**, 203-213 (2001).
9. Hanahan, D. & Weinberg, R.A. The hallmarks of cancer. *Cell* **100**, 57-70 (2000).
10. Olivier, B.G. & Snoep, J.L. Web-based kinetic modelling using JWS Online. *Bioinformatics* **20**, 2143-2144 (2004).
11. Schellenberger, J., Park, J.O., Conrad, T.M. & Palsson, B.O. BiGG: a Biochemical Genetic and Genomic knowledgebase of large scale metabolic reconstructions. *BMC Bioinformatics* **11** (2010).
12. Ma, H.W. *et al.* The Edinburgh human metabolic network reconstruction and its functional analysis. *Mol. Syst. Biol.* **3** (2007).
13. Duarte, N.C. *et al.* Global reconstruction of the human metabolic network based on genomic and bibliomic data. *Proc. Natl. Acad. Sci. U. S. A.* **104**, 1777-1782 (2007).
14. Westerhoff, H.V. *et al.* in International Conference on Industrial and Applied Mathematics 7-34 (Springer, Zurich, Switzerland; 2009).
15. Jerby, L., Shlomi, T. & Ruppin, E. Computational reconstruction of tissue-specific metabolic models: application to human liver metabolism. *Mol. Syst. Biol.* **6** (2010).
16. Agren, R. *et al.* Reconstruction of Genome-Scale Active Metabolic Networks for 69 Human Cell Types and 16 Cancer Types Using INIT. *PLoS Comp. Biol.* **8** (2012).
17. Warburg, O., Wind, F. & Negelein, E. The metabolism of tumors in the body. *The Journal of general physiology* **8**, 519-530 (1927).
18. Richardson, A.D., Yang, C., Osterman, A. & Smith, J.W. Central carbon metabolism in the progression of mammary carcinoma. *Breast Cancer Res. Treat.* **110**, 297-307 (2008).
19. Alberts, B. *Molecular biology of the cell*, Edn. 5th. (Garland Science, New York ; Abingdon; 2008).
20. Kim, J.W. & Dang, C.V. Cancer's molecular sweet tooth and the Warburg effect. *Cancer Res.* **66**, 8927-8930 (2006).
21. Voet, D. & Voet, J.D. *Biochemistry*, Edn. 4th. (John Wiley & Sons, 2011).
22. Feron, O. Pyruvate into lactate and back: From the Warburg effect to symbiotic energy fuel exchange in cancer cells. *Radiother. Oncol.* **92**, 329-333 (2009).
23. Pedersen, P.L. Warburg, me and hexokinase 2: Multiple discoveries of key molecular events underlying one of cancers' most common phenotypes, the "Warburg Effect", i.e., elevated glycolysis in the presence of oxygen. *J. Bioenerg. Biomembr.* **39**, 211-222 (2007).
24. Diaz-Ruiz, R., Uribe-Carvajal, S., Devin, A. & Rigoulet, M. Tumor cell energy metabolism and its common features with yeast metabolism. *Biochim. Biophys. Acta* **1796**, 252-265 (2009).
25. Warburg, O. Origin of cancer cells. *Science* **123**, 309-314 (1956).
26. Christofk, H.R. *et al.* The M2 splice isoform of pyruvate kinase is important for cancer metabolism and tumour growth. *Nature* **452**, 230-U274 (2008).
27. Czernin, J. & Phelps, M.E. Positron emission tomography scanning: Current and future applications. *Annu. Rev. Med.* **53**, 89-112 (2002).
28. Owen, O.E., Kalhan, S.C. & Hanson, R.W. The key role of anaplerosis and cataplerosis for citric acid cycle function. *J. Biol. Chem.* **277**, 30409-30412 (2002).
29. Colquhoun, A. & Newsholme, E.A. Aspects of glutamine metabolism in human tumour cells. *Biochem. Mol. Biol. Int.* **41**, 583-596 (1997).
30. Ruan, K., Song, G. & Ouyang, G.L. Role of Hypoxia in the Hallmarks of Human Cancer. *J. Cell. Biochem.* **107**, 1053-1062 (2009).
31. Klimova, T. & Chandel, N.S. Mitochondrial complex III regulates hypoxic activation of HIF. *Cell Death Differ.* **15**, 660-666 (2008).
32. Hockel, M. & Vaupel, P. Tumor hypoxia: Definitions and current clinical, biologic, and molecular aspects. *J. Natl. Cancer Inst.* **93**, 266-276 (2001).

33. Griffiths, J.R. *et al.* Metabolic changes detected by in vivo magnetic resonance studies of HEPA-1 wild-type tumors and tumors deficient in hypoxia-inducible factor-1 beta (HIF-1 beta): Evidence of an anabolic role for the HIF-1 pathway. *Cancer Res.* **62**, 688-695 (2002).
34. Sonveaux, P. *et al.* Targeting lactate-fueled respiration selectively kills hypoxic tumor cells in mice. *J. Clin. Invest.* **118**, 3930-3942 (2008).
35. Wang, G.L., Jiang, B.H., Rue, E.A. & Semenza, G.L. Hypoxia-Inducible Factor 1 is a basic-helix-loop-helix-PAS heterodimer regulated by cellular O_2 tension. *Proc. Natl. Acad. Sci. U. S. A.* **92**, 5510-5514 (1995).
36. Wang, G.L. & Semenza, G.L. Purification and characterization of Hypoxia-Inducible Factor-1. *J. Biol. Chem.* **270**, 1230-1237 (1995).
37. Semenza, G.L. Targeting HIF-1 for cancer therapy. *Nature Reviews Cancer* **3**, 721-732 (2003).
38. Troy, H. *et al.* Metabolic profiling of hypoxia-inducible factor-1 beta-deficient and wild type Hepa-1 cells: effects of hypoxia measured by H-1 magnetic resonance spectroscopy. *Metabolomics* **1**, 293-303 (2005).
39. Masson, N., Willam, C., Maxwell, P.H., Pugh, C.W. & Ratcliffe, P.J. Independent function of two destruction domains in hypoxia-inducible factor-alpha chains activated by prolyl hydroxylation. *EMBO J.* **20**, 5197-5206 (2001).
40. Jaakkola, P. *et al.* Targeting of HIF-alpha to the von Hippel-Lindau ubiquitylation complex by O-2-regulated prolyl hydroxylation. *Science* **292**, 468-472 (2001).
41. Lando, D. *et al.* FIH-1 is an asparaginyl hydroxylase enzyme that regulates the transcriptional activity of hypoxia-inducible factor. *Genes Dev.* **16**, 1466-1471 (2002).
42. Kaelin, W.G. The von Hippel-Lindau tumour suppressor protein: O-2 sensing and cancer. *Nature Reviews Cancer* **8**, 865-873 (2008).
43. Kelly, C., Smallbone, K. & Brady, M. Tumour glycolysis: The many faces of HIF. *J. Theor. Biol.* **254**, 508-513 (2008).
44. Esteban, M.A. & Maxwell, P.H. HIF, a missing link between metabolism and cancer. *Nat. Med.* **11**, 1047-1048 (2005).
45. Kim, J.-w., Tchernyshyov, I., Semenza, G.L. & Dang, C.V. HIF-1-mediated expression of pyruvate dehydrogenase kinase: A metabolic switch required for cellular adaptation to hypoxia. *Cell Metabolism* **3**, 177-185 (2006).
46. Baker, L.C.J. *et al.* The HIF-pathway inhibitor NSC-134754 induces metabolic changes and anti-tumour activity while maintaining vascular function. *Br. J. Cancer* **106**, 1638-1647 (2012).
47. Dunn, W.B. Current trends and future requirements for the mass spectrometric investigation of microbial, mammalian and plant metabolomes. *Phys Biol* **5**, 11001 (2008).
48. Lhoste, E.F. *et al.* The human colonic microflora influences the alterations of xenobiotic-metabolizing enzymes by catechins in male F344 rats. *Food Chem. Toxicol.* **41**, 695-702 (2003).
49. Benson, D.A. *et al.* GenBank. *Nucleic Acids Res.* **40**, D48-D53 (2012).
50. Fiehn, O. *et al.* The metabolomics standards initiative (MSI). *Metabolomics* **3**, 175-178 (2007).
51. Turner, E. & Bolton, J. Required steps for the validation of a Laboratory Information Management System. *Quality assurance (San Diego, Calif.)* **9**, 217-224 (2001).
52. Scholz, M. & Fiehn, O. Setup X - A public study design database for metabolomic projects, in *Pacific Symposium on Biocomputing 2007* 169-1802007).
53. Brown, M. *et al.* Mass spectrometry tools and metabolite-specific databases for molecular identification in metabolomics. *Analyst* **134**, 1322-1332 (2009).
54. Kind, T. *et al.* FiehnLib: Mass Spectral and Retention Index Libraries for Metabolomics Based on Quadrupole and Time-of-Flight Gas Chromatography/Mass Spectrometry. *Anal. Chem.* **81**, 10038-10048 (2009).
55. Brown, M. *et al.* Automated workflows for accurate mass-based putative metabolite identification in LC/MS-derived metabolomic datasets. *Bioinformatics* **27**, 1108-1112 (2011).
56. Tulpan, D., Leger, S., Belliveau, L., Culf, A. & Cuperlovic-Culf, M. MetaboHunter: an automatic approach for identification of metabolites from H-1-NMR spectra of complex mixtures. *BMC Bioinformatics* **12** (2011).
57. Ye, J. *et al.* Pyruvate kinase M2 promotes de novo serine synthesis to sustain mTORC1 activity and cell proliferation. *Proc. Natl. Acad. Sci. U. S. A.* **109**, 6904-6909 (2011).
58. Sava, A.C. *et al.* Ex Vivo High Resolution Magic Angle Spinning Metabolic Profiles Describe Intratumoral Histopathological Tissue Properties in Adult Human Gliomas. *Magn. Reson. Med.* **65**, 320-328 (2011).
59. Sreekumar, A. *et al.* Metabolomic profiles delineate potential role for sarcosine in prostate cancer progression. *Nature* **457**, 910-914 (2009).
60. Kind, T., Tolstikov, V., Fiehn, O. & Weiss, R.H. A comprehensive urinary metabolomic approach for identifying kidney cancer. *Anal. Biochem.* **363**, 185-195 (2007).

61. Dunn, W.B. *et al.* Procedures for large-scale metabolic profiling of serum and plasma using gas chromatography and liquid chromatography coupled to mass spectrometry. *Nature Protocols* **6**, 1060-1083 (2011).
62. Kenny, L.C. *et al.* Robust Early Pregnancy Prediction of Later Preeclampsia Using Metabolomic Biomarkers. *Hypertension* **56**, 741-749 (2010).
63. Dunn, W.B. *et al.* A GC-TOF-MS study of the stability of serum and urine metabolomes during the UK Biobank sample collection and preparation protocols. *Int. J. Epidemiol.* **37**, 23-30 (2008).
64. Kell, D.B. *et al.* Metabolic footprinting and systems biology: The medium is the message. *Nature Reviews Microbiology* **3**, 557-565 (2005).
65. Teng, Q., Huang, W., Collette, T., Ekman, D. & Tan, C. A direct cell quenching method for cell-culture based metabolomics. *Metabolomics* **5**, 199-208 (2009).
66. Sellick, C.A., Hansen, R., Stephens, G.M., Goodacre, R. & Dickson, A.J. Metabolite extraction from suspension-cultured mammalian cells for global metabolite profiling. *Nature Protocols* **6**, 1241-1249 (2011).
67. Frezza, C. *et al.* Haem oxygenase is synthetically lethal with the tumour suppressor fumarate hydratase. *Nature* **477**, 225-U132 (2011).
68. Tomlinson, I.P.M. *et al.* Germline mutations in FH predispose to dominantly inherited uterine fibroids, skin leiomyomata and papillary renal cell cancer. *Nat. Genet.* **30**, 406-410 (2002).
69. Isaacs, J.S. *et al.* HIF overexpression correlates with biallelic loss of fumarate hydratase in renal cancer: Novel role of fumarate in regulation of HIF stability. *Cancer Cell* **8**, 143-153 (2005).
70. Hoffmann, E.d. & Stroobant, V. *Mass spectrometry : principles and applications*, Edn. 3rd. (J. Wiley, Chichester, England ; Hoboken, NJ; 2007).
71. Halket, J.M. *et al.* Chemical derivatization and mass spectral libraries in metabolic profiling by GC/MS and LC/MS/MS. *J. Exp. Bot.* **56**, 219-243 (2005).
72. Zelena, E. *et al.* Development of a Robust and Repeatable UPLC-MS Method for the Long-Term Metabolomic Study of Human Serum. *Anal. Chem.* **81**, 1357-1364 (2009).
73. Qiu, Y. *et al.* Urinary Metabonomic Study on Colorectal Cancer. *Journal of Proteome Research* **9**, 1627-1634 (2010).
74. Dunn, W.B. *et al.* Changes in the Metabolic Footprint of Placental Explant-Conditioned Culture Medium Identifies Metabolic Disturbances Related to Hypoxia and Pre-Eclampsia. *Placenta* **30**, 974-980 (2009).
75. Makarov, A. *et al.* Performance evaluation of a hybrid linear ion trap/orbitrap mass spectrometer. *Anal. Chem.* **78**, 2113-2120 (2006).
76. Zimmermann, D., Hartmann, M., Moyer, M.P., Nolte, J. & Baumbach, J.I. Determination of volatile products of human colon cell line metabolism by GC/MS analysis. *Metabolomics* **3**, 13-17 (2007).
77. Chan, E.C.Y. *et al.* Metabolic Profiling of Human Colorectal Cancer Using High-Resolution Magic Angle Spinning Nuclear Magnetic Resonance (HR-MAS NMR) Spectroscopy and Gas Chromatography Mass Spectrometry (GC/MS). *Journal of Proteome Research* **8**, 352-361 (2009).
78. Qiu, Y. *et al.* Serum Metabolite Profiling of Human Colorectal Cancer Using GC-TOFMS and UPLC-QTOFMS. *Journal of Proteome Research* **8**, 4844-4850 (2009).
79. Walker-Samuel, S. *et al.* Non-invasive in vivo imaging of vessel calibre in orthotopic prostate tumour xenografts. *Int. J. Cancer* **130**, 1284-1293 (2011).
80. Caprioli, R.M., Farmer, T.B. & Gile, J. Molecular imaging of biological samples: Localization of peptides and proteins using MALDI-TOF MS. *Anal. Chem.* **69**, 4751-4760 (1997).
81. Takats, Z., Wiseman, J.M., Gologan, B. & Cooks, R.G. Mass spectrometry sampling under ambient conditions with desorption electrospray ionization. *Science* **306**, 471-473 (2004).
82. Petucci, C. *et al.* Direct analysis in real time for reaction monitoring in drug discovery. *Anal. Chem.* **79**, 5064-5070 (2007).
83. Heeren, R.M.A., Smith, D.F., Stauber, J., Kükrer-Kaletas, B. & MacAleese, L. Imaging Mass Spectrometry: Hype or Hope? *J. Am. Soc. Mass Spectrom.* **20**, 1006-1014 (2009).
84. Fletcher, J.S. & Vickerman, J.C. A new SIMS paradigm for 2D and 3D molecular imaging of bio-systems. *Anal Bioanal Chem* **396**, 85-104 (2009).
85. Benabdellah, F. *et al.* Mass spectrometry imaging of rat brain sections: nanomolar sensitivity with MALDI versus nanometer resolution by TOF-SIMS. *Anal. Bioanal. Chem.* **396**, 151-162 (2010).
86. Karas, M. & Hillenkamp, F. Laser desorption ionization of proteins with molecular masses exceeding 10000 daltons. *Anal. Chem.* **60**, 2299-2301 (1988).
87. Reyzer, M.L. & Caprioli, R.M. MALDI-MS-based imaging of small molecules and proteins in tissues. *Curr. Opin. Chem. Biol.* **11**, 29-35 (2007).
88. Hart, P.J., Francese, S., Claude, E., Woodroofe, M.N. & Clench, M.R. MALDI-MS imaging of lipids in ex vivo human skin. *Anal. Bioanal. Chem.* **401**, 115-125 (2011).
89. Berry, K.A.Z. *et al.* MALDI imaging MS of phospholipids in the mouse lung. *J. Lipid Res.* **52**, 1551-1560 (2011).

90. Reyzer, M.L., Hsieh, Y.S., Ng, K., Korfmacher, W.A. & Caprioli, R.M. Direct analysis of drug candidates in tissue by matrix-assisted laser desorption/ionization mass spectrometry. *J. Mass Spectrom.* **38**, 1081-1092 (2003).
91. Cohen, S.L. & Chait, B.T. Influence of matrix solution conditions on the MALDI-MS analysis of peptides and proteins. *Anal. Chem.* **68**, 31-37 (1996).
92. Reyzer, M.L. *et al.* Early changes in protein expression detected by mass spectrometry predict tumor response to molecular therapeutics. *Cancer Res.* **64**, 9093-9100 (2004).
93. Jackson, S.N. *et al.* MALDI-ion mobility-TOFMS imaging of lipids in rat brain tissue. *J. Mass Spectrom.* **42**, 1093-1098 (2007).
94. Khatib-Shahidi, S., Andersson, M., Herman, J.L., Gillespie, T.A. & Caprioli, R.M. Direct molecular analysis of whole-body animal tissue sections by imaging MALDI mass spectrometry. *Anal. Chem.* **78**, 6448-6456 (2006).
95. Vickerman, J.C. & Gilmore, I.S. *Surface analysis : the principal techniques*, Edn. 2nd. (John Wiley & Sons Ltd., Chichester; 2009).
96. Ostrowski, S.G., Van Bell, C.T., Winograd, N. & Ewing, A.G. Mass Spectrometric Imaging of Highly Curved Membranes During Tetrahymena Mating. *Science* **305**, 71-73 (2004).
97. Benninghoven, A. Untersuchungen zum Spektrum und den Anfangsenergien negativer Sekundärionen. *Zeitschrift für Physik A Hadrons and Nuclei* **199**, 141-156 (1967).
98. Gillen, G. & Roberson, S. Preliminary evaluation of an SF5+ polyatomic primary ion beam for analysis of organic thin films by secondary ion mass spectrometry. *Rapid Commun. Mass Spectrom.* **12**, 1303-1312 (1998).
99. Davies, N. *et al.* Development and experimental application of a gold liquid metal ion source. *Appl. Surf. Sci.* **203-204**, 223-227 (2003).
100. Touboul, D., Kollmer, F., Niehuis, E., Brunelle, A. & Laprévote, O. Improvement of biological time-of-flight-secondary ion mass spectrometry imaging with a bismuth cluster ion source. *J. Am. Soc. Mass Spectrom.* **16**, 1608-1618 (2005).
101. Wong, S.C.C. *et al.* Development of a C60+ ion gun for static SIMS and chemical imaging. *Appl. Surf. Sci.* **203-204**, 219-222 (2003).
102. Fletcher, J.S., Lockyer, N.P. & Vickerman, J.C. Developments in molecular SIMS depth profiling and 3D imaging of biological systems using polyatomic primary ions. *Mass Spectrom. Rev.* **30**, 142-174 (2009).
103. Altelaar, A.F.M. *et al.* Gold-Enhanced Biomolecular Surface Imaging of Cells and Tissue by SIMS and MALDI Mass Spectrometry. *Anal. Chem.* **78**, 734-742 (2006).
104. Vickerman, J.C. Molecular imaging and depth profiling by mass spectrometry-SIMS, MALDI or DESI? *Analyst* (2011).
105. Carado, A. *et al.* C60 Secondary Ion Mass Spectrometry with a Hybrid-Quadrupole Orthogonal Time-of-Flight Mass Spectrometer. *Anal. Chem.* **80**, 7921-7929 (2008).
106. Fletcher, J.S. *et al.* A New Dynamic in Mass Spectral Imaging of Single Biological Cells. *Anal. Chem.* **80**, 9058-9064 (2008).
107. Johansson, B. ToF-SIMS imaging of lipids in cell membranes. *Surf. Interface Anal.* **38**, 1401-1412 (2006).
108. McQuaw, C.M., Sostarecz, A.G., Zheng, L., Ewing, A.G. & Winograd, N. Investigating lipid interactions and the process of raft formation in cellular membranes using ToF-SIMS. *Appl. Surf. Sci.* **252**, 6716-6718 (2006).
109. Ostrowski, S.G., Kurczy, M.E., Roddy, T.P., Winograd, N. & Ewing, A.G. Secondary Ion MS Imaging To Relatively Quantify Cholesterol in the Membranes of Individual Cells from Differentially Treated Populations. *Anal. Chem.* **79**, 3554-3560 (2007).
110. Touboul, D. *et al.* MALDI-TOF and cluster-TOF-SIMS imaging of Fabry disease biomarkers. *Int. J. Mass spectrom.* **260**, 158-165 (2007).
111. Monroe, E.B., Jurchen, J.C., Lee, J., Rubakhin, S.S. & Sweedler, J.V. Vitamin E Imaging and Localization in the Neuronal Membrane. *J. Am. Chem. Soc.* **127**, 12152-12153 (2005).
112. Piehowski, P.D. *et al.* Time-of-Flight Secondary Ion Mass Spectrometry Imaging of Subcellular Lipid Heterogeneity: Poisson Counting and Spatial Resolution. *Anal. Chem.* **81**, 5593-5602 (2009).
113. Fletcher, J.S., Lockyer, N.P., Vaidyanathan, S. & Vickerman, J.C. TOF-SIMS 3D Biomolecular Imaging of Xenopus laevis Oocytes Using Buckminsterfullerene (C60) Primary Ions. *Anal. Chem.* **79**, 2199-2206 (2007).
114. Fletcher, J.S., Lockyer, N.P. & Vickerman, J.C. Molecular SIMS imaging; spatial resolution and molecular sensitivity: have we reached the end of the road? Is there light at the end of the tunnel? *Surf. Interface Anal.* **43**, 253-256 (2011).
115. Maxwell, P.H. *et al.* Hypoxia-inducible factor-1 modulates gene expression in solid tumors and influences both angiogenesis and tumor growth. *Proc. Natl. Acad. Sci. U. S. A.* **94**, 8104-8109 (1997).

116. Roberts, D.L. *et al.* Contribution of HIF-1 and drug penetrance to oxaliplatin resistance in hypoxic colorectal cancer cells. *Br. J. Cancer* **101**, 1290-1297 (2009).
117. Mosmann, T. Rapid colorimetric assay for cellular growth and survival: Application to proliferation and cytotoxicity assays. *J. Immunol. Methods* **65**, 55-63 (1983).
118. Burrows, N. *et al.* Expression of hypoxia-inducible factor 1 alpha in thyroid carcinomas. *Endocrine-Related Cancer* **17**, 61-72.
119. Cowen, R.L. *et al.* Hypoxia targeted gene therapy to increase the efficacy of tirapazamine as an adjuvant to radiotherapy: Reversing tumor radioresistance and effecting cure. *Cancer Res.* **64**, 1396-1402 (2004).
120. Bondar, R.J.L. & Mead, D.C. Evaluation of Glucose-6-Phosphate Dehydrogenase from Leuconostoc mesenteroides in the Hexokinase Method for Determining Glucose in Serum. *Clin. Chem.* **20**, 586-590 (1974).
121. Cattaneo, M.V. & Luong, J.H.T. Monitoring glutamine in animal cell cultures using a chemiluminescence fiber optic biosensor. *Biotechnol. Bioeng.* **41**, 659-665 (1993).
122. Barham, D. & Trinder, P. An improved colour reagent for the determination of blood glucose by the oxidase system. *Analyst* **97**, 142-145 (1972).
123. Kim, D.-H. *et al.* Combining metabolic fingerprinting and footprinting to understand the phenotypic response of HPV16 E6 expressing cervical carcinoma cells exposed to the HIV anti-viral drug lopinavir. *Analyst* **135**, 1235-1244 (2009).
124. Christian, G.D. (ed.) *Analytical Chemistry*, Edn. 6. (Wiley International Edition, 2004).
125. Winder, C.L., Gordon, S.V., Dale, J., Hewinson, R.G. & Goodacre, R. Metabolic fingerprints of Mycobacterium bovis cluster with molecular type: implications for genotype-phenotype links. *Microbiology-Sgm* **152**, 2757-2765 (2006).
126. Martens, H., Nielsen, J.P. & Engelsen, S.B. Light scattering and light absorbance separated by extended multiplicative signal correction. Application to near-infrared transmission analysis of powder mixtures. *Anal. Chem.* **75**, 394-404 (2003).
127. Fifield, F.W. & Kealey, D. *Principles and Practice of Analytical Chemistry*, Edn. 5th. (Blackwell Science, 2000).
128. Begley, P. *et al.* Development and Performance of a Gas Chromatography-Time-of-Flight Mass Spectrometry Analysis for Large-Scale Nontargeted Metabolomic Studies of Human Serum. *Anal. Chem.* **81**, 7038-7046 (2009).
129. Sumner, L.W. *et al.* Proposed minimum reporting standards for chemical analysis. *Metabolomics* **3**, 211-221 (2007).
130. Babushok, V.I. *et al.* Development of a database of gas chromatographic retention properties of organic compounds. *J. Chromatogr.* **1157**, 414-421 (2007).
131. Kopka, J. *et al.* GMD@CSB.DB: the Golm Metabolome Database. *Bioinformatics* **21**, 1635-1638 (2005).
132. Smith, C.A., Want, E.J., O'Maille, G., Abagyan, R. & Siuzdak, G. XCMS: Processing mass spectrometry data for metabolite profiling using Nonlinear peak alignment, matching, and identification. *Anal. Chem.* **78**, 779-787 (2006).
133. Jones, E.A., Lockyer, N.P. & Vickerman, J.C. Mass spectral analysis and imaging of tissue by ToF-SIMSâ€"The role of buckminsterfullerene, C60+, primary ions. *Int. J. Mass spectrom.* **260**, 146-157 (2007).
134. Fletcher, J.S., Kotze, H.L., Armitage, E.G., Lockyer, N.P. & Vickerman, J.C. Time-of-Fight Secondary Ion Mass Spectrometry for Metabolomics – Challenges for In Situ Metabolite Identification and Quantification (Submitted). *Metabolomics* (2012).
135. Schwartz, S.A., Reyzer, M.L. & Caprioli, R.M. Direct tissue analysis using matrix-assisted laser desorption/ionization mass spectrometry: practical aspects of sample preparation. *J. Mass Spectrom.* **38**, 699-708 (2003).
136. Passarelli, M.K. & Winograd, N. Lipid imaging with time-of-flight secondary ion mass spectrometry (ToF-SIMS). *Biochimica et Biophysica Acta (BBA) - Molecular and Cell Biology of Lipids* **1811**, 976-990 (2011).
137. Steuer, R., Morgenthal, K., Weckwerth, W. & Selbig, J. A gentle guide to the analysis of metabolomic data. *Methods Mol. Biol.* **358**, 105-126 (2007).
138. Hogg, R.V. & Ledolter, J. *Engineering Statistics*. (Macmillan publishing company, New York; 1987).
139. Storey, J.D. The positive false discovery rate: A Bayesian interpretation and the q-value. *Annals of Statistics* **31**, 2013-2035 (2003).
140. Hollander, M. & Wolfe, D.A. *Nonparametric Statistical Methods*, Edn. 2nd. (John Wiley & Sons, 1999).
141. Jolliffe, I.T. *Principal Component Analysis* Edn. 2nd. (Springer, New York; 2002).
142. Wold, S., Esbensen, K. & Geladi, P. Principal component analysis. *Chemometrics Intellig. Lab. Syst.* **2**, 37-52 (1987).

143. Mellinger, M. Multivariate data-analysis - its methods. *Chemometrics Intellig. Lab. Syst.* **2**, 29-36 (1987).
144. Stuart, A. & Ord, J.K. *Kendall's advanced theory of statistics*, Edn. 5th. (Griffin and co, London; 1987).
145. Steuer, R. in Institut für Physik, Vol. PhD 130 (Universität Potsdam, Potsdam; 2005).
146. Keating, S.M., Bornstein, B.J., Finney, A. & Hucka, M. SBMLToolbox: an SBML toolbox for MATLAB users. *Bioinformatics* **22**, 1275-1277 (2006).
147. Hoffman, E.C. *et al.* Cloning of a factor required for activity of the AH (Dioxin) receptor. *Science* **252**, 954-958 (1991).
148. Brown, L.M. *et al.* Reversing hypoxic cell chemoresistance in vitro using genetic and small molecule approaches targeting hypoxia inducible factor-1. *Mol. Pharmacol.* **69**, 411-418 (2006).
149. DeBerardinis, R.J. *et al.* Beyond aerobic glycolysis: Transformed cells can engage in glutamine metabolism that exceeds the requirement for protein and nucleotide synthesis. *Proceedings of the National Academy of Sciences* **104**, 19345-19350 (2007).
150. Wise, D.R. *et al.* Myc regulates a transcriptional program that stimulates mitochondrial glutaminolysis and leads to glutamine addiction. *Proc. Natl. Acad. Sci. U. S. A.* **105**, 18782-18787 (2008).
151. Yang, C., Richardson, A., Osterman, A. & Smith, J. Profiling of central metabolism in human cancer cells by two-dimensional NMR, GC-MS analysis, and isotopomer modeling. *Metabolomics* **4**, 13-29 (2008).
152. Gardner, L.B. *et al.* Hypoxia inhibits G(1)/S transition through regulation of p27 expression. *J. Biol. Chem.* **276**, 7919-7926 (2001).
153. Schmaltz, C., Hardenbergh, P.H., Wells, A. & Fisher, D.E. Regulation of proliferation-survival decisions during tumor cell hypoxia. *Mol. Cell. Biol.* **18**, 2845-2854 (1998).
154. Liu, W., Xin, H., Eckert, D.T., Brown, J.A. & Gnarra, J.R. Hypoxia and cell cycle regulation of the von Hippel-Lindau tumor suppressor. *Oncogene* **30**, 21-31.
155. Denko, N.C. Hypoxia, HIF1 and glucose metabolism in the solid tumour. *Nature Reviews Cancer* **8**, 705-713 (2008).
156. Firth, J.D., Ebert, B.L. & Ratcliffe, P.J. Hypoxic regulation of lactate-dehydrogenase-A - interaction between Hypoxia-Inducible Factor-1 and cAMP response elements. *J. Biol. Chem.* **270**, 21021-21027 (1995).
157. Ullah, M.S., Davies, A.J. & Halestrap, A.P. The plasma membrane lactate transporter MCT4, but not MCT1, is up-regulated by hypoxia through a HIF-1 alpha-dependent mechanism. *J. Biol. Chem.* **281**, 9030-9037 (2006).
158. Baggetto, L.G. Deviant energetic metabolism of glycolytic cancer-cells. *Biochimie* **74**, 959-974 (1992).
159. Fiehn, O. *et al.* Metabolite profiling for plant functional genomics. *Nat. Biotechnol.* **18**, 1157-1161 (2000).
160. Roessner, U. *et al.* Metabolic profiling allows comprehensive phenotyping of genetically or environmentally modified plant systems. *Plant Cell* **13**, 11-29 (2001).
161. Davey, M.P., Burrell, M.M., Woodward, F.I. & Quick, W.P. Population-specific metabolic phenotypes of Arabidopsis lyrata ssp petraea. *New Phytol.* **177**, 380-388 (2008).
162. Ali, K. *et al.* Alterations in grapevine leaf metabolism upon inoculation with Plasmopara viticola in different time-points. *Plant science : an international journal of experimental plant biology* **191-192**, 100-107 (2012).
163. Park, C., Yun, S., Lee, S.Y., Park, K. & Lee, J. Metabolic Profiling of Klebsiella oxytoca: Evaluation of Methods for Extraction of Intracellular Metabolites Using UPLC/Q-TOF-MS. *Appl. Biochem. Biotechnol.* **167**, 425-438 (2012).
164. Allen, J. *et al.* High-throughput classification of yeast mutants for functional genomics using metabolic footprinting. *Nat. Biotechnol.* **21**, 692-696 (2003).
165. Baudoin, E., Benizri, E. & Guckert, A. Metabolic fingerprint of microbial communities from distinct maize rhizosphere compartments. *Eur. J. Soil Biol.* **37**, 85-93 (2001).
166. Castrillo, J.I., Hayes, A., Mohammed, S., Gaskell, S.J. & Oliver, S.G. An optimized protocol for metabolome analysis in yeast using direct infusion electrospray mass spectrometry. *Phytochemistry* **62**, 929-937 (2003).
167. Sreekumar, A. *et al.* Metabolomic profiles delineate potential role for sarcosine in prostate cancer progression. *Nature* **457**, 910-914 (2009).
168. Teul, J. *et al.* Improving Metabolite Knowledge in Stable Atherosclerosis Patients by Association and Correlation of GC-MS and H-1 NMR Fingerprints. *Journal of Proteome Research* **8**, 5580-5589 (2009).
169. Godzien, J., García-Martínez, D., Martinez-Alcazar, P., Ruperez, F. & Barbas, C. Effect of a nutraceutical treatment on diabetic rats with targeted and CE-MS non-targeted approaches. *Metabolomics*, 1-15 (2011).

170. Bollard, M.E. *et al.* Metabolic profiling of the effects of D-galactosamine in liver spheroids using H-1 NMR and MAS-NMR spectroscopy. *Chem. Res. Toxicol.* **15**, 1351-1359 (2002).
171. Welthagen, W. *et al.* Comprehensive two-dimensional gas chromatography-time-of-flight mass spectrometry (GC x GC-TOF) for high resolution metabolomics: biomarker discovery on spleen tissue extracts of obese NZO compared to lean C57BL/6 mice. *Metabolomics* **1**, 65-73 (2005).
172. Wedge, D.C. *et al.* Is Serum or Plasma More Appropriate for Intersubject Comparisons in Metabolomic Studies? An Assessment in Patients with Small-Cell Lung Cancer. *Anal. Chem.* **83**, 6689-6697 (2011).
173. Shrestha, B. & Vertes, A. In Situ Metabolic Profiling of Single Cells by Laser Ablation Electrospray Ionization Mass Spectrometry. *Anal. Chem.* **81**, 8265-8271 (2009).
174. Armitage, E.G. *et al.* Time-of-flight SIMS as a novel approach to unlocking the hypoxic properties of cancer. *Surf. Interface Anal.* (2012).
175. Kotze, H.L. *et al.* ToF-SIMS as a tool for metabolic profiling small biomolecules in cancer systems. *Surf. Interface Anal.* (2012).
176. Tejedor, M.L., Mizuno, H., Tsuyama, N., Harada, T. & Masujima, T. In Situ Molecular Analysis of Plant Tissues by Live Single-Cell Mass Spectrometry. *Anal. Chem.* **84**, 5221-5228 (2012).
177. Sabatine, M.S. *et al.* Metabolomic identification of novel biomarkers of myocardial ischemia. *Circulation* **112**, 3868-3875 (2005).
178. Wang, C. *et al.* Plasma phospholipid metabolic profiling and biomarkers of type 2 diabetes mellitus based on high-performance liquid chromatography/electrospray mass spectrometry and multivariate statistical analysis. *Anal. Chem.* **77**, 4108-4116 (2005).
179. Farag, M.A., Ryu, C.M., Sumner, L.W. & Pare, P.W. GC-MS SPME profiling of rhizobacterial volatiles reveals prospective inducers of growth promotion and induced systemic resistance in plants. *Phytochemistry* **67**, 2262-2268 (2006).
180. Bedair, M. & Sumner, L.W. Current and emerging mass-spectrometry technologies for metabolomics. *TrAC, Trends Anal. Chem.* **27**, 238-250 (2008).
181. Semenza, G.L. HIF-1: upstream and downstream of cancer metabolism. *Curr. Opin. Genet. Dev.* **20**, 51-56 (2010).
182. Kanehisa, M. & Goto, S. KEGG: Kyoto Encyclopedia of Genes and Genomes. *Nucleic Acids Res.* **28**, 27-30 (2000).
183. Wishart, D.S. *et al.* HMDB: a knowledgebase for the human metabolome. *Nucleic Acids Res.* **37**, D603-D610 (2009).
184. Fahy, E., Sud, M., Cotter, D. & Subramaniam, S. LIPID MAPS online tools for lipid research. *Nucleic Acids Res.* **35**, W606-W612 (2007).
185. Karp, P.D. *et al.* Expansion of the BioCyc collection of pathway/genome databases to 160 genomes. *Nucleic Acids Res.* **33**, 6083-6089 (2005).
186. Knox, C. *et al.* DrugBank 3.0: a comprehensive resource for 'Omics' research on drugs. *Nucleic Acids Res.* **39**, D1035-D1041 (2011).
187. Gradin, K. *et al.* Functional interference between hypoxia and dioxin signal transduction pathways: Competition for recruitment of the Arnt transcription factor. *Mol. Cell. Biol.* **16**, 5221-5231 (1996).
188. Rebouche, C.J. & Seim, H. Carnitine metabolism and its regulation in microorganisms and mammals. *Annu. Rev. Nutr.* **18**, 39-61 (1998).
189. Gerner, E.W. & Meyskens, F.L. Polyamines and cancer: Old molecules, new understanding. *Nature Reviews Cancer* **4**, 781-792 (2004).
190. Meyskens, F.L. & Gerner, E.W. Development of difluoromethylornithine (DFMO) as a chemoprevention agent. *Clin. Cancer. Res.* **5**, 945-951 (1999).
191. Kim, K. *et al.* Lysophosphatidylserine induces calcium signaling through Ki16425/VPC32183-sensitive GPCR in bone marrow-derived mast cells and in C6 glioma and colon cancer cells. *Arch. Pharmacal Res.* **31**, 310-317 (2008).
192. Capiod, T., Shuba, Y., Skryma, R. & Prevarskaya, N. Calcium signalling and cancer cell growth, in *Subcellular Biochemistry*, Vol. 45 405-427 (Springer, Po Box 17, 3300 Aa Dordrecht, Netherlands, 2007).
193. Reynolds, C.P., Maurer, B.J. & Kolesnick, R.N. Ceramide synthesis and metabolism as a target for cancer therapy. *Cancer Lett.* **206**, 169-180 (2004).
194. Yin, J., Miyazaki, K., Shaner, R.L., Merrill Jr, A.H. & Kannagi, R. Altered sphingolipid metabolism induced by tumor hypoxia â€“ New vistas in glycolipid tumor markers. *FEBS Lett.* **584**, 1872-1878 (2010).
195. Varki, A., Cummings, R. & Esko, J. (eds.) *Essentials of Glycobiology*. (Cold Spring Harbor Laboratory Press, 1999).
196. Fuster, M.M. & Esko, J.D. The sweet and sour of cancer: Glycans as novel therapeutic targets. *Nature Reviews Cancer* **5**, 526-542 (2005).

197. Yin, J. *et al.* Hypoxic culture induces expression of sialin, a sialic acid transporter, and cancer-associated gangliosides containing non-human sialic acid on human cancer cells. *Cancer Res.* **66**, 2937-2945 (2006).
198. Semenza, G.L. HIF-1 and tumor progression: pathophysiology and therapeutics. *Trends Mol. Med.* **8**, S62-S67 (2002).
199. Cheng, K.C., Cahill, D.S., Kasai, H., Nishimura, S. & Loeb, L.A. 8-Hydroxyguanine, an abundant form of oxidative DNA damage, causes CAUSES G -> T and A -> C substitutions. *J. Biol. Chem.* **267**, 166-172 (1992).
200. Gillespie, M.N., Pastukh, V.M. & Ruchko, M.V. Controlled DNA "damage" and repair in hypoxic signaling. *Respiratory Physiology & Neurobiology* **174**, 244-251.
201. Kietzmann, T. & Gorlach, A. Reactive oxygen species in the control of hypoxia-inducible factor-mediated gene expression. *Seminars in Cell & Developmental Biology* **16**, 474-486 (2005).
202. Camacho, D., de la Fuente, A. & Mendes, P. The origin of correlations in metabolomics data. *Metabolomics* **1**, 53-63 (2005).
203. Rodgers, J.L. & Nicewander, W.A. Thirteen Ways to Look at the Correlation Coefficient. *The American Statistician* **42**, 59-66 (1988).
204. Shirato, K. *et al.* Hypoxic regulation of glycosylation via the N-acetylglucosamine cycle. *Journal of Clinical Biochemistry and Nutrition* **48**, 20-25 (2011).
205. Bruick, R.K. & McKnight, S.L. A conserved family of prolyl-4-hydroxylases that modify HIF. *Science* **294**, 1337-1340 (2001).
206. Griffin, J.L. & Shockcor, J.P. Metabolic profiles of cancer cells. *Nature Reviews Cancer* **4**, 551-561 (2004).
207. Herszènyi, L. *et al.* The role of cysteine and serine proteases in colorectal carcinoma. *Cancer* **86**, 1135-1142 (1999).
208. Greene, J.G., Porter, R.H.P., Eller, R.V. & Greenamyre, J.T. Inhibition of succinate-dehydrogenase by malonic-acid produces an exocitotoxic lesion in rat striatum. *J. Neurochem.* **61**, 1151-1154 (1993).
209. Dang, L. *et al.* Cancer-associated IDH1 mutations produce 2-hydroxyglutarate *Nature* **465**, 966-966 (2010).
210. Griffiths, J.R. & Stubbs, M. Opportunities for studying cancer by metabolomics: preliminary observations on tumors deficient in hypoxia-inducible factor 1. *Adv. Enzyme Regul.* **43**, 67-76 (2003).
211. Benyoseph, O., Badargoffer, R.S., Morris, P.G. & Bachelard, H.S. Glycerol-3-phosphate and lactate as inhibitors of the cerebral cytoplasmic redox state in severe and mild hypoxia respectively - a C-13-NMR and P-31-NMR study. *Biochem. J.* **291**, 915-919 (1993).
212. Gordan, J.D., Thompson, C.B. & Simon, M.C. HIF and c-Myc: sibling rivals for control of cancer cell metabolism and proliferation. *Cancer Cell* **12**, 108-113 (2007).
213. Brunelle, A., Touboul, D. & Laprévote, O. Biological tissue imaging with time-of-flight secondary ion mass spectrometry and cluster ion sources. *J. Mass Spectrom.* **40**, 985-999 (2005).
214. Fletcher, J.S. Cellular imaging with secondary ion mass spectrometry. *Analyst* **134**, 2204-2215 (2009).
215. McDonnell, L.A., Heeren, R.M.A., de Lange, R.P.J. & Fletcher, I.W. Higher sensitivity secondary ion mass spectrometry of biological molecules for high resolution, chemically specific imaging. *J. Am. Soc. Mass Spectrom.* **17**, 1195-1202 (2006).
216. McDonnell, L.A. & Heeren, R.M.A. Imaging mass spectrometry. *Mass Spectrom. Rev.* **26**, 606-643 (2007).
217. Parry, S. & Winograd, N. High-resolution TOF-SIMS imaging of eukaryotic cells preserved in a trehalose matrix. *Anal. Chem.* **77**, 7950-7957 (2005).
218. Nygren, H.k., Malmberg, P., Kriegeskotte, C. & Arlinghaus, H.F. Bioimaging TOF-SIMS: localization of cholesterol in rat kidney sections. *FEBS Lett.* **566**, 291-293 (2004).
219. Chandra, S. & Morrison, G.H. Sample preparation of animal tissues and cell cultures for secondary ion mass spectrometry (SIMS) microscopy. *Biol. Cell* **74**, 31-42 (1992).
220. Piwowar, A.M., Lockyer, N.P. & Vickerman, J.C. Salt Effects on Ion Formation in Desorption Mass Spectrometry: An Investigation into the Role of Alkali Chlorides on Peak Suppression in Time-of-Flight-Secondary Ion Mass Spectrometry. *Anal. Chem.* **81**, 1040-1048 (2009).
221. Lobjois, V.r., Frongia, C.l., Jozan, S., Truchet, I. & Valette, A. Cell cycle and apoptotic effects of SAHA are regulated by the cellular microenvironment in HCT116 multicellular tumour spheroids. *Eur. J. Cancer* **45**, 2402-2411 (2009).
222. Friedrich, J. *et al.* A reliable tool to determine cell viability in complex 3-D culture: The acid phosphatase assay. *J. Biomol. Screen.* **12**, 925-937 (2007).
223. Horai, H. *et al.* MassBank: a public repository for sharing mass spectral data for life sciences. *J. Mass Spectrom.* **45**, 703-714 (2010).

224. Jones, E.A., Lockyer, N.P., Kordys, J. & Vickerman, J.C. Suppression and enhancement of secondary ion formation due to the chemical environment in static-secondary ion mass spectrometry. *J. Am. Soc. Mass Spectrom.* **18**, 1559-1567 (2007).
225. Samudio, I. *et al.* Pharmacologic inhibition of fatty acid oxidation sensitizes human leukemia cells to apoptosis induction. *J. Clin. Invest.* **120**, 142-156 (2010).
226. Bennett, B.D., Yuan, J., Kimball, E.H. & Rabinowitz, J.D. Absolute quantitation of intracellular metabolite concentrations by an isotope ratio-based approach. *Nature Protocols* **3**, 1299-1311 (2008).
227. Glunde, K., Bhujwalla, Z.M. & Ronen, S.M. Choline metabolism in malignant transformation. *Nature Reviews Cancer* **11**, 835-848 (2011).
228. Galons, J.P., Job, C. & Gillies, R.J. Increase of GPC levels in cultured-mammalian-cells during acidosis -A P-31 MR spectroscopy study using a continuous bioreactor system. *Magn. Reson. Med.* **33**, 422-426 (1995).
229. Glunde, K. *et al.* Hypoxia regulates choline kinase expression through hypoxia-inducible factor-lot signaling in a human prostate cancer model. *Cancer Res.* **68**, 172-180 (2008).
230. Temes, E. *et al.* Role of diacylglycerol induced by hypoxia in the regulation of HIF-1Î± activity. *Biochem. Biophys. Res. Commun.* **315**, 44-50 (2004).
231. Furuta, E. *et al.* Fatty acid synthase gene is up-regulated by hypoxia via activation of Akt and sterol regulatory element binding protein-1. *Cancer Res.* **68**, 1003-1011 (2008).
232. Deng, W. *et al.* Role of ornithine decarboxylase in breast cancer. *Acta Biochimica Et Biophysica Sinica* **40**, 235-243 (2008).
233. Matteucci, E., Modora, S., Simone, M. & Desiderio, M.A. Hepatocyte growth factor induces apoptosis through the extrinsic pathway in hepatoma cells: favouring role of hypoxia-inducible factor-1 deficiency. *Oncogene* **22**, 4062-4073 (2003).